

***In vivo* imaging of host – pathogen
interactions in *Staphylococcus aureus*
infection**

Justyna Jadwiga Serba

Submitted for the degree of Doctor of Philosophy

Department of Infection and Immunity

University of Sheffield

June 2015

Abstract

S. aureus has evolved strategies to manipulate host-pathogen interactions to its own ends, and avoid killing by professional phagocytes. It has been suggested that *S. aureus* can reside and survive inside professional phagocytes – mainly neutrophils and macrophages. Moreover, the intracellular environment, instead of being disruptive could constitute a beneficial “niche”.

My hypothesis is that *S. aureus* evade elimination by subverting one or more of uptake and intracellular processes. Internalisation and autophagy are host response processes already reported to favour pathogenesis of other bacteria. Widefield fluorescence and confocal microscopy has been used to track pathogens inside of the transparent zebrafish embryo. *S. aureus* strains were stained before injection with pH-sensitive and insensitive fluorescent dyes to assess the stage of endosome maturation by pH decrease. Transgenic zebrafish lines were developed during this study to specifically mark autophagosomes (LC3 fused with GFP and RFP). Nomarski DIC combined with high power fluorescence microscopy enabled imaging of pathogen uptake, phagocyte-to-phagocyte interactions and bacterial acidification *in vivo*.

Results of whole body counts of bacteria internalised by phagocytes showed more intake into macrophages than into neutrophils. Quantification of bacteria labelled with pH sensitive bacterial cell wall dyes indicated different acidic conditions in bacteria-containing endosomes and lower acidification rates in neutrophils. Bacterial cells co-localise with LC3 protein in neutrophils. The presence of bacteria in LC3 tagged vesicles suggests that autophagy may be involved in *S. aureus* intake and intracellular processing. *In vivo* quantification combined with real time imaging have the potential to help increase our understanding of host – pathogen interactions at different stages of infection.

Acknowledgements

First I would like to thank my supervisors, Steve Renshaw and Simon Foster for making it possible for me to work on this project. I have got opportunity to develop many skills and learn to collaborate in an international network. I am also thankful for their help, inspiring advices and for training in critical thinking and writing.

I would also like to thank my personal tutor Mark Thomas for his guidance and support.

I wish to thank Nikolay Ogryzko for training in microscopy, generation of transgenic zebrafish lines, for his technical advice and for helping me during writing up of my thesis. It would have been much more difficult without your support.

Many thanks to Tomasz Prajsnar for training in zebrafish infection, imaging and for scientific advice and guidance during the project. I wish to thank Aleksandra Bojarczuk for training in zebrafish experimental work, her constant support and helping me to accommodate in Sheffield. I would also like to thank members of Renshaw and Foster Labs for being so welcoming and creating such a positive working atmosphere.

I would also like to acknowledge collaborators and participants of the FishForPharma Initial Training Network. It was a great experience to work with other students, under a very supportive and motivating supervision. I am very grateful to Annemarie Meijer and Jean-Pierre Levraud for allowing me to work in their laboratories during secondments.

Finally very special thanks go to Natasja Barki, Sara Cruz, Justina Mischewski and Lucyna Serba for their patience, understanding and moral support.

This work was a part of Marie Curie Initial Training Network funded by the 7th Framework People Programme of the European Commission.

Abbreviations

agr: Accessory gene regulator; **ALRs**: absent-in-melanoma (AIM)-like receptors; **APC**: Antigen presenting cells; **ARDS**: Acute respiratory distress syndrome; **Atg**: Autophagy-related genes; **BHI**: Brain heart infusion; **bp**: Base pairs; **CFU**: Colony forming units; **CGD**: Chronic granulomatous disease; **cLC3**: cytoplasmic LC3; **ClfB**: Clumping factor B; **Cna**: Collagen adhesion; **COPD**: Chronic obstructive pulmonary disease; **CTLs**: C-type lectins; **°C**: Degrees Celsius; **DIC**: Differential interference contrast; **DNA**: Deoxyribonucleic acid; **dNTPs**: Deoxyribonucleoside-5' –phosphate; **dpf**: Days post fertilisation; **dpi**: Days post infection; **DRAM1**: DNA-damage regulated autophagy modulator 1; **Ebp**: Elastin-binding protein; **ECM**: Extracellular matrix; **ER**: Endoplasmic reticulum; **FnBPA**: Fibronectin-binding protein A; **FnBPB**: Fibronectin-binding protein B; **GAPs**: GTPase-activating proteins; **GAS**: Group A *Streptococcus*; **GEFs**: Guanine nucleotide exchange factors; **GFP**: Green fluorescence protein; **hpf**: Hours post fertilisation; **hpi**: Hours post infection; **Hsp60**: Human heat shock protein 60; **HUVECs**: Human umbilical vein endothelial cells ; **IRF8**: Interferon regulatory factor 8; **LAP**: LC3 associated phagocytosis; **LB**: Luria Bertani medium; **LLO**: Listeriolysin O; **LPS**: Lipopolysaccharide; **LWT**: London wild type; **M**: Molar; **MAMPs**: microbial associated molecular patterns; **MB**: Methylene blue; **MBL**: Mannose binding lectin ; **min**: minutes; **MO**: Morpholino oligonucleotide; **MPO**: Myeloperoxidase; **MR**: Mannose receptor; **mROS**: Mitochondrial-derived Reactive oxygen species; **MRSA**: Methicillin-resistant *Staphylococcus aureus*; **MSCRAMMs**: Microbial-Surface Components Recognising Adhesive Matrix Molecules; **mTOR**: Mammalian target of rapamycin; **NA**: Numerical aperture; **NDP52**: Nuclear dot protein 52 kDa; **OatA**: O-acetyltransferase A; **PAMPs**: Pathogen associated molecular patterns; **PAS**: Pre-autophagosomal structure; **PBS**: Phosphate buffered saline; **PCR**: Polimerase chain reaction; **PE**: Phosphatidylethanolamine; **pLC3**: Phagocytic LC3; **PPRs**: Pattern recognition receptors; **PSMs**: Phenol soluble modulins; **PV**: Parasitophorus vacuole; **RLRs**: (RIG-I)-like receptors; **RNA**: ribonucleic acid; **ROS**: Reactive oxygen species; **rpm**: revolutions per minute; **sar**: *Staphylococcal* Accessory Regulator; **SCV**: *Salmonella*-containing vacuole; **SCVs**: Small colony variants; **SEM**: Standard error of the mean; **SLO**: Streptolysin O; **SOK**: Surface factor promoting resistance to oxidative killing; **SRs**: Scavenger receptors; **TBK1**: Tank-binding kinase 1; **TGF-β1**: Transforming growth factor-β1; **TLRs**: Toll-like receptors; **V-ATPases**: Vacuolar ATPases; **WT**: Wild type; **WTA**: Wall teichoic acids.

Table of contents

	Page number
Title page.....	1
Abstract.....	3
Acknowledgements.....	4
Abbreviations.....	5
Table of Contents.....	6
Figures and Tables.....	12
Chapter 1: Introduction.....	17
1.1. Staphylococcus aureus.....	17
1.1.1. <i>S. aureus</i> in disease.....	17
1.1.2. <i>S. aureus</i> virulence determinants.....	18
1.2. Cells of the innate immune system.....	22
1.2.1. Elements of the host innate immune response.....	22
1.2.2. The role of innate immune system cells in <i>S. aureus</i> infection.....	25
1.2.3. Interaction between innate immune system cells.....	26
1.3. <i>S. aureus</i> internalisation into host cells.....	27
1.3.1. Uptake pathways.....	27
1.3.1.1. Phagocytosis.....	27
1.3.1.1.2. Differing phagocytosis in macrophage and neutrophil.....	28
1.3.1.2. Macropinocytosis.....	29
1.4. The intracellular fate of <i>S. aureus</i>.....	33
1.4.1. pH of endosome compartments.....	33
1.4.2. Autophagy.....	34
1.4.2.1. Components of autophagy.....	35
1.4.2.2. Regulators of autophagy.....	37
1.4.2.3. Noncanonical autophagy.....	38
1.4.2.4. Pathogen evasion of autophagy.....	39
1.4.2.5. <i>S. aureus</i> and autophagy.....	39
1.4.3. Intracellular fate and escape from killing.....	40
1.4.3.1. <i>S. aureus</i> escape from killing.....	43
1.5. Tools for investigating host-pathogen interaction <i>in vivo</i>.....	45
1.5.1. Zebrafish transgenic reporters.....	45
1.5.2. The <i>S. aureus</i> infection model in zebrafish.....	46
1.5.3. Live imaging with the use of fluorescence labelling of <i>S. aureus</i>	48
1.5.3.1. Staining of <i>S. aureus</i> with pH indicators.....	48
1.6. Thesis aims.....	50

Chapter 2: Materials and methods.....	52
2.1. Materials.....	52
2.1.1. Media and Buffers.....	52
2.1.1.1. Brain heart infusion (BHI).....	52
2.1.1.2. Phosphate buffered saline (PBS) pH 4, pH 7.4 and pH 9....	52
2.1.1.3. Tris washing buffer.....	52
2.1.1.4. E3 medium.....	53
2.1.1.5. Methylcellulose.....	53
2.1.2. Antibiotics.....	53
2.1.3. <i>S. aureus</i> strains.....	54
2.1.4. Zebrafish strains.....	55
2.1.5. Morpholinos.....	55
2.2. Methods.....	56
2.2.1. <i>S. aureus</i> procedures and protocols.....	56
2.2.1.1. Determining bacterial cell density and size of inoculum....	56
2.2.1.1.1. Spectrophotometric measurement (OD600).....	56
2.2.1.1.2. 2500 CFU in 1 nl dose calculation.....	56
2.2.1.1.3. Direct cell counts (CFU/ml).....	56
2.2.1.2. Bacterial growth kinetics.....	57
2.2.1.3. Succinimidyl ester staining of <i>S. aureus</i> laboratory strains	57
2.2.1.3.1. Staining procedure of <i>S. aureus</i> laboratory	
strains.....	58
2.2.1.3.2. Washing of stained bacteria.....	58
2.2.1.3.3. Injection with CellROX® indicator.....	58
2.2.1.3.4. Preparing bacteria sample for inverted	
microscopy <i>in vitro</i>	59
2.2.2. Zebrafish procedures.....	59
2.2.2.1. Zebrafish embryo generation.....	59
2.2.2.2. Zebrafish husbandry.....	59
2.2.2.3. Zebrafish breeding.....	59
2.2.2.4. Zebrafish embryo anaesthesia.....	60
2.2.2.5. Tail transection of transgenic embryos at 72 hpf.....	60
2.2.2.6. Zebrafish embryo mounting.....	61
2.2.2.6.1. Zebrafish embryo mounting for standard	
injections (3.5 % methylcellulose).....	61
2.2.2.6.2. Zebrafish embryo mounting in 1.75 %	
methylcellulose.....	61
2.2.2.6.3. Zebrafish embryo mounting in agarose.....	61
2.2.2.6.4. Zebrafish embryo mounting for screening	
procedures.....	62
2.2.2.7. Microinjections.....	63
2.2.2.7.1. Morpholino microinjection.....	63
2.2.2.7.2. Injection of pHrodo™ Red <i>S. aureus</i> Bioparticle®	
Conjugate.....	63

2.2.2.7.3. Microinjection of viable <i>S. aureus</i> into zebrafish embryo.....	64
2.2.2.8. Determination of zebrafish embryo mortality upon infection (“survival test”).....	64
2.2.3. Transgenic zebrafish line generation.....	64
2.2.3.1. Bioinformatic study.....	64
2.2.3.2. Tol2 mRNA synthesis.....	65
2.2.3.3. PCR amplification.....	65
2.2.3.4. PCR product purification.....	67
2.2.3.5. Construct generation.....	67
2.2.3.5.1. BP recombination cloning.....	67
2.2.3.5.2. BP product transformation.....	68
2.2.3.5.3. DNA purification.....	68
2.2.3.5.6. Sequencing result analysis.....	68
2.2.3.5.7. LR recombination cloning and restriction digest	69
2.2.3.5.8 pDEST(mpeg1: mTurquoise.snx1).....	69
2.2.3.5.9 pDEST(lyzC:mTurquoise.snx1).....	70
2.2.3.5.10 pDEST(lyzC:RFP.GFP.LC3) and	
pDEST(mpeg1:RFP.GFP.LC3).....	70
2.2.3.5.11 Line generation and maintenance.....	70
2.2.4. Imaging.....	71
2.2.4.1. Imaging of <i>S. aureus</i> infected zebrafish embryo <i>in vivo</i>	71
2.2.4.2. Real-time imaging of <i>S. aureus</i> -host interaction in infected zebrafish embryo <i>in vivo</i>	71
2.2.4.3. High power imaging for transgenic progeny screening and selection.....	72
2.2.5. Imaging data collection and statistical analysis.....	72
Chapter 3: Quantification of phagocyte and bacterial dynamics during <i>Staphylococcus aureus</i> infection in a zebrafish model.....	73
3.1. Introduction.....	73
3.1.1. A model of <i>S. aureus</i> infection in zebrafish embryos.....	73
3.1.2. <i>In vivo</i> imaging assays for phagocyte and bacterial enumeration in zebrafish embryos.....	75
3.1.3. Hypotheses.....	78
3.1.4. Aims.....	78
3.2. Results.....	79
3.2.1 Effect of injection of fluorescently-labelled <i>S. aureus</i> strains on zebrafish embryo survival.....	79
3.2.2 Impact of infection on professional phagocyte number in the zebrafish embryo.....	81
3.2.2.1. Number of professional phagocytes in infected zebrafish embryo 1 hpi	81
3.2.2.2. Number of professional phagocytes in infected zebrafish embryos at 20 hpi.....	84

3.2.2.3. Professional phagocyte number dynamics in infected zebrafish embryos over time.....	86
3.2.2.4. Professional phagocyte number dynamics in infected neutrophil and macrophage double-labelled embryos.....	88
3.2.2.5. Impact of imaging-related procedures on survival of infected embryo.....	91
3.2.2.6. Impact of professional phagocyte number on survival of infected embryo.....	93
3.2.3. Whole body analysis of bacteria distribution in professional phagocytes during <i>S. aureus</i> infection.....	97
3.2.3.1. Enumeration of bacteria in infected phagocytes.....	99
3.2.3.2. Percentage of uninfected neutrophils in infected embryos over time.....	101
3.2.4. High magnification phagocyte-specific analysis of <i>S. aureus</i> internalisation rates.....	105
3.2.5. Distribution of <i>S. aureus</i> mixed inoculum in professional phagocytes	109
3.2.5.1. Infection with 1:1 CFP and YFP labelled bacteria.....	109
3.2.5.2. Re-infection of infected embryos at 50 hpf.....	113
3.3. Discussion.....	115
Chapter 4: Generation of the novel fluorescently tagged transgenic zebrafish reporters.....	121
4.1. Hypotheses and aims.....	121
4.1.1. Hypotheses.....	121
4.1.2. Aims.....	121
4.2. Sorting nexin 1 macropinosome maturation reporter.....	122
4.2.1. Introduction.....	122
4.2.2. Gateway® Three-Fragment Vector Construction.....	124
4.2.3. Cloning and fluorescently tagged SNX1 mTurquoise vector construction.....	125
4.2.4. Fusion protein expression and embryo screening.....	131
4.2.5. Discussion.....	135
4.3. LC3 autophagy reporter.....	138
4.3.1. Introduction.....	138
4.3.2. Fusion protein expression and embryo screening.....	140
4.4. Characterisation of <i>Tg(lyz:RFP.GFP.LC3)</i> transgenic zebrafish line.....	149
4.4.1. <i>S. aureus</i> internalisation in labelled neutrophils.....	149
4.4.2. Classification of LC3 aggregates in neutrophils.....	152
4.4.3. Impact of methylene blue on LC3 function in neutrophils.....	157
4.4.4. Imaging of infection in neutrophil-specific LC3 reporter line.....	157
4.5. <i>Tg(mpeg:RFP.GFP.LC3)</i> transgenic zebrafish line.....	159
4.5.1. Classification of LC3 aggregates in macrophages.....	159
4.5.2. Imaging of infection in macrophage-specific LC3 reporter line.....	160
4.6. Discussion.....	162

Chapter 5: Investigation of intracellular pathogen processing <i>in vivo</i>.....	165
5.1. Introduction.....	165
5.1.1. Hypotheses.....	169
5.1.2. Aims.....	169
5.2. IAcidification of internalised <i>S. aureus</i>.....	170
5.2.1. Acidification of injected pHrodo particles.....	170
5.2.2. <i>S. aureus</i> cell wall staining with low pH indicators.....	173
5.2.3. Simultaneous visualisation of <i>S. aureus</i> acidification and viability in bloodstream phagocytes.....	178
5.2.4. <i>S. aureus</i> killing in cellular compartments of different pH.....	180
5.3. Intracellular processing of <i>S. aureus</i> by autophagy machinery.....	185
5.3.1. ROS generation and colocalisation with LC3 in neutrophils during <i>S. aureus</i> infection.....	188
5.3.2. <i>S. aureus</i> co-localises with different classes of LC3 aggregates in neutrophils.....	192
5.3.3. ROS generation and colocalisation with LC3 in macrophages during <i>S. aureus</i> infection.....	197
5.3.4. LC3 interacts with bacteria internalised by neutrophils and macrophages in distinct ways.....	200
5.3.5. LC3 vesicles content in <i>S. aureus</i> infected phagocytes.....	202
5.4. <i>S. aureus</i> co-localisation with LC3 upon treatment with carbamazepine and chloroquine.....	211
5.4.1. LC3 recruitment and ROS generation in <i>Tg(LyzC.RFP.GFP.LC3)</i> embryos.....	211
5.4.2. LC3 vesicles content in neutrophils of infected <i>Tg(LyzC.RFP.GFP.LC3)</i> embryos.....	220
5.4.3. LC3 recruitment and ROS generation in <i>Tg(mpeg1.RFP.GFP.LC3)</i> embryos.....	223
5.4.4. LC3 vesicles content in macrophages of infected <i>Tg(mpeg1.RFP.GFP.LC3)</i> embryos.....	232
5.5. Neutrophil LC3 colocalisation with different <i>S. aureus</i> strains.....	232
5.5.1. USA300, USA300 Δ hla and SH1000 Δ hla strains.....	235
5.5.2. 6850 and 6850 Δ psm α strains.....	239
5.6. Acidification of 6850 and 6850Δpsmα <i>S. aureus</i> strains in neutrophils and macrophages.....	242
5.7. Discussion.....	244
Chapter 6: Observation of host-pathogen interactions in <i>S. aureus</i> infection.....	255
6.1. Introduction.....	255
6.1.1. Pathogen internalisation into host cells.....	255
6.1.2. Phagocyte-phagocyte pathogen transfer.....	257
6.1.3. Hypotheses.....	259
6.1.4. Aims.....	259
6.2. Results.....	260
6.2.1. Internalisation of bacteria in the bloodstream.....	260
6.2.2.1. DIC imaging of membrane ruffling and <i>S. aureus</i> uptake.....	260

6.2.1.2. Differences in internalisation mode between macrophages and neutrophils.....	267
6.2.1.3. Phagocyte motility and actin rearrangements during <i>S. aureus</i> uptake.....	275
6.2.1.4. Size of vesicles containing bacteria at 1 hpi.....	277
6.2.1.5. Infection of Snx5 morphants.....	287
6.2.2 Neutrophil to macrophage transfer of <i>S. aureus</i>	292
6.2.2.1. Quantification of neutrophil to macrophage transfer in actin.mRuby transgenic embryos.....	294
6.2.2.2. Phagocyte-phagocyte colocalisation in double phagocyte-specific transgenic lines.....	296
6.2.2.3. Fluorescently labelled CAAX protein transfer during <i>S. aureus</i> infection.....	301
6.2.2.4. Observed cases of neutrophil to macrophage <i>S. aureus</i> transfer.....	307
6.3. Discussion.....	310
6.3.1. Host cells internalise <i>S. aureus</i> using different pathways.....	310
6.3.2. <i>S. aureus</i> is transferred from neutrophils to macrophages.....	313
Chapter 7: Discussion.....	315
7.1. Neutrophils and macrophages interact with <i>S. aureus</i> in distinct ways during infection.....	315
7.2. <i>S. aureus</i> is capable of intracellular replication in zebrafish professional phagocytes.....	318
7.3. Final remarks and future work.....	321
References.....	322

Figures and Tables

Figure 1.1. <i>S. aureus</i> virulence determinants.....	19
Figure 1.2. Macropinosome formation, shape and size.....	30
Table 2.1. Antibiotics used in the study.....	54
Table 2.2. <i>S. aureus</i> strains used in the study.....	54
Table 2.3. Morpholinos used in the study.....	55
Figure 2.1. Zebrafish embryo mounting for screening procedure.....	62
Figure 3.1. Fluorescently labelled <i>S. aureus</i> strains do not differ in pathogenicity in the zebrafish bloodstream infection.....	80
Figure 3.2. Number of neutrophils and macrophages in embryos 1 hpi.....	83
Figure 3.3. Number of neutrophils and macrophages in embryos 20 hpi.....	85
Figure 3.4. Number of neutrophils (A) and macrophages (B) in larvae increases during 20 hpi.....	87
Figure 3.5. Low magnification imaging of neutrophil and macrophage fluorescently labelled embryo 50 hpf.....	89
Figure 3.6. Relative neutrophil and macrophage numbers during infection with <i>S. aureus</i> at 1 (A) and 20 hpi (B).....	90
Figure 3.7. The imaging procedure has no effect on embryo survival kinetics.....	92
Figure 3.8. Phagocyte kinetics 20 hpi and the length of embryo survival.....	94
Figure 3.9. Survival of embryos classified by the number of neutrophils evaluated during microscopy observation.....	96
Figure 3.10. Imaging infection in the whole body of infected embryo using low magnification, high numerical aperture objectives.....	98
Figure 3.11. Number of bacteria in neutrophils and macrophages counted during whole embryo imaging analysis.....	100
Figure 3.12. Percentage of neutrophils containing bacteria in infected embryos...	102
Figure 3.13. Correlation between the percentage of neutrophils containing bacteria and bacterial number during infection.....	104
Figure 3.14. Macrophages contain more bacteria than neutrophils.....	106
Figure 3.15. Percentage of neutrophils and macrophages containing bacteria imaged at high magnification.....	108
Figure 3.16. Bacterial population dynamics in phagocytes of embryos with 1:1 mixed inoculum.....	112
Figure 3.17. Example images of phagocytes internalising bacteria injected at two different time points.....	114
Figure 4.1. Sorting nexin phylogenetic tree.....	126
Figure 4.2. ClustalW analysis of <i>snx1a</i> and <i>snx1b</i> (source ZFIN, Zebrafish Zv9) and <i>Danio rerio</i> SNX1 (NCBI) transcripts.....	128
Figure 4.3. ClustalW analysis of human SNX1 and <i>Danio rerio</i> SNX1 transcripts.....	129
Figure 4.4. Protein blast analysis of <i>Danio rerio</i> SNX1 and Human SNX1 transcripts.....	130
Figure 4.5. SH1000-GFP <i>S. aureus</i> co-localises with SNX1 in embryo injected with pDEST(<i>lyz</i> :mTurquoise. <i>snx1</i>).....	133

Figure 4.6. Fluorescently labelled cells circulating in the bloodstream of embryos from F1 <i>Tg(mpeg:mTurquoise.snx1)</i>	134
Figure 4.7. pDEST(<i>lyz:RFP.GFP.LC3</i>) expression in neutrophils of embryos injected with SH1000-GFP.....	142
Figure 4.8. RFP and GFP expression in neutrophils of pDEST(<i>lyzC:RFP.GFP.LC3</i>) injected embryo infected with SH1000-GFP.....	144
Figure 4.9. Imaging of several z stacks of a neutrophil in pDEST(<i>lyzC:RFP.GFP.LC3</i>) injected embryo infected with SH1000-GFP.....	145
Figure 4.10. Fluorescently labelled cells are recruited to the site of injury in <i>Tg(mpeg:RFP.GFP.LC3)</i> embryos.....	147
Figure 4.11. SH1000 <i>S. aureus</i> internalised by macrophages of <i>Tg(mpeg:RFP.GFP.LC3)</i>	148
Figure 4.12. Number of fluorescently labelled neutrophil cells.....	151
Figure 4.13. Illustration of LC3 classes.....	153
Figure 4.14. The occurrence of LC3 classes in neutrophils of infected and uninfected larvae 1 hpi.....	154
Figure 4.15. <i>S. aureus</i> co-localisation with LC3 classes in neutrophils 1 hpi.....	156
Figure 4.16. Imaging of <i>Tg(lyz:RFP.GFP.LC3)</i> embryos infected with CFP/ YFP inoculum shows overlap between spectra channels.....	158
Figure 4.17. Imaging of <i>Tg(mpeg:RFP.GFP.LC3)</i> macrophages internalising differently labelled SH1000.....	161
Figure 5.1. pHrodo™ Red <i>S. aureus</i> BioParticles® conjugates allow visualisation of phagocyte acidification <i>in vivo</i>	172
Figure 5.2. Schematic interpretation of pHrodo™ intracellular low pH indication...	175
Figure 5.3. <i>In vitro</i> and <i>in vivo</i> imaging of pH sensitive dyes.....	176
Figure 5.4. <i>S. aureus</i> uptake followed by gradual acidification.....	177
Figure 5.5. <i>In vivo</i> imaging of <i>S. aureus</i> carrying plasmid-encoded GFP reporter, simultaneously stained with pHrodo™ indicator and Alexa Fluor 350 pH-insensitive dyes.....	179
Figure 5.6. Survival of LWT embryos infected with 2500 CFU of SH1000-GFP stained with s-ester fluorescent dyes.....	181
Figure 5.7. Imaging analysis of <i>S. aureus</i> viability and acidification in neutrophils and macrophages 1hpi.....	183
Figure 5.8. Fluorescence intensity measures of pHrodo™ stained, GFP expressing SH1000 cells internalised by neutrophils and macrophages.....	184
Figure 5.9. Imaging of <i>Tg(lyz:RFP.GFP.LC3)</i> embryo injected with SH1000-mCherry <i>S. aureus</i> and CellROX® ROS indicator.....	186
Figure 5.10. Imaging of <i>Tg(mpeg:RFP.GFP.LC3)</i> embryo injected with SH1000-mCherry <i>S. aureus</i> and CellROX® ROS indicator.....	187
Figure 5.11. Generation of ROS in neutrophils of infected <i>Tg(lyz:RFP.GFP.LC3)</i> embryos.....	189
Figure 5.12. Mean number of <i>S. aureus</i> internalised by neutrophils of <i>Tg(lyz:RFP.GFP.LC3)</i> embryos.....	190
Figure 5.13. Direct co-localisation of <i>S. aureus</i> with ROS-active compartments in neutrophils of infected <i>Tg(lyz:RFP.GFP.LC3)</i> embryos.....	191

Figure 5.14. Percentage of bacteria co-localised in neutrophils with different classes of LC3 at 1 hpi.....	194
Figure 5.15. Percentage of bacteria co-localised in neutrophils with different classes of LC3 at 20 hpi.....	195
Figure 5.16. Percentage of <i>S. aureus</i> co-localised with different classes of LC3 at various time points post infection.....	196
Figure 5.17. Generation of ROS in macrophages of infected <i>Tg(mpeg:RFP.GFP.LC3)</i> embryos.....	198
Figure 5.18. Mean number of bacteria internalised in ROS ⁺ and ROS ⁻ macrophages.....	199
Figure 5.19. Co-localisation of <i>S. aureus</i> with LC3 in macrophages 1 hpi.....	201
Figure 5.20. ROS generation within LC3 vesicles in neutrophils 1 and 20 hpi.....	203
Figure 5.21. LC3 puncta presence within LC3 vesicles in neutrophils 1 and 20 hpi.	204
Figure 5.22. Percentage of LC3 vesicles not containing bacteria.....	207
Figure 5.23. Percentage of LC3 vesicles not containing bacteria in ROS ⁺ and ROS ⁻ vesicles.....	208
Figure 5.24. ROS and LC3 puncta within LC3 vesicles in macrophages 1 hpi.....	210
Figure 5.25. LC3 aggregates in neutrophils of uninfected 2dpf <i>Tg(lyz:RFP.GFP.LC3)</i> embryos.....	212
Figure 5.26. Proportion of neutrophils containing bacteria in <i>Tg(lyz:RFP.GFP.LC3)</i> embryos upon treatment with autophagy regulators.....	214
Figure 5.27. Percentage of neutrophils containing bacteria in <i>Tg(lyz:RFP.GFP.LC3)</i> embryos upon treatment with autophagy regulators with relation to ROS generation.....	215
Figure 5.28. Bacteria co-localisation with ROS and LC3 in <i>Tg(lyz:RFP.GFP.LC3)</i> embryos upon treatment with autophagy regulators.....	217
Figure 5.29. <i>S. aureus</i> co-localisation with LC3 classes in <i>Tg(lyz:RFP.GFP.LC3)</i> neutrophils upon treatment with autophagy regulators.....	219
Figure 5.30. The presence of ROS species and LC3 puncta within LC3 vesicles in neutrophils upon treatment.....	221
Figure 5.31. The occurrence of empty LC3 vesicles in neutrophils of <i>Tg(lyz:RFP.GFP.LC3)</i> embryos upon treatment with autophagy regulators.....	222
Figure 5.32. LC3 formation in macrophages of uninfected 2dpf <i>Tg(mpeg:RFP.GFP.LC3)</i> embryos upon treatment with autophagy regulators.....	224
Figure 5.33. General generation of LC3 in macrophages upon infection in treated embryos.....	226
Figure 5.34. ROS generation in macrophages of <i>Tg(mpeg:RFP.GFP.LC3)</i> 2 dpf embryo upon treatment with autophagy regulators.....	227
Figure 5.35. ROS co-localisation with bacteria in macrophages of 2 dpf <i>Tg(mpeg:RFP.GFP.LC3)</i> embryos upon treatment with autophagy regulators.....	228
Figure 5.36. Bacteria co-localisation with LC3 in macrophages of 2 dpf <i>Tg(mpeg:RFP.GFP.LC3)</i> embryos upon treatment with autophagy regulators.....	230
Figure 5.37. Mean number of bacteria residing in macrophages.....	231
Figure 5.38. <i>hla</i> mutant strains are less efficient in killing infected embryos.....	234

Figure 5.39. Internalisation of different <i>S. aureus</i> strains and <i>hla</i> mutants in neutrophils of <i>Tg(lyz:RFP.GFP.LC3)</i> embryos.....	236
Figure 5.40. USA300 <i>S. aureus</i> is abundant in the bloodstream of infected <i>Tg(lyz:RFP.GFP.LC3)</i> larvae.....	237
Figure 5.41. LC3 classes co-localisation with SH1000 and USA300 <i>S. aureus</i> strains and <i>hla</i> mutants.....	238
Figure 5.42. 6850 and 6850 Δ psma <i>S. aureus</i> strains internalisation in neutrophils and co-localisation with LC3 classes.....	240
Figure 5.43. Internalisation of 1:1 mixed inoculum of 6850 and 6850 Δ psma <i>S. aureus</i> strains in neutrophils and co-localisation with LC3 classes.....	241
Figure 5.44. Acidification of 6850 and 6850 Δ psma <i>S. aureus</i> strains in neutrophils and macrophages.....	243
Figure 5.45. LC3 recruitment to <i>S. aureus</i> containing phagosomes upon ROS generation.....	252
Figure 6.1. Long membrane extensions visualised in infected larvae.....	263
Figure 6.2. <i>S. aureus</i> uptake by macrophage.....	264
Figure 6.3. <i>S. aureus</i> uptake by neutrophil.....	265
Figure 6.4. Macrophages of infected embryos protrude long membrane extensions.....	266
Figure 6.5. Phagocyte internalises blood-borne <i>S. aureus</i> after forming a cup-like actin structure.....	268
Figure 6.6. Phagocyte internalises blood-borne <i>S. aureus</i> using protruded lamellipodia.....	270
Figure 6.7. Phagocytes internalise <i>S. aureus</i> in distinct actin-dependent manners....	273
Figure 6.8. Actin “pulsing” during <i>S. aureus</i> internalisation by phagocytes of <i>Tg(mpx:Lifact-Ruby)</i>	274
Figure 6.9. Phagocytes show different internalisation efficiency in the presence of <i>S. aureus</i>	276
Figure 6.10. Different size of compartments containing bacteria in neutrophils.....	278
Figure 6.11. Imaging-based assessment of the size of compartments containing bacteria in neutrophils and macrophages.....	279
Figure 6.12. Correlation between the number of bacteria and size of the vesicle in neutrophils and macrophages 1 hpi.....	281
Figure 6.13. <i>S. aureus</i> resides in numerous vesicles of different sizes in infected neutrophils.....	283
Figure 6.14. <i>S. aureus</i> resides in numerous vesicles of different sizes in infected macrophages.....	284
Figure 6.15. Uninfected neutrophils and macrophages show different vesicular phenotypes.....	285
Figure 6.16. Lamellipodium structure visualised in the membrane-labelled macrophage.....	286
Figure 6.17. Sorting nexin 5 morphants showed impaired development.....	289
Figure 6.18. Sorting nexin 5 morphants are highly susceptible to <i>S. aureus</i> infection.	290
Figure 6.19. SNX5 knock down does not prevent the formation of spacious vesicles.	291
Figure 6.20. Multiple <i>S. aureus</i> cells transferred from neutrophil to macrophage.....	293

Figure 6.21. Actin remodelling during phagocyte-to-phagocyte transfer of <i>S. aureus</i> cells.....	296
Figure 6.22. Infection decreases the number of unpaired neutrophils and macrophages observed in the bloodstream.....	299
Figure 6.23. Neutrophil-macrophage pairing rate in phagocyte population is increased upon infection with <i>S. aureus</i>	300
Figure 6.24. Fluorescent CAAX reporter in <i>Tg(mpx:GFP.CAAX/mpeg1:mCherry.CAAX)</i>	303
Figure 6.25. Imaging analysis of the transfer of the fluorescently labelled CAAX protein.....	304
Figure 6.26. Transfer of the fluorescently labelled CAAX protein in uninfected embryos.....	305
Figure 6.27. Transfer of the fluorescently labelled CAAX protein in infected embryos.....	306
Figure 6.28. Neutrophil to macrophage multiple <i>S. aureus</i> cells transfer and subsequent acidification in the recipient cell.....	308
Figure 6.29. Neutrophil to macrophage multiple <i>S. aureus</i> cells transfer observed in <i>Tg(LyzC:RFP.GFP.LC3)</i> embryo.....	309

Chapter 1: Introduction

1.1. *Staphylococcus aureus*

1.1.1. *S. aureus* in disease

S. aureus is a common, opportunistic, Gram-positive pathogen permanently carried in the nares and skin of about one-third of healthy individuals (Kluytmans et al., 1997). Typically this colonisation is harmless, but in certain circumstances results in infection, thought to be due to the spread of colonising bacteria (Lowy, 1998). *S. aureus* is capable of causing both local and systemic diseases, with significant morbidity and mortality. The diverse array of infections ranges from relatively minor local cutaneous lesions to life-threatening conditions such as endocarditis, toxic shock syndrome and sepsis (Chesney, 1989, Johnson, 1993, Lowy, 1998). Though the pathogen is able to invade virtually any tissue of the host, bloodstream bacteraemia caused by *S. aureus* is one of the most serious common infections worldwide. Studies performed in the United States show that *S. aureus* causes more fatalities than any other bacterial infection (Shorr *et al.*, 2006), in the United Kingdom about 4,000 deaths are reported out of 12,500 cases of *S. aureus* bacteraemia annually (Wyllie et al., 2006).

Once *S. aureus* enters the bloodstream, it can cause metastatic infection of almost any organ, resulting in destruction of tissue and the formation of abscesses from pus retained within the tissue (Lowy, 1998). Successful treatment is additionally complicated by the differences between infections of foreign bodies, implanted prosthetic materials and those of natural tissues (Chu et al., 2005, Lalani et al., 2008). Additionally, bacteraemia can rarely be treated solely with antibiotics and if persistent over 2 days increases the probability of complications developing. As a consequence, death may occur due to the severe inflammatory response and multi-organ dysfunction (Fowler et al., 2003, Cosgrove and Fowler, 2008).

Hospital patients are at higher risk for *S. aureus* infection, as the majority of these cases are a complication of vascular access devices. Usually pathogens can gain entry

via a central or peripheral venous catheter, as well as from surgical or minor tissue wounds (Chang *et al.*, 2003). However, it is unclear how this occurs in people who have not been in hospital prior to infection and the emergence of community-acquired *S. aureus* infections constitutes an important issue to public health (Lowy, 1998).

Most infections caused by *S. aureus* are treatable with known antimicrobial drugs, but the appearance of methicillin- and vancomycin-resistant strains has raised concerns over future treatments (Weichhart *et al.*, 2003). Therefore, the fact that *S. aureus* is able to develop multidrug resistance and survive a course of antibiotics has renewed interest in both elucidating host defence mechanisms and understanding the mechanisms of pathogen virulence.

1.1.2. *S. aureus* virulence determinants

S. aureus has evolved an array of potential virulence determinants, which include either bacterial cell membrane components or substances secreted extracellularly (Novick, 2003, Weichhart *et al.*, 2003) (Figure 1.1.). The first group of factors comprise those facilitating adhesion to host cells, while the second group comprises several specific toxins and enzymes. Both play important roles in establishing infection and increase the complexity of *S. aureus* virulence strategies. Moreover, Gordon and Lowy (Gordon and Lowy, 2008) point out a level of functional variability in virulence factors of *S. aureus*: a virulence factor may perform several functions, while several virulence factors may perform the same function.

Figure 1.1. *S. aureus* virulence determinants

The figure shows some of the *S. aureus* virulence factors from both groups: bacterial cell membrane components and substances secreted extracellularly. Image cannot be shown, adapted from (Defres et al., 2009).

S. aureus binding surface proteins - MSCRAMMs (Microbial-Surface Components Recognising Adhesive Matrix Molecules) - are responsible for establishing infection in the host. Proteins such as elastin-binding protein (Ebp), fibronectin-binding protein (FnBP), clumping factor (Clf) or collagen adhesin (Cna) mediate adherence to host tissues (Foster and Höök, 1998). *S. aureus* strains display a variety of MSCRAMM constellations, which result in different levels of virulence (Menzies, 2003). Additionally to disturb the action of a host's adaptive immune system, *S. aureus* expresses protein A on the cell surface. This protein binds to the Fc fragment of antibodies, preventing bacterial recognition and subsequent opsonisation and phagocytosis.

During later stages of infection, *S. aureus* employs extracellularly secreted agents, such as chemotaxis inhibitory protein, which interferes with neutrophil extravasation and recruitment to the site of infection (Foster, 2005). Additionally, leukocyte destruction may be performed by cell membrane pore-forming leukocidins – another staphylococcal extracellular product (Gladstone and Van Heyningen, 1957). Haemolysins and leukocidins cause damage to host immune cells, whereas numerous enzymes, such as lipases and proteases produced by *S. aureus* during infection allow the pathogen to penetrate more deeply into tissue. The pathogen activates and interacts with the host immune system and coagulation pathways resulting in septic shock (Bhakdi and Tranum-Jensen, 1991).

Phenol soluble modulins (PSMs) are *S. aureus* peptides which recently have been shown to play key roles in *S. aureus* virulence, demonstrated in animal models of skin infection and bacteraemia (Wang *et al.*, 2007; Kobayash *et al.*, 2011). Although PSMs can be expressed in virtually all strains, it has been shown that the pathogenicity of some of them can be enhanced, also emerging among CA-MRSA strains (Otto; 2010). There are several activities that cause the PSMs to have an impact on the *S. aureus* pathogenicity: they cause biofilm structuring and detachment, inhibit T-helper cell differentiation thereby affecting the adaptive immune system, and are able to perform cytolytic activity (including lysis of neutrophils) (Periasamy *et al.*, 2012; Wang *et al.*, 2011; Chatterjee *et al.*, 2013; Surewaard *et al.*, 2013; Geiger *et al.*, 2012; Schreiner *et al.*, 2013; Peschel and Otto, 2013). It has been reported by several

studies that the PSM α -related neutrophil lysis by *S. aureus* was facilitated after phagocytosis of bacteria (Chatterjee *et al.*, 2013; Surewaard *et al.*, 2013; Geiger *et al.*, 2012). The recent study reports that PSM α toxin plays an important role in the context of phagosomal escape of *S. aureus* (Grosz *et al.*, 2014).

The expression of virulence factors is timed and coordinated to provide pathogens with the necessary “arms” required during the process of infection; this ability making *S. aureus* capable of successful colonisation and invasion of host cells. MSCRAMMs are expressed during logarithmic growth, whereas secretion toxins are produced in the stationary phase. Although many loci regulate this coordination, there are two well characterised global systems: *agr* (Accessory Gene Regulator) and *sar* (Staphylococcal Accessory Regulator) (Yarwood and Schlievert, 2003, Novick, 2003). The *agr* quorum-sensing system enables bacteria to respond to changing cell density, for instance PSMs are expressed in *agr*-dependent manner, divided into two operons PSM α and PSM β . Mutation in *agr* and inactivation of the *sar* global regulator system were shown to lead to decreased virulence in several mammalian models of *S. aureus*-related diseases (Abdelnour *et al.*, 1993, Cheung *et al.*, 1994, Chan *et al.*, 1998).

Interestingly, host susceptibility to staphylococcal disease may also be affected by previous carriage. For instance, it has been reported that former colonisation may confer some protective immunity in hospitalised patients. Although carriers were more likely to develop *S. aureus* bacteraemia and in most cases the subsequent infection was caused by colonising strains, the all-cause mortality was higher in non-carriers (Wertheim *et al.*, 2004).

1.2. Cells of the innate Immune system

Following a breach of epidermal defences the innate immune system provides host protection against pathogens. It acts together with the adaptive immune system and is necessary to establish the adaptive immune response.

1.2.1. Elements of the host innate immune response

Pathogen recognition is the key mechanism initiating the innate immune system response and is mediated by specific receptors – PRRs (pattern recognition receptors). These are able to identify structures that can be important for bacterial survival, called PAMPs (pathogen associated molecular patterns) (Yokoyama and Colonna, 2008) or MAMPs (microbial associated molecular patterns) (Akira et al., 2006). PRRs are organised in the host in a spatial manner, and they can be divided into several main types based on their localisation (reviewed by Sellge and Kufer, 2015). Considering their additional genetic and functional differences, PRRs were classified into five families (Motta, 2015). The two major ones are TLRs and nucleotide-binding and oligomerization domain (NOD)-like receptors (NLRs), followed by retinoic acid inducible gene-I (RIG-I)-like receptors (RLRs), C-type lectins (CTLs), and absent-in-melanoma (AIM)-like receptors (ALRs) (Shah et al., 2008, Barton, 2008, Motta, 2015). TLRs and CTLs are mainly located in the plasma membrane, whereas other classes of PRRs are located intracellularly.

Toll-like receptors (TLRs) were identified already 20 years ago as the first PRRs described (Lemaitre et al., 1996). This family of innate immune receptors is evolutionarily conserved, and has an important role in the first-line defence against pathogens (Takeda and Akira, 2005, Kawai and Akira, 2010). TLRs are present in both immunocompetent cells, for instance macrophages and in non-immune cells such as epithelial cells (Zarembler and Godowski, 2002). The membrane PRRs react to both extracellular and endosomal stimuli, lipopeptide (TLR2), lipopolysaccharide (TLR4) and flagellin (TLR5) fall into the first group and recognise a variety of microbial molecules (Barton and Medzhitov, 2002). Binding of bacterial lipopolysaccharides (LPS) to the neutrophil plasma membrane receptor TLR4 triggers an intracellular

signalling cascade followed by activation of transcription factors like NF- κ B (nuclear factor- κ B) (Medzhitov, 2007, Barton, 2008). NF- κ B regulates the activation of transcription and release of pro-inflammatory mediators, including chemokines, adhesion molecules and cytokines (Nathan, 2002). Intracellular TLRs are expressed in the endosomal compartments of cells and their role is to sense nucleic acids common in bacterial and viral genomes. These include double-stranded RNA (TLR3), single-stranded RNA (TLR7 and TLR8) or unmethylated single-stranded DNA containing cytosine–phosphate–guanine (CpG) motifs (TLR9) (Barton and Medzhitov, 2002).

NLRs, the second major group of PRRs, recognises PAMPs from pathogen structures, which triggers innate immune response (Jeong and Lee, 2011). There are 22 known human NLRs (Zhong et al., 2013). They share common organization with a central domain NOD (NACHT: NAIP, CIITA, HET-E, and TP-2) important in dNTPase activity and oligomerization and C-terminal leucine-rich repeats (LRRs) domain which is involved in ligand binding (Koonin and Aravind, 2000). The N-terminus domain performs effector functions by interacting with other proteins (Ting et al., 2008). NLRs are classified into four subfamilies based on their N-terminal domain: the acidic transactivation domain (NLRA), the baculoviral inhibitory repeat-like domain (NLRB), the caspase activation and recruitment domain (CARD; NLRC), and the pyrin domain (NLRP) (Ting et al., 2008). The MHC-II transactivator (CIITA) and the NAIP are the only members of NLRA and NLRB families, accordingly. The NLRC subfamily consists of: NLRC1 (NOD1), NLRC2 (NOD2), NLRC3, NLRC4, NLRC5, and NLRX1 (Ting et al., 2008, Schroder and Tschopp, 2010, Motta, 2015). 14 members are classified into the NLRP family, named NLRP1-14 (Zhong et al., 2013).

Pathogen strategies to avoid recognition by PRRs often consist on establishment of a safe location in the host cells, a protective niche. This may include creating specific compartments and escaping the killing pathways of host immune cells. Innate immune cells act in an independent manner, constituting an indispensable element of a successful immune response. A variety of cell types exist to provide pathogen identification and elimination: macrophages, neutrophils, dendritic cells, natural killer cells, basophils, eosinophils and mast cells. This study discusses the role of neutrophils and macrophages in host defence during infection.

Neutrophils and macrophages pursue invading pathogens throughout the body, exploiting the circulatory system and bloodstream as the route of transit. Neutrophils are relatively short-lived, with a circulation time of a few hours, although it has been reported, that their presence in circulation may be extended to several days (Kennedy and DeLeo, 2009, Summers et al., 2010). This increase in longevity is possibly related to adaptation to the environment and influence on surrounding cells at sites of inflammation (Walmsley et al., 2005). Human neutrophils normally represent 50% to 60% of the total circulating leukocytes and during the acute phase of inflammation are the first innate immune system cells migrating toward the site of infection, directed by a chemotactic gradient. They can be recruited from the vasculature by macrophages and mast cells present in the infected tissue. This process is called chemotaxis and it consists of rolling of neutrophils to endothelial cells where they adhere (Nathan, 2002, Muller, 2003). Neutrophils are critical for host defence because they deploy a variety of functions to eliminate pathogens and augment the inflammatory response. Macrophages engaged in the inflammatory response are known to phagocytose invading bacteria, and may also neutralise antigens and act as antigen presenting cells (APC) initiating the adaptive immune response (Murray and Wynn, 2011). Macrophages reside within tissues and produce a broad spectrum of chemicals: regulatory factors such as interleukins, enzymes and complement proteins.

For effective host defence it is crucial to maintain the circulation of neutrophils during infection, but after pathogen invasion has been subsided, it is equally important to restore homeostasis by neutrophil clearance and removal. Successful resolution helps to avoid the deleterious effects of neutrophil death and disintegration: restored inflammation, autoimmunity and tissue damage. Release of cell cargo and histotoxic products, such as cathepsin G, reactive oxygen species (ROS) and proteases can lead to a wide range of infectious and autoimmune illnesses such as ARDS (acute respiratory distress syndrome) or COPD (chronic obstructive pulmonary disease) (Nordenfelt and Tapper, 2011). Neutrophil removal is an active process preceded by a switch in mediator production – from inflammatory to anti-inflammatory signals – e.g. resolvins, lipoxins, transforming growth factor- β 1

(TGF- β 1) and protectins (Serhan and Savill, 2005). Neutrophil clearance can also be completed by cell apoptosis with subsequent recognition and phagocytosis (of neutrophil corpses) by macrophages (Savill et al., 1989).

1.2.2. The role of innate immune system cells in *S. aureus* infection

As mentioned previously, *Staphylococcus aureus* is capable of causing multiple well-characterised illnesses, although the mechanism it uses to evade killing activity of host innate immune cells is unclear (Lâm *et al.*, 2010). The invasion pathways and post-invasion events are only partially understood, and there are important gaps in our understanding of *S. aureus* infection mechanisms, for instance the cellular level of host-pathogen interactions (Gresham et al., 2000, Prajsnar et al., 2008).

S. aureus presence and invasion in host tissues provokes rapid migration of both macrophages and neutrophils, key elements in the innate immune response (Foster, 2005, DeLeo et al., 2009). The main mechanism of pathogen killing in cells is an antibody- and complement-enhanced phagocytosis (Rooijackers et al., 2005), therefore bacterial defence mechanisms mainly aim to avoid these uptake mechanisms (Serruto et al., 2010). However, recent data suggest that the ability to re-establish infection and evade killing is not solely determined by pathogen virulence factors. Multiple lines of evidence suggest that phagocytes may provide an intracellular niche for *S. aureus* during infection, providing an optimal environment in which pathogens reside without being digested, and acting as a “Trojan horse” in bacterial invasion (Gresham et al., 2000, Kubica et al., 2008, Thwaites and Gant, 2011, Prajsnar et al., 2012).

It has been shown in several experiments where ablation of either neutrophils or macrophages was harmful to the host during *S. aureus*-related conditions, that both cell lines are indispensable in preventing overwhelming infection (Verdrengh and Tarkowski, 1997, Verdrengh and Tarkowski, 2000). However, their mechanisms of action differ greatly. Macrophages ingest bacteria with greater efficiency, whereas neutrophils are more prone to form a niche for bacteria during infection. Moreover, additional data suggest that the latter are also responsible for infection progression and dissemination (Gresham et al., 2000, Kobayashi et al., 2010).

Data from the zebrafish model of *S. aureus* infection confirmed the previous evidence from other models that bacteria need to be injected in a relatively high inoculum in order to initiate infection (Prajsnar *et al.*, 2008). This suggests a limited number of host niches, where bacteria can reside to eventually trigger the fatal infection. A more recent study in the same model show that there is an “immunological bottleneck” in the development of *S. aureus* bacteraemia, supporting the hypothesis of few effective niches (Prajsnar *et al.*, 2012).

For many years *S. aureus* was considered an extracellular pathogen, but most recent reports have questioned this assumption. It has been shown that it is able to survive in human professional phagocytes such as neutrophils (Gresham *et al.*, 2000) and macrophages (Kubica *et al.*, 2008). The key question now would be: how do so few *S. aureus* mount the fatal infection – if they are able to avoid phagocyte killing by subverting host cells and taking advantage of a niche? Answering this question would allow us to develop successful treatment against *S. aureus* infection, possibly targeting intracellular bacteria.

1.2.3. Interaction between innate immune system cells

Neutrophils and macrophages are both capable of pathogen internalisation and immunomodulatory activities, however during differentiation they specialise to provide different antimicrobial components (Pozzi *et al.*, 2015). Both immune cell types demonstrate complementary characteristics and promote the cooperative participation in innate immunity, which is important for a successful response against the pathogen (Silva, 2010).

Macrophages can constitute an important source of neutrophil-attracting chemokines (Abtin *et al.*, 2014) but also interact with them in a more direct manner, for instance by removing of *S. aureus* cells ensnared within NETs (Neutrophil extracellular traps) (Farrera and Fadeel, 2013). Interestingly, the latter interaction can be impeded by the fact, that *S. aureus* expresses adenosine synthase and nuclease, resulting in the generation of deoxyadenosine from NETs, an agent inducing apoptosis in macrophages (Thammavongsa *et al.*, 2013).

The use of the zebrafish model allowed visualisation of another neutrophil-macrophage interaction, transfer of cytoplasm portions from neutrophils to macrophages, accompanied by pseudopodial activity, and followed by neutrophil migration away from the site of interaction (Ellett *et al.*, 2011). Additionally, it has been shown using imaging in the zebrafish reporter lines, that macrophages phagocytose apoptotic neutrophils during inflammation (Loynes *et al.*, 2010; Ellett *et al.*, 2011).

1.3. *S. aureus* internalisation into host cells

1.3.1. Uptake pathways

Pathogens use different pathways to gain entry into the cells of the host innate immune system. Independently of their mechanism of invasion, pathogens initially interact with the cell membrane of targeted cells.

1.3.1.1. Phagocytosis

The process of phagocytosis is an actin-dependent (Kaplan, 1977; May and Machesky, 2001) and receptor-mediated pathway of bacterial internalisation initiated by attachment to PAMPs, promoting cytoskeletal rearrangements, leading to the formation of a membrane-bound vacuole. As a consequence, a phagosome is shaped, with the plasma membrane extended around the engulfed target. Pathogens can first interact with opsonins, such as C3b and antibodies, which facilitate attachment and internalisation. The enzymes that control actin movements are regulated by GAPs (GTPase-activating proteins), guanine nucleotide exchange factors (GEFs) and small GTPases. Neutrophils, macrophages and other professional phagocytes may then internalise opsonised pathogens in the complement component C3bi receptor (CR3)-mediated phagocytosis, Fc receptor (FcR)-mediated phagocytosis and clathrin-independent manner, depending upon small G proteins (Swanson, 2008, Doherty and McMahon, 2009).

After internalisation, *S. aureus* reside in phagosome vacuoles, exposed to a spectrum of antimicrobial substances released from specific cellular organelles after fusion. These reagents include antimicrobial peptides and proteins (e.g. lysozyme, cathepsins, leukocyte proteinase 3 and α -defensins) together with reactive oxygen and nitrogen intermediates. That set of agents is usually sufficient to kill the bacteria, although multiple studies have reported that *S. aureus* is capable of evading killing (Rogers and Tompsett, 1952, Gresham et al., 2000, Kubica et al., 2008, Thwaites and Gant, 2011). To elucidate the mechanisms of survival it is necessary to improve the current knowledge on pathogen intracellular fate.

1.3.1.1.2. Differing phagocytosis in macrophage and neutrophil

The understanding of phagocytosis and phagosome maturation mechanisms in neutrophils is limited, as most of this information has been obtained from studies in macrophages (Lee et al., 2003). However, there are multiple differences in internalisation progress, phagosome maturation and, finally, in the outcome of the process of phagocytosis (Nordenfelt and Tapper, 2011).

Firstly, macrophages have the larger array of PRRs, though neutrophils also express a large repertoire of receptors (Hayashi et al., 2003, Ekman and Cardell, 2010). In terms of phagosome maturation, macrophage phagosomes follow the endocytic pathway, with processes transforming it into a phagolysosome (Vieira et al., 2002), while in neutrophils the phagosome integrates with preformed granules. The fusion is precisely regulated and its components activate the NADPH oxidase complex to generate ROS (reactive oxygen species). Neutrophil granules have various sizes, and are generally divided into three groups: azurophilic granules (peroxidase positive, primary), the secondary or specific granule and gelatinase granule (tertiary). The first type – azurophilic – is the most important for bacterial killing, as granule components constitute, for instance, pore-forming peptides and lytic enzymes (Faurischou and Borregaard, 2003). Additionally, macrophages and neutrophils differ in Rab GTPase effectors during the phagosome maturation process – in macrophages and

neutrophils Rab5 and Rab7 are recruited (Minakami et al., 2010, Perskvist et al., 2002).

Uptake into neutrophils is more effective when bacteria are surface-bound, as has been shown in studies of *B. subtilis* and *E. coli* infection in zebrafish models (Colucci-Guyon *et al.*, 2011). Fluid-borne pathogens are not efficiently phagocytosed unless it adheres to the wall of the infected bloodstream. Same study suggested that macrophages are capable of microbial internalisation regardless the anatomical site of infection and the macropinocytic activity may enhance internalisation of bacteria present in zebrafish body fluids. Moreover, bacteria freely circulating in the bloodstream can preferentially adhere to macrophages which extend long membrane pseudopodia, and also due to macrophage-specific expression of range of receptors (Bowdish and Gordon, 2009; Colucci-Guyon *et al.*, 2011; Levraud *et al.*, 2009).

1.3.1.2. Macropinocytosis

Macropinocytosis, has been long perceived as an unregulated process, and its components were studied relatively recently, showing that this clathrin-independent pathway for cellular endocytosis consists of a series of well-co-ordinated signalling events (Sandvig and van Deurs, 1990). Unlike phagosomes, macropinosomes are not shaped by the ingested particles, as they may be formed in the absence of a solid cargo target. Therefore macropinosomes are usually larger, with size ranging from 0.2 to 10 μm in diameter (Figure 1.2.) and mainly recognised by their size, however the addition of dextran dye to the cell containing media is also applied to help macropinosome visualisation (Hewlett *et al.*, 1994; Swanson and Watts, 1995).

Figure 1.2. Macropinosome formation, shape and size

Images cannot be shown.

- a. Transmission electron micrograph showing membrane ruffling surrounding the *Mycobacterium tuberculosis* H37Rv strain in A549 cells (García-Pérez et al., 2003).
- b. Picture from a time-lapse microscopy showing Macrophage infected with the *Mycobacterium avium* strain (Bermudez et al., 2004).
- c. Brightfield DIC microscopy showing zebrafish neutrophil of *Tg(mpx:GFP)i114* line infected with SH1000 *S. aureus* strain. Picture captured *in vivo*, bacteria reside in the compartments of different sizes (this study) 60x objective.

Although both macropinocytosis and phagocytosis require a dynamic actin cytoskeleton, macropinosome morphogenesis occurs spontaneously or in response to stimulation by several growth factors. Subsequently, the cell membrane forms extensions of surface filaments, forming protrusions called ruffles or lamellopodia, depending on their shape (Swanson, 2008). The kinase PAK1 is implied in macropinocytosis and is indispensable in the induction of the process. Additionally, the activities of PI3K and ras promote the process and cholesterol is required for the recruitment of activated rac1 to PAK1 (Doherty and McMahon, 2009).

Macropinosomes also undergo maturation, which is unlikely to occur by a common pathway in different cells. For instance, it may include acquirement of rab7 – a late endosome marker and finally merge with tubular lysosomal compartments. Recent studies have indicated that the sorting nexin (SNX) family may have an important role in the regulation of macropinocytosis (Lim et al., 2008, Lim and Gleeson, 2011). Five out of twelve SNX-PX-BAR family members have been shown to regulate macropinosome formation and maturation (Wang *et al.*, 2010), with the leading impact of SNX1 and SNX5, having a direct relationship between the level of this cell surface protein and macropinocytic activity.

Infectious pathogens such as viruses, protozoa and prions, have been reported to take advantage of macropinocytosis to gain entry into the host cells (reviewed by Lim and Gleeson, 2011). The bacterial uptake in this pathway has already been reported for various pathogens, including *Mycobacterium tuberculosis* and *Legionella pneumophila* (Watarai et al., 2001, García-Pérez et al., 2003), additionally bacteria from *Salmonella spp.* were shown to use this pathway to gain entry into macrophages, which enabled the essential for their virulence survival within these host cells (Alpuche-Aranda *et al.*, 1994). Macropinocytosis during infection can therefore determined by ruffling of membrane towards the bacteria and closing of the lamellipodia into macropinosomes containing the pathogen cargo (Alpuche-Aranda *et al.*, 1994). Macropinocytosis has been proposed as an internalisation route of *S. aureus*, by Gresham *et al.* (Gresham *et al.*, 2000) leading to the hypothesis that the outcome of infection changes with the uptake mode. Bacteria reside in spacious

vacuoles, which may not be competent for integration with azurophil granules, possibly constituting a neutral environment for *S. aureus* survival.

Macropinocytosis, apart from constituting an alternative pathway for pathogen internalisation into innate immune system cells, may play an important role for other features of the immune response. As it is associated with actin-dependent ruffling, the process is also implied in cell motility. Moreover, macropinocytosis is considered to be significant in the chemotactic response of highly mobile cells such as neutrophils (Carpentier *et al.*, 1991). Interestingly, it may also play a role in antigen presenting cells like macrophages. These cells undergo extensive constitutive macropinocytosis (able to internalise up to 200% of their surface area every hour), to sample their immediate environment for antigens (Carpentier *et al.*, 1991, Norbury *et al.*, 1995).

Taking into account the above information it will be important to analyse the importance of macropinocytosis in immune system activities, and develop strategies for *in vivo* experiments in this area.

1.4. The intracellular fate of *S. aureus*

Staphylococcus aureus in disease is commonly characterised as an extracellular pathogen due to its clinical presentation as furuncles (hair follicle infection), carbuncles (draining pus), impetigo (skin infections), and multiple forms of abscesses, biofilm formation or septicaemia (reviewed by Fraunholz and Sinha, 2012). However, *S. aureus* uptake into host cells can result in its intracellular survival, leading to development of strategies allowing it to escape the killing by host defence system (Schröder et al., 2006b) (Jarry and Cheung, 2006).

1.4.1. pH of endosome compartments

The phagosome compartment is acidified during maturation and maintained at low pH by vacuolar ATPases (V-ATPases) (Haas, 2007). However, as mentioned before in this review, the phagosomes of innate immune cells function in miscellaneous ways. The differences also apply to intracellular pH regulation, especially neutrophil phagosome fusion with a number of specific azurophilic granules, which vary significantly from the macrophage phagosome pathway, which slowly acidifies alongside the phagolysosomal pathway. Thus macrophage lysosomes are acidic, with a pH below 5, whereas a fraction of neutrophil ones can maintain neutral pH (Claus *et al.*, 1998). However, this assumption may seem quite surprising, due to the fact that neutrophils function as effective pathogen killers. It should be taken into consideration that actual pH may be much lower than what is obtained during *in vitro* approaches, or as indicated in different studies, a low pH is not an absolute requirement for phagosome function (Odeberg and Olsson, 1976).

Alternatively, Ip *et al.* (Ip *et al.*, 2010) have recently suggested that phagosome maturation and acidification are necessary for efficient immune system response to *S. aureus* infection. In this case, digestion of the Gram-positive cell wall is indispensable for cryptic PRR ligand liberation and TLR-dependent response activation.

To summarise, it could be suggested that a possible alternative pathway for *S. aureus* internalisation – macropinocytosis – contributes to formation of large endosomes containing neutral extracellular fluid. Together with the fact that various mechanisms for phagosome maturation exist in neutrophils and macrophages, it makes pH changes an important factor for future studies on host immune system-pathogen interactions.

1.4.2. Autophagy

The term autophagy has first been coined by Christian de Duve and derived from the Greek meaning “eating of self”. The mechanisms first described almost 50 years ago mainly consisted on the degradation of intracellular structures, including mitochondria and was observed in rat liver perfused with glucagon, the pancreatic hormone (Deter *et al.*, 1967). Regulation of the process and its molecular components has mainly been investigated in the yeast model *Saccharomyces cerevisiae* (Nakatogawa *et al.*, 2009, Klionsky, 2007,). Several screening studies lead to the identification of over 30 autophagy-related genes (Atgs) in yeast (Nakatogawa *et al.*, 2009). Atgs have been identified and together with signalling complexes are responsible for the initiation and course of the process. Orthologues of these genes have been found in other organisms, demonstrating the conservation of autophagic machinery throughout eukaryotes.

Currently, autophagy is a known, catabolic mechanism of degradation, which acts in order to remove unnecessary or dysfunctional cellular components through lysosomal activity. This process has an important role in eliminating pathogens, and it has been shown to be mediated by PGRP receptors that recognise bacterial peptidoglycans in drosophila (Yano *et al.*, 2008). Different TLRs induce signalling upon binding pathogen-derived ligands, to trigger autophagy during innate and adaptive immune responses (He and Klionsky, 2009). Moreover, it has been suggested that autophagosomes provide the grounds for escape of *S. aureus*, giving another possible hypothesis for its successful pathogenicity (Schnaith *et al.*, 2007).

1.4.2.1. Components of autophagy

Macroautophagy is one of the three known types of autophagy, the other two described as microautophagy (processed by invagination of lysosomal membrane and engulfment of small portions of cytoplasm) and chaperone-mediated autophagy (defined by the direct translocation of the soluble proteins through the lysosome membrane) (Li *et al.*, 2013; Pareja and Colombo 2013). Macroautophagy is a process described to have impact on innate and adaptive immunity and is involved in bacterial infections, therefore being the most relevant to this study, and referred to as “autophagy” herein.

Autophagy is a well-controlled process, and its components vary depending on the degradation target, as well as the environmental conditions. It can be triggered by cell starvation, oxidative stresses and generally plays a role in cellular adaptation to stressful stimuli. It can also be employed as a basic cellular process facilitating the degradation of protein aggregates and intracellular debris (Levine and Kionsky 2004). However, basic key stages can be distinguished in most cases.

The induction of autophagy can be regulated by inhibition of the serine/threonine kinase mTOR (mammalian target of rapamycin). Inhibition of the protein by nutrient deprivation causes increased autophagic activity, thereby informing cellular metabolism (Carrera, 2004; Noda and Ohsumi, 1998). When active, the protein inhibits autophagy by targeting downstream effectors that interact with transcription and translation of the autophagic components or by regulating the Atg proteins responsible for the formation of the autophagosome. Other serine/threonine kinases responsible for the induction of autophagy are ULK1 and ULK2 (Chan *et al.*, 2007). Together in complex with Atg13, Atg101 and FIP200 these proteins are crucial for autophagosome formation (Kilonsky, 2005; Mercer *et al.*, 2009). In mammalian cells, autophagy is initiated by the creation of structures called phagophores. These are formed from elongated membranes originating from endoplasmic reticulum and after the formation of the double membrane they enclose into vesicles called autophagosomes (Mitello and Colombo 2011). Upon the initiation of autophagy the ULK1-Atg13-FIP200 complex binds to the phagopore and interacts with mTOR,

inhibiting ULK1 and ULK2 activity, resulting in the subsequent association of Atg proteins and formation of an autophagosome (Hosokawa *et al.*, 2009).

Autophagosome formation requires a few steps for its completion, including the Atg12-Atg5 conjugation system. Proteins are covalently attached and require Atg7 and Atg10 to catalyse the conjugation reaction. Subsequently, Atg16L1 protein is associated to the conjugate, designating the site for further LC3 lipidation. The Atg12-Atg5-Atg16L1 structure is a characteristic phagophore marker, dissociating after progressing autophagosome formation (Fujita *et al.*, 2008 both). Growth of the autophagic membrane is driven by protein-lipid conjugation systems that include proteins like Atg12 and LC3-II (Atg8-PE) (Mizushima *et al.*, 1998; Mizushima, 2002; Hanada *et al.*, 2007). LC3 is the mammalian homolog of Atg8, its conjugation and presence in isolation membranes requires processing and activation by Atg4, Atg7 and Atg3 proteins. Atg4 is a cysteine protease that cleaves pro-LC3 in order to expose Gly in its C-terminus. After processing, LC3 undergoes ATP-dependent activation by Atg7, followed by conjugation regulated by the Atg3 enzyme. Phosphatidylethanolamine (PE) membrane lipid conjugates with LC3 through an amide bond between its amine group and the LC3 Gly C-terminus (Pareja and Colombo, 2013). The LC3 protein is processed and conjugated with the extending membrane of the future autophagosome, and targets destined for degradation are captured within. The entrapped cytoplasmic cargo is further degraded together with the inner membrane of the autophagosome, after subsequent maturation and fusion with lysosomal organelles (Levine and Klionsky, 2004; Glick *et al.*, 2010).

Double-membrane autophagosomes sequester intracellular cargos, such as long lived protein aggregates, debris, impaired organelles and ribosomes (Mizushima, 2007). The by-products of this degradation, for example amino acids, can be exported back to the cytoplasm, through the action of lysosomal permeases and transporters (Mizushima, 2007). Removing non-functional organelles and redundant proteins underlines the role autophagy plays in damage control. One can also conclude that this mechanism is important for energy efficiency through ATP generation and molecule recycling.

1.4.2.2. Regulators of autophagy

Autophagy is a highly conserved process enabling cell homeostasis. This process, along with metabolic adaptation, can elevate the cell's chances of survival, but excessive autophagy can cause cell death (Yoshimori, 2004). Excessive autophagy and impaired regulation or autophagosome assembly can both result in defective autophagy, and as such constitute cause of increased aging and the pathogenesis of various diseases, ranging from infection, neuronal degeneration to cancer (Pareja and Colombo, 2013).

mTOR can be found in two distinct complexes, mTORC1 and mTORC2 and works as a sensor of nutrient signals and the energy status of the cell, in response to those mTORC1 functions in plasma membrane to downregulate autophagy through Akt kinase. mTOR is informed about the cellular energy state by AMP-activated kinase, which is activated by decreased ATP/AMP levels, therefore acting as a hypoxia sensor (Noda and Ohsumi, 1998). Additionally, PtdIns3K is activated by receptor tyrosine kinases that autophosphorylate upon association with growth factors, which results in activation of mTORC1 (Brazil and Hemmings, 2001; Axe *et al.*, 2008).

hVps34 (the yeast ortholog of class III PI3K) can also regulate autophagic machinery at the autophagosome formation step, in complex with Beclin 1, by enabling Atg protein recruitment to the pre-autophagosomal structure. Moreover, Rab 5, known as the small GTPase regulating early endocytosis, interacts and activates the Beclin 1/hVps34 complex to increase autophagosome assembly. Furthermore, autophagosome formation is also promoted by the complex-related generation of PI3P, which subsequently allows the recruitment of DFCP1 and Wipi (Atg18) via FYVE and PH domains, respectively (Itakura and Mizushima, 2010; Matsunaga *et al.*, 2010). Additionally, as hVps34 does not compete with the anti-apoptotic protein Bcl-2 for binding to Beclin 1, it allows the interaction to cause a switch between autophagy and apoptosis, which has been reported to be exploited by pathogens (Kang *et al.* 2011). Interestingly, even proteins initially known only for their role in autophagy can have a pro-apoptotic function, for example Atg5 changes its regulatory properties when cleaved by calpain (Yousefi *et al.*, 2006).

1.4.2.3. Noncanonical autophagy

Autophagy is a cellular process already reported to contribute to host-pathogen interactions during infection with bacteria defined as having an intracellular invasion phenotype. However, recently described autophagic machinery activity mediated by phagocytosis, also known as LC3-associated phagocytosis, increased interest in understanding how those two processes cooperate during infection. Such noncanonical autophagy would be initiated by cell membrane receptors and utilised to degrade phagocytosed extracellular pathogens, in contrast to canonical autophagy that progresses through autophagosome formation in order to engulf cytosolic pathogens. In noncanonical autophagy direct recruitment of the autophagy protein LC3 is induced by activation of TLR receptors upon phagocytosis (Sanjuan *et al.*, 2007). LC3 associates with the phagosome membrane and can be found within the phagosome as well. Moreover, there is evidence indicating that LC3-enriched phagosomes are more efficient in cargo degradation and able to modulate the immune response (Mehta *et al.*, 2014). Engagement of TLR signalling triggers LC3 recruitment to phagosomes (Sanjuan *et al.*, 2007). It is unknown how signalling and recruitment are related, but such interaction promotes phagosome maturation and bacterial killing. The ability of LC3 to tether and partially fuse with other vesicles may have a key role in the process. NOX2 NADPH oxidase is assembled in the nascent phagosomal membrane and acts in pathogen killing downstream of phagocytosis. Its role is to transfer electrons from cytosolic NADPH to oxygen inside the phagosome which causes the generation of superoxide and reactive oxygen species (ROS) and results in bacterial killing. NOX2 generated ROS play a few roles related to infection, for instance they regulate pH levels and are involved in direct antimicrobial activity (Huang *et al.*, 2009). ROS generation has recently been shown to antibacterial autophagy, resulting in LC3 recruitment to phagosomes upon TLR signalling.

1.4.2.4. Pathogen evasion from autophagy

Although the autophagy pathway can restrict pathogens in several different ways, some of the intracellular pathogens have respectively evolved strategies to avoid being entrapped by its components. For instance, while actin and septin-generated cages usually help to capture and destroy intracellular bacteria, *Listeria monocytogenes* uses an actin-based motility to escape from autophagy in the cytoplasm (Mostowy *et al.*, 2011). Another mechanism used by several pathogens consists of downregulation of autophagy-related gene expression. *Burkholderia cenocepacia* suppresses autophagy by targeting Atg12, Atg5 and Atg8 genes (Abdulrahman *et al.*, 2011). Another pathogen, *Legionella Spp.*, evades the autophagy pathway by secretion of a protein called RavZ, which cleaves the C-terminal region of lipid-conjugated LC3 disrupting autophagosome formation (Choy *et al.*, 2012).

1.4.2.5. *S. aureus* and autophagy

S. aureus has been shown to interact with autophagy and subvert the process in nonprofessional phagocytes. In the study performed in an infected epithelial cell line *S. aureus* became encapsulated by autophagosomes, which enabled its survival and replication in a protective niche (Schnaith *et al.*, 2007). Autophagosomes containing *S. aureus* differed from those studied in the conventional autophagic pathway, both in function and molecular composition. During the course of the conventional autophagic pathway, autophagosomes fuse with lysosomes, which are determined by the acquisition of lysosomal proteins, for example LAMP-2 and the decrease of pH in the autophagosomal lumen. Uniquely, *S. aureus* co-localised with LC3 after infection but did not acquire LAMP-2, which indicated a lack of fusion with lysosomes (Dorn, 2001). Subversion of autophagosome maturation and intracellular growth were both dependent on the secretion of virulence factors, managed by the global regulator *agr* (Schnaith *et al.*, 2007).

On the other hand, a different study, performed in tumour cells proposed that *S. aureus* autophagosome-like vesicles were created in response to inhibited

functionality of the lysosomal compartment (Mauthe et al., 2012). Moreover, such interaction has been proposed to be a result of the growth of intracellular *S. aureus*. Pathogen presence stimulated a response where proteins such as Atg5 and LC3 are recruited upon binding of WIPI-1 to PtdIns(3)P at the phagophore (Mauthe et al., 2012), Itakura and Mizushima, 2010), causing bacterial entrapment in autophagosome-like vesicles.

Another study has proposed that *S. aureus* pore-forming haemolysin α can trigger an autophagic response, where LC3 protein is recruited to vacuoles perforated by this toxin (Mestre et al., 2010). Authors proposed the involvement of non-canonical autophagy pathway which responds to the activity of this virulence factor, however, the elicited response pathway is dysfunctional (Mestre et al., 2010). Further study performed by the same research group postulated that RAPGEF3 and RAP2B, are recruited to the *S. aureus*-containing phagosome (Mestre and Colombo, 2012).

Virtually all host cells are capable of performing autophagy, however it is possible that the process is employed distinctively, depending on the cell type. However, the role of autophagy performed in professional phagocytes, host first defence during *S. aureus* bacteraemia, remained long unknown. Recently, it has been suggested, that Agr-active *S. aureus* block autophagic flux, which demonstrates as an accumulation of autophagosomes (O'Keeffe et al., 2015). These autophagosomes constituted a protective environment and likely facilitated the dissemination of the pathogen. So far these results have not been confirmed in any *in vivo* model, and study performed in zebrafish has a potential to fill this gap, which I am discussing further in the introduction and in the presented work.

1.4.3. Intracellular fate and escape from killing

Bacteria have evolved strategies to avoid host defences and survive intracellular killing mechanisms. A broad spectrum of tactics exist in different species, for instance, *Helicobacter pylori* bacteria disrupt the targeting of NADPH oxidase to the phagosome (Allen et al., 2005). Activation of the NADPH oxidase plays an important role in the killing of fungi and bacteria (Babior, 2004). It has been proved that defects

in the enzyme subunits resulted in CGD (Chronic granulomatous disease), a potentially fatal disorder (Segal, 2005).

Another potential survival strategy is escape from the phagosome, as occurs in *F. tularensis* infections, where the pathogen disrupts the phagosome membrane in macrophages (Mohapatra et al., 2007). *Listeria monocytogenes* is a Gram-positive bacterium known to secrete a pore forming listeriolysin O (LLO), which allows it to escape from phagosomes. Interestingly, the low pH of the phagosomal compartment is optimal for the action of LLO (Goldfine and Wadsworth, 2002; Kayal and Charbit, 2006). *Shigella flexneri*, a Gram-negative bacterial pathogen becomes phagocytosed by macrophages and dendritic cells at early stages of infection, subsequently it escapes from the phagocytic vacuole and causes macrophage apoptosis. *S. flexnerii* is able to create small junctions, move through the cytoplasm and spread intercellularly by being phagocytosed into neighbouring cells (Sansone et al., 1986; Blocker et al., 1999). *Streptococcus pyogenes*, also known as Group A *Streptococcus* (GAS) produces diverse pathogenic factors, for instance streptolysin O (SLO), which is allowing GAS to escape the endosome-lysosomal pathway (Nakagawa et al., 2004). Interestingly, it has been reported that upon escape to cytoplasm, GAS is recaptured by autophagy, and therefore SLO may function as autophagy inducer (Nakagawa et al., 2004).

Instead of escaping from the phagosome compartment, several bacterial pathogens are modifying it to avoid intracellular killing or increase dissemination in host organism. *Legionella pneumophila*, Gram negative bacteria, is a facultative intracellular pathogen, able to alter phagosome membrane within 15 minutes post uptake. *Legionella*-containing compartment membrane lacks endocytic markers which impounds its interaction with lysosomes and maturation pathway (Clemens and Horwitz, 1992; Marra and Shuman, 1992). When the legionella containing compartments are eventually labelled by lysosomal markers and become acidified, the pathogen is already able to replicate intracellularly, spread cell to cell and induce pyroptosis in macrophages, which in consequence allows bacterial release to the extracellular environment (Sturgill-Koszycki and Swanson, 2000). Another Gram-negative bacterium, *Salmonella typhimurium*, is capable of modulating the intracellular

environment to its own favour by injecting virulence factors into the host cell cytosol in order to promote self-engulfment into a specific vacuole, called *Salmonella*-containing vacuole (SCV) (Brumell et al 1999, Brumell and Grinstein 2004). Replication of *Salmonella* as well as manipulation of its trafficking inside the host cell requires *Salmonella*-induced filaments, present in the membrane of SCV (Brumell et al., 2002; Birmingham et al., 2005, Brumell et al., 2001). Maintained Rab5 recruitment postpones vacuole maturation, and although SCV acquire late endosomal markers, LAMP-1 for instance, it lacks cathepsin D and further components necessary to fuse with lysosomal compartments. Therefore, bacteria can replicate in optimal conditions within late SCV (Brumell and Grinstein, 2004). Another bacterium able to survive in infected macrophages by not allowing the maturation of the phagosomes and their fusion with lysosomes is *Mycobacterium tuberculosis* (Armstrong and Hart, 1971; Russell et al., 2002). To achieve this, *M. tuberculosis* produces lipids involved in modulating phagosome maturation, for instance lipoarabinomannan, and manipulates the function and recruitment of Rab proteins, molecules involved in intracellular trafficking (Fratti et al., 2001, 2003; Kasmajpour et al., 2012).

Some of the bacterial pathogens instead of alternating the phagosomal compartment, have evolved strategies allowing them to survive and replicate in a potentially disruptive ones. *Coxiella Burnetti*, an obligate intracellular bacterium, manages the biogenesis of a “parasitophorus vacuole” (PV), where it resists the acidic pH of 5, necessary for its metabolic activation (Voth and Heinzen, 2007). Interestingly, PV compartments interact with autophagy and associate LC3 protein on the limiting membrane. This occurs early after infection, within less than 10 minutes, and favours bacteria replication in a replicative vacuole (Gutierrez et al., 2005; Romano et al., 2007). The systems seems quite cooperative, as bacterial protein synthesis is necessary for the formation of the PV, and *C. burnetti* manipulates host cell processes and presence of factors such as LC3 for its successful replication (Howe et al., 2003).

1.4.3.1. *S. aureus* escape from killing

Intracellular pathways, bacterial fates and possible tactics for evading killing may be cell line specific and are likely to differ between neutrophils and macrophages (Lâm et al., 2010, Nordenfelt and Tapper, 2011). Although intracellular fate of *S. aureus* still remains unclear, there is evidence for its prolonged presence within acidic cellular compartments up to 5 days post internalisation, without signs of escape (Schröder et al., 2006b). On the other hand, *S. aureus* has been reported to escape from the phagosome to the cytoplasm during invasion of nonprofessional phagocytes (Jarry and Cheung, 2006).

As mentioned, results published by Prajsnar *et al.* (2012) suggest that neutrophils may establish a niche for *S. aureus*, contributing to its pathogenicity. Similar paradoxical roles of neutrophils have been shown in a large prospective comparisons of bloodstream infections in neutropaenic and non-neutropaenic adults, where the former group had less metastatic infections, shorter duration of bacteraemia and higher survival than the latter (Venditti *et al.*, 2003). Successful subversion of killing activity and intracellular survival of bacteria may contribute to the long lasting infections and fatal conditions also from the therapeutic point of view. Intracellular bacteria may survive the course of antibiotics if, for example, molecular size, charge or concentration of the antibiotic are relevant to its ability to penetrate cells (Van Bambeke et al., 2006). Interestingly, the activity of some antibiotics is reduced in the acidic environments found within phagolysosomes (Carryn *et al.*, 2003).

Activated neutrophils produce reactive oxygen species (ROS), a complex mixture composed of highly reactive molecules that can damage internalised pathogens (Hampton *et al.*, 1998). Molecular oxygen is reduced in the space between an internalised pathogen and the phagosome membrane, with the subsequent assembly of NADPH-dependent oxidase generating high levels of superoxide (Babior only 1999). Superoxide is reduced to hydrogen peroxide as a result of an influx of protons and other cations. These emerge in the phagosome to compensate for the presence of electrons pumped into its lumen (Babior only 1999). The active, antibacterial compounds such as hydroxyl radicals, hydroperoxyl radicals, chloramines, singlet oxygen and peroxynitrite are generated in secondary reactions

(Klebanoff only 2005; reviewed by Spaan *et al.* 2013). Neutrophil MPO catalyses the association of hydrogen peroxide with chloride into hypochlorous acid and mediates augmentation of the NADPH oxidase, enabling more effective response to infection in neutrophils (Babior, 1999; reviewed by Spaan *et al.*, 2013). *S. aureus* strains evolved strategies for their defence against ROS, for instance staphyloxanthin allows partial resistance to killing by peroxide and singlet oxygen (Liu *et al.*, 2005). Moreover, catalase, an enzyme from the staphylococcal cytoplasm contributes to resistance against ROS, by converting the degradative compound to oxygen and water (Mandell, 1975). Additionally, SOK (surface factor promoting resistance to oxidative killing) is another protein which also confers resistance to singlet oxygen (Malachowa *et al.*, 2011).

Another feature facilitating killing evasion of *S. aureus* is its insensitivity to lysozyme. Lysozyme causes lysis of the bacteria by degradation of the cell wall peptidoglycan matrix (Schindler *et al.*, 1977). *S. aureus* uses its O-acetyltransferase A (OatA) enzyme, which performs O-acetylation of the peptidoglycan, protecting it from the muramidase activity of lysozyme (Bera *et al.*, 2005; Herbert *et al.*, 2007).

S. aureus is also capable of resisting the attack of defensins and disruption of its cell wall integrity. The resistance of *S. aureus* cell membrane is increased by a modification of phosphatidylglycerol with L-lysine (Peschel *et al.*, 1999, 2001). Furthermore, *S. aureus* secretes staphylokinase, which directly binds with α -defensins and inhibits the bactericidal effect of these antibacterial compounds (Jin *et al.*, 2004).

Altogether, many studies have shown that *S. aureus* can persist and grow inside different host cells. However, this depends on the strain causing the infection and the colonised cell defence mechanisms used (Krut *et al.*, 2003).

1.5. Tools for investigating host-pathogen interaction *in vivo*

Bacterial pathogens behave differently *in vivo* and *in vitro*, with mechanisms of action changing when transferred from the host to cell culture, for instance in terms of gene expression as shown for *Mycobacterium tuberculosis* (Ramakrishnan et al., 2000). However, *S. aureus* demonstrates regular logarithmic growth in *in vitro* culture, although *in vivo* growth would be constrained by the dynamic host environment. Cell culture studies simulate the actual host-pathogen interactions in a less complex way than those in living organisms, in the ongoing immune response.

Mammalian infectious disease models used in the past are laborious and expensive, especially in the case of high-throughput screens performed in mice and rabbits (Mukhopadhyay and Peterson, 2006). On the other hand, experiments on non-vertebrate organisms, as *Caenorhabditiselegans*, *Drosophila melanogaster* and *Arabidopsis thaliana* were less successful due to the lack of important constituents of the immune response (Rahme et al., 1995, Ewbank, 2002, Hoffmann, 2003). There has been a need to identify a model organism providing features associated with human immunity and pathogenesis (e.g. leukocytes, innate and adaptive immunity, the complement pathway), as well as able to decipher pathogen virulence factors.

The zebrafish model was first used for developmental studies, and more recently infection models have been developed in experimental work on various bacterial and viral infections. Established models already exist for *Mycobacterium marinum* (Davis et al., 2002), *Salmonella typhimurium* (van der Sar et al., 2003) and *Staphylococcus aureus* (Prajsnar et al., 2008).

1.5.1. Zebrafish transgenic reporters

The zebrafish model allows us to increase our understanding of the processes occurring in an infected organism *in vivo*. Observation of the involvement of the whole immune system is essential in investigating host-pathogen interactions. Several molecular biology techniques, for instance the Gateway® system and the tol2 kit subsequently developed from it (Kwan et al., 2007) described further in this study,

allowed the generation of transgenic zebrafish, containing fluorescently labelled immune cells or proteins crucial for the processes of interest. Thus, the creation of credible neutrophil and macrophage reporter lines was enabled (Renshaw, *et al.*, 2006; Ellet *et al.*, 2011).

As described above, autophagy plays an important role in bacterial infections. The zebrafish model was also useful in determining the role of autophagy using microscopy approaches. LC3 fluorescent reporters have been designed for this purpose allowing this protein to be successfully used as a marker of autophagy (Klionsky, 2012; Mizushima *et al.*, 2010). To validate the analysis of autophagy in this model, several methods such as LC3-immunoblotting, LysoTracker staining and GFP-LC3 microscopy, were applied (He and Kilonsky, 2010). Additionally, zebrafish larvae can be treated with autophagy inducers and inhibitors, which allows observation of how such regulation affects different stages of the process. The use of an *in vivo* system helps us to understand how the host responds to the infection upon drug treatment, and to elucidate the impact of the process to the course and outcome of a condition. A zebrafish LC3 transgenic line has already been used to study *Shigella flexneri* infection, postulating several benefits arising from the use of this model (Mostowy *et al.*, 2013). More recently, work performed in the zebrafish model led to discovery that DRAM1 (DNA-damage regulated autophagy modulator 1) protects the host during the infection with *Mycobacterium marinum* (Meijer and van der Vaart, 2014). This pathogen is a close relative to dangerous human pathogen *Mycobacterium tuberculosis*.

1.5.2. *S. aureus* infection model in zebrafish

Zebrafish (*Danio rerio*) are a relatively small – 4 cm, freshwater tropical fish – vertebrate organism, equipped with both innate and adaptive immune systems (Trede *et al.*, 2004). Additionally, the model has a well-developed complement system that functions by the classical, alternative or lectin pathways, similar to mammals (Boshra *et al.*, 2006). Moreover, microbial detection in zebrafish is

mediated by TLRs (which show high homology to their counterparts, including humans) and are upregulated by infection (Meijer et al., 2004, Phelan et al., 2005).

Zebrafish embryos possess leukocytes, including phagocytes, crucial for the innate immune response (neutrophils and macrophages), present in the bloodstream within 25 – 30 hours post fertilisation (Lieschke et al., 2001). They are able to phagocytose intravenously injected bacteria and mount an effective immune response, preventing overwhelming infections (Davis et al., 2002, van der Sar et al., 2003).

The zebrafish embryo model has been shown to be useful in successfully elucidating important mechanisms of *S. aureus* infection and dissection of host-pathogen interactions (Prajsnar et al., 2008). At this stage of development, fish are protected against bacteria by myeloid cells, TLRs and NLRs (Trede et al., 2004, Laing et al., 2008). In this model, injection of *S. aureus* into the bloodstream causes systemic infection and bacteraemia is well modelled in the circulation. Additionally, as zebrafish are unlikely to be adapted to *S. aureus* infection, they are more capable of showing factors that increase host resistance to a new pathogen, and make bacteria pathogenic to a new host (Prajsnar et al., 2008).

Several traits make the zebrafish a very useful tool for genetic manipulation and experiments are aided by the generation of transgenic lines. Breeding zebrafish is relatively easy, a single pair may lay up to 200 eggs per mating. Zebrafish reach sexual maturity at 3 months post-fertilisation, which makes generation time very short, facilitating the creation of the new transgenic lines. This tool, as well as gene targeting, enables elucidation of genes with potentially important roles in pathogenesis and assessment of the importance of innate immune system components in host defence against pathogens. Morpholino technology provides the tool for the rapid knock-down experiments (Nasevicius and Ekker, 2000). Moreover, because of their small size, zebrafish are a perfect tool for rapid, high-throughput screening. It is the only vertebrate model enabling large-scale small-molecule tests to be performed with thousands of compounds and in living organisms. Several screens have already been performed for developmental pathways and mutant phenotype modifiers (Khersonsky et al., 2003).

Zebrafish constitute a complex model for research into the mechanisms of innate immune responses (Prajsnar *et al.*, 2008) and compared to other infection model organisms, including mammals, zebrafish are more appropriate for real-time tracking of the developing infection.

1.5.3. Live imaging with the use of fluorescence labelling of *S. aureus*

In vivo study aims to better characterise phagocytes and dynamics of the host – pathogen interaction during infection. The zebrafish embryo infection model facilitates this goal mainly because of larval transparency. Most of the experiments are performed on zebrafish before the fifth day post fertilisation, as by then they are capable of independent feeding, which is important in terms of Home Office legislation. At early stages of development, embryonic skin mostly lacks pigment, allowing the observation of inner tissues of a living organism, by using light and confocal microscopy. The use of differential interference contrast (DIC) microscopy enabled the distinguishing of various immune cell lineages *in vivo* based on their cytomorphological features (Le Guyader *et al.*, 2008, Colucci-Guyon *et al.*, 2011). Individual cells can be imaged at subcellular resolution; moreover, a strong fluorescence signal is visible even at lower magnification, allowing placement and assessment of a process within the whole organism.

1.5.3.1. Staining of *S. aureus* with pH indicators

Different types of fluorescence labelling can be used in this model, enabling detailed visualisation of molecular processes and intra- or extracellular environment features, such as pH changes. Transgenic zebrafish lines are useful when the main feature or marker for the hypothesis is known, or when we want to establish the background for the study.

The zebrafish model for *S. aureus* infection provides additional insights into the dynamics of pathogenesis – it can be combined with fluorescent labelling of the pathogen. It has been shown in many previous reports, that this brings great

potential for observation of pathogenesis mechanisms (Prajsnar *et al.*, 2008). This can be performed using different methods, for instance, by expression of plasmid-encoded fluorescence proteins. Interestingly, the loss of expression of GFP in different *S. aureus* strains can be used as a tool to determine their killing in host cells (Schwartz *et al.*, 2009). Bacteria may also be stained by dyes reacting with components of its cell wall (Figure 1.3.). Altogether, these methods enable visualisation of bacteria localisation, growth, as well as disposition – important especially when two (or more) competitive strains are tested (Prajsnar *et al.*, 2012).

Tools that allow the visualisation of pH changes with the use of fluorescence microscopy are important for investigating the response of immune system cells during infection – especially for elucidating bacterial fate within intracellular compartments. Multiple compounds may be used to illuminate low pH compartments within the phagocyte, for example LysoTracker® (Ip *et al.*, 2010) or to stain bacterial cell walls. pH sensitive reagents available for cell wall staining may be either brighter at low pH – like the pHrodo™ Indicator, or get quenched in low pH – a known feature of FITC(Lâm *et al.*, 2010, Han and Burgess, 2010). All of these tools provide a broad array of complex approaches for a better understanding of immunity and infection patterns.

1.6. Thesis aims

Despite discovery of various antimicrobial treatments, life-threatening infections with *Staphylococcus aureus* constitute a major problem worldwide (WHO. 2014. Antimicrobial resistance- Global Report on Surveillance). Recurring infections and increased bacterial persistence substantially impede battling blood infections caused by *S. aureus* and are related to poor outcome of patients suffering from MRSA bacteraemia (Seidl *et al.*, 2011; Park *et al.*, 2012; Chong *et al.*, 2013).

It has been suggested that innate immune cells, the major components of host defence, can play an important role in prolonged *S. aureus* lifespan (Koziel *et al.*, 2009) and dissemination of the pathogen (Thwaites and Gant, 2011), and therefore favour bacterial persistence.

The zebrafish model of *S. aureus* infection was shown an appropriate system to study mechanisms involved in pathogen presence in the host bloodstream (Prajsnar *et al.* 2008). Moreover, it was useful in showing that innate immune cells provide *S. aureus* with a beneficial niche (Prajsnar *et al.*, 2012, McVicker *et al.*, 2014).

In this thesis, I hypothesise that an internalisation pathway, or intracellular pathogen handling-related mechanism, characteristic for neutrophils or macrophages, is subverted by *S. aureus* to favour its expansion and survival. In the chapters that follow, host-pathogen interaction leading to bacterial survival and proliferation was observed using *in vivo* microscopy experiments conducted in infected zebrafish embryo, followed by quantitative analysis of collected data.

The aims of presented experimental work:

- Quantification of neutrophil, macrophage and bacterial dynamics during *S. aureus* bloodstream infection (Chapter 3).
- Generation of fluorescent transgenic reporters of processes potentially involved in *S. aureus* intracellular persistence: macropinocytotic uptake (Gresham *et al.*, 2000, Lim *et al.*, 2011), and autophagy (Schnaith *et al.* 2007), under neutrophil and macrophage-specific promoters (Chapter 4).
- Observation of neutrophil and macrophage intracellular environment and antimicrobial host components during *S. aureus* infection (Chapter 5).
- High power microscopy analysis of *S. aureus* internalisation pathways in neutrophils and macrophages, including observation of interaction between the two immune cell lineages (Chapter 6).

Chapter 2: Materials and methods

2.1. Materials

2.1.1. Media and Buffers

2.1.1.1. Brain heart infusion (BHI)

Brain heart infusion (Oxoid) 37 g l⁻¹

Oxoid agar No. 1 was used for BHI agar (1.5 % (w/v)).

Medium was prepared using distilled water and sterilised by autoclaving for 40 min at 121 °C and 15 psi.

2.1.1.2. Phosphate buffered saline (PBS) pH 4, pH 7.4 and pH 9

NaCl 8 g l⁻¹

Na₂HPO₄ 1.4 g l⁻¹

KCl 0.2 g l⁻¹

KH₂PO₄ 0.2 g l⁻¹

The pH was adjusted to 7.4 or 9 using NaOH.

The pH was adjusted to 4 using H₃PO₄.

Working solutions were sterilised using micropore filtration (0.33 µm pore size).

2.1.1.3. Tris washing buffer

0,3 g of Tris powder (brand) was dissolved in 100 ml of distilled water to the final concentration of 25 mM. pH was adjusted to 8,5 using HCl.

Working solution was sterilised using micropore filtration (0.22 µm pore size).

2.1.1.4. E3 medium

NaCl	5 mM
KCl	170 μ M
CaCl ₂	330 μ M
MgSO ₄	330 μ M
methylene blue	0.00005%

Before use the 10 x stock was diluted in distilled water to 1x solution and subsequently methylene blue was added to prevent fungal growth. Working solution was stored in 28.5 °C.

2.1.1.5. Methylcellulose

1.75 % and 3.5 % (w/v) solutions of methylcellulose were prepared in the working solution of E3. The suspensions were then mixed, partially frozen and defrost several times in order to facilitate methylcellulose solubilisation. The solutions were subsequently aliquoted into 20 ml syringes and stored at -20 °C. For use and short-term storage methylcellulose solutions were kept at 28.5 °C. To use the 1.75 % methylcellulose as a mounting medium, tricaine was added to the final concentration of 0.02 % (w/v). The syringe with mixed medium was then stored for short term in the dark.

2.1.2. Antibiotics

Antibiotics were stored in stocks in -20 °C, prepared by dissolving in appropriate solvent and sterilised by filtering (0.22 μ m pore). For use in BHI agar plates stock solutions were added after autoclaving to cooled media (55 °C). For use in liquid BHI medium the antibiotics were added shortly in sterile conditions, just before use. The antibiotics used in this study are listed in Table 2.1.

Antibiotic	Stock concentration (mg/ml)	Stock -solvent	Working concentration (µg/ml)
Chloraphenicol (Cm)	10	100 % ethanol	10
Tetracycline (Tet)	5	100 % ethanol	5

Table 2.1. Antibiotics used in the study

2.1.3. *S. aureus* strains

S. aureus strains used in this study are listed in the Table 2.2. For short-term storage, strains were kept on plates containing the appropriate antibiotics if applicable for resistance marker maintenance, at 4 °C. For long-term storage a single colony was put into bead stocks and placed into -80 °C freezer.

Strain	Genotype
SH1000	Functional <i>rsbU</i> ⁺ derivative of 8325-4
SJF2850	SH1000 carrying pTKP003- <i>rfp</i>
SJF2848	SH1000 carrying pTKP004- <i>cfp</i>
SJF2849	SH1000 carrying pTKP005- <i>yfp</i>
SJF4405	SH1000-pMV158-GFP
SJF4308	SH1000-pMV158-mCherry

Table 2.2. *S. aureus* strains used in the study

2.1.4. Zebrafish strains

London Wild Type (LWT) strain was used for zebrafish experiments.

The transgenic line *Tg(mpx:GFP)ⁱ¹¹⁴* (i114), was generated by Renshaw *et al.* from AB wild-type strain (Renshaw *et al.*, 2006). Transgenic lines *Tg(mpeg:FRET)^{SH266}* and *Tg(mpeg:mCherry.CAAX)^{SH378}* were generated from AB and nacre wild type strains (unpublished, kind gift of Dr Nikolay Ogryzko). Transgenic line *Tg(mpeg:mCherry.CAAX/mpx:GFP.CAAX)* was generated from AB wild type strain (Unpublished, kind gift of Dr Felix Ellett). *Tg(mpx:Lifeact-Ruby)* was a gift from Anna Huttenlocher (Yoo *et al.*, 2010). *Tg(lyz:RFP.GFP.LC3)^{SH383}* and *Tg(mpeg:RFP.GFP.LC3)* were generated from LWT wild type strain (this study).

2.1.5. Morpholinos

Morpholino-modified antisense oligomers (MOs) were obtained from Gene Tools or Open Biosystems. In order to knock down a gene of interest, morpholino oligonucleotides were digested to block the start of translation. All morpholinos used in this study are listed in Table 2.3.

MO	Sequence (5'-3')	Quantity per embryo	Reference
<i>irf8</i>	TCAGTCTGCGACCGCCCGAGTTCAT	0.5 pmole	(Li <i>et al.</i> , 2011)
<i>pu.1</i>	GATATACTGATACTCCATTGGTGGT	0.5 pmole	(Rhodes <i>et al.</i> , 2005)
<i>snx5</i>	CAGAGTTAGACTCACGCCTCAAGTT	0.5 pmole	(Yoo <i>et al.</i> , 2006)
<i>snx5</i> control	CGTGATCTTCAGGACATATTTGGCT	0.5 pmole	(Yoo <i>et al.</i> , 2006)

Table 2.3. Morpholinos used in the study

2.2. Methods

2.2.1. *S. aureus* procedures and protocols

2.2.1.1. Determining bacterial cell density and size of inoculum

For growth on solid media bacteria were inoculated from -80 °C strain stocks directly on BHI agar plates. For growth in liquid media strains were grown aerobically at 37 °C. For standard growth, a single colony was used to inoculate 10 ml liquid media in a sterile universal tube. The culture was grown at 37 °C overnight on a rotary shaker at 250 rpm. 0.5 ml of overnight pre-culture was then used to inoculate 50 ml fresh media in a sterile 250 ml conical flask. Bacterial cultures were then grown for 1.5 h – 2 h (according to strain requirements) at 37 °C, on a rotary shaker at 250 rpm, until the OD₆₀₀ of ~ 1 was reached. 40 ml of prepared bacteria were spun down and resuspended in the precise volume of PBS, according to 2500 CFU dose equation.

2.2.1.1.1. Spectrophotometric measurement (OD₆₀₀)

To quantify bacterial yield of a culture, spectrophotometric measurements at 600 nm were performed using WPA Biowave spectrophotometer. Overnight culture samples were diluted 1:10 in sterile culture medium.

2.2.1.1.2. 2500 CFU in 1 nl dose calculation

To estimate colony forming unit (CFU) counts, the precise OD₆₀₀ value of each sample was included into ratio equation, basing on the constant value:

$$\text{OD}_{600}: 1 = 2 \times 10^8 \text{ CFU/ml.}$$

2.2.1.1.3. Direct cell counts (CFU/ml)

Direct cell counts were performed for quantification of viable cell numbers. Bacterial samples were serially diluted in PBS in triplicate. 5 µl samples of each dilution were

spotted onto BHI agar plates containing antibiotics where necessary. After overnight incubation at 37 °C the number of colony forming units (CFU) was determined.

For the 2500 CFU dose control test, using the same needle as for zebrafish injections, bacteria were diluted 250000x by injecting 4 x 1 nl into 1000 µl of sterile PBS. 10 µl samples per each needle loaded in the experiment were spotted in triplicate onto BHI agar plates containing antibiotics where necessary. After overnight incubation at 37 °C the number of colony forming units (CFU) was determined.

2.2.1.2. Bacterial growth kinetics

In order to recover bacteria from infected embryos, groups of 5 zebrafish embryos were individually transferred (together with 100 µl of E3 medium) to Precellys 0.5ml tubes containing 1.4 mm ceramic beads and mechanically homogenised using the Precellys 24 Bertin Technologies homogeniser. The homogenates were serially diluted and plated onto solid BHI media to determine *S. aureus* numbers within infected embryos. This procedure was repeated every 24 h in a 4 days following the injection.

2.2.1.3. Succinimidyl ester staining of *S. aureus* laboratory strains

S-esters, Alexa Fluor, pHrodo™ Red and Fluorescein-5-EX, were supplied from Life Technologies™. According to protocols provided by the supplier, dyes were dissolved in DMSO to the final concentrations of 10 mM (pHrodo) and 16.95 mM (Fluorescein). For the working concentration pHrodo™ was subsequently diluted 4 x in DMSO and stored in 8 µl aliquots. All stocks are stored in the dark at -20 °C.

2.2.1.3.1. Staining procedure of *S. aureus* laboratory strains

All *S. aureus* strains were stained with S-esters accordingly to the same procedure.

40 ml of bacteria prepared following the protocol (2.2.1.1.) were spun down and the pellet was resuspended in PBS pH 9 to the final concentration of 2500 CFU/nl. If used simultaneously for double staining the dyes were defrosted and placed at the bottom of the eppendorf tubes in appropriate volumes: 0,5 µl of pHrodo and 1,5 µl Fluorescein and then mixed thoroughly. 200 µl of bacterial suspension were added and promptly mixed up and down several times with the pipette. Additional 30 s of vortex was performed to avoid clumping of bacterial cells.

The tubes were covered with aluminium foil (as the dyes are light-sensitive) and incubated 30 min at 37 °C with gentle rotating of solution.

2.2.1.3.2. Washing of stained bacteria

To remove the excess of the dyes, bacteria were washed during 3 step procedure: addition of 1 ml of PBS pH 8, 1 ml of Tris pH 8.5, again 1ml of PBS pH 8; followed by 30 s of vortex (until the pellet was completely suspended), 2 min of centrifugation in 13400 rpm and gentle removal of the supernatant. After washing, bacterial pellet was resuspended in 200 µl of PBS pH 7.4. The solution was kept on ice before using.

2.2.1.3.3. Injection with CellROX® indicator

CellROX® indicator was diluted to 10x working concentration according to the protocol supplied by Life Technologies™, disposed into 2 µl aliquots and kept away from the light, at -20 °C. *S. aureus* strains were prepared according to the protocol (2.2.1.1.) and further re-suspended in PBS pH 7.2. 18µl of suspended culture were mixed with 2µl of 10X CellROX®. Samples were incubate for 30 minutes at 37 °C, 100 r.p.m. shaking. Subsequently, 1 nl of the mixture was injected directly into the bloodstream.

2.2.1.3.4. Preparing bacteria sample for inverted microscopy *in vitro*

5 µl of stained bacterial suspensions were transferred onto glass slides and covered with the microscopy cover slip number 0. The low pH samples were acidified with addition of PBS pH 4 in the 1:10 ratio.

2.2.2. Zebrafish procedures

2.2.2.1. Zebrafish embryo generation

All zebrafish experiments and transgenic line maintenance were performed under a Home Office animal-handling license to conform to Animals (Scientific Procedures) act 1986.

2.2.2.2. Zebrafish husbandry

Adult zebrafish were kept at 28 °C in a continuous closed aquarium system with day/night light cycle of 14/10 hours respectively. Zebrafish embryos derived from adults were kept in E3 medium at 28.5 °C. Zebrafish experiments were performed on embryos not protected under the Animals (Scientific Procedures) Act, as embryos used were younger than 5 dpf and incapable of independent feeding.

2.2.2.3. Zebrafish breeding

Tanks of fish with a 1:1 male:female sex ratio, were marbled overnight. The marbling procedure consists on placing a mesh bottomed, marble containing plastic box into a solid plastic box inside the fish tanks, in which it was left overnight. The mesh base of the upper container allows newly laid eggs to sink into the lower container, separating the eggs from the adults. The eggs were collected from the boxes during the first 3 hpf.

For experiments involving microinjections into embryos during the 1 - 4 cell stage, and for line crosses, embryos were generated by pair mating. A single female and

male fish were placed together in a double bottom mating tank and separated with a plastic divider. Dividers were removed sequentially in the first hour of fish day cycle to allow collection and injection of embryos within the first 20 minutes post fertilisation.

Regardless the method of breeding all eggs were sorted into 30 ml of E3 buffer, with a maximum of 80 embryos per plate before any experimental procedures. For longer experiments, all embryos were kept in a designated fish incubator at 28.5 °C. All embryos designated for autophagy-related experiments were transferred to fresh E3 medium without methylene blue from 1 dpf, before dechoriation or hatching.

2.2.2.4. Zebrafish embryo anaesthesia

A stock solution of 0.4 % (w/v) 3-amino benzoic acid ester (tricaine, Sigma) was prepared in 20mM Tris-HCl (pH adjusted to 7) and stored at -20 °C. The working stock was stored at 4 °C in the dark. Zebrafish embryos were anaesthetised in the final concentration of 0.02 % (w/v) tricaine until cessation of movement prior to microinjections, bacterial injections and microscopic observations.

2.2.2.5. Tail transection of transgenic embryos at 72 hpf

72 hpf embryos were anaesthetised, dechorionated, placed onto a petri dish with fresh E3 media and gently aligned at the bottom of the plate. The tail fin was amputated very closely to the most distal point of the tail under a dissecting microscope. Before imaging embryos were placed into fresh E3 immediately post injury and kept at 28 °C for 6 hours to allow wound healing and innate immune cell recruitment to the site of injury.

2.2.2.6. Zebrafish embryo mounting

2.2.2.6.1. Zebrafish embryo mounting for standard injections (3.5 % methylcellulose)

Embryos were embedded in 3.5 % (w/v) methylcellulose on the glass slides. After injections embryos were washed and incubated for 1 hour in E3 buffer in order to dissolve the remaining methylcellulose. Before experiments or visualisation embryos were transferred to fresh E3 medium.

2.2.2.6.2. Zebrafish embryo mounting in 1.75 % methylcellulose

Anaesthetised embryos were mounted in 1,75 % (w/v) methylcellulose on a No.0 microscopy glass coverslip (SLS) over puncture in a plastic Petri dish. Before injections embryos were mounted flat on the coverslip and transferred to the microscope on the same dish promptly after.

2.2.2.6.3. Zebrafish embryo mounting in agarose

Zebrafish embryos at fixed time post injection were anaesthetised and placed on a Petri dish with a section of the base replaced by a No.0 microscopy glass coverslip. They were then immobilised and mounted in 0.8 % low-melting point agarose (Sigma) solution in E3 medium (without methylene blue) containing 0.02 % tricaine. The embryos and agarose were prevented from drying by a layer of E3 solution supplemented with 0.02% (w/v) tricaine. For the imaging of the early stage of infection, 10 - 15 anaesthetised embryos were first mounted with the ventral side facing the cover glass, in a small amount of 0.8 % low-melting point agarose. Secondly, embryos were injected with *S. aureus* inoculum, covered with a second, shallow layer of 0.8 % low-melting point agarose shortly after injection, and subsequently imaged in a previously set up microscope. Prevention from drying, was provided during acquisition.

2.2.2.6.4. Zebrafish embryo mounting for screening procedures

Low number of transgenic marker positive embryos was selected and anaesthetised between 1 – 3 dpf. A distinct mounting method has been designed in order to enable fish recovery from the analysis with simultaneous minimalizing of embryo damage and time necessary for the high power imaging of high numbers of embryos (Figure 2.1.). 1 % agar solution in MiliQ water was heated and poured onto a cover slip attached to the microscopy plate (Figure 2.1.A-C). 10 rectangular boxes were further cut off with the use of special pipette tip forming two columns of wells (Figure 2.1.D). Anaesthetised embryos were subsequently placed in the wells, one fish per well, and aligned against the cover slip. After the imaging all embryos were gently removed from wells and put into fresh E3 media at 28 °C for recovery (Figure 2.1.F). Subsequent groups of 10 fish were then analysed in the same plate for the completion of screening and selection of best founders.

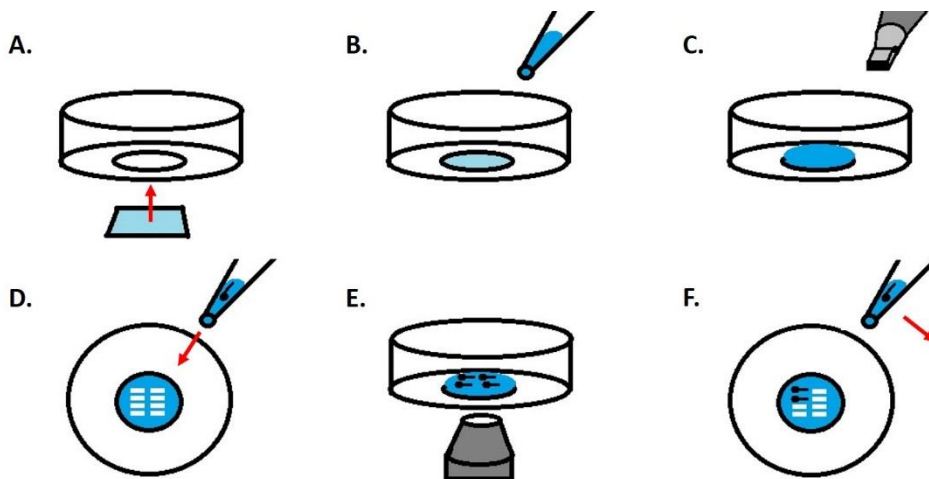


Figure 2.1. Zebrafish embryo mounting for screening procedure

Screening procedure required high power imaging of injected fish and F0 progeny. To prevent damaging of larvae and allow their maintenance after the screening procedure anaesthetised embryos were placed in agar wells. Procedure description see 2.2.2.6.4.

2.2.2.7. Microinjections

All microinjections were performed on anaesthetised embryos using a pneumatic micropump (WPI), a micromanipulator (WPI) and a dissecting microscope. Embryos were injected individually using a Kwik-Fil™ borosilicate glass capillaries (WPI) previously pulled by an electrode puller in order to obtain a fine tip. The end of the needle was broken off using fine forceps to create the injection aperture (~50 µm – 150 µm in diameter). Injected solutions were loaded in the needle using a gel loading pipette tip. The volume injected was calibrated using a graticule slide and its consistency during injections was ensured by a pneumatic picopump and air compressor.

50 embryos were collected and aligned along a microscopy slide and placed onto a Petri dish. Morpholino nucleotides or construct DNA were injected (0.5 – 1 nl solution per embryo) into the yolk ball. Following injections, the eggs were promptly placed back in E3 medium at 50 embryos per plate and incubated at 28.5 °C before they reached 30 hpf.

2.2.2.7.1. Morpholino microinjection

Embryos were collected and injected no more than 20 minutes post fertilisation during the 1 - 4 cell stage. 50 embryos were collected and aligned onto a microinjection plate (without methylcellulose mounting). Morpholino nucleotides were microinjected (0.5 – 1 nl solution per embryo) into the yolk sac. Following injections, the eggs were placed in E3 medium at 50 embryos per plate and incubated at 28.5 °C before they reached 30 hpf.

2.2.2.7.2. Injection of pHrodo™ Red *S. aureus* Bioparticle® Conjugate

The pHrodo™ Red *S. aureus* Bioparticles® (Life Technologies™) were prepared from 1 mg/ml stock to the working solution of 0.5 mg/ml by 1:1 suspending in PBS pH 7.4. The needle was loaded with the 7 µl of the solution and the drop volume of 1 nl was calibrated using a graticule. Mechanically dechorionated embryos were mounted on

3.5 % methylcellulose and injected individually into the yolk sac circulation valley. Embryos were then washed and incubated 1 hour in fresh E3 medium at 28.5 °C.

2.2.2.7.3. Microinjection of viable *S. aureus* into zebrafish embryo

Microinjections of 1 nl of bacterial suspension were performed either on the 3.5 % or 1.75 % methylcellulose accordingly to the type of the experiment performed. To confirm bacterial numbers in each injection the direct cell counts dose control test was performed. Depending on the mounting type, embryos were washed and incubated for at least 1 hour in fresh E3 medium at 28.5 °C or imaged promptly after injections.

2.2.2.8. Determination of zebrafish embryo mortality upon infection (“survival test”)

After injections with *S. aureus* embryos were washed and incubated in fresh E3 for 1 hour at 28.5 °C and then placed in a 96-well microtitre dish (each fish in a separate well). For each mortality test a single *S. aureus* strain was injected into a group of at least 20-50 embryos. Following infection, embryos were observed for signs of mortality several times a day (up to 120 hpf) and dead embryo numbers were recorded at each time point. Data collected was then transfer to the Prism[®] v6 software (GraphPad) in order to analyse and generate figures.

2.2.3. Transgenic zebrafish line generation

2.2.3.1. Bioinformatic study

Genes of interest were researched using Ensembl browser and updated according to the zebrafish genome assembly (<http://www.ensembl.org/index.html>). Alignment analysis was performed using BLAST (Basic Local Alignment Tool) from the National Centre for Biotechnology (NCBI) database (<http://blast.ncbi.nlm.nih.gov/>). Protein alignments were performed with the use of clustalW.

2.2.3.2. Tol2 mRNA synthesis

PCS2FA-transposase construct (plasmid 396) from the Tol2Kit was used to generate Tol2 mRNA. Linearised plasmid was transcribed using a Sp6 mMACHINE[®] kit (Ambion). The reaction was assembled with 1 µg of template DNA, 2 µl enzyme mix, 2 µl reaction buffer, 10 µl NTP/CAP, adjusted to a total volume of 20 µl with nuclease-free water. The reaction was mixed thoroughly with a pipette and briefly centrifuged before incubation for 2 hours at 37 °C. 1 µl of TURBO DNase was added to the reaction in order to degrade the template DNA, digested for 15 minutes at 37 °C. Transcribed RNA was recovered using phenol: chloroform extraction and isopropanol precipitation. 15µl of ammonium acetate stop solution was added together with 115 µl of nuclease-free water for a final volume of 150 µl and the reaction was mixed thoroughly by flicking. An equal volume (150 µl) of phenol: chloroform was added and sample was vortexed briefly, then centrifuged at 14000 rpm for 10 minutes. The aqueous layer was moved to a new tube, after recording its exact volume. An equal volume of chloroform was added, the reaction was vortexed briefly and centrifuged at 14000 rpm for 10 minutes. The aqueous layer was moved to a new tube, after recording its exact volume. RNA was precipitated in the reaction by adding an equal volume of isopropanol, vortexing thoroughly and incubating for 1 hour at -20 °C. The reaction was centrifuged at 14000 rpm for 10 minutes at 4 °C to pellet RNA. The supernatant was carefully removed and RNA was resuspended in RNase-free water). The yield of RNA was estimated on an agarose gel. The amount of RNA was calculated based on comparison with HyperLadder™ (Bioline) marker, then aliquoted into a 2x working concentration. Aliquots were stored at - 80 °C.

2.2.3.3. PCR amplification

Primers were resuspended to a concentration of 100 µM in a volume of MiliQ water calculated from the enclosed specification sheet and aliquoted to a working concentration of 10 µM. Stock and aliquots were stored at - 20 °C.

PCR reaction:

1 µl of 10µM dNTPs (Promega), 0.5 µl Phusion polymerase (NEB), 1.25 µl each of 10 µM forward and reverse primers, 100 ng of template DNA and 4 µl of 5x HF buffer (snx1) or Phusion GC buffer (NEB) (snx5) in total volume of 20 µl nuclease free water.

Gradient PCR with four temperatures ranging between 55 and 65 °C was performed in order to optimise the annealing step. cDNA for snx1 was obtained from a day 4 library, for snx5 from a day 2 library. Known primers were used in control probes.

PCR conditions:

98 °C for 3 minutes

30 cycles of:

Denaturation: 98 °C for 30 seconds;

Annealing: 63.1 °C (snx1), 55 °C (snx5) for 50 seconds (55 °C for the control probe);

Extension: 72 °C for 45 seconds.

72 °C for 10 minutes

4 °C final temperature

The results were verified on a 1 % agarose gel.

PCR primers

Gateway sequencing primers

5' forward sequencing CTATGACCATGATTACGCCAAGCTA

5' reverse sequencing CTGCTTTTTTGTACAAACTTG

ME forward sequencing CAAGTTTGTACAAAAAAGCAG

ME reverse sequencing CCACTTTGTACAAGAAAGCTG

3' forward sequencing CAGCTTTCTTGTACAAAGTGG

3' reverse sequencing CAGTGAATTATCAACTATGTA

2.2.3.4. PCR product purification

Gel extraction was performed using a QIAGEN gel extraction kit. Respective DNA bands corresponding to the size of *snx1* or *snx5* were cut from the agarose gel and weighed for the appropriate use of extraction kit buffers. These were then incubated for 10 minutes at 50 °C in 3x V/weight QG buffer. When the solution colour became yellow, 1 V/weight of isopropanol was added and mixed. Solution was applied to a column and centrifuged 1 minute at 13000 rpm. The flow-through was discarded and column was washed with 750 µl of PE buffer, centrifuged for 1 minute at 13000 rpm. The flow-through was discarded again and the column was centrifuged for 1 minute at 13000 rpm. The column was placed in a new tube, 10 µl of MiliQ water was added. The column was left for 2 minutes to saturate the membrane, and then centrifuged for 1 minute at 13000 rpm to elute the DNA. The DNA solution was stored at - 20 °C.

2.2.3.5. Construct generation

Constructs were generated using the Gateway[®] System (Invitrogen), described in Chapter 4.

2.2.3.5.1. BP recombination cloning

The gene of interest was amplified by PCR reaction using primers containing attB sites and purified as described. 35 ng of the *snx1* PCR product and 58.5 ng of *snx5* PCR product were each combined with 100ng of the donor vector in 5x BP buffer, then 2 µl of BP clonase (Gateway BP Clonase Enzyme Mix) was added in a total volume of 10 µl and vortexed briefly. The reaction was performed at room temperature for 2 hours then stopped by adding 2 µl of Proteinase K to each sample followed by a 10 minute incubation at 37 °C. The reaction product was stored in - 20 °C before transformation into competent cells.

2.2.3.5.2. BP product transformation

Competent Top10 cells (Invitrogen) were defrosted on ice. 2.5 µl of each plasmid (snx1 and snx5) was added to the 25 µl of cells in separate tubes, and gently mixed. To allow the plasmids to enter the cells, the heat shock method was used. Cells were first incubated for 30 minutes on ice, then heat shocked for 45 seconds at 42 °C, then left on ice for 10 minutes. 200 µl of room temperature SOC medium (Invitrogen) was then added to the cells, which were incubated in a shaker at 250 rpm, 37 °C for 1 hour. During that time selection plates, already made with autoclaved LB agar and kanamycin antibiotic at 50µg/ml, were incubated at 37 °C. The liquid culture in SOC was then plated out onto these selection plates and incubated overnight at 37 °C. Colonies were kept on selection plates at 4 °C before selection.

2.2.3.5.3. DNA purification

Several bacterial colonies were selected for each construct, snx1 and snx5, and inoculated into 5ml of sterile LB broth with at 50µg/ml kanamycin and incubated overnight in a shaker at 250rpm, 37 °C. Plasmids were purified from cultures following the QIAgen Plasmid Mini Kit protocol. Larger volumes of DNA (50 µl) from constructs made by BP cloning and tested by diagnostic restriction digest and colonies representing correctly recombined vectors were purified following the high speed midiprep protocol (QIAgen) before the transformation step. DNA concentration was measured using a Nanodrop™ 1000 spectrophotometer (Thermo Scientific). All obtained plasmids were sequenced with M13 forward and reverse primers.

2.2.3.5.6. Sequencing result analysis

ApE software was used to analyse sequencing results, assemble vector maps and sequences and to design restriction maps for diagnostic digests (<http://biologylabs.utah.edu/jorgensen/wayned/ape/>). The ApE recombination tool was used to generate sequences of entry clones and expression vectors.

2.2.3.5.7. LR recombination cloning and restriction digest

10 femtomoles of destination vector and 5 femtomoles of each entry clone were added to a microcentrifuge tube in a final volume of 4 μ l. Femtomolar quantities were calculated based on the equation:

$$ng = (\text{femtomoles required}) \times (\text{size in bp}) \times \frac{660}{1000000}$$

mTurquoise: 3500 bp

snx1: 4600 bp

1 μ l of LR clonase (Invitrogen) was last added to the reaction. The mixture was vortexed briefly and kept overnight at 18 °C then transformed into Top10 cells and plated onto carbenicillin selection plates. After overnight incubation at 37 °C selected colonies were minipreped and tested for correct integration. pDEST(lyzC:mTurquoise.snx1) and pDEST(mpeg1:mTurquoise.snx1) were subjected to diagnostic restriction digest with XhoI enzyme (NEB) at 37 °C, for 2-3 hours. The restriction pattern was analysed using gel electrophoresis on 1 % agarose resolving gel in order to verify correct recombination. Appropriate clones were then purified in midi prep and used for further transformation.

2.2.3.5.8 pDEST(*mpeg1: mTurquoise.snx1*)

The mpeg1 5' entry clone (Ellett *et al.*, 2011) was recombined using LR cloning with the pME-mTurquoise (a kind gift of Nikolay Ogryzko, University of Sheffield), p3E-snx1 in the pDEST cryCFP backbone. pDEST(*mpeg1:snx1.mTurquoise*) correct recombination was confirmed using an XhoI (NEB) restriction digest. Before microinjections the working concentration was determined using a Nanodrop™ 1000 spectrophotometer (Thermo Scientific).

2.2.3.5.9 pDEST(*lyz:mTurquoise.snx1*)

The p5E-lyzC entry clone (a kind gift of Xingang Wang, Institute of Molecular and Cell Biology, Singapore) was recombined using LR cloning with the pME-mTurquoise, p3E-sn_{x1} in the pDEST cryCFP backbone. pDEST(*lyz:mTurquoise.snx1*) correct recombination was confirmed with the use of XhoI (NEB) restriction digest. Before microinjection the working concentration was determined using a Nanodrop™ 1000 spectrophotometer (Thermo Scientific).

2.2.3.5.10 pDEST(*lyz:RFP.GFP.LC3*) and pDEST(*mpeg1:RFP.GFP.LC3*)

The zebrafish RFP.GFP.LC3 middle entry clone was a kind gift of Angeleen Fleming (Molecular Biology, Cell Biology and Genetics, The University of Cambridge, UK). LR recombination with *lyz* and *mpeg1* promoters had been performed in the Renshaw Lab prior to this study.

2.2.3.5.11 Line generation and maintenance

Embryos of wild type zebrafish lines (Nacre and LWT) were injected with transgenic expression constructs together with the tol2 transposase. Positive embryos were selected for mosaic expression under a fluorescence dissecting microscope by CFP eye marker in *Tg(MPEG1:mTurquoise.snx1)* and *Tg(lyzC:mTurquoise.snx1)* lines and GFP heart marker in *Tg(MPEG1.RFP.GFP.LC3)* and *Tg(lyzC:RFP.GFP.LC3)* lines. For the latter two the visibility of fluorescence expressed in macrophages and neutrophils (accordingly) was an additional factor during selection, higher fluorescent intensity having greater utility in microscopy assays. Selected embryos were grown at a density of 30 per tank, 3 tanks per transgenic line to allow high numbers of fish to be screened, increasing the probability of isolating a line founder. After 2 – 3 months sexually mature fish were screened by outcrossing to wild type fish. The offspring of about 90 potential founders were screened for transgene expression. For the *Tg(lyzC:RFP.GFP.LC3)* line multiple founders were identified, the individual selected as a line founder was designated with the allele number SH383. Single potential

founders were identified for *Tg(mpeg1:mTurquoise.snx1)* and *Tg(lyz:mTurquoise.snx1)* lines.

The *Tg(mpeg1:mTurquoise.snx1)*, *Tg(lyz:mTurquoise.snx1)* and *Tg(mpeg:RFP.GFP.LC3)* lines fish showed very low rates of allele transmission to progeny and low transgene expression in most embryos. For these lines more profound analysis was applied in order to select the best founder and embryos raised over the next generations. The analysis involved tail injury and high power microscopy.

2.2.4. Imaging

2.2.4.1. Imaging of *S. aureus* infected zebrafish embryo *in vivo*

Images were acquired using a Nikon TE-2000 U microscope with a Hamamatsu Orca-AG camera. Image acquisition and processing were performed running Volocity™ imaging software (Perkin Elmer). Objectives of following parameters have been used: 4x Nikon Plan Fluor objective NA 0.13; 10x Nikon Plan Fluor objective NA 0.30 and 60x Nikon Plan Apo oil objective NA 1.4. Fluorophores were excited with 488 nm (green) and 543 nm (red). Images and videos were captured with the 1 or 1.5 µm z spacing. For imaging of cells in circulation valley upper and lower limits of focal depth were defined for each embryo. Gain was set 100-150 depending on the fluorophore used and exposure times kept to a minimum.

2.2.4.2. Real-time imaging of *S. aureus*-host interaction in infected zebrafish embryo *in vivo*

Images were acquired using UltraVIEW VoX spinning disk confocal microscope (Perkin Elmer) running Volocity™ imaging software (Perkin Elmer). The mCherry channel was acquired using 561 nm laser line for excitation and 525/640 nm dual band-pass filter for emission. CFP was acquired using 440 nm laser line for excitation and a 485/705 nm dual band-pass filter for emission. YFP was acquired using 514 nm

laser line for excitation and 587 nm filter for emission. The time lapse acquisition was performed at maximum speed over a focal depth of 20 μm with 15 z-planes.

2.2.4.3. High power imaging for transgenic progeny screening and selection

Embryos were mounted according to the procedure described in this chapter (2.2.2.6.4.). Anaesthetised larvae were imaged using Images were acquired using UltraVIEW VoX spinning disk confocal microscope (Perkin Elmer) running Volocity™ imaging software (Perkin Elmer) as described above (2.2.4.2.).

2.2.5. Imaging data collection and statistical analysis

Data was collected using Volocity™ software and analysed using measurement tools available in the software. Number of immune cells per embryo, bacterial cells as well as protein aggregates for quantitative analysis was counted using point tool in the Volocity™ software. Number of bacteria per immune cell, and number of bacteria per vesicle were determined by drawing region of interest around immune cell and vesicle, respectively. Compartmentalisation tool was further used to assign number of bacteria to the region of interest.

Measurement values were further input manually into Prism® (Graphpad) for figure generation and statistical analysis. Means of two unmatched sets of data were compared using unpaired t test. For sets of data containing 3 or more groups, One-way ANOVA analysis was used with appropriate after test. The Tukey's test when comparing every mean with every other mean, Dunnett's test when comparing every mean with a control mean, and Šídák when not all groups in the set were compared. Two-way ANOVA method was used when two factors were affecting the result of experiment. Survival experiment data was analysed using log rank test.

A representative number of minimum 5 embryos and (or 20 phagocytes where applicable) was imaged per experimental group during each microscopy approach. The researcher was blinded to avoid experimental bias.

Chapter 3: Quantification of phagocyte and bacterial dynamics during *Staphylococcus aureus* infection in a zebrafish model

3.1. Introduction

3.1.1. A model of *S. aureus* infection in zebrafish embryos

Staphylococcus aureus is an opportunistic pathogen which persistently or intermittently colonises the human body, for example on the skin and in the nares (Archer, 1998). Such colonisation may be harmless and approximately 60 % of the human population will carry *S. aureus* at some point in their life (Wertheim *et al.*, 2004, Kuehnert *et al.*, 2006). However, this pathogen is capable of causing a spectrum of conditions, ranging from skin infections and cutaneous lesions, to life-threatening bacteraemia resulting in 30 % mortality in UK hospitals (Thwaites and Gant, 2011).

A zebrafish *S. aureus* infection model has been established to enable rapid, high throughput analysis of host and pathogen-derived determinants of disease (Prajsnar *et al.*, 2008). These vertebrates are unlikely to have host-specialisation towards *S. aureus*, which constitutes an advantage in elucidating factors responsible for host resistance to a pathogen it has never met before. Zebrafish has a well-developed innate immune system and it possesses toll-like receptors showing high homology to humans (Kasahara *et al.*, 2004, Meijer *et al.*, 2004). Additionally, it gives a potential model to observe which strategies *S. aureus* uses in its pathogenicity. The infection model has been designed in the zebrafish embryo, before the larvae reaches 5 days post fertilisation (dpf) and become capable of independent feeding. Fish can be easily bred, single pair mating results in 100-200 embryos. Zebrafish reach their sexual maturity at the age of 2 – 3 months which facilitates their maintenance and allows short times for the generation of transgenic lines.

The infection model developed by Prajsnar *et al.* (2008) and employed in this study, involves injection of *S. aureus* inoculum into the bloodstream. Such route simulates those by which *S. aureus* enters mammalian blood, leading to bacteraemia. Human infection commonly follows skin puncture, but bacteraemia can also occur after

several diseases, for instance pneumonia. *S. aureus* infection can also occur during surgery, often associated with indwelling medical devices such as catheters. However, regardless of whether infection is iatrogenic or not, there is increasing number of studies suggesting that phagocytes play an important role in the dissemination of the pathogen (Thwaites and Gant, 2011). Thus, in my study of host-pathogen interaction, *S. aureus* interaction with bloodstream phagocytes was investigated as a major component of host defence and pathogen dissemination.

During experiments, the time of death was assigned to individuals, to determine mortality rates upon infection. Such analysis was called “survival tests”. Embryos were injected at 30 hours post fertilisation (hpf) with a dose of 1500 – 2500 CFU of *S. aureus*, which has been showed to cause death of 50 % of population within 5 days (Prajsnar *et al.*, 2008). Hence, such a set up allows observation of both: successful host defence and successful pathogen virulence strategies. At the 30 hpf time point embryos have no adaptive immune system and their protection against infection with *S. aureus* is mostly provided by myeloid cells and innate immune signalling molecules including TLRs (Trede *et al.*, 2004), NLRs (Stein *et al.*, 2007) amongst others (Wang *et al.* 2008). However, it has been reported that morpholino knock down of MyD88 had no effect on the outcome of infection (Prajsnar *et al.*, 2008). In contrast, *S. aureus* growth in embryos could not be contained in the absence of myeloid cells, and thus bacterial uptake by those cells is important for the resistance to bacteraemia (Prajsnar *et al.*, 2012).

Macrophages are present in the bloodstream by 25 hpf (Herbomel *et al.*, 1999) and neutrophils appear from 30 hpf (Lieschke *et al.*, 2001). Both immune cell lineages are capable of internalising intravenously injected bacteria (Herbomel *et al.*, 1999) and virtually all *S. aureus* cells are internalised in the initial 3 hpi (Prajsnar *et al.*, 2012). In order to visualise host-pathogen interaction, transgenic lines with fluorescent proteins expressed under macrophage and neutrophil-specific promoters were used. *mpx* constitutes faithful neutrophil marker in *Tg(mpx:GFP)* (Renshaw *et al.*, 2006), thus, herein this line was mainly used to label neutrophils. To label macrophages, the *mpeg1* gene has recently been proposed as a credible marker of embryonic

macrophages. This marker co-localises with the macrophage marker *fms* and is independent of neutrophil markers such as *mpx/mpo* and *lyz* (Ellett *et al.*, 2011).

Studies carried out on bacterial population dynamics in the zebrafish infection model have shown skewing of the population ratio in embryos infected with 1:1 mixed inoculum of strains isogenic other than from an antibiotic resistance marker (Prajsnar *et al.*, 2012, McVicker *et al.*, 2014). High bacterial ratio variance was not observed in larvae after using a morpholino against *pu.1* (Prajsnar *et al.*, 2012), a transcription factor essential for development of myeloid cells (Rhodes *et al.*, 2005). This suggests the existence of a population bottleneck within the host and bloodstream phagocytes are responsible for that bottleneck. Likely, these cells can constitute a niche facilitating *S. aureus* dissemination and replication. A mathematical model was developed that demonstrated a small number of host cells were necessary to warrant significant difference in bacterial population variance. Hence, high numbers of bacteria present in the inoculum are required to reach a relatively low number of niches provided by host cells. Subsequently, a small number of *S. aureus* cells escape their niche to mount the fatal infection, resulting in clonal population expansion in up to 30 % of embryos.

Zebrafish constitutes an appropriate model to follow on these findings. Embryos are transparent and their optical accessibility allows the use of various imaging techniques, helping to increase our understanding of the processes occurring in professional phagocytes during infection with *S. aureus*.

3.1.2. *In vivo* imaging assays for phagocyte and bacterial enumeration in zebrafish embryos

Microscopy experiments provide a detailed insight into host-pathogen interaction, however choosing the appropriate time points for imaging experiment is crucial to successfully capture features of a dynamic process. Moreover, prolonged imaging of anaesthetised and immobilised fish increases the risk of additional physiological stress and obtaining non-specific results. Microscopy also impedes the maintenance of conditions important for an experimental design, for instance presence and

activity of drug compounds or photostability of fluorescence markers. Altogether, in my opinion limiting the length of the imaging process serves to increase the stability of the experimental setup, reproducibility of results and also lowers the probability of obtaining false results. Given the large sizes of imaging data files, reducing image acquisition time facilitates quantitative analysis. It also increases the representative number of embryos analysed within relatively similar time point.

Initially, several image acquisition approaches and a pilot analysis were used to find the most informative imaging time frame for this work. As a result, in this study most of the experiments were performed with two time points – within first 2 hours post infection and the second at approximately 20 hpi. Bloodstream phagocytes internalise intravenously injected bacteria during the first 2-3 hours (Prajsnar *et al.*, 2008). Quantitative analysis of bacteria residing in macrophages and neutrophils at early stages of infection also aimed to determine internalisation rates of those professional phagocytes. The 20 hpi time point aimed visualisation of processes occurring after phagocytosis and at the beginning of the phase of pathogen population expansion. According to survival tests, 10 % of larvae had died within 20 hpi and observation of the remaining population showed that a fraction of embryos presented various symptoms of infection, for instance oedema and abscesses. This indicates that the larvae in the population display different stages and severity of infection at that time point. An injected dose of 1200-2500 CFU is chosen such that by 100 hpi, 50 % of embryos will die of infection. However by 20 hpi most embryos had not died, the remaining proportion that would eventually succumb could be identified. Altogether this indicates that a decisive threshold initiating *S. aureus* growth inside of the host and fatal bacteraemia is likely to occur within 20 hpi.

However, infection is an ongoing process and complex factors can influence its outcome at different stages. One of the hypotheses of this study is that phagocytes, likely neutrophils, constitute a niche for *S. aureus* and individual bacterial cells are able to evade intracellular defence mechanisms. This would happen within 20 hpi, however it is difficult to anticipate an exact time point. First of all, even if the escape is mediated by a common mechanism, it can occur at different time points in different embryos. Furthermore, currently we do not know if *S. aureus* is predisposed

to take advantage of its niche shortly before the escape and dissemination. It may be that after a failure in its degradation or neutrophil pathogen-driven apoptosis *S. aureus* is released from phagocytes and starts to replicate. Alternatively, it subverts a crucial process long before killing the host. Hence, between 1 and 20 hpi constitutes a useful time frame for experiments to determine the pathway that leads to the eventual survival of pathogen or host.

Several microscopy approaches were used in this initial study. Images taken using 2x-20x objectives were described as “low magnification” microscopy, and those taken with 40x or 60x objectives was referred as “high magnification”. Low magnification objectives allowed imaging and counts of labelled phagocytes within live embryos. The additional use of the higher numerical apertures enabled higher resolution image acquisition. High resolution images permitted the enlargement of fine details and quantification of bacteria in whole larvae, when used during low magnification acquisition. This enabled the determination of the percentage of infected phagocytes and initial analysis of the number of bacteria residing in immune cells.

High magnification imaging was performed to verify number of bacteria contained in neutrophils and macrophages at different time points post infection. For this purpose, neutrophil and macrophage reporter lines were infected with *S. aureus* carrying fluorescence marker mCherry, enabling precise counts of pathogen cells.

3.1.3. Hypotheses

The main hypothesis underlying work presented in this thesis is that professional phagocytes are responsible for the *S. aureus* population bottleneck, and that zebrafish neutrophils provide niches in which *S. aureus* can avoid host killing. In this chapter I hypothesise that distinctive bacterial uptake events determining the outcome of infection occur during the first 24 hpi in the zebrafish bacteraemia model. Within this time, the neutrophil population would contain different numbers of bacteria, and show different proportion of cells containing bacteria, than the macrophage population. Furthermore, bacterial population dynamics change intracellularly and clonal expansion of *S. aureus* population could occur inside of professional phagocytes.

3.1.4. Aims

Aims of experiments presented in this chapter:

- Quantification of phagocyte and bacterial dynamics during first 24 hpi
- Determination of host immune system cells kinetics in response to *S. aureus* infection.
- Quantification of the number of bacteria contained in neutrophils and macrophages.
- Determination of the proportion of immune cells containing bacteria in neutrophil and macrophage populations.
- The use of microscopy approaches to observe dissemination of *S. aureus* within the host.
- Observation of bacterial population dynamics inside of professional phagocytes.

3.2. Results

3.2.1 Effect of injection of fluorescently-labelled *S. aureus* strains on zebrafish embryo survival

The imaging of infection inside of the zebrafish bloodstream requires brightly fluorescent bacteria with no alteration in pathogenicity. Plasmid-encoded fluorescence was used to track *S. aureus* distribution within larval bloodstream and internalisation into professional phagocytes. Both observations require dynamic acquisition, thus low exposure times provided by strong fluorophores play an important role in the real time *in vivo* imaging. For this study, two new fluorescent *S. aureus* SH1000 derived strains were used having either green or red fluorescence. SH1000 carrying pMV158-GFP (SJF4405, Prajsnar and Foster, unpublished) and SH1000 carrying pmV158-mCherry (SJF4308, this study, unpublished) were injected intravenously into 30 hpf LWT embryos and tested for their pathogenicity, compared to the parental strain SH1000. The survival test demonstrated that all strains injected at the dose of 1200-2300 CFU caused death of 40-60% percent of infected embryos within 100 hpi (Figure 3.1.). Within the same experiment the survival dynamics matched those previously observed (Prajsnar *et al.*, 2008). Therefore, the plasmid based *S. aureus* reporters did not affect pathogenicity in this model of infection.

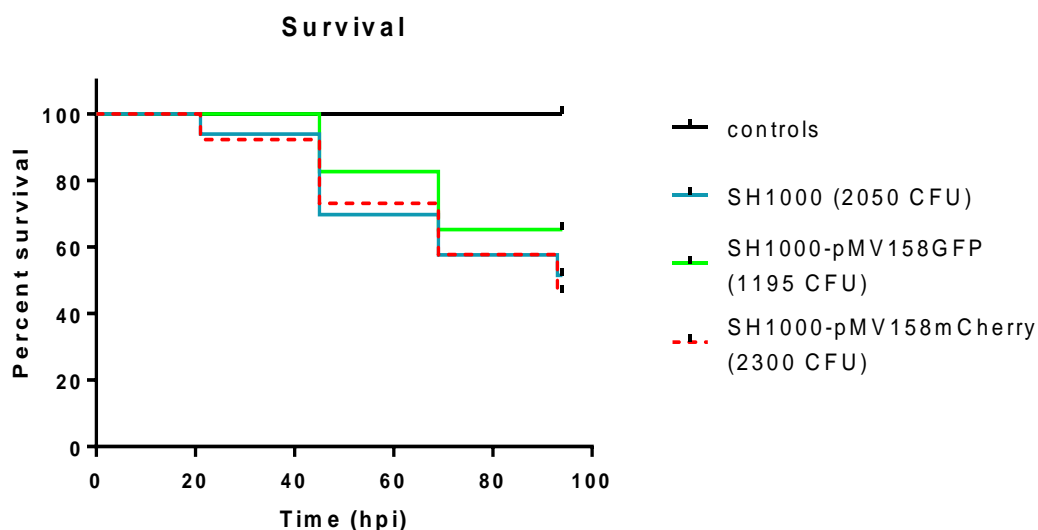


Figure 3.1. Fluorescently labelled *S. aureus* strains do not differ in pathogenicity in the zebrafish bloodstream infection.

Embryos ($n = 20$ per group) were injected intravenously into the yolk sac circulation valley with approximately 1200-2500 CFU of various *S. aureus* strains as shown in the legend. Not injected and PBS injected fish were used as control groups. Log rank test of fluorescently tagged strains versus wild type SH1000 shown no significant difference in virulence of tested strains (log rank test, $p = 0.65$ for SH1000-GFP, $p = 0.83$ for SH1000-mCherry).

3.2.2 Impact of infection on professional phagocyte number in the zebrafish embryo

The aim of quantitative analysis of the number of neutrophils and macrophages was to enable further reference of any more detailed analysis to the general phagocyte kinetics. Phagocyte counts were performed using stable fluorescence reporter transgenic lines, both neutrophil – *Tg(mpx:GFP)* and macrophage-specific – *Tg(mpeg:mCherry.CAAX)*.

As described in the introduction, quantitative data was collected at two time points post infection – after 1 and 20 hours. Introducing counts at 1 hpi time point provided an overview of phagocyte number after internalisation of the majority of injected *S. aureus*. The 20 hpi time point may be representative for a predicted outcome of infection, therefore it was important to analyse how the condition of the host is reflected in phagocyte number and if it has a potential impact on successful bacterial clearance from the bloodstream.

3.2.2.1. Number of professional phagocytes in infected zebrafish embryo 1 hpi

The experiment aimed determination, whether infection with *S. aureus* influences neutrophil and macrophage numbers early after bacterial presence in the bloodstream. Embryos from the transgenic line *Tg(mpx:GFP)* were infected with 2500 CFU dose of SH1000-mCherry *S. aureus* strain to enable counts of GFP-positive neutrophil cells. Before imaging, all embryos from the *S. aureus*-injected group were observed by imaging and confirmed to contain fluorescently labelled *S. aureus*. Embryos from the transgenic line *Tg(mpeg:mCherry.CAAX)* line were infected with 2500 CFU dose of SH1000-GFP *S. aureus* strain for the quantification of mCherry-positive macrophages cells.

Fluorescence microscopy at low magnification enabled visualisation of neutrophils and macrophages at 1 hpi (31 hpf) in three groups: infected, PBS injected and uninjected. Cells were counted by eye in three independent experiments. At this time point most embryos from all groups had 10 – 60 neutrophils and 15 – 80

macrophages (Figure 3.2. A and B). A small fraction of embryos had neutrophils or macrophage number increased to about 100. *Tg(mpx:GFP)*, embryos from the PBS injected group had significantly less neutrophils than embryos of the uninjected control group. Nevertheless both early neutrophils and macrophages are functional phagocytes, capable of internalising *S. aureus* at that time point (Prajsnar *et al.* 2008).

No significant difference was found in the number of neutrophils between PBS injected and infected groups (Figure 3.2A). Furthermore, embryos of all groups contained similar numbers of macrophages (Figure 3.2B). At 1 hpi (31 hpf) embryos contain significantly more macrophages than neutrophils, regardless if they have been infected or injected with PBS (Figure 3.2C). That suggests infection does not influence the number of professional phagocytes during the first hour after injection of *S. aureus*.

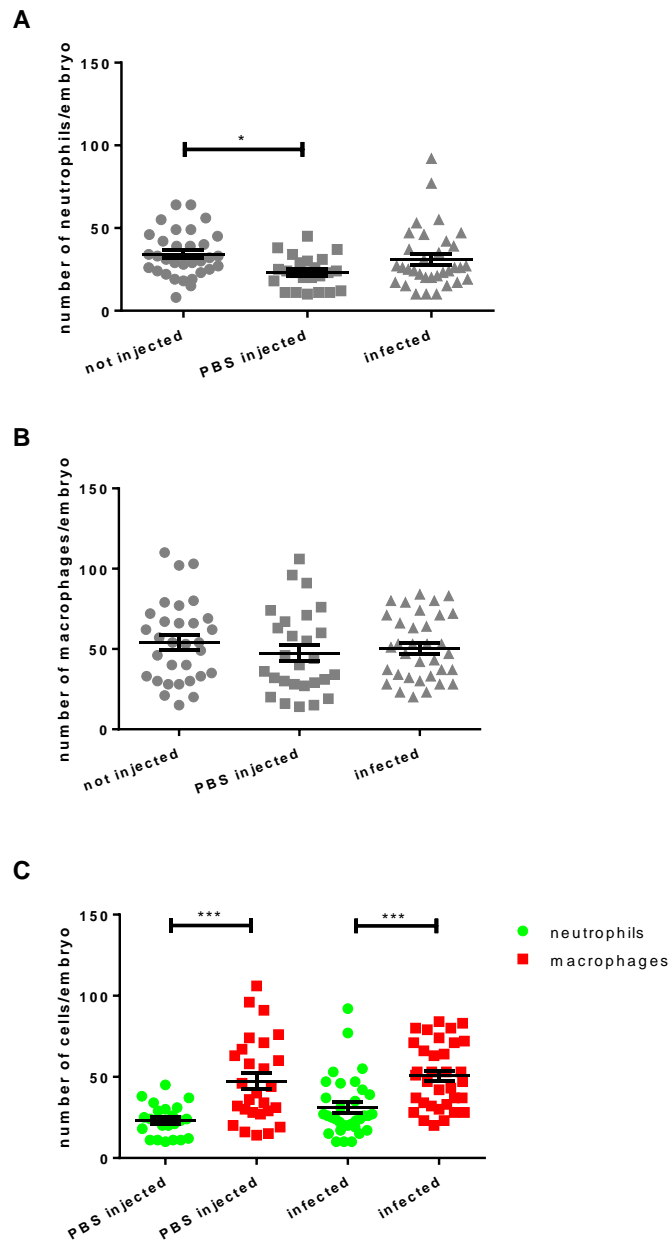


Figure 3.2. Number of neutrophils and macrophages in embryos 1 hpi.

A, number of GFP-positive neutrophil cells (*Tg(mpx:GFP)* line); B, mCherry-positive macrophage cells (*Tg(mpeg:mCherry.CAAX)* line) were counted in 3 groups of embryos: not injected, PBS injected and infected with 2500 CFU SH1000. No significant differences were found in number of macrophages. PBS injected embryos contained significantly less neutrophils than not injected ones (A. $p = 0.0172$, One-way ANOVA, Dunnett's test). C, at 1 hpi (31 hpf) the number of macrophages per embryo was significantly higher than the number of neutrophils per embryo, regardless if they were PBS injected (unpaired t test, $p = 0.0001$) or infected (unpaired t test, $p = 0.0001$). A representative number of minimum 5 embryos was imaged in each experimental group, experiment repeated $n = 3$.

3.2.2.2. Number of professional phagocytes in infected zebrafish embryos at 20 hpi

The number of neutrophils and macrophages was not influenced 1 hpi, and further experiment aimed to determine if the phagocyte numbers will be influenced at the later stages of infection with *S. aureus*. Therefore, *Tg(mpx:GFP)* and *Tg(mpeg:mCherry.CAAX)* embryos of all 3 groups: not injected, PBS injected and infected with *S. aureus*, were imaged again 20 hpi.

The analysis showed no significant differences between the numbers of neutrophils in all groups (Figure 3.3A). The number of macrophages was significantly lower in infected and PBS injected embryo groups (Figure 3.3B) compared to control embryos. This suggested that injection procedure can influence phagocyte numbers and to elucidate the impact of infection, PBS injected embryos were further used as control for *S. aureus* injected group.

PBS injected embryos contained similar number of macrophages and neutrophils at 50 hpf (Figure 3.3C). In the infected embryos, neutrophils seemed to be more numerous in analysed embryos. However, to be certain it would be important to count macrophages and neutrophils in the same embryo.

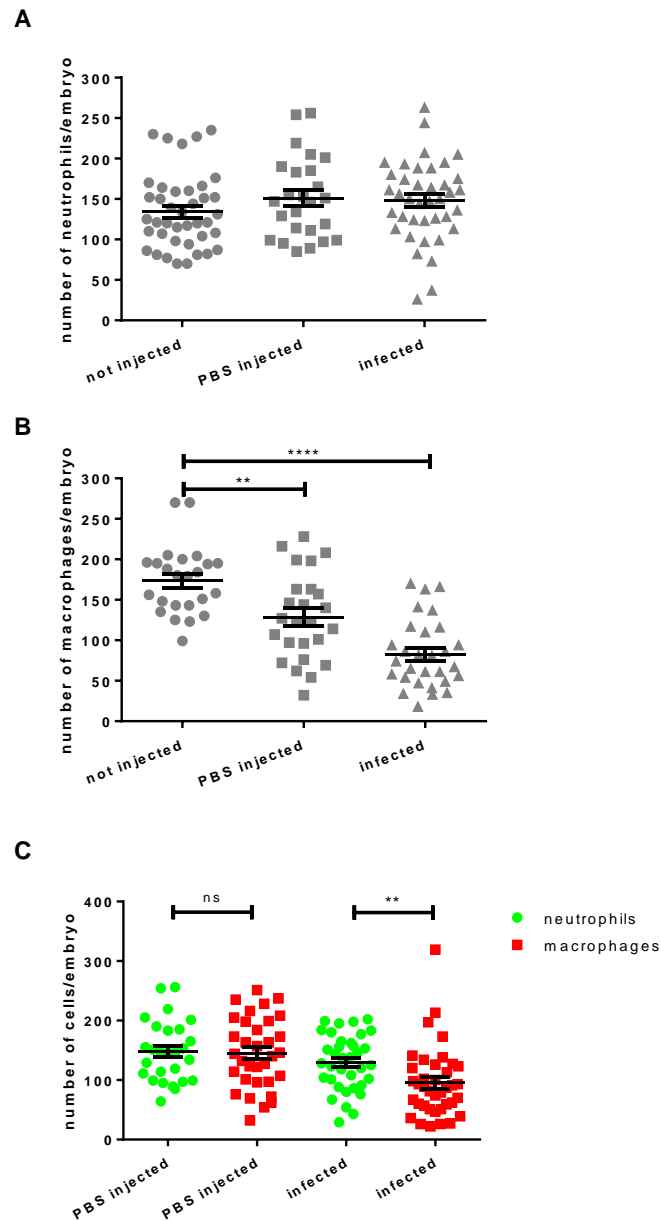


Figure 3.3. Number of neutrophils and macrophages in embryos 20 hpi

A, number of GFP-positive neutrophil cells (*Tg(mpx:GFP)* line) and B, mCherry-positive macrophage cells (*Tg(mpeg:mCherry.CAAX)* line) was counted in 3 groups of embryos: not injected, PBS injected and infected with 2500 CFU SH1000. No significant differences were found in number of neutrophils (A). PBS injected and infected embryos contained significantly less macrophages than not injected ones (B. $p = 0.002$ and $p < 0.0001$, respectively, One-way ANOVA, Dunnett's test). C, at 20 hpi (50 hpf) number of macrophage per embryo was not significantly different than number of neutrophil per embryo in PBS injected (unpaired t test, $p = 0.0012$), and significantly lower in infected group (unpaired t test, $p = 0.0067$). A representative number of minimum 5 embryos was imaged in each experimental group, experiment repeated $n = 3$.

3.2.2.3. Professional phagocyte number dynamics in infected zebrafish embryos over time

It has been previously shown that between 20-50 hpi numbers of neutrophils in non infected *Tg(mpx:GFP)* embryos expand by approximately 30 % per day (T. K. Prajsnar, PhD Thesis, University of Sheffield 2009). At this stage of development, the increase appears constant, caused by the development of the immune system. After infection with *S. aureus*, neutrophil numbers are either maintained or decrease in response to bacteraemia. However, such study was not performed for macrophage population, and additionally it remained unknown how phagocyte kinetics change during first 20 hpi. Thus, data collected during counts performed 1 and 20 hpi was subsequently used to analyse the difference in phagocyte number over time.

The counts of phagocyte number allowed the determination of how phagocytes change between 1 and 20 hpi (30 – 50 hpf) (Figure 3.4.). The results showed threefold increase in the number of neutrophils in both infected and PBS injected embryos (Figure 3.4A). During that time course the number of macrophages per embryo also increases (Figure 3.4B). This demonstrates considerable development of the immune system in embryos.

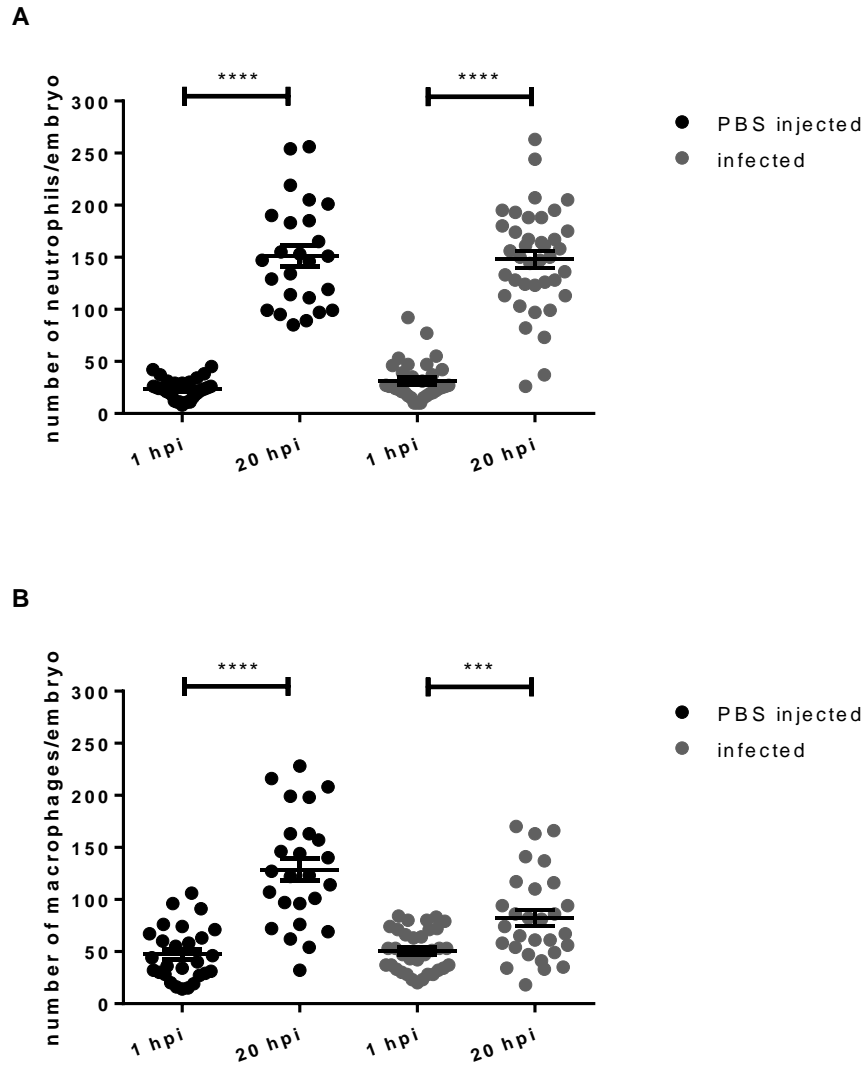


Figure 3.4. Number of neutrophils (A) and macrophages (B) in larvae increases during 20 hpi.

Tg(mpx:GFP) and *Tg(mpeg:mCherry.CAAX)* embryos were injected with PBS or 2500 CFU of SH1000 *S. aureus*. Number of neutrophils (A) and macrophages (B) significantly expands in larvae between 1 and 20 hpi (unpaired t test, A. $p < 0.0001$ for both infected and PBS injected groups, B. $p < 0.0001$ for PBS injected, $p = 0.0002$ for infected). A representative number of minimum 5 embryos was imaged in each experimental group, experiment repeated $n = 3$.

3.2.2.4. Professional phagocyte number dynamics in infected neutrophil and macrophage double-labelled embryos

Counts performed in neutrophil and macrophage-specific reporter lines provided an overview on phagocyte dynamics during infection. To verify how neutrophil and macrophage numbers are related it was necessary to examine both populations in one embryo.

Thus, neutrophil and macrophage labelled embryos were generated by crossing fish of *Tg(mpx:GFP)* and *Tg(mpeg:mCherry.CAAX)*, and quantification of imaging data was performed to assess if neutrophil and macrophage numbers are regulated independently upon infection with *S. aureus* (Figure 3.5.). Embryos were divided in 3 groups: non injected, PBS injected and infected, and imaged at 1 and 20 hpi.

Neutrophil and macrophage numbers were counted in each embryo and compared graphically (Figure 3.6.). At 1 hpi, embryos contained more macrophages than neutrophils in each larvae from each group (Figure 3.6A). At 20 hpi embryos in not injected, PBS injected and infected groups fell into two categories – those that contained more neutrophils than macrophages and more macrophages than neutrophils (Figure 3.6B). The result was not related to the infection and suggests that neutrophil and macrophage numbers are regulated independently upon infection at both time points. Counts of neutrophils and macrophages also shown that the number of cells of each population vary between individuals.

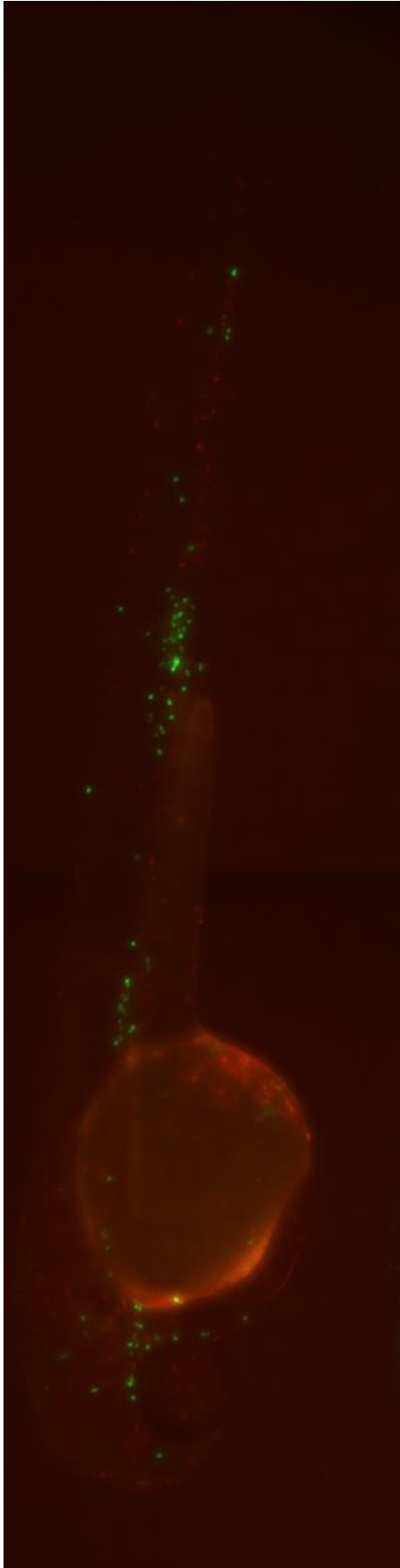


Figure 3.5. Low magnification imaging of neutrophil and macrophage fluorescently labelled embryo 50 hpf.

Image shows uninfected embryo 50 hpf. Visualisation of phagocytes was enabled in embryos generated by crossing of *Tg(mpx:GFP)* and *Tg(mpeg:mCherry.CAAX)* fish. Fluorescent reporters of neutrophils and macrophages (respectively) are expressed simultaneously in offspring larvae. 4x objective.

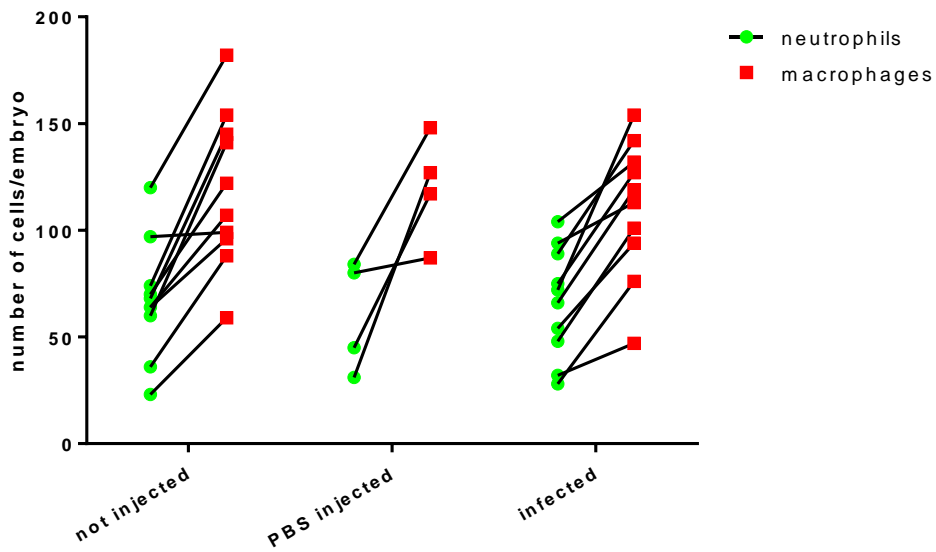
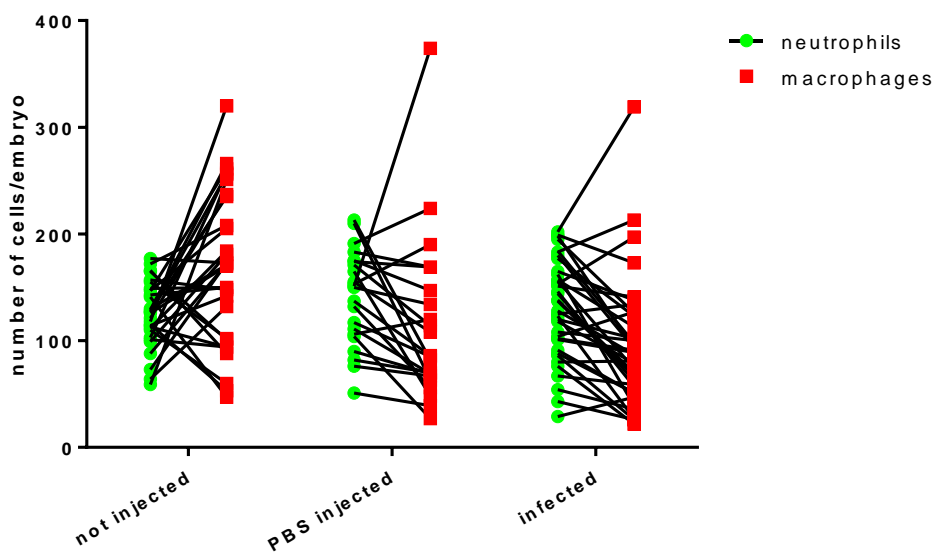
A**B**

Figure 3.6. Relative neutrophil and macrophage numbers during infection with *S. aureus* at 1 (A) and 20 hpi (B).

Counts were performed in imaged embryos generated by crossing *Tg(mpx:GFP)* fish with *Tg(mpeg:mCherry.CAAX)* fish - the lines connect the neutrophil and macrophage number within the same embryo. Embryos contain more macrophages than neutrophils 1 hpi (A) and but not at 20 hpi (B) in all tested groups of individuals. A representative number of minimum 5 embryos was imaged in each experimental group, experiment repeated n = 3.

3.2.2.5. Impact of imaging-related procedures on survival of infected embryo

The experiment aimed to determine whether anaesthesia, imaging and the procedure of release from the agarose impacted embryo survival. *Tg(mpx:GFP);Tg(mpeg:mCherry.CAAX)* embryos were divided into three groups: non injected, PBS injected and infected at 30 hpf with 2500 CFU dose of SH1000 *S. aureus*. Embryos of all groups were further imaged 1 day post infection (1 dpi). Subsequently, larvae were retrieved from the mounting medium in order to perform the survival test.

Survival dynamics were compared with larvae of all tested groups that had not been subjected to imaging. Both imaged and not imaged embryos of all groups did not show significant differences in survival (Figure 3.7.).

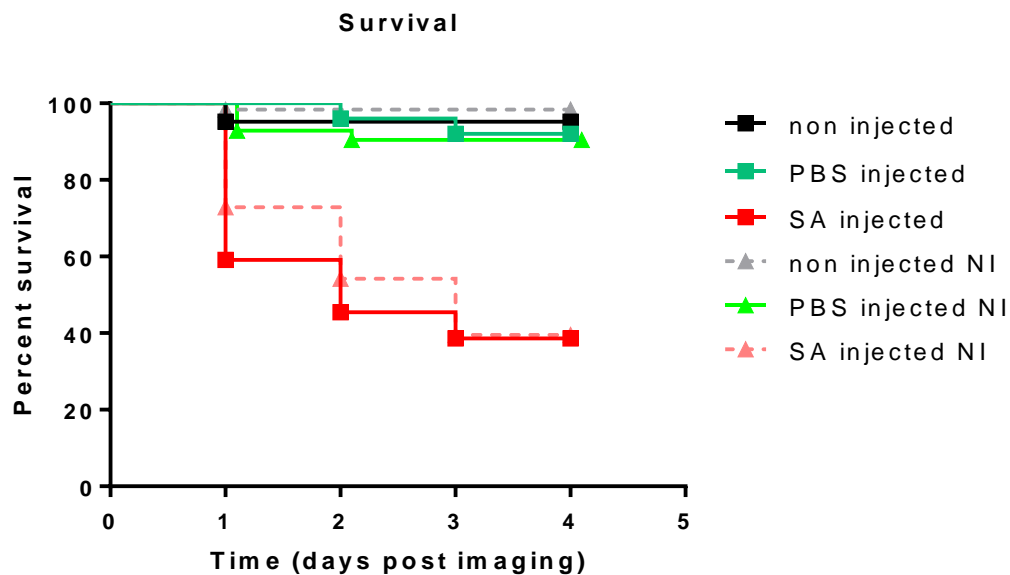


Figure 3.7. The imaging procedure has no effect on embryo survival kinetics

Tg(mpx:GFP) embryos were divided into 3 groups: non injected, PBS injected and infected with 2500 CFU SH1000 *S. aureus*. 10 embryos from each group were imaged at 20 hpi in the phagocyte count experiment. After imaging embryos were removed from mounting agarose and the survival test was performed together with not imaged (NI) embryos from each experimental group (n = 10). No significant differences in survival were shown for imaged and NI embryos of each group (log rank test, p = 0.95 non injected, p = 0.90 PBS injected, p = 0.86 infected). A representative number of minimum 20 embryos was imaged in each experimental group, experiment repeated n = 3.

3.2.2.6. Impact of professional phagocyte number on survival of infected embryo

While phagocyte counts results demonstrated that numbers of neutrophils and macrophages vary between individuals, it remained unclear if these differences can impact embryo survival. Hence, several experiments were performed to verify whether the number of neutrophils and macrophages is related to the survival of infected zebrafish larvae.

Imaging procedure did not affect embryo survival and therefore could be applied in order to determine phagocyte numbers in this experiment. Myeloid cells were counted in each embryo 1 dpi, and embryo survival was observed 2, 3 and 4 dpi. A fraction of embryos survived the infection. As a result, number of neutrophils and macrophages at 1 dpi, as well as time of death was known for each individual. Embryos were further divided into 4 groups, based on whether they survived, or by which time point they died (2, 3, or 4 dpi). Numbers of neutrophils and macrophages were plotted for each group and compared between surviving embryos and the remaining 3 groups (Figure 3.8.).

Embryos which died in the first 2 dpi had significantly lower number of neutrophils at the time of imaging than those which survived over the course of 4 dpi (Figure 3.8A). No relation was demonstrated between neutrophil numbers at 1 dpi and embryo survival until 3 and 4 dpi. This indicates that neutrophil numbers fall shortly before infection-induced death, as it has been shown previously (Prajnsnar *et al.* 2008). Macrophage numbers were not significantly lower in embryos which died 2, 3 or 4 dpi, than in the surviving group (Figure 3.8A). Therefore neutrophil number in embryo could constitute a prognostic for its survival in the short term, but would not predict the exact length of survival during *S. aureus* infection.

Analysis performed measuring neutrophil and macrophage numbers in one embryo showed that these myeloid cells kinetics within an embryo are not related to the length of its survival during infection (Figure 3.8B).

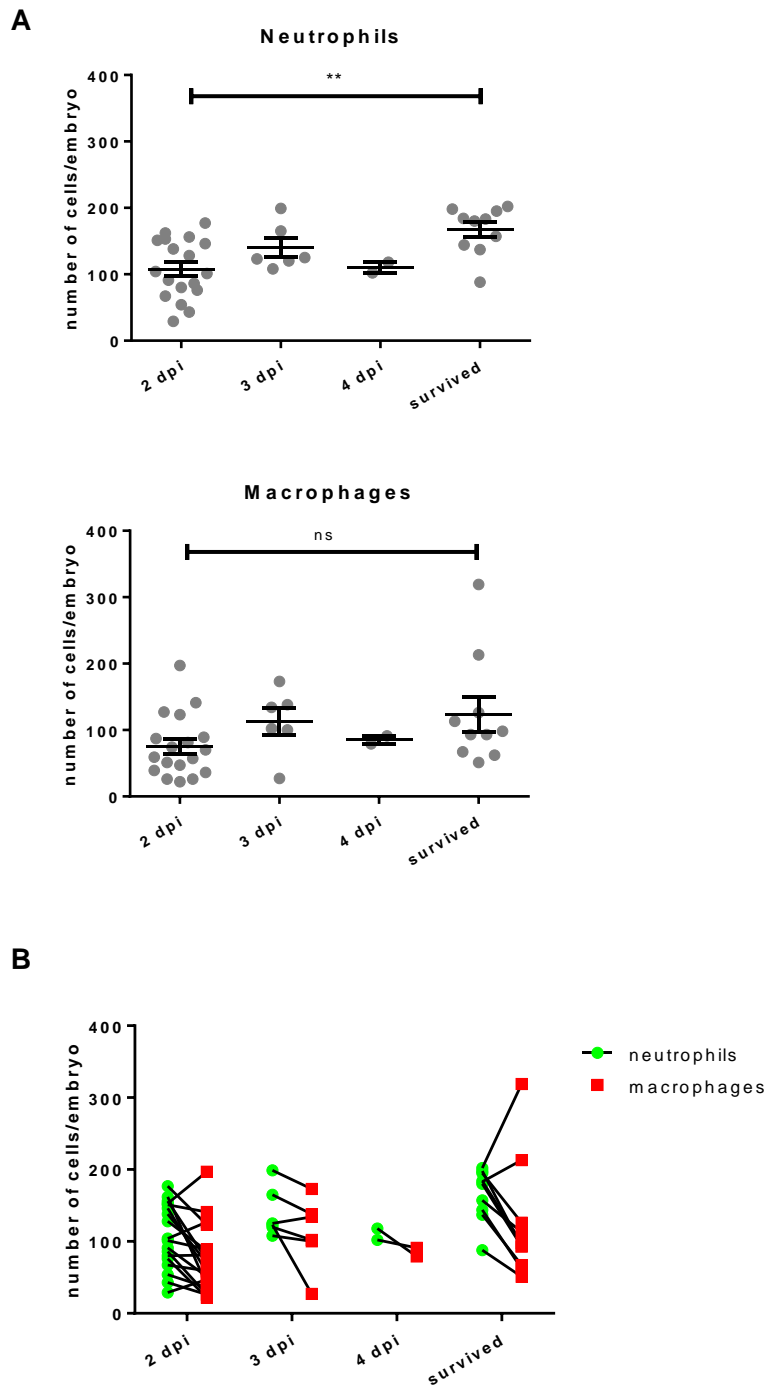


Figure 3.8. Phagocyte kinetics 20 hpi and the length of embryo survival.

Embryos surviving up to 2 dpi had significantly less neutrophils 20 hpi than those which survived over the course of 4 dpi (A. One-way ANOVA, Tukey's test, $p = 0.0022$). No significant relation was found between the number of macrophages and length of its survival (A). Macrophage and neutrophil kinetics within an embryo are not related to the length of its survival during infection (B). A representative number of minimum 5 embryos was imaged in each experimental group, experiment repeated $n = 3$.

Since the number of neutrophils in infected embryo significantly drops before the host death I decided to test, whether it can be verified based on an observation made without imaging procedure. *Tg(mpx:GFP)* larvae were infected with 2500 CFU SH1000 *S. aureus* and at 1 dpi divided into 3 groups based on the amount of GFP-positive neutrophils observed on the low magnification bench fluorescence microscope: high, intermediate and low (Figure 3.9A). Embryo survival was subsequently evaluated for each group. More fish died in the intermediate group compared to high, and more in the low group than in the intermediate (Figure 3.9B). This suggests that low number of neutrophils could predicts poor survival of embryo infected with *S. aureus* and it can be verified during microscopy observation, avoiding imaging procedure.

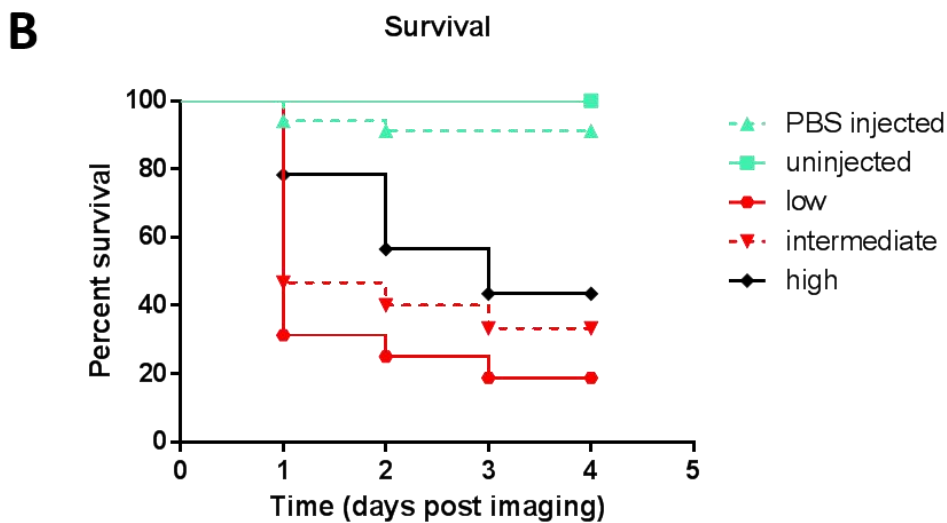
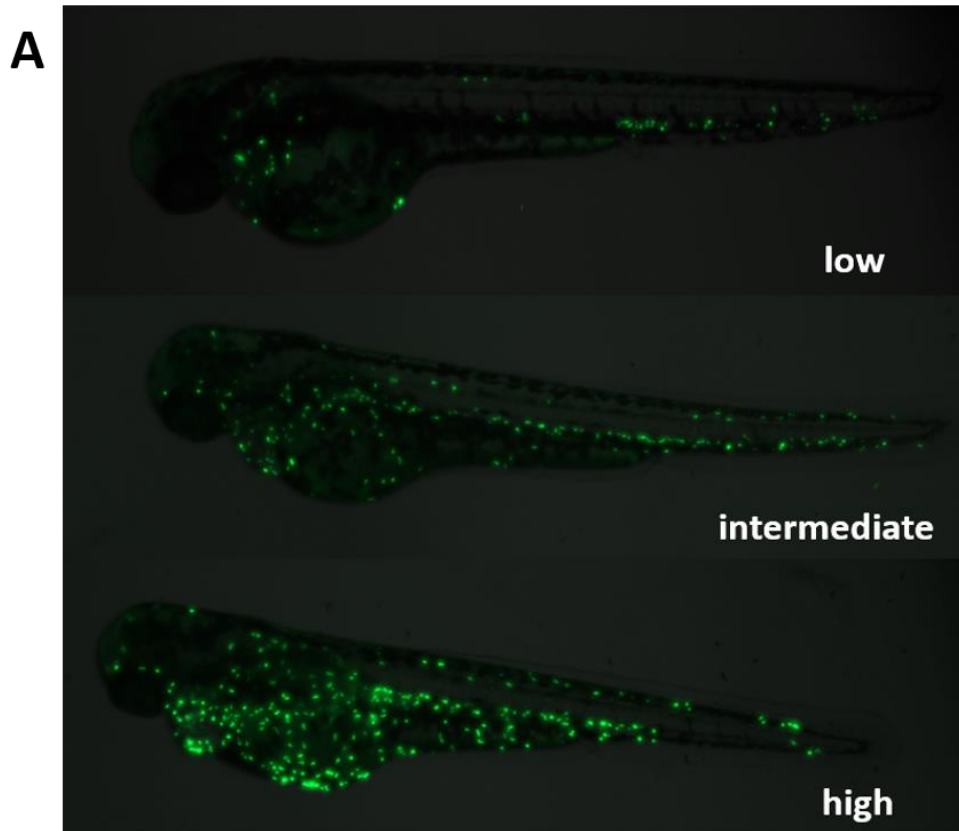


Figure 3.9. Survival of embryos classified by the number of neutrophils evaluated during microscopy observation

1 dpi embryos were divided into 3 groups based on the amount of neutrophils per embryo. Classification was not based on the neutrophil count, but on the observation (A). Survival test of the 3 different groups showed that most embryos survived in the high group, less in the intermediate and least in the low one (B) (log rank test, $p = 0.045$ low to high). A representative number of minimum 20 embryos was imaged in each experimental group, experiment repeated $n = 3$. 4x objective.

3.2.3. Whole body analysis of bacteria distribution in professional phagocytes during *S. aureus* infection

Initial quantitative analysis helped determine zebrafish phagocyte kinetics during *S. aureus* infection. Subsequently, I aimed to observe how bacteria disseminate in host neutrophils and macrophages and within the whole embryo. Microscopy-based whole body analysis of *S. aureus* distribution was impeded by the low resolution of images generated using low magnification lenses. Bacterial cells could only be visualised using high magnification imaging, however this could not be performed in the whole larvae with existing technology.

The numerical aperture of a microscope objective is the measure of its ability to gather light and to resolve fine detail. High numerical apertures allow smaller structures to be visualised with higher clarity and increase the resolution of the microscope system. Numerical apertures are generally higher in high magnification objectives, however can also be used in low magnification objectives. Higher values of numerical aperture enable generation of images, which subsequently may be enlarged (Figure 3.10.). In my study, “high magnification” refers to 40x and 60x objectives, low magnification to 2x, 4x and 10x lenses, while “low magnification with high numerical aperture” refers to 20x objective NA = 0.75. Low magnification objectives with high numerical aperture were used in this study and allowed microscopy-based analysis of *S. aureus* within the host. Visualisation of the whole embryo in high resolution became possible, however it required prolonged acquisition. Thus, in order to increase the number of embryos (n = 11 - 13), the first time point was extended to 1 - 5 hpi, and the second 24 - 28 hpi. The injected dose was decreased to 1500 CFU to facilitate precise counts.

Fluorescent SH1000-mCherry *S. aureus* was used to visualise bacteria present in the larvae. The use of *Tg(mpx:GFP)* embryos allowed recognition of GFP-positive neutrophils. Due to the long time of acquisition and lack of wider range of strong fluorophores, macrophages were not labelled in this experiment. Instead, bacteria residing in groups of more than 1 cell were considered to be phagocytosed by bloodstream macrophages, as preliminary imaging indicated these groups of bacteria are likely to have been internalised by macrophages.

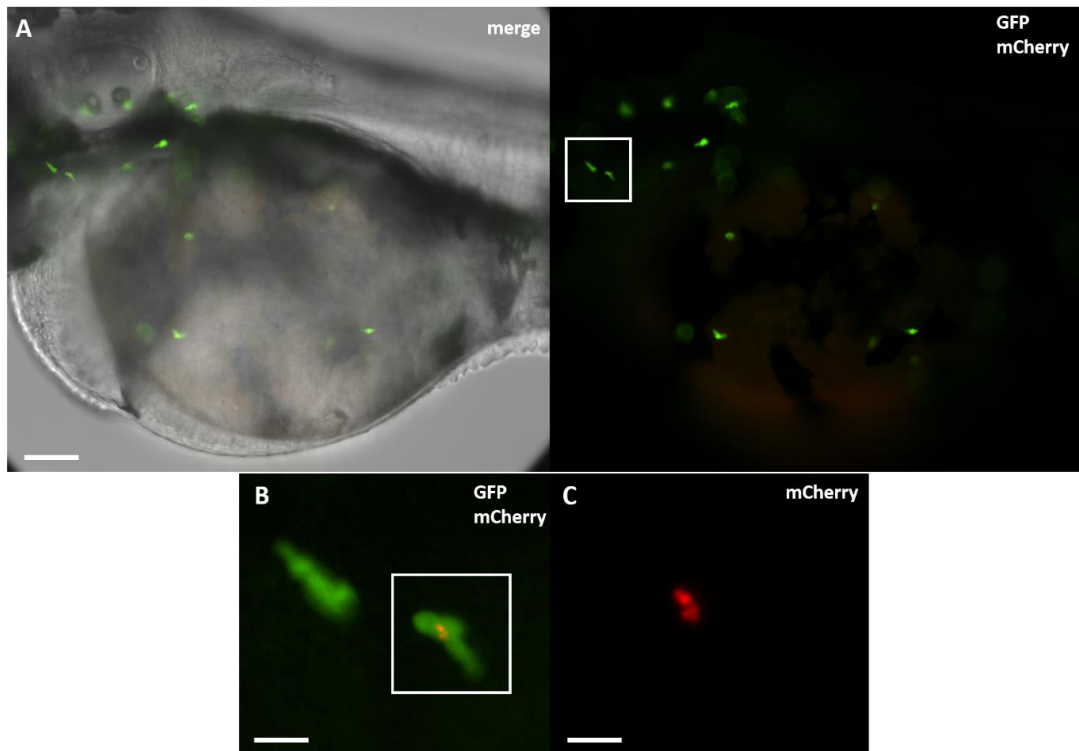


Figure 3.10. Imaging infection in the whole body of infected embryo using low magnification, high numerical aperture objectives.

Figure shows *Tg(mpx:GFP)* embryo infected with 1500 CFU of SH1000-mCherry *S. aureus*. A, upper panel shows initial field of view, captured using 20x magnification, all channels are merged on the left hand side picture. Right hand side picture shows GFP-positive neutrophils and *S. aureus* marked with mCherry fluorescent protein, not detectable without increasing the magnification (scale bar: 80 μm).

B, using high numerical aperture lenses enabled obtaining high resolution images. Increasing the magnification of a picture allows visualisation of GFP-positive neutrophil containing SH1000-mCherry *S. aureus* cells (scale bar: 20 μm).

C, Further increase of the image magnification enables counting of single *S. aureus* cells present in the embryo (scale bar: 10 μm).

20x objective NA = 0.75.

3.2.3.1. Enumeration of bacteria in infected phagocytes

As described in the previous paragraph, whole body imaging of infected embryos allowed enumeration of bacteria contained in neutrophils and macrophages, and therefore to observe *S. aureus* dissemination.

Statistically macrophages internalised 2 times more *S. aureus* than neutrophils within 5 hpi (Figure 3.11.). At 24 – 28 hpi, an average neutrophil still contained 2 fold lower number of bacteria than an average macrophage.

Observations made in my study shown that the number of *S. aureus* bacteria per cell can be increased up to a 100 and more. Precise counting of bacteria was possible when the number of cells did not exceeded 100. Therefore, whenever an analysed phagocyte contained ≥ 100 *S. aureus* cells, it was scored the value of 100, which set the maximum limit for the analysis. At 24 hpi in both cell lineages studied, the number of phagocytes containing ≥ 100 *S. aureus* increased 2 x (Figure 3.11.1).

Both types of professional phagocytes contained more bacteria at 1 - 5 hpi than 24 - 28 hpi, although the difference between mean numbers was significantly larger in macrophages (Figure 3.11.2B) than in neutrophils (Figure 3.11.2A).

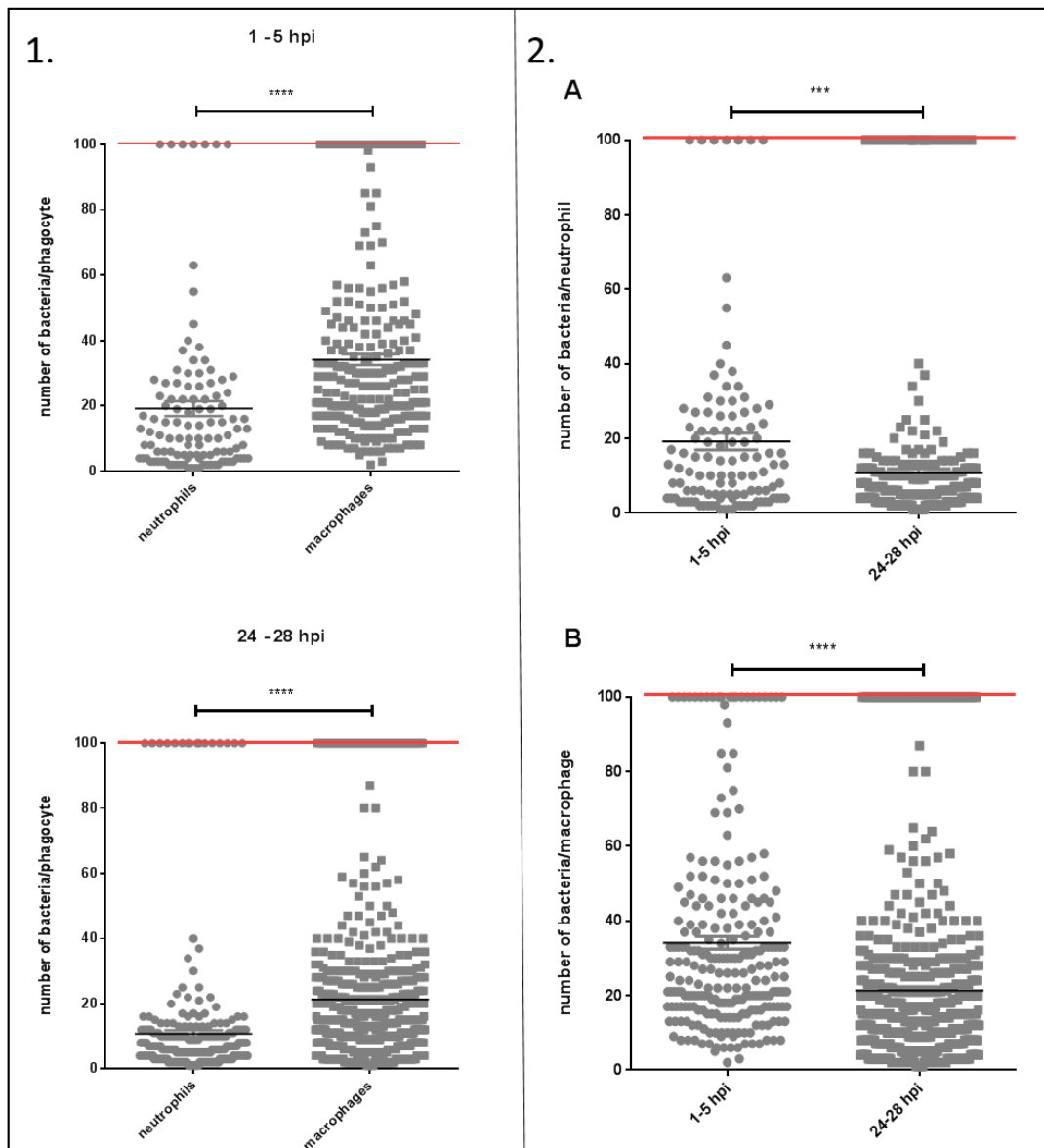


Figure 3.11. Number of bacteria in neutrophils and macrophages counted during whole embryo imaging analysis.

1. *Tg(mpx:GFP)* embryos were injected with 1500 CFU of SH1000-mCherry *S. aureus*. Plots show number of bacteria internalised in neutrophils and macrophages in embryos ($n = 11 - 13$) at two different time points. At both time points macrophages contain significantly more *S. aureus* cells compared to neutrophils (unpaired t test, $p < 0.0001$). A representative number of minimum 5 embryos (and 20 phagocytes per larvae) was imaged in each experimental group, experiment repeated $n = 3$.

2. Plots show number of bacteria contained in neutrophils (A) and macrophages (B) in embryos ($n = 11 - 13$) at time points: 1 - 5 and 24 - 28 hpi. Both neutrophils and macrophages contain significantly more *S. aureus* at the earlier stage of infection (unpaired t test, $p = 0.0004$, $p < 0.0001$, respectively). A representative number of minimum 5 embryos (and 20 phagocytes per larvae) was imaged in each experimental group, experiment repeated $n = 3$.

3.2.3.2. Percentage of uninfected neutrophils in infected embryos over time

Whole body imaging of *Tg(mpx:GFP)* embryos allowed recognition of GFP-positive neutrophils. The analysis of bacterial numbers in these cells during *S. aureus* infection revealed the existence of a fraction of GFP-positive neutrophil cells, which did not contain bacteria. Nearly 60 % of neutrophils had bacteria 1 - 5 hours post infection but only 20 % at the later stage of infection (24 - 28 hpi Figure 3.12.). The 80 % of empty neutrophils could possibly include cells which had killed internalised bacteria. Additionally, due to embryo development, the population of neutrophils would increase by about 30 % within 1 day post infection (Prajnsnar *et al.*, 2008). Newly generated phagocytes could remain empty if extracellular bacteria were no longer available, however the formation of abscesses was observed in a group of analysed embryos at that time point (n = 3). Thus, potentially some of the neutrophils do not phagocytose *S. aureus* even in the presence of extracellular organisms.

The ability of neutrophils to phagocytose and kill bacteria is a critical determinant of the outcome of infection. However, either phagocytosis or killing could become overwhelmed during infection *in vivo* leading to a failure to cope with the infectious burden. In order to assess whether zebrafish neutrophils were able to ingest and kill bacteria effectively *in vivo*, across a range of bacterial burdens, *Tg(mpx:GFP)* zebrafish were infected with 1500-200 *S. aureus* CFU and the numbers of infected neutrophils were counted.

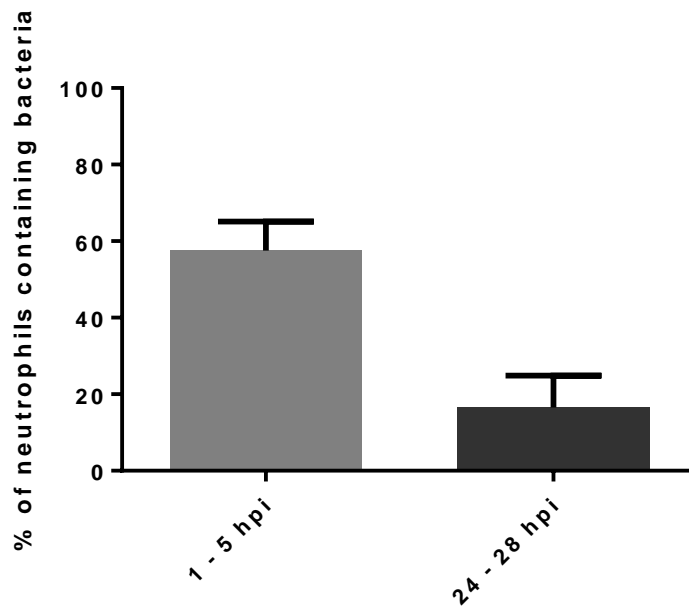


Figure 3.12. Percentage of neutrophils containing bacteria in infected embryos.

Neutrophils were counted in the whole *Tg(mpx:GFP)* larvae. Fluorescent labelling of *S. aureus* allowed determination of proportion of the neutrophils containing bacteria at two time points. At the early stage of infection nearly 60 % of neutrophils contain bacteria. This fraction drops 24 - 28 hpi when only about 20 % of neutrophils contain *S. aureus* (dose injected 1500 CFU). A representative number of minimum 5 embryos (and 20 phagocytes per larvae) was imaged in each experimental group, experiment repeated n = 3.

The number of bacteria contained within a whole larva was correlated with the percentage of neutrophils containing bacteria and plotted. Embryos were injected with the dose of 1500 CFU and at 1 - 5 hpi the number of bacterial cells did not exceed 2000 in all analysed fish (Figure 3.13A). 3 out of 11 embryos had only 500 *S. aureus* cells, which indicated that the host was able to successfully kill the majority of injected bacteria during the first 5 hours post infection (or less). All neutrophils contained bacteria in only one of the embryos, with 1200 bacterial cells. Two embryos with lowest fraction of neutrophils containing bacteria (less than 40 %) showed bacterial numbers varied significantly at this time point: 200 and 2000. The number of neutrophils containing bacteria increases with the number of bacteria in an embryo, however there is no significant correlation between bacteria load and number of neutrophil containing bacteria.

At 24 - 28 hpi the number of bacteria has increased overall but with a large spread between less than 200 to nearly 4500 *S. aureus* cells per embryo (Figure 3.13B). 3 out of 13 larvae were found to have visible *S. aureus* abscesses (Figure 3.13C red points). Abscesses precluded accurate counting of bacterial numbers. No significant correlation was found between the overall number of bacteria and the percentage of neutrophils containing *S. aureus*. In most embryos (n = 8), the fraction of neutrophils containing bacteria varied between 15 and 25 %, regardless to the total amount of *S. aureus*. One could speculate that larvae containing less bacteria will survive. In the remaining group of embryos higher numbers of *S. aureus* will more likely predict a lethal outcome of infection. However, a study of population variance showed that very few *S. aureus* cells are necessary to initiate a fatal infection (Prajnsar *et al.*, 2012). It would be interesting to follow bacterial dynamics and distribution in fish at multiple time points within first 24 hpi using microscopy approach established in this study.

Although the number of bacteria seems to correlate more with the percentage of infected neutrophils at earlier stage of infection, the difference between the two time points is not significant (Figure 3.13C). Values of 1 - 5 hpi data set seem to be more scattered in the proportion of infected neutrophils, and in 24 - 28 hpi analysis amounts of bacteria per embryo are strongly diversified.

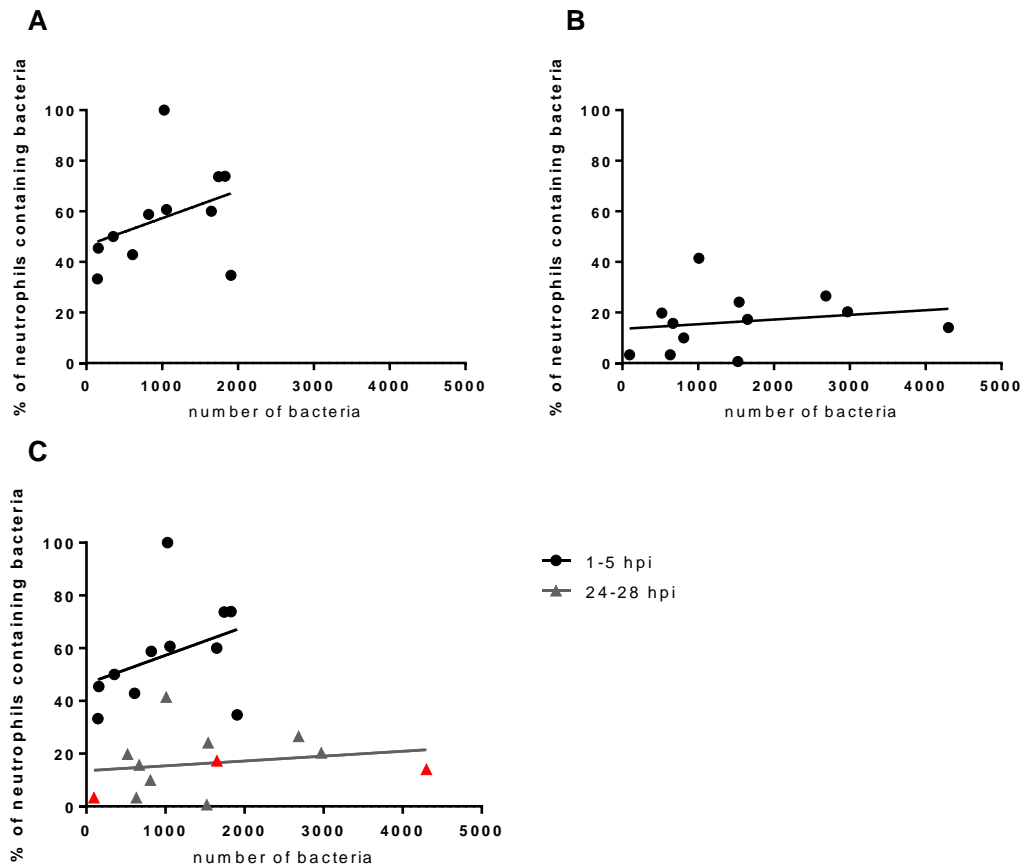


Figure 3.13. Correlation between the percentage of neutrophils containing bacteria and bacterial number during infection.

A, data collected from embryos at 1-5 hpi. Linear regression analysis showed that there is a relationship between X and Y data sets, however it is not significant ($r^2 = 0.1367$; slope not significantly non-zero, $p = 0.2630$).

B, data collected from embryos at 24-28 hpi. Linear regression analysis showed that there is a relationship between X and Y data sets, however it is not significant ($r^2 = 0.03848$; slope not significantly non-zero, $p = 0.5412$).

C, the differences between the slopes from the two time points are not significant ($p = 0.2977$). The Y intercepts of both lines are significantly different for both lines ($p < 0.0001$), which means that the elevation of Y values is significantly higher in the 1-5 hpi data set and there is a higher percentage of neutrophils is containing bacteria at that time point for a particular number of bacteria. Points belonging to larvae containing abscesses were marked red.

A representative number of minimum 5 embryos (and 20 phagocytes per larvae) was imaged in each experimental group, experiment repeated $n = 3$.

3.2.4. High magnification phagocyte-specific analysis of *S. aureus* internalisation rates

Neutrophils and macrophages take up *S. aureus* injected intravenously into 30 hpf zebrafish embryo. Although both phagocytes are capable of internalisation, it is likely they handle the pathogen in distinct ways. To determine the differences between neutrophil and macrophage internalisation and the potential effects on infection outcome, quantification of pathogen handling by professional phagocytes was measured by determination of their bacterial internalisation rates. The analysis previously performed in the whole embryo allowed the determination of size of the fraction of neutrophils containing bacteria and estimate the number of *S. aureus* residing in neutrophils and macrophages. This method enables examination of the whole neutrophil population, however it does not provide a reliable source of information concerning macrophages.

Imaging was performed in three independent repeats, at two time points, 1 and 20 hpi, in a representative group of embryos (5 – 10 embryos/repeat). Neutrophil internalisation rates were determined in GFP-positive neutrophils of *Tg(mpx:GFP)* embryos and macrophage internalisation was assessed in CFP and YFP expressing cells of *Tg(mpeg:FRET)* embryos. Both groups of embryos were infected with 1500 CFU of SH1000-mCherry *S. aureus*. Acquisition was localised to the yolk circulation valley bloodstream area. Altogether this resulted in visualisation of bacteria residing in over 120 neutrophil and 160 macrophage cells.

At 1 hpi, significantly more bacteria were in macrophages than neutrophils (average of 25 and 15 respectively Figure 3.14.). Mean values counted in cells imaged during the whole body approach were about 10 bacterial cells per phagocyte higher in both cell lineages.

At 20 hpi average numbers of bacteria internalised by neutrophils of macrophages corresponded with those determined in the low magnification approach (Figure 3.11.1). Although macrophages showed a trend towards increased internalisation of *S. aureus* at that time point, the difference between cell lineages was not significant. This may have been due to the lower number of neutrophils available for analysis at that time point.

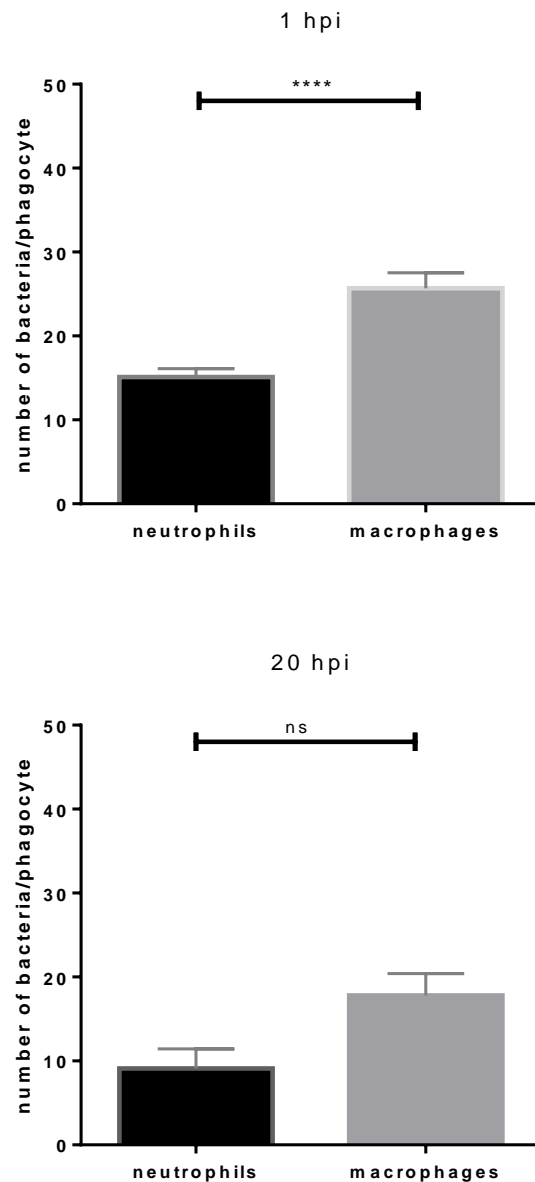


Figure 3.14. Macrophages contain more bacteria than neutrophils.

Neutrophil-specific *Tg(mpx:GFP)* embryos and macrophage-specific *Tg(mpeg:FRET)* embryos were injected with 1500 CFU of SH1000-mCherry *S. aureus* and imaged at 1 and 20 hours post infection in the yolk circulation valley. Plots show number of bacteria contained in neutrophils and macrophages, giving a measure of the mean number of bacteria per phagocyte. At 1 hpi macrophages contain significantly more *S. aureus* than neutrophils ($p < 0.0001$, unpaired t-test, $n=34$ fish per group). A representative number of minimum 5 embryos (and 20 phagocytes per larvae) was imaged in each experimental group, experiment repeated $n = 3$.

The phagocyte-specific reporter lines allowed assessment of the proportion of phagocytes containing bacteria at 1 and 20 hpi. In this experiment, the imaging area was limited to yolk sac circulation valley, where innate cells can be readily visualised and most importantly, bloodstream infection may be observed relating it to bacteraemia condition.

The amount of professional phagocytes containing *S. aureus* could indicate the ability of immune cells to kill pathogen. Therefore it was important to observe how it changes over the time course of infection. The proportion bacteria-containing neutrophils was compared between 1 hpi and 20 hpi time points. Same comparison was performed for macrophages. Significantly more neutrophils and macrophages contain bacteria at 1 hpi than 20 hpi (Figure 3.15.).

Almost all neutrophils and macrophages contained bacteria at 1 hpi, demonstrating high internalisation efficiency of both cell lineages during the initial stages of bloodstream bacteraemia (Figure 3.15.). A significantly smaller fraction of macrophages contained bacteria 20 hpi compared to the earlier time point.

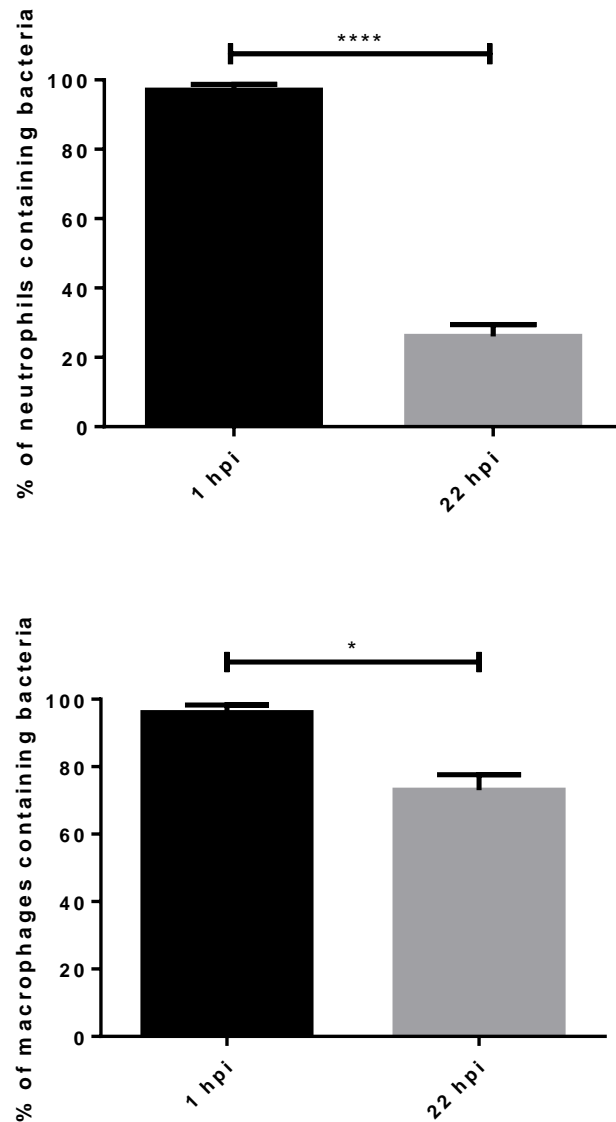


Figure 3.15. Percentage of neutrophils and macrophages containing bacteria imaged at high magnification.

Tg(mpx:GFP) and *Tg(mpeg:FRET)* (neutrophil and macrophage reporter lines, respectively) embryos were infected with approx.. 1500 CFU of SH1000-mCherry *S. aureus* and imaged 1 and 20 hpi. Imaging analysis shown that a significantly larger fraction of neutrophils and macrophages contained bacteria at 1 hpi than at 20 hpi (unpaired t test; $p < 0.0001$, $p = 0.0112$ respectively). A representative number of minimum 5 embryos (and 20 phagocytes per larvae) was imaged in each experimental group, experiment repeated $n = 3$.

3.2.5. Distribution of *S. aureus* mixed inoculum in professional phagocytes

3.2.5.1. Infection with 1:1 CFP and YFP labelled bacteria

S. aureus replication and persistence has already been shown in macrophages (Kubica *et al.*, 2008). Results in my study indicated a possible intracellular growth of bacteria in neutrophils and macrophages.

It has been shown that *S. aureus* undergoes clonal expansion when injected into zebrafish embryos (Prajsnar *et al.*, 2012). Isogenic strains carrying different fluorescence markers and antibiotic resistant properties have been shown to pass through a “bottleneck” inside the larvae when injected in 1:1 ratio. As a result, in about 30 % of fish one of the two simultaneously injected strains was significantly prevalent. This implies the existence of a niche which facilitates expansion of a few bacterial cells and eventual killing of the host. Results published in the same study showed that professional phagocytes are required for the clonal expansion.

The aim of the mixed strain 1:1 inoculum experiments in my study, was to determine at which stage of infection the population segregation could be observed. Additionally, it aimed to elucidate if *S. aureus* grows intracellularly. Replication could be observed as an over representation of one of the fluorescently labelled strains.

During survival tests the first embryos succumb to infection around 20 hpi. My work has shown bacterial internalisation by 3 hpi suggesting the initial clonal expansion occurs between 3 - 20 hpi. Therefore, several time points between complete internalisation of injected bacteria and potential intracellular growth and events leading to *S. aureus* spread were used.

Both neutrophils and macrophages express fluorescent actin in 30 - 40 hpf *Tg(mpx:Lifeact-Ruby)* embryos (Yoo *et al.*, 2010), thus counts of bacteria could be taken in all phagocytes present in the bloodstream during the time course of the experiment. Additionally, these phagocytes are labelled with red fluorescence marker, which allows acquisition set up including two additional fluorophores expressed by *S. aureus* strains, CFP (blue) and YFP (yellow), as the three spectral classes can be easily separated. 30 hpf *Tg(mpx:Lifeact-Ruby)* embryos were infected

intravenously with 1:1 inoculum of CFP and YFP-expressing SH1000 *S. aureus* strains (total dose 2500 CFU) and numbers of bacteria residing in bloodstream phagocytes were counted from images captured 3, 6 and 9 hpi. A three hour interval was calculated to be long enough to identify changes, and sufficiently frequent for detailed analysis.

The number of CFP and YFP-expressing *S. aureus* cells was counted for each phagocyte and a higher value was further divided by the lower one to determine the ratio. Values were subsequently grouped into 5 classes, ranging from lower than 1.5, and indicating similar number of both colours, through higher than 1.5-fold, 2-fold and 3-fold to 4-fold prevalence of one of the strains. A separate group was distinguished for phagocytes that contained bacteria of “one colour only”, regardless of the total number of bacteria in phagocytes. The number of immune cells in each group was represented as a fraction of the whole analysed population on a plot for each time point (Figure 3.16A). At 3 hpi a third of phagocytes contained a ratio similar to that initially injected, 1:1. Only 20 % of phagocytes contained one colour only. At 6 hpi, the fraction of phagocytes containing one colour only increases to 45 % and becomes the largest group. Interestingly, at 9 hpi, the prevalence of the “one colour only” fraction decreased by 10 % and the number of phagocytes in 3-fold and 4-fold groups grows by approximately 10 % each, compared to the previous time point.

The fraction of phagocytes containing 1:1 colour ratio reduces over the time course of experiment. This implies that the population imbalance is already initiated in phagocytes during first hours of infection. The increase in phagocytes containing only one *S. aureus* strain at 6 hpi indicates that population skewing, starts to occur between 3 and 6 hpi. The 10 % decrease in this fraction of phagocytes observed at 9 hpi could suggest that phagocytes may lyse upon *S. aureus* expansion. It may be that the increase in 3-fold and 4-fold groups at 9 hpi reflects more phagocytes showing initial changes in the strain proportion, leading to the prevalence of one strain.

Phagocytes of the “one colour only” group could theoretically contain any number of bacteria. In this experiment it has never been less than 2 *S. aureus* cells. At 3 hpi the number of *S. aureus* in these phagocytes did not exceed 10 (average = 5.4). At 6 and 9 hpi number of bacteria in phagocytes containing one strain was elevated, ranging

up to 20 and 24 *S. aureus* cells, respectively. The average number of bacteria per phagocyte at 6 hpi was 9.35, and at 9 hpi it was 9.1.

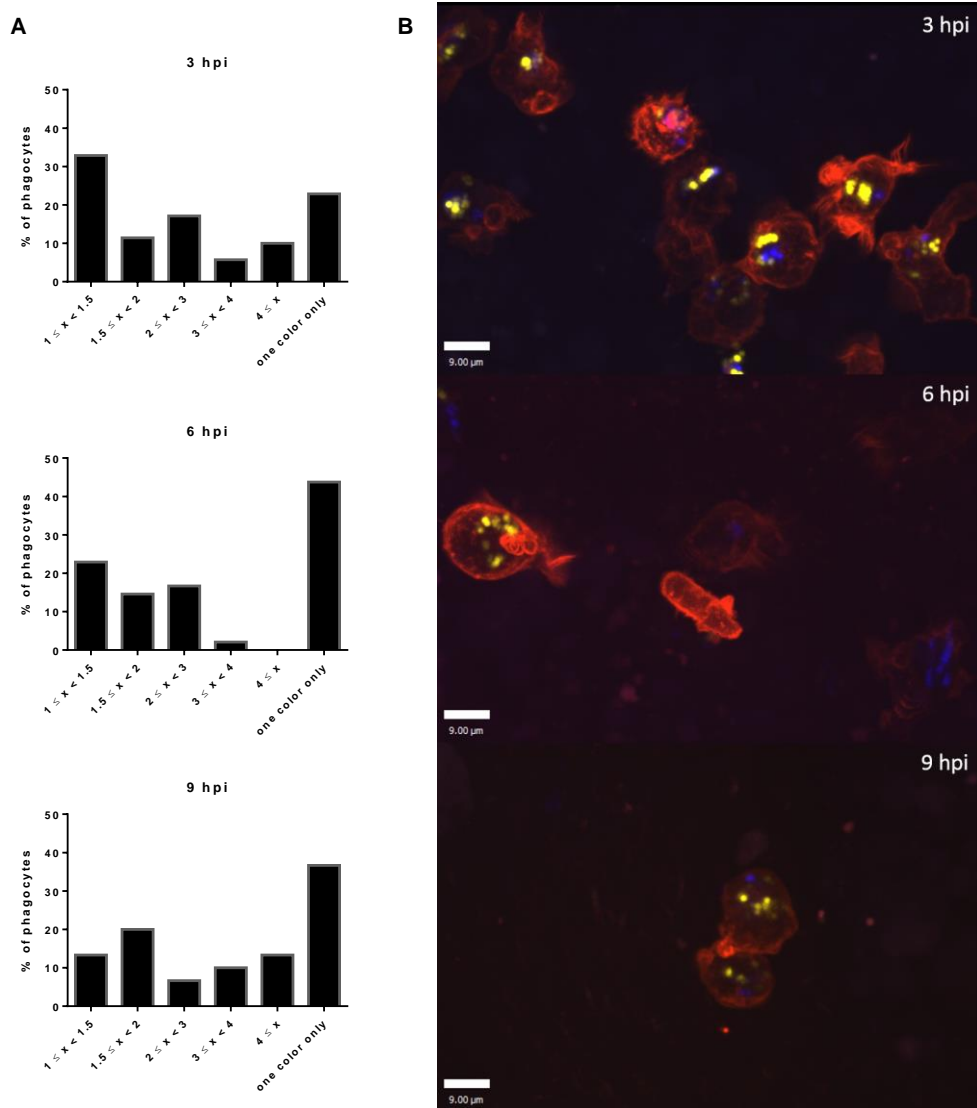


Figure 3.16. Bacterial population dynamics in phagocytes of embryos with 1:1 mixed inoculum.

A. *Tg(mpx:Lifeact-Ruby)* embryos were infected with 2500 CFU inoculum containing 1:1 mix of SH1000-CFP and SH1000-YFP *S. aureus* strains. At each time point a group of embryos (n = 5) was imaged and the number of each bacterial strain in phagocyte was quantified.

B. Example images of phagocytes captured at 3, 6 and 9 hpi. At 3 hpi each of presented phagocytes contained both *S. aureus* strains. At 6 and 9 hpi phagocytes containing more than 10 cells of one fluorescent strains were more common.

A representative number of minimum 5 embryos (and 20 phagocytes per larvae) was imaged in each experimental group, experiment repeated n = 2. 40x objective.

3.2.5.2. Re-infection of infected embryos at 50 hpf

The re-injection experiment was designed to test whether neutrophils and macrophages of embryos infected at 30 hpf were still capable of internalising extracellular bacteria at 50 hpf. A fraction of uninfected phagocytes has been observed during quantification analysis of macrophages and neutrophils at 20 hpi (Figure 3.12., Figure 3.15.).

Tg(mpx:GFP) embryos were infected with 2500 CFU of SH1000-mCherry 30 hpf, and subsequently with 2500 CFU of SH1000-GFP, 20 hours post the initial infection (50 hpf).

The imaging data has shown that both neutrophils and macrophages were able to internalise the bacteria injected at the latter time point (Figure 3.17.). Moreover, macrophages already demonstrated to have higher capacity (Figure 3.11, Figure 3.14.), were capable of internalising SH100-GFP *S. aureus* despite containing a substantial amount of the SH1000-mCherry (Figure 3.17B). Altogether the results indicate that phagocytes are functional and able to take up bacteria present in the bloodstream. Therefore, the strategy which allows bacteria to grow and cause the fatal condition is probably not related to phagocytic incapability of host cells.

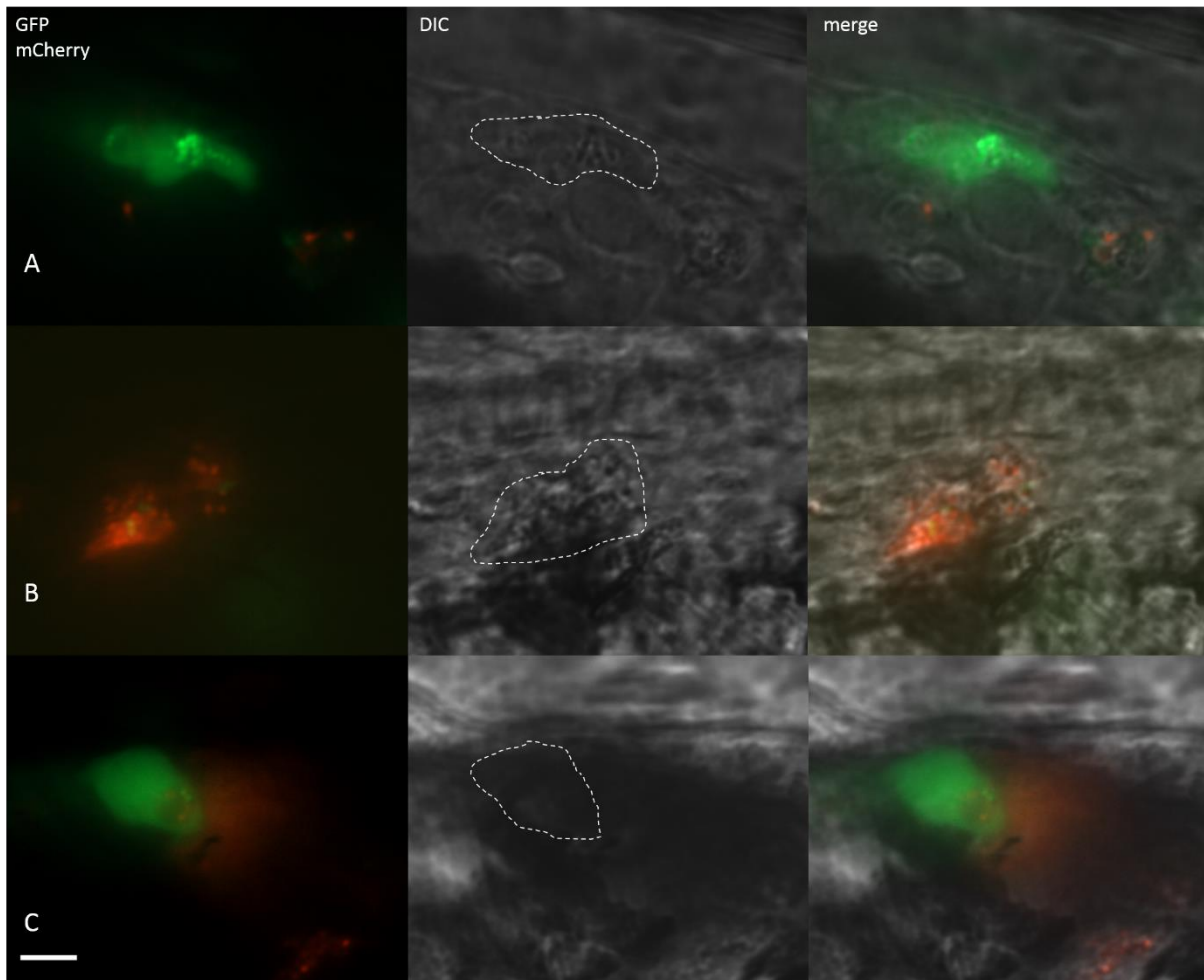


Figure 3.17. Example images of phagocytes internalising bacteria injected at two different time points.

At 30 hpf *Tg(mpx:GFP)* embryos were infected with 2500 CFU of SH1000-mCherry and at 50 hpf with 2500 CFU of SH1000-GFP *S. aureus*. A representative number of minimum 5 embryos (and 20 phagocytes per larvae) was imaged in each experimental group, experiment repeated n = 3.

A. GFP-positive neutrophil cells internalised GFP *S. aureus*. The presence of GFP-positive bacteria only suggests that the neutrophil did not contain bacteria prior to re-injection.

B. Macrophages are GFP-negative phagocytes, distinguishable with the use of DIC imaging. The macrophage internalised SH1000-GFP *S. aureus* despite containing a substantial amount of SH1000-mCherry bacteria.

C. Infected neutrophils were also capable of internalising bacteria injected at 50 hpf (scale bar 15 μ m). 60x oil objective.

3.3. Discussion

Immune cells constitute an important component of host defence in *S. aureus* infection of zebrafish and have been shown to play a role in the bacteria dissemination (Prajsnar *et al.*, 2012). The number of neutrophils and macrophages, variable upon infection, constitutes an important insight into first systemic response to *S. aureus* bacteraemia.

The kinetics of neutrophil and macrophage numbers during *S. aureus* bacteraemia infection in the zebrafish model have been previously evaluated using *Tg(mpx:GFP)* neutrophil reporter line, combined with Neutral Red live staining or L-plastin/Cy3-TSA phagocyte staining methods (T.K. Prajsnar, PhD thesis, University of Sheffield 2009, Prajsnar *et al.* 2008). Counts of neutrophils and macrophages were taken at 20, 30 and 50 hours post infection (hpi), and demonstrated that the two myeloid line phagocytes respond differently to *S. aureus* infection. However staining techniques do not constitute an accurate method for macrophage counting, for instance neutral red stains only a third to half of macrophages (Mostowy *et al.*, 2013, Herbomel *et al.*, 2001). Hence, in this study, phagocyte counts were performed using stable fluorescence reporter transgenic lines, both neutrophil – *Tg(mpx:GFP)* and macrophage-specific – *Tg(mpeg:mCherry.CAAX)*.

The number of phagocytes embryos are generally different within a population, probably caused by minor differences in the time of fertilisation. Light-controlled diurnally-synchronised egg fertilisation sets the similar start point of larvae generation, however embryos are being laid during the following hour. Collected embryos laid at slightly different times are kept together in a petri dish and therefore mixed. Embryo selection involves the early evaluation of development stage to minimise age differences between larvae, however small variations are still inevitable. The first 30-50 hpf are the period of generation of myeloid cells and first fully functional phagocytes circulating in the bloodstream, hence, the number of fluorescence-positive phagocytes may vary between embryos. However, the variance seems reproducible in all groups, indicating that its cause is not related to infection.

Quantitative analysis performed in *Tg(mpeg:mCherry.CAAX)* embryos demonstrated that the macrophage population contracts upon infection at 20 hpi. This result may reflect a specific effect of *S. aureus* on macrophage survival or an infection-mediated effect on the physiology of the larvae. The macrophage number is decreased by 30 % and at that time point 60% of macrophages the circulation valley contain bacteria. Alternatively, *mpeg* gene expression could become down regulated upon infection as it has been shown for *Mycobacterium marinum* and *Salmonella typhimurium* infections in the zebrafish model (Benard *et al.*, 2015). The encoded protein, MPEG1/perforin-2 is an integral macrophage membrane component, and in vertebrates it has been shown to be involved in the killing of bacteria by pore forming activity (Fields *et al.*, 2013). Thus, the results presented in this study should encourage more in depth study elucidating its role in *S. aureus* infection.

The significant decrease in the number of macrophages in PBS injected control embryos is surprising and could be explained by non-specific infection if the PBS stock was contaminated with pathogen a after media sterilisation. However, such an explanation is not very likely, as the same stock has been used in control injections for survival tests (Figure3.1.) and did not affect embryo survival. Moreover, the *S. aureus* inoculum was always resuspended in PBS and plated after infection as a dose control, showing that only *S. aureus* cells grew on the BHI agar medium (no selective antibiotics added). The result obtained for the PBS injected group is an intermediate between values recorded in non injected and infected groups, therefore possibly was not caused by unintended infection with *S. aureus*. Interestingly, number of neutrophils in PBS injected embryos also tends to resemble values in infected group, rather than in not injected one (however, differences are not significant). Furthermore, the outcome of both neutrophil and macrophage counts remained constant in all 3 independent repeats. One can speculate that although anaesthesia, injection and mounting do not influence survival of PBS infected larvae, those procedures can affect well-being of a fragile 2 dpf larvae. Infection and imaging protocols, although thoughtful and well controlled, could put fish through physiological stress and influence phagocyte numbers. Although the hypothetical

mechanisms of such change remains unknown, it seems important to be aware of such relation when interpreting phagocyte counts results.

It has been suggested that in *S. aureus* infection low numbers of neutrophils precede death of infected embryos (Prajsnar *et al.*, 2008), similarly as leukopenia is regarded as a poor prognostic sign in clinical infection (Fine *et al.*, 1996). However, infection did not seem to affect mean neutrophil numbers in *Tg(mpx:GFP)* at 1 and 20 hpi time points. Data presented in this chapter shows although that the neutrophil number drop shortly before death of an embryo. A low survival prediction based on the neutrophil population demonstrates, that such a preselection could be applied in drug screening, enabling a quick estimate of larvae condition prior to, or upon treatment with different compounds. It also has a potential use in high throughput fluorescence-based embryo selection (Veneman *et al.*, 2013).

A whole body imaging approach was important to visualise systemic distribution and dissemination of bacteria. The existing technology does not allow to effectively image the entire body of living zebrafish embryo, however in future this may be enabled using Multiview light sheet fluorescence microscope. In my study, bacterial dissemination within embryo was assessed using low magnification objectives with high numerical aperture. High resolution images could be enlarged during analysis, which demonstrated that most of bacteria seemed to be contained within phagocytes up to 28 hpi. However, the number of bacteria contained within neutrophils and macrophages decreased over time. Given that macrophages initially internalise more, the reduction in bacterial number becomes even more significant. This could indicate that macrophages are more efficient in killing internalised bacteria within 24 hpi. It could also suggest that *S. aureus* is more likely to persist in large numbers or replicate in neutrophils during that time. Nevertheless, such conclusions should be verified in an experimental set up allowing labelling of macrophages. Herein, imaging was performed in neutrophil specific reporter line *Tg(mpx:GFP)*, and thus the counts of bacteria contained in macrophages could possibly include extracellular *S. aureus* cells.

At 24 hpi in both cell lineages studied, the number of phagocytes containing ≥ 100 *S. aureus* increased. This could indicate intracellular growth of bacteria inside those

phagocytes, and *S. aureus* has the potential to replicate intracellularly (Schnaith *et al.*, 2007, Grosz *et al.*, 2014), it can also become internalised as larger groups of cells. Also, a fraction of initially phagocytosed bacteria could escape back to the bloodstream and become internalised again. Extracellular growth, or re-internalisation into phagocytes which already contain large amount of *S. aureus*, could therefore cause their increased intracellular abundance.

A large proportion of neutrophil did not contain bacteria at 24-28 hpi time point even in the presence of extracellular pathogen. This finding seems important as neutrophils are supposed to play a crucial role in immune defence of zebrafish larvae. Thus, it raised a question whether neutrophils become incapable of internalising *S. aureus* at the later stages of infection. The re-injection experiment confirmed internalisation ability of neutrophils 20 hpi. Therefore my study shows that during the final dissemination of the *S. aureus* cells, their potential to avoid internalisation by bloodstream phagocytes is not related to neutrophils phagocytic inactivity.

The infection rates of professional phagocytes were determined using various microscopy approaches. The infection and internalisation rates seemed to be increased in high magnification study, compared to the whole body study for both neutrophils and macrophages. This is likely caused by the fact that acquisition in high magnification is performed close to the injection site, yolk circulation valley. For the study of *S. aureus* bacteraemia it is important to observe presentation of the host cell - pathogen interaction occurring in the bloodstream. Increased infection rates help investigating pathogen interaction with cells. Additionally, yolk circulation valley has been chosen the main imaging site due to its optical accessibility. Therefore, high magnification allows precise quantification and forms grounds for microscopy experiments performed in this area, but concerning other aspects of pathogens intracellular fate.

Macrophages have been reported to be most important cells for the ingestion of *S. aureus* (Le Guyader *et al.*, 2008), although their further role in the infection can be diverse. It has been suggested by Prajsnar *et al.* (2008) that macrophages are capable of internalising larger numbers of bacteria compared to neutrophils, however, the exact numbers and internalisation rates in the zebrafish model remained to be

determined. Results of experiments performed during my study in neutrophil and macrophage reporter lines demonstrated that throughout the experiment macrophages internalised and contained more *S. aureus* than neutrophils. However, macrophages stored but did not necessarily kill internalised *S. aureus*. This potentially supports pathogen persistence, given that these immune cells are able to act as a reservoir of infection (Kubica *et al.*, 2008). The ability to survive in human cells is proposed to be one of the factors enhancing incidence of recurrent infections (Sendi and Proctor, 2009, Garzoni and Kelley, 2009). *S. aureus* cells surviving inside of the phagocytes can use them to disseminate within host organism (Schröder *et al.*, 2006a).

Additionally, it may be that *S. aureus* replicates within these cells. One of the components facilitating such use of immune cells is the cytoprotective effect of *S. aureus* phagocytosis on infected macrophages. For instance, anti-apoptotic activity and prolonged lifespan of host cell lead to them being perceived as a pathogen's "Trojan horse" (Koziel *et al.*, 2009).

Potential intracellular growth of SH1000 laboratory strain was assessed by microscopy-based observation of 1:1 mixed CFP and YFP inoculum dynamics, followed by quantification of colour proportion in phagocytes over time. The fraction of phagocytes containing 1:1 colour ratio reduces over the time course of experiment. This result implies that potentially the population skewing previously observed by Prajsnar *et al.* (2012) was initiated in phagocytes during the first hours of infection. The fraction of phagocytes containing only one from the *S. aureus* strains starts to grow by 6 hpi. Additionally the number of *S. aureus* contained in phagocytes of that group increases as well. This indicates that a process implied in the population skewing, occurs already before 6 hpi.

This important finding also suggests that microscopy approaches established during my study constitute a set of tools valuable for carrying out bacterial population dynamics study. These up to now could only be assessed by plating bacteria contained within the whole larvae, omitting important role of phagocytes in clonal expansion.

Potentially, it would be also interesting to follow the intracellular population dynamics in mixed inoculum created by re-injection. This could help elucidate whether the strain which was invading hosts organism first has an advantage over the one injected later.

Altogether the data presented in this chapter shows that neutrophils and macrophages interact with *S. aureus* in distinct ways, which initially is demonstrated by different internalisation and infection rates. Although population dynamic study strongly suggests that *S. aureus* niche is arranged inside of bloodstream phagocytes, it does not necessarily mean that the phagocyte, itself, constitutes one. Further experimental work presented in the following chapters aimed to determine possible factors enabling *S. aureus* to subvert immune cells and escape killing.

Chapter 4: Generation of the novel fluorescently tagged transgenic zebrafish reporters

4.1. Hypotheses and aims

4.1.1. Hypotheses

In my study the important hypothesis is that *S. aureus* subverts one of the internalisation and intracellular pathways to escape killing in professional phagocytes.

Macropinocytosis is a process used by several pathogens to enter the host cells (García-Pérez *et al.*, 2003; Watarai *et al.*, 2001). Autophagy is a process known to favour bacterial existence (Mostowy *et al.* 2011, Choy *et al.*, 2012) it has also been reported to allow *S. aureus* replication in non professional phagocytes (Schnaith *et al.* 2007).

In this chapter I hypothesise that macropinocytosis and/or autophagy have a role in *S. aureus* evasion of host killing.

4.1.2. Aims

Aims of experiments presented in this chapter:

- Determination of a useful macropinocytosis marker.
- Generation of fluorescent reporter transgenic line to study macropinocytosis.
- Generation of stable lines expressing fluorescent LC3 autophagy reporter under neutrophil and macrophage specific promoters.
- Functional characterisation of *Tg(lyz:RFP.GFP.LC3)* and *Tg(mpeg:RFP.GFP.LC3)* lines.

4.2. Sorting nexin 1 macropinosome maturation reporter

4.2.1. Introduction

Virtually all cells are capable of engaging in macropinocytosis. This process allows a cell to engulf large amounts of extracellular liquid and is performed independently of solid cargo. Despite its non-selective nature, macropinocytosis may cause internalisation of bacterial cells and has been implied in host cell uptake of pathogens, for example *Mycobacterium tuberculosis* and *Legionella pneumophila* (Watarai *et al.*, 2001, García-Pérez *et al.*, 2003). I hypothesise that *S. aureus* is able to subvert the macropinocytosis internalisation pathway to avoid intracellular killing in professional phagocytes. Macropinocytosis is a compelling alternative pathway of *S. aureus* uptake, due to its known involvement in other bacterial infections, as well as its potential to establish intracellular compartments where bacteria can escape killing. Macropinosomes containing neutral extracellular liquid would therefore provide *S. aureus* a niche for prolonged persistence in phagocytes, with potential for subsequent replication or escape from innate immune cells.

S. aureus populations can undergo clonal expansion inside of zebrafish larvae (Prajsnar *et al.*, 2012). It was shown, that when embryos were injected with 1:1 ratio of two isogenic *S. aureus* strains, in 30 % of individuals only one of those would gain an advantage, grew into an abscess and led to host death. Presence of professional phagocytes, neutrophils and macrophages, was necessary for this significant population variance to occur (Prajsnar *et al.*, 2012). Study performed in neutrophil- and macrophage-ablated larvae suggested, that neutrophils may be responsible for the immunological bottleneck. However, clonal expansion also suggests, that a fatal infection is often caused from the growth of a small number of bacteria. Prajsnar *et al.* (2012) postulated, that the host offers a limited number of niches, facilitating one or a few *S. aureus* cells to subvert the host defence mechanism. I aimed at address the question of whether an alternative uptake pathway may be involved in this large, phagocyte-related population variance. Macropinocytosis has already been suggested to constitute an alternative *S. aureus* internalisation route in polymorphonuclear neutrophils (Gresham *et al.* 2010), however the result has never been confirmed in an *in vivo* model. The generation of transgenic lines with

macropinocytotic vesicles marked with fluorescent protein was therefore useful to follow the previous study on *S. aureus* population dynamics (Prajsnar *et al.*, 2012). The existence of phagocyte-specific promoters allowed to design this study in neutrophils, but also in macrophages. Although it is known that macrophages perform macropinocytosis constitutively, no study has been performed to specifically look at the involvement of macropinocytic internalisation by these cells during infection. Given that the infection model used in this study mimics systemic infection caused by *S. aureus* present in the bloodstream, it was also important to determine if macrophages uptake bacteria via macropinocytosis.

The work presented in chapters 5 and 6 uses a number of measures of the volume of bacteria-containing vesicles and their acidification rates to demonstrate different modes of *S. aureus* internalisation and intracellular trafficking in professional phagocytes. However, none of these methods has yielded unequivocal results confirming or excluding macropinocytosis as an alternative uptake pathway. Therefore, there was a need to create a new tool to stably and specifically label macropinosomes in an *in vivo* model suitable for dynamic imaging.

To image the internalisation of bacteria by macropinocytosis *in vivo*, it was important to create a fluorescently tagged reporter line. The uptake of *S. aureus* by professional phagocytes is a dynamic process and takes place in a relatively short time (often less than 20 minutes post infection). It was therefore important to establish an efficient method allowing to distinguish innate immune system cells of interest for well-targeted high resolution imaging. I decided to generate two cell-specific lines, one to label macropinocytosis in neutrophils and the other in macrophages, where the construct would be expressed under *lyz* and *mpeg1* promoters, respectively.

During bacterial uptake, macropinocytosis does not require specific components which would unequivocally differ it from phagocytosis. This is mainly because membrane reorganisation is actin dependent in both cases, and thus finding the appropriate protein to uniquely label macropinosomes was the most challenging part of vector design. While both macropinosomes and phagosomes are capable of fusing with lysosomes, the maturation and intracellular pathways of both are performed in a different manner. Sorting nexins (SNX), a large family of proteins containing the

Phox domain (PX), are associated with the regulation of endocytosis, degradation and intracellular sorting of vesicles (Cullen, 2008). SNX family members are present in all eukaryotes, ranging from yeast to mammals, and out of 33 SNX family genes, SNX1 was discovered first, as a protein required for the lysosomal degradation of epidermal growth factor receptor (Kurten *et al.*, 1996). The SNX family members have also been shown to regulate macropinosome formation and are particularly related to that type of endosome, differentiating it from phagosomes. SNX1 and SNX5 are leading components of the maturation process, acting within the first 0 – 5 minutes post macropinosome formation and maturation (Lim and Gleeson, 2011). I therefore decided to use them in order to label macropinosomes in zebrafish.

4.2.2. Gateway® Three-Fragment Vector Construction

In this study pDEST(*lyz:mTurquoise.snx1*) and pDEST(*mpeg:mTurquoise.snx1*) vectors were generated with use of the Tol2Kit (Kwan *et al.*, 2007). This method of transgenic vector construction is based on the Gateway™ recombination system (Invitrogen, (Walhout *et al.*, 2000), which consists of two recombination steps, BP and LR reaction. The first step concerns the generation of an entry clone, by the recombination of AttB sites flanking the sequence of interest with AttP sites of a donor vector using the BP clonase enzyme. Successful recombinants can be selected due to kanamycin resistance encoded in plasmid. The second stage is the LR reaction, which allows the recombination of AttL and AttR sites using LR clonase in order to generate the final expression vector. Vector selection is facilitated by ampicillin resistance. Non-recombined empty donor vectors and plasmids will not be expressed in competent cells, as they carry *ccdb* suicide gene between the att recombination sites, removed only as a result of recombination (Bernard and Couturier, 1992). The complete construct contains the 5' insert, a promoter driving the remaining sequence encoded downstream, a middle entry insert and 3' insert. Such tools provide a very powerful system for a construction of vectors with a variety of promoters, and reporters expressed together with a gene of interest. The modification of entry clones and possible fusion of two proteins under a tissue specific promoter enables the fluorescent labelling of a protein in a defined range of

zebrafish structures/development-related sites/population of cells. Therefore, the Tol2Kit was generated based on Gateway™ to allow easy transposition of the destination vector into the zebrafish genome. This was performed by inserting Tol2 transposable elements on either side of the Att recombination sites of the destination vector (Kwan *et al.*, 2007).

4.2.3. Cloning and fluorescently tagged SNX1 mTurquoise vector construction

Macropinocytosis is usually considered a non-regulated process and its regulation, as well as processes involved in macropinosome formation, has only been studied relatively recently. PI3-kinase, Ras, Rac1, Cdc42 and sorting nexins are examples of potential macropinocytotic regulators (Lim and Gleeson, 2011). Members of the sorting nexin family were studied in order to determine their role in macropinosome formation. 5 out of 12 proteins screened: SNX1, SNX5, SNX9, SNX18 and SNX33 were found to increase macropinosome formation upon their overexpression (Wang *et al.* 2010). Among those proteins, SNX5 is currently the best characterised. Its subcellular localisation has been identified by the generation of HEK293 cells expressing SNX5 protein fused to GFP (Merino-Trigo *et al.* 2004). Epidermal growth factor stimulation of these cells resulted in the formation of large SNX5 positive endosomal structures, described as macropinosomes (Kerr *et al.*, 2006). During the maturation of macropinosomes, SNX5-labelled tubules were dynamically extended, and subsequently the surface area of the macropinosome was reduced (Kerr *et al.*, 2006). Further maturation steps comprised macropinosome transition into Rab7-positive vesicles, followed by its fusion with late endosomes/lysosomes. The lipid binding PX domain of SNX5 binds preferentially to PI(3)P and PI(3,4)P₂, and the BAR domain has been hypothesised to act as a membrane deforming factor (Peter *et al.*, 2004, Merino-Trigo *et al.*, 2004, Carlton *et al.*, 2004). Both are typical for sorting nexins, and the latter could possibly form complexes with other sorting nexins such as SNX1, in order to regulate the extension of tubular elements (Kerr *et al.*, 2006, Carlton *et al.*, 2004).

Although the important role of SNX5 in the regulation of macropinocytosis has already been shown (Lim *et al.*, 2008), little is known about the specific steps of the process, nor the role of other 4 SNX proteins. Moreover, it is difficult to anticipate possible rearrangements in macropinosome formation and changes in its trafficking in relation to bacterial infection. Therefore in my study I first considered all 5 sorting nexins as a possible marker of macropinosomes.

The phylogenetic analysis presented on the tree graph (Figure 4.1.) suggests that the evolution of these particular sorting nexins appears to occur prior to the divergence of the tetrapod lineage from fish. Initially I decided to aim for the generation of SNX1 and SNX5 transgenic reporter lines, because the two sorting nexins family members were best described in the literature and seemed to play an important role in macropinosome maturation. Cloning of the SNX5 did not result in obtaining correct sequence, possibly due to a poor primer specificity. However, both proteins – SNX1 and SNX5 – possibly have similar function in macropinosome maturation and intracellular signalling (Lim and Gleeson 2011). Therefore I continued the generation of the transgenic line using only the SNX1 protein.

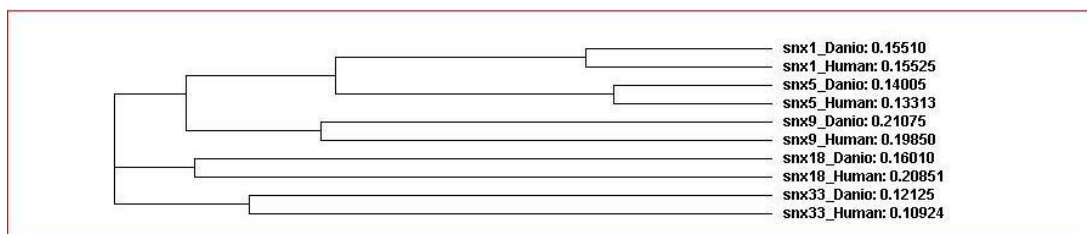


Figure 4.1. Sorting nexin phylogenetic tree.

The phylogenetic analysis of 5 sorting nexins potentially involved in macropinosome formation. The evolution of particular sorting nexins probably occurred prior to the divergence of the tetrapod lineage from fish. The generation of the transgenic line was performed for the SNX1 protein.

Two transcripts of SNX1 were found in Ensembl database (Zebrafish Zv9): *snx1a* and *snx1b*. Those were compared with the use of ClustalW against *Danio rerio* SNX1 transcript found in the NCBI database. The cluster shows very good conservation of *snx1a* transcript compared to the one found in the NCBI database, and therefore this transcript was chosen for further work (Figure 4.2.). Similarly, human SNX1 transcript was analysed against the *Danio rerio* sequence showing good conservation, probably indicating important function of the protein as evolution has not changed it (Figure 4.3.). However, as 5' of the transcript tends to diverge more, additional analysis of the encoded domains was performed in BLAST. Although the SNX domain is recognised as SNX1, it is less conserved than the BAR and PX domains of the protein (Figure 4.4.). Both conserved domains have functional significance, for instance SNX5 recruits to the cytoplasmic side of plasma membrane via its PX domain, and the levels of surface SNX5 are related to the activity of macropinocytotic uptake. By analogy, in SNX1 the PX domain could potentially mediate association to the early macropinosome. The BAR domain has been suggested to have a direct role in membrane deformation and in the formation of sorting nexins complexes (Teasdale *et al.*, 2001, Carlton *et al.*, 2004). Given the information above, both conserved domains are the ones likely to be functioning in membrane dynamics, thus the zebrafish SNX1 protein had a potential to usefully label the macropinosome regardless of the difference in its SNX1 domain.

```

CLUSTAL 2.1 multiple sequence alignment

snx1-201_Ensembl_ENSDART000000    MAASSERSPPFPDSEEPLELDSDEGADAFGTISISEMDSPPDTHGS 50
snx1_NCBI_NP_001122143.2          MAASSERSPPFPDSEEPLELDSDEGADAFGTISISEMDSPPDTHGS 50
snx1_zgc_114075-201_ENSDART000    MSGSCGRNPPFPDNE---LE-----AIDARVLDSDDE- 32
*:.*.*****:* **                :*: * :

snx1-201_Ensembl_ENSDART000000    KDIFSDPAEDIFSDPLSDINSEPKKNSDVKIPSPASDEAVDLFSDPLDDD 100
snx1_NCBI_NP_001122143.2          KDIFSDPAEDIFSDPLSDINSEPKKNSDVKIPSPASDEAVDLFSDPLDDD 100
snx1_zgc_114075-201_ENSDART000    -----DEGEDIFG-----ARSKPTTPTSAPDEG-DIFSE----- 61
* .*****: .                .*. . :*: * :

snx1-201_Ensembl_ENSDART000000    EPSEMSSPEVQNFVPDLSNEPAEFPKSDNKKPIFEPAKVKGKAASSELFD 150
snx1_NCBI_NP_001122143.2          EPSEMSSPEVQNFVPDLSNEPAEFPKSDNKKPIFEPAKVKGKAASSELFD 150
snx1_zgc_114075-201_ENSDART000    EGSYIRS----- 68
* * : *

snx1-201_Ensembl_ENSDART000000    DDEDLFQESFKFVKPKQASVPLDVYEVKVKPKVQKDDPTDLFTFEALT 200
snx1_NCBI_NP_001122143.2          DDEDLFQESFKFVKPKQASVPLDVYEVKVKPKVQKDDPTDLFTFEALT 200
snx1_zgc_114075-201_ENSDART000    -----

snx1-201_Ensembl_ENSDART000000    PPASKPAANTRINGVHS-EEQDLFSEATVELSLDSPHNDRKKKKSVNPSV 249
snx1_NCBI_NP_001122143.2          PPASKPAANTRINGVHS-EEQDLFSEATVELSLDSPHNDRKKKKSVNPSV 249
snx1_zgc_114075-201_ENSDART000    -----DVHHTINGLHSDLELDLFEATVELLINTIS-QGRREIIGPTA 111
. : **:* ** **:*:*****: * . . . : : : :*:

snx1-201_Ensembl_ENSDART000000    SAP-AAPVASSSSKP--PSKILEEEEESEDKFDLNVSIINPEKVGDM 296
snx1_NCBI_NP_001122143.2          SAP-AAPVASSSSKP--PSKILEEEEESEDKFDLNVSIINPEKVGDM 296
snx1_zgc_114075-201_ENSDART000    SACNTHVPSILKPSIVTKMEELEEEESGDQFELNIAVTNPEKIGDM 161
** : * . * ** :*:***** * :*:*:*:*:*:*:*:

snx1-201_Ensembl_ENSDART000000    NAYMVYKVESTQTSLSMFRSKITVRRRFSDFLGLYEKLEKHSQNGYIVP 346
snx1_NCBI_NP_001122143.2          NAYMVYKVESTQTSLSMFRSKITVRRRFSDFLGLYEKLEKHSQNGYIVP 346
snx1_zgc_114075-201_ENSDART000    TAYMSYKVESTQITLPMFANKITVRRRFSDFLGLYERMSAKNSLMGCIIIP 211
.*** *****:*.** .*****:*****:* *:* * *:*

snx1-201_Ensembl_ENSDART000000    PPPEKSIIMGMTKVKVKGEDPSSAEFVERRRAALERYLQRVVSHPSLLQDP 396
snx1_NCBI_NP_001122143.2          PPPEKSIIMGMTKVKVKGEDPSSAEFVERRRAALERYLQRVVSHPSLLQDP 396
snx1_zgc_114075-201_ENSDART000    PAPQKSVVGMTKVKVKGEDSSSAEFVEKRAALERYLQRVVAHPSLLQDP 261
* :*:*:*****:*****:*****:*****:*****:

snx1-201_Ensembl_ENSDART000000    DVREFLEKEELPRAVSTQTLGAGFLKMLNKAIDAVSKMIIKMQDQVWF 446
snx1_NCBI_NP_001122143.2          DVREFLEKEELPRAVSTQTLGAGFLKMLNKAIDAVSKMIIKMQDQVWF 446
snx1_zgc_114075-201_ENSDART000    DVREFLERDELPRVNTQTLGSGPGLKMINRASDAVNKMTIINKINESDNWF 311
*****:*****.*****.*:***:*:*:***.*****:* **

snx1-201_Ensembl_ENSDART000000    DEKIQDVENEEQLLRKLVHVMVESLVNHRKELSGNTAAFAKSVAMLGSSD 496
snx1_NCBI_NP_001122143.2          DEKIQDVENEEQLLRKLVHVMVESLVNHRKELSGNTAAFAKSVAMLGSSD 496
snx1_zgc_114075-201_ENSDART000    ESKLQEVENEEQLLRRLHAAVDSLVNHRKELCINTAVFSKSVAMLGSSVEE 361
.:*:*:*****:*. * :*****. ***.*:***** *

snx1-201_Ensembl_ENSDART000000    NTALSRLSQLAEVEDRIEQLHRDQAANDFFTFAELLADYIRLLGAVRGC 546
snx1_NCBI_NP_001122143.2          NTALSRLSQLAEVEDRIEQLHRDQAANDFFTFAELLADYIRLLGAVRGC 546
snx1_zgc_114075-201_ENSDART000    NSALSRLSQLAEVEDKMEQLHQQAFAFDFFILAELLADYVRLGAVRCC 411
*:*****:*****:***.*** :*****:***** *

snx1-201_Ensembl_ENSDART000000    FDQRMKAWQRWQDAESMLQKKREAEAKLLWANKPKLQQAQKDEIAEWEAK 596
snx1_NCBI_NP_001122143.2          FDQRMKAWQRWQDAESMLQKKREAEAKLLWANKPKLQQAQKDEIAEWEAK 596
snx1_zgc_114075-201_ENSDART000    FEQRMKAVQRLQEAQITLQKKREAEAKLLWANKPEKLQQAQKDDINEWESK 461
*:***.*** *:* :*****:*****:*****.* **:*

snx1-201_Ensembl_ENSDART000000    VTQYERDFERISATVQKDVIRFDKKEKARDFKRQIIKYLESLLSQQQLIK 646
snx1_NCBI_NP_001122143.2          VTQYERDFERISATVQKDVIRFDKKEKARDFKRQIIKYLESLLSQQQLIK 646
snx1_zgc_114075-201_ENSDART000    VSQYERDFERVTCIVRKEVLRFE----- 484
*:*****:*.***:*:***:

snx1-201_Ensembl_ENSDART000000    YWEAFLPEAKAIA 659
snx1_NCBI_NP_001122143.2          YWEAFLPEAKAIA 659
snx1_zgc_114075-201_ENSDART000    -----

```

Figure 4.2. ClustalW analysis of snx1a and snx1b (source ZFIN, Zebrafish Zv9) and *Danio rerio* SNX1 (NCBI) transcripts.

Snx1a (ENSDART00000075184) is the top sequence; *Danio rerio* SNX1 (NP_001122143.2) middle sequence; Snx1b (ENSDART00000104763) bottom sequence.

Two transcripts of SNX1 a and b, found in Ensembl database (Zebrafish Zv9) were compared in ClustalW against *Danio rerio* SNX1 transcript found in the NCBI database. Good conservation of snx1a transcript was shown compared to *Danio rerio* SNX1 transcript.

CLUSTAL 2.1 multiple sequence alignment

```

snx1_Danio      MAAS-----SERSPPFPDSEEPLEDSDEGADAFGTGTSISEMDSPPDITGHSKDIF 54
snx1_Human     MASGGGGCSASERLPPFPFG-----LEPESEGAAGG-----SEPEAGDSDETEGE--DIF 47
                **:.      *** *****.      ** ..*** .      ** :: .** *.  ***

snx1_Danio      SDPAEDIFSDPLSDINSEPKKNSDVKIPSPASDEAVDLFSDPLDDDEPSEMSSPEVQNFV 114
snx1_Human     TG-----A-AVVSKHQSPKITTSL 65
                :.      * : .**:: ...

snx1_Danio      PDLSEPAEPPKSDNKKPIFEPAAKVKAASSELFDDDEDLFQESFKFVIKPKQASVPPL 174
snx1_Human     LPINNGSKE-----NGIHE-----EQDQ----- 83
                :.* . *      : *.*      :*:

snx1_Danio      DVYTEVVKVKPQVKDDPTDLFTEEALTPPASKPAANTRTINGVHSEEQDLFSEATVELSLDS 234
snx1_Human     -----EPQDLFADATVELSLDS 100
                * ****:*****

snx1_Danio      PHNDRKKKDSVNPVSAPAAPVASSSSKPPSKTLEEEEEESEDKFDLNVISITNPEKVG 294
snx1_Human     TQNNQKK---VLAKTLISLSPQEAATNSSKQPITYEELEEEEQEDQFDLTVGITDPEKIG 157
                .:*** * ... .:* :*. * * *****.***:***.*:***:***

snx1_Danio      GMNAYMVYKVSTQTSLSMFRSKFTVRRRFSDFLGLYEKLEKHSQNGYIVPPPEKSIM 354
snx1_Human     GMNAYVAYKVTITQSLPLFRSKQFAVKRRFSDFLGLYEKLEKHSQNGFIVPPSPEKSLI 217
                *****:***:*****.:*** *.:*****:*****:*****:*****:

snx1_Danio      GMTKVKVGKEDPSSAEFVERRAALERYLQRVVSHPSLLQDPDVREFLEKEELPRAVSTQ 414
snx1_Human     GMTKVKVGKEDSSSAEFLEKRRALERYLQRIVNHPTMLQDPDVREFLEKEELPRAVGTQ 277
                *****:*****:*****:*****:*****:*****:*****:

snx1_Danio      TLGAGFLKMLNKATDAVSKMTIKMNEQDVWFDEKIQDVENEQQLLRKHLHVMVESLVNHR 474
snx1_Human     TLGAGLLKMFNKATDAVSKMTIKMNESDIWFEEKLQVEVECEEQLRKLHAVVETLVNHR 337
                *****:***:*****:*****:*****:*****:*****:*****:

snx1_Danio      KELSGNTAAFAKSVAMLGSSDNTALSRLSQLAEVEDRIEQLHRDQAANDFFTFAELLA 534
snx1_Human     KELALNTAQFAKSLAMLGSSDNTALSRLSQLAEVEEKIEQLHQEQANNDFFLLAELLS 397
                ***: *** *****:*****:*****:*****:*****:*****:

snx1_Danio      DYIRLLGAVRGCFDQRMKAWQRWQDAESMLQKKREAEAKLLWANKPDKLQQAQKDEIAEWE 594
snx1_Human     DYIRLLAIVRAAFDQRMKTWQRWQDAQATLQKKREAEARLLWANKPDKLQQAQKDEILEWE 457
                *****: * .*****:*****: *****:*****:*****:*****

snx1_Danio      AKVTQYERDFERISATVQKDVIRFDKEKARDFKRQIIKYLESLLSHQQLIKYWEAFLPE 654
snx1_Human     SRVTQYERDFERISTVVRKEVIRFEKEKSKDFKNHVIKYLETLLYSQQQLAKYWEAFLPE 517
                :*****:*.:*:*****:*****:*****:*****:*****:*****

snx1_Danio      AKAIA 659
snx1_Human     AKAIS 522
                ****:

```

Figure 4.3. ClustalW analysis of human SNX1 and *Danio rerio* SNX1 transcripts.

Both transcripts were found in NCBI database. *Danio rerio* SNX1 (NCBI Reference Sequence: NP_001122143.2) and Human SNX1 (GenBank: AAC17182.1).

Human SNX1 transcript analysed against the *Danio rerio* sequence showing good conservation.

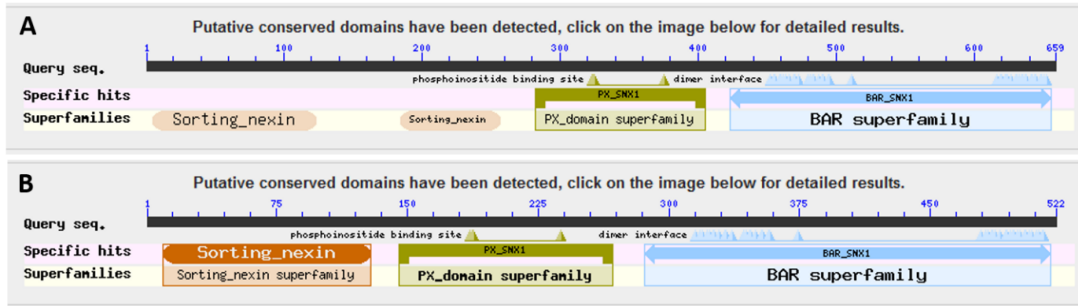


Figure 4.4. Protein blast analysis of *Danio rerio* SNX1 and Human SNX1 transcripts.

BAR and PX domains of the protein are well conserved. Both conserved domains have functional significance, in sorting nexins recruitment and membrane dynamics.

A. *Danio rerio* SNX1

B. Human SNX1

4.2.4. Fusion protein expression and embryo screening

pDESTcry:CFP(*lyz:mTurquoise.snx1*) was injected into LWT wild type embryos alongside *tol2* transposase mRNA. Transformed embryos were screened at 1-2 dpf and positive embryos were selected based on the expression of the blue eye marker. 30 positive embryos were selected for raising and after 2 – 3 months each fish was outcrossed by pairing with a wild type LWT. The progeny were screened to determine whether any of the raised fish could be a potential founder. 3 potential founders have been designated, based on high percentage of eye marker-positive embryos in their offspring. Fluorescent signal from neutrophil cells could not be observed with the use of dissecting fluorescence microscope, thus I decided to image several eye marker-positive embryos using confocal microscopy. To shorten the acquisition time and limit the mounting and rescue procedures required in that type of imaging, I designed a method to immobilise anaesthetised fish without mounting them in agarose (see Materials and Methods). Offspring of the one of potential founders was confirmed to contain mTurquoise labelled cells circulating in the bloodstream.

Although those cells were similar in shape to neutrophils, as observed in *Tg(mpx:GFP)* (Renshaw *et al.*, 2006), I tested their ability to phagocytose bacteria. Intravenously injected bacteria are internalised by both neutrophils and macrophages, whereas those residing on solid surfaces are more likely to be phagocytosed by neutrophils (Colucci-Guyon *et al.*, 2011). Therefore, SH1000-GFP *S. aureus* was injected into the somite of 3 dpf embryo in order to increase neutrophil recruitment and phagocytosis. The expression of the SNX1 protein fused to mTurquoise in neutrophil cells could be visualised, although the signal was weak. However, adjusting laser gain sensitivity allowed the fluorophore to be visualised with 500 ms exposure time, simultaneously allowing the acquisition of good quality images. The observed mTurquoise-labelled protein seemed to form circular aggregates and colocalised with SH1000-GFP *S. aureus* (Figure 4.5.). Although the mTurquoise aggregates seemed to be distinct from the round-shaped *S. aureus* cells, one could speculate that those were an artefact, resulting from the similar spectra of mTurquoise and GFP, and the strong GFP signal of transgenic *S. aureus*.

The pDEST(*mpeg:mTurquoise.snx1*) construct was injected into LWT embryos alongside *tol2* mRNA to visualise expression. Similar screening procedures as described above were applied to screen *Tg(mpeg.mTurquoise.snx1)* embryos. Fluorescently labelled cells circulating in the bloodstream were identified in progeny of one potential founder (Figure 4.6.).

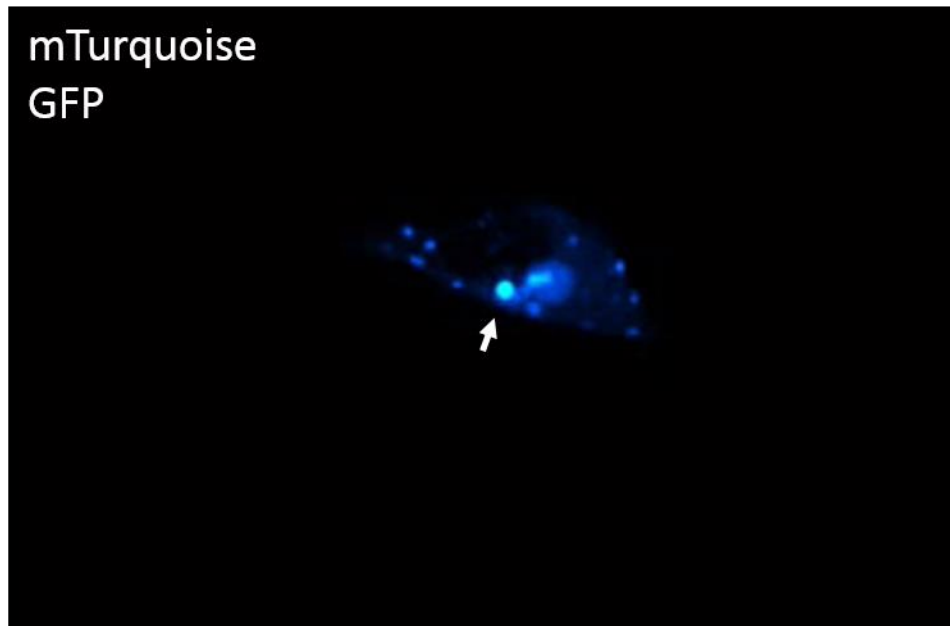


Figure 4.5. SH1000-GFP *S. aureus* co-localises with SNX1 in embryo injected with pDEST(*lyz:mTurquoise.snx1*).

Embryos were injected with pDEST(*lyz:mTurquoise.snx1*) construct at 1-4 cell stage and subsequently 3 dpf infected with 2500 CFU SH1000-GFP *S. aureus* strain injected into somite. Image shows one of the phagocytes recruited to the site of infection. These are predominantly neutrophils. Intracellular mTurquoise-labelled protein appears in smaller aggregates and co-localises with SH1000-GFP *S. aureus* (white arrow). 40x objective.

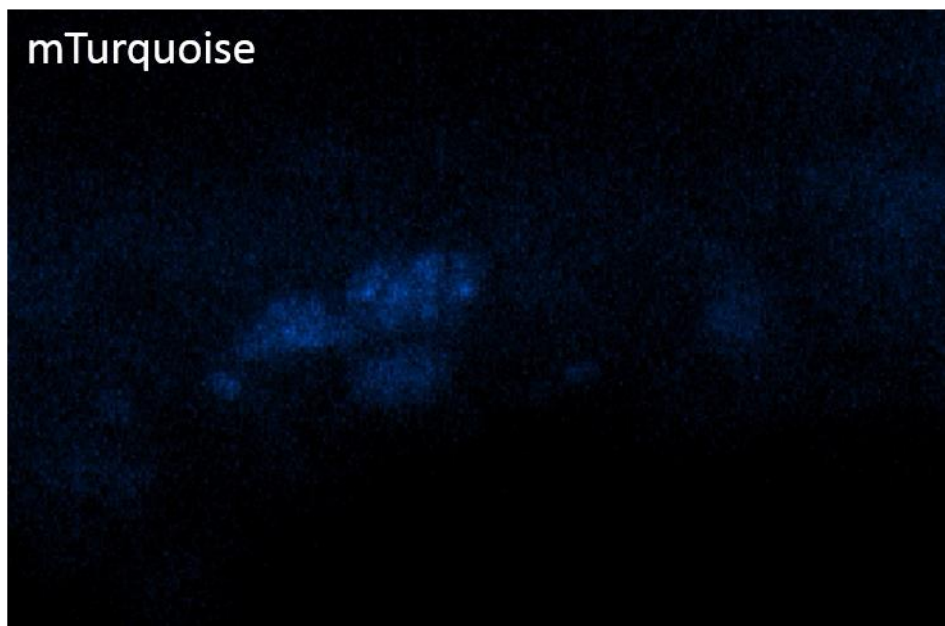


Figure 4.6. Fluorescently labelled cells circulating in the bloodstream of embryos from F1 *Tg(mpeg:mTurquoise.snx1)*.

Embryos were injected with pDEST(*mpeg:mTurquoise.snx1*) construct at 1-4 cell stage and subsequently imaged 3 dpf. Image shows one of observed phagocytes containing intracellular mTurquoise-labelled protein appearing in small aggregates. 40x objective.

4.2.5. Discussion

Tg(mpeg:mTurquoise.snx1) and *Tg(lyz:mTurquoise.snx1)* transgenic reporters of sorting nexin 1 were generated with the use of the Gateway™ system which allowed fusion with fluorescent protein mTurquoise and expression under two different promoters: neutrophil and macrophage-specific. The strategy included the use of “no-stop” mTurquoise as the middle entry clone and SNX1 as the 3’ insert and aimed to maintain the intracellular function and localisation of SNX1 protein and its domains. The correct insertion of the complete *snx1* coding sequence was confirmed by sequencing after performing BP recombination. Successful vector generation was confirmed and embryo transgenesis yielded an eye marker-positive larval population, which was confirmed to contain fluorescently labelled phagocytes. The result of transient expression of pDESTcry:CFP(*lyz:mTurquoise.snx1*) followed by *S. aureus* infection demonstrated the presence of fluorescent signal in intracellular aggregates. These structures are consistent with vesicles created during bacterial uptake, supported by their colocalisation with bacteria (Figure 4.5). Further generation of inbred F1 adults aimed to obtain homozygous embryos in order to potentially increase the number and brightness of labelled cells in embryo. Despite careful selection of positive embryos and engagement of high power microscopy in the process, there was a significant loss in quantity of cells and quality of fluorescence signalling in subsequent generations of fish. Particularly, the expression of the fluorescence marker was decreased, precluding the functional study and embryo infection microscopy due to prolonged exposure times. Enabling short exposure time is important in preserving a sample from bleaching, moreover in this study, it was crucial for a dynamic acquisition of *in vivo* internalisation process. Notably, macropinocytosis of single bacteria takes less than 10 seconds and the whole maturation process, from membrane engulfment to fusion with lysosomes can be completed within 8 - 20 minutes (Kerr *et al.*, 2006). Therefore imaging approaches are most informative when performed in real-time, and that requires high intensity fluorescence of the marker protein.

Although macrophages are known to perform macropinocytosis constitutively when they are sampling the extracellular environment (Carpentier *et al.*, 1991, Norbury *et*

al., 1995), macrophages of *Tg(mpeg.mTurquoise.snx1)* were shown to have less detectable fluorescence than neutrophils of *Tg(lyz:mTurquoise.snx1)* fish. There are a few possible reasons for decreased fluorescence of fused mTurquoise SNX1 fusion proteins. One possible reason is that the protein is not abundantly recruited during the regulation of macropinocytosis. Little is known about the regulation of macropinocytosis and the role that sorting nexin family plays in the process. Although we can suggest possible roles of the PX and BAR domains (Merino-Trigo *et al.*, 2004, Carlton *et al.*, 2004, Peter *et al.*, 2004), it is difficult to anticipate the role of individual sorting nexins. Additionally, we would have to assume that the longevity of a particular sorting nexin within the cell and on the macropinosome membrane could also vary between different sorting nexins. Depending on what role they play in macropinosome formation, maturation or tubular structure generation, the presence of a SNX1 protein could be transient, specific for a characteristic stage or solely associated in a temporary complex.

However, the cell-specific fluorescence seemed to be entirely lost in the maintained generations of *Tg(mpeg.mTurquoise.snx1)* line, despite presence of eye marker positive embryos in offspring. A plausible explanation for such outcome could be that the founder chosen for the stable line generation had two insertions of the transgene, and one of those was a partial insertion. The latter one would not contain the fused proteins of interest but only the CFP selection marker. Inbred F1 *Tg(mpeg.mTurquoise.snx1)* fish were outcrossed with LWT wild type and the impaired version would be inherited to the next generation. Additionally, the CFP marker coding sequence could be transferred alone to the next generation during a recombination event, and then the fused protein sequence would be replaced with the wild type gene part. However, it is very unlikely to occur due to the close proximity of the transgene and transgenic marker on the chromosome.

The quality of the fluorescence is also dependent on the fluorescence protein itself. Blue fluorescence variants are made after cloning GFP protein from *Aequorea Victoria* by mutagenesis (Tsien, 1998). Generally the perceived brightness of a fluorescent protein depends on several variable factors, such as the intrinsic brightness of the protein, the optical properties of the imaging setup and camera

sensitivity to the emission spectrum. Illumination wavelength and spectra of filters were specifically adjusted for the imaging on the confocal spinning disk microscope, although the system seems to be most efficient during the imaging of proteins of the GFP and RFP spectrum.

Sorting nexins have a great potential to constitute macropinosome maturation reporters, notably when fused to a fluorescent protein. The Tol2Kit allows efficient generation of an *in vivo* zebrafish model for the study of macropinocytosis and its role in pathogenesis. The flexibility of the system allows generation fluorescent protein variants of such model. Possibly, further investigation would result in determination of the most appropriate one, and the generation of a bright and precise macropinocytosis marker. Although the generation of transgenic reporter of the macropinocytotic uptake remains in progress, the findings described here will enable this work to be done in future.

4.3. LC3 autophagy reporter

4.3.1. Introduction

Autophagy is a catabolic mechanism of degradation aiming to remove unnecessary or dysfunctional cellular components through lysosomal activity. LC3 (protein light chain 3) is a microtubule associated protein encoded by the mammalian homologue of Atg8, involved in the later stages of autophagosome formation. In the majority of cell types it is first expressed as a full length protein which is further processed by proteolytic cleavage, upon autophagic machinery activation. Furthermore, the processed LC3-II is constantly recruited and integrated to the growing phagophore, making it a useful readout of the ongoing process. Therefore, LC3 protein has been widely used as a marker of autophagy (Klionsky, 2012; Mizushima *et al.*, 2010). It acts during the formation of autophagosomes, and its recruitment is an important step in the targeting of cargo designated for destruction. The autophagic process has an important role in eliminating pathogens mediated by PGRP receptors that recognise bacterial peptidoglycans (Yano *et al.*, 2008). Different TLRs induce signalling upon binding pathogen-derived ligands to trigger autophagy during the innate and adaptive immune response (He and Klionsky, 2009). LC3 is present during the processing of cytoplasmic debris, including bacteria-related targets, additionally it associates with phagosome membranes upon infection-triggered TLR signalling (Huang *et al.*, 2009). Altogether, this indicates that LC3 is also a good marker for infection-related autophagy.

The zebrafish model allows us to increase our understanding of the application of autophagic mechanisms in an *in vivo* model. This is essential in investigating host-pathogen interactions, and an animal model offers the involvement of the whole innate immune system. Zebrafish LC3, similar to mammalian LC3, is an Atg8 homologue, and the use of zebrafish GFP-LC3 transgenic lines have been previously described: methods such as LC3-immunoblotting, LysoTracker staining and transiently expressed GFP-LC3 microscopy, were validated for the analysis of autophagy in this model (He and Klionsky, 2010). GFP-LC3 confocal fluorescence microscopy has resulted in the observation that LC3 is largely cytosolic under normal conditions and after rapamycin induction of autophagy localises to distinct puncta

(He and Klionsky, 2010). The zebrafish LC3 transgenic line has also been used to study host-pathogen interaction (Mostowy *et al.*, 2013). Several bacterial pathogens, including *L. monocytogenes*, *M. marinum* and *S. flexineri*, have been shown to translocate from the phagosome to cytosol, where they are recognised by the autophagy pathway. These processes have also been studied in known zebrafish infection models (Levraud *et al.*, 2009). The above suggests that experiments in zebrafish have the potential to help elucidate mechanisms of pathogenicity for those organisms, including the subversion of autophagy. Moreover, the study of *S. flexineri* infection has shown that zebrafish constitute a valuable system to observe pathogen clearance in relation to the autophagic machinery (Mostowy *et al.*, 2013). Additionally, the relatively low temperature used for zebrafish husbandry did not impair *S. flexineri* virulence factors required for bacterial escape from the phagosome and replication in the cytoplasm. GFP tagged LC3 was shown to be recruited to intracellular *Shigella spp.*, validating the applicability of transgenic zebrafish larvae in investigating the *in vivo* manipulation of autophagy by the pathogen (Mostowy *et al.*, 2013).

The involvement of autophagy in *S. aureus* infection has never been studied in an *in vivo* model. Studies performed in infected epithelial cell lines show that *S. aureus* invasion of non-phagocytic cells is autophagy-related. Schnaith *et al.* (2007) suggest that *S. aureus* cells are encapsulated by autophagosomes while in a transition process. Instead of resulting in bacterial degradation, this encapsulation allows them to survive and replicate in a protective niche. Escape to the cytoplasm and eukaryotic cell death is the final outcome of such interaction. Thus, based on the data, it has been suggested that autophagosomes provide the means of escape of *S. aureus*, giving another possible hypothesis for its successful pathogenicity (Schnaith *et al.*, 2007).

The zebrafish *S. aureus* infection model has been established in Sheffield, providing a great tool to study the systemic infection and bacterial population dynamics in a living organism (Prajsnar *et al.*, 2008, 2012). As discussed above, the zebrafish larvae model is a useful tool to study the interaction of the autophagy process with the pathogen *in vivo* (Mostowy *et al.*, 2013). Therefore, we aimed to create a transgenic

line expressing a fluorescently tagged zebrafish LC3 reporter, and use it to investigate the role of autophagy in *S. aureus* infection.

It has been suggested that *S. aureus* autophagosome-like vesicles were created in infected human tumour cells in response to inhibited functionality of the lysosomal compartment (Mauthe *et al.*, 2012). *S. aureus* was captured in phagosome-like vesicles and its presence stimulated a response in which Atg5 and LC3 were recruited upon binding of WIPI-1 to PtdIns(3)P at the phagophore (Mauthe *et al.*, 2012). Thus WIPI-stimulation lead to selective autophagy occurring even in nutrient-rich conditions. Such interaction was proposed to be initiated by the growth of intracellular *S. aureus*. Phagophore membranes of endoplasmic reticulum became WIPI-1 positive to trigger sequestering of bacterial cells, while they were using their niche to replicate. Subsequently, *S. aureus* particles were trapped in autophagosome-like vesicles. LC3-II is bound to both the internal and external membranes of the autophagosome, which enables it to play role in hemifusion of membranes and in targeting cargo for degradation. This also means that LC3 may be exposed to intracellular compartments of different acidification levels. Thus, labelling LC3 protein with both RFP and GFP in tandem allows indication of low pH, as GFP becomes quenched in acidified compartments but RFP does not (Kimura *et al.*, 2007). Therefore we decided to use a pDestCMV:RFP.GFP.LC3 (Schiebler *et al.*, 2015) plasmid to generate macrophage and neutrophil-specific transgenic zebrafish lines.

4.3.2. Fusion protein expression and embryo screening

pDEST(*lyz*:RFP.GFP.LC3) was injected into LWT wild type embryos alongside *tol2* transposase mRNA. Offspring were screened at 1 dpf in order to select potential founders. The expression vector carried the GFP heart muscle selection marker, however, in a fraction of heart marker-positive embryos, strongly fluorescent bloodstream cells were also detectable under a dissecting fluorescence microscope. pDEST(*lyz*:RFP.GFP.LC3) injections into LWT embryos were repeated in order to determine function of fluorescent cells and verify their ability to internalise *S. aureus*.

SH1000-GFP *S. aureus* bacteria were injected into the bloodstream of 30 hpf larvae and imaged at 1 hpi to allow the time for bacteria uptake by bloodstream innate immune cells. When a similar method was used to study internalisation of bacteria performed by neutrophils of *Tg(lyz:mTurquoise.snx1)* line embryos, the infection route was changed to muscle somite injection in order to allow higher numbers of neutrophils to be recruited to the site of infection. However, embryos transiently expressing the vector seemed to have strong fluorescence signal in circulating cells, hence I decided to perform the experiment using the standard intravenous injection approach.

This imaging demonstrated that a fraction of immune cells was fluorescently labelled and able to internalise injected SH1000-GFP (Figure 4.7.). The presence of unlabelled cells could be explained by the mosaic expression within the neutrophil population of the transiently injected embryo. However, it is possible the non-fluorescent phagocytes are macrophages - supported by the higher numbers of internalised bacteria (see chapter 3 for internalisation rates). Although the fluorescence inside the cells was ubiquitous, protein aggregates of different shapes could also be distinguished. Fluorescent structures best described as puncta and circular vesicles are often related to autophagic mechanisms, where LC3 is recruited to phagosomal membranes and intracellular pathogens.

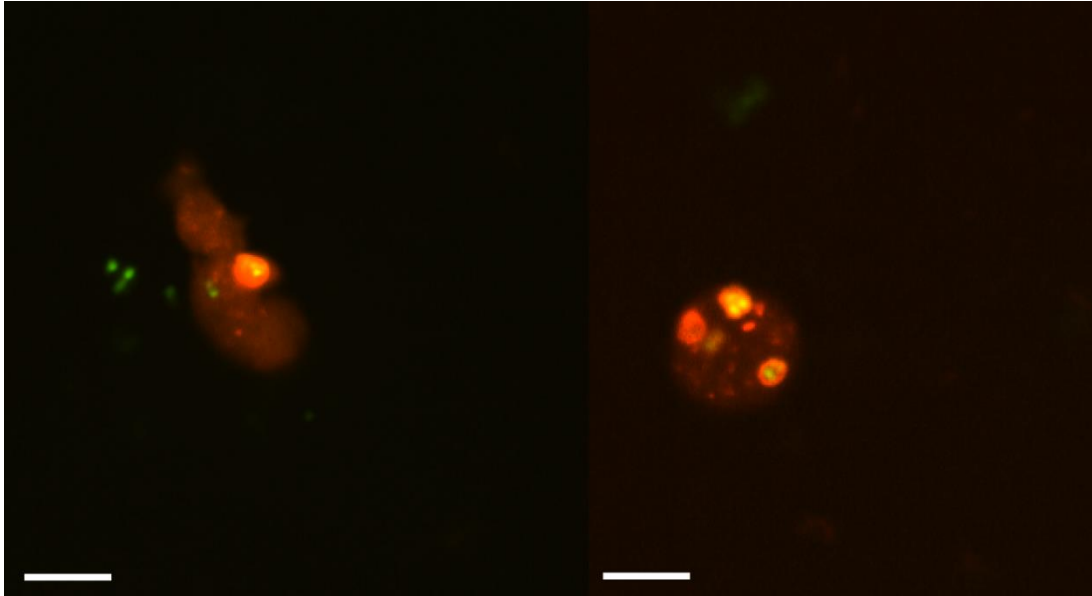


Figure 4.7. pDEST(*lyz:RFP.GFP.LC3*) expression in neutrophils of embryos injected with SH1000-GFP.

Embryos were injected with pDEST(*lyz:RFP.GFP.LC3*) construct at 1-4 cell stage and subsequently 30 hpf infected with 2500 CFU SH1000-GFP *S. aureus* strain injected intravenously. Image shows LC3 positive structures associated with phagocytosed bacteria. (Scale bar 15 μ m). 40x objective.

Additionally, as shown in Figure 4.8, LC3 positive structures were fluorescent in both RFP and GFP channels. The GFP protein expression seemed to be less bright however in the case of this particular imaging experiment this could be caused by the relatively strong expression of *S. aureus* plasmid-encoded GFP signal. During the setup of these acquisition experiments, exposure times were adjusted to image the structure most strongly expressing a particular fluorophore. This occurs for example when two elements expressing the same fluorescence protein, or proteins of the same spectral class, are imaged simultaneously – here the GFP encoded on the bacterial plasmid and the GFP fused with LC3. Ideally, the custom settings of exposure time and laser gain are then tailored to a level that would allow visualisation of both sources of fluorescence signal, but not causing over-saturation of the image.

Interestingly, initial pictures taken in an embryo expressing the fluorescently labelled LC3 have demonstrated the complexity of interaction between this autophagy protein and *S. aureus* bacteria. Imaging and analysis of possible associations between this intracellular pathway and pathogen requires in-depth analysis of several z stack images taken of individual neutrophils (Figure 4.9.).

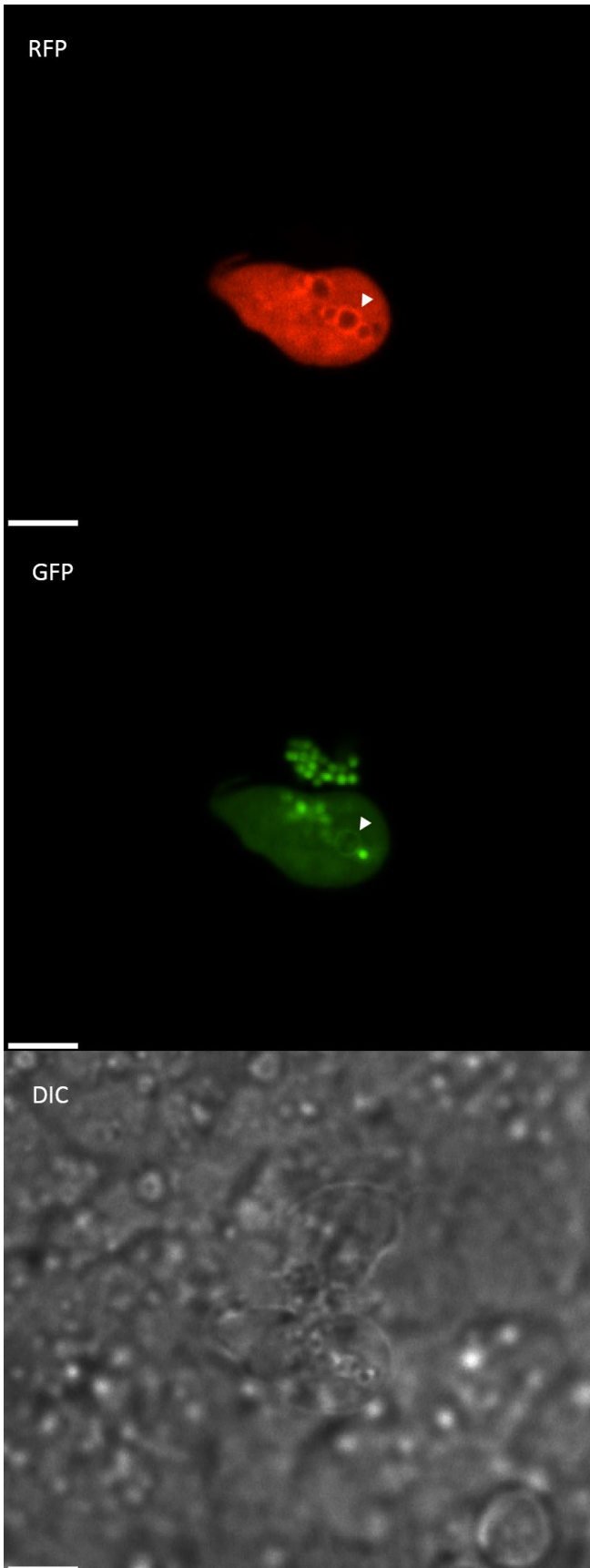


Figure 4.8. RFP and GFP expression in neutrophils of *pDEST(lyzC:RFP.GFP.LC3)* injected embryo infected with SH1000-GFP.

Embryos were injected with *pDEST(lyz:RFP.GFP.LC3)* construct at 1-4 cell stage and subsequently 30 hpf infected with 2500 CFU SH1000-GFP *S. aureus* strain injected intravenously. Image shows that LC3 aggregates were labelled with both RFP and GFP fluorescent proteins.

(Scale bar 10 μ m)

40x objective.

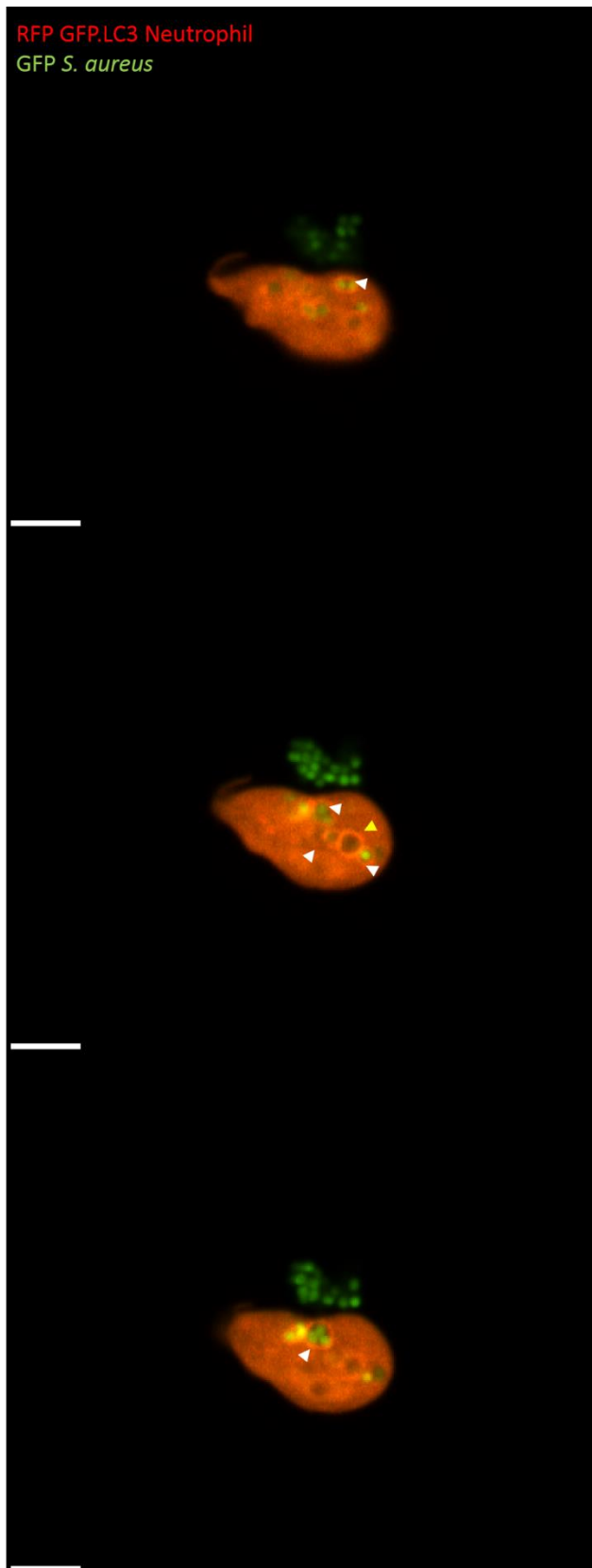


Figure 4.9. Imaging of several z stacks of a neutrophil in pDEST(*lyzC:RFP.GFP.LC3*) injected embryo infected with SH1000-GFP.

Embryos were injected with pDEST(*lyzC:RFP.GFP.LC3*) construct at 1-4 cell stage and subsequently 30 hpf infected with 2500 CFU SH1000-GFP *S. aureus* strain injected intravenously. Image shows that fluorescently labelled LC3 is recruited to intracellular *S. aureus*. Recruited LC3 forms structures around bacteria (white arrow heads).

LC3 can also be observed recruited to empty vesicles (yellow arrow head).

A group of green cells observed next to the neutrophil is internalised in a not labelled phagocyte, possibly macrophage.

(Scale bar 10 μ m)

40x objective.

pDEST(*mpeg:RFP.GFP.LC3*) was injected into LWT wild type embryos alongside *tol2* transposase mRNA and offspring was screened for GFP heart marker positive embryos 1 dpf in order to select potential founders. Unlike the screening of pDEST(*lyz:RFP.GFP.LC3*) injected embryos, only the green heart marker fluorescence was visible with the use of a dissecting fluorescence microscope. Thus a group of marker-positive embryos were selected and first analysed on a high power confocal microscope. To verify the presence of fluorescently labelled cells in the bloodstream and simultaneously assess their function in the immune system response, I performed the tail transection of 72 hpf embryos, followed by high power imaging of the site of injury. Injury would recruit cells and concentrate them in an easily imaged area. Fluorescently labelled cells were recruited 6 hours post injury (Figure 4.10.). Uninjured, heart marker positive embryos from the same batch were raised with the aim of screening for a founder and generating a stable transgenic line.

Fish from the stable *Tg(mpeg:RFP.GFP.LC3)* line were inbred in order to increase the quantity of labelled cells and quality of the fluorescence. Offspring of the F2 generation had brightly fluorescent macrophages circulating in the bloodstream 1 dpf, detectable also with the use of a dissecting fluorescence microscope. Selected larvae were injected with a standard 2500 CFU dose of wild type SH1000 and bloodstream cells were imaged on the confocal microscope to verify their ability to phagocytose bacteria. SH1000 cells were internalised into fluorescently labelled cells, morphologically similar to macrophages. The GFP fluorescence appeared to be quite ubiquitous in the cytoplasm of cells, whereas RFP labelled LC3 aggregated in puncta and colocalised with phagocytosed *S. aureus* (Figure 4.11.). This functional study formed the basis for further imaging experiments involving the *Tg(mpeg:RFP.GFP.LC3)* line.

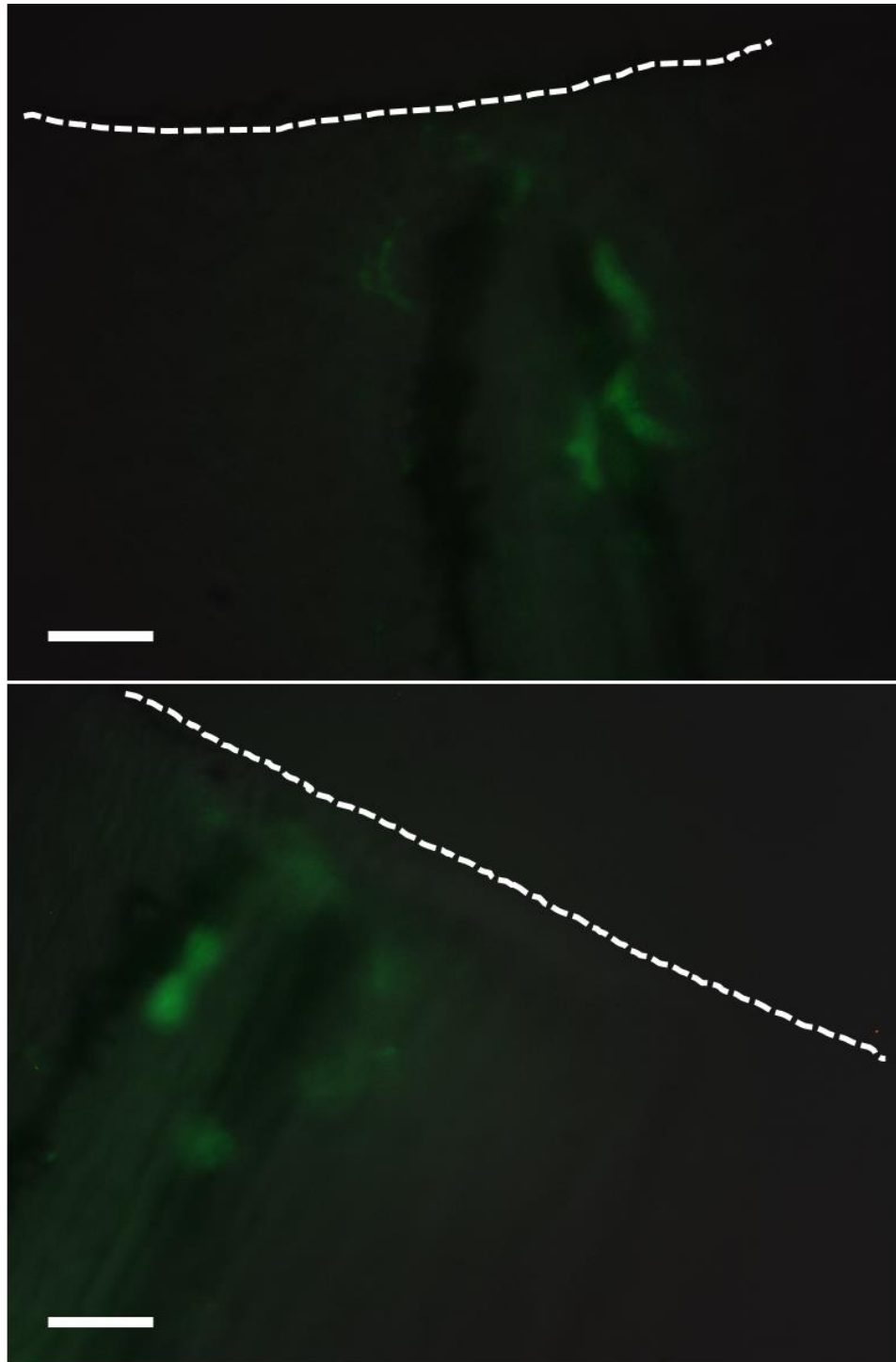


Figure 4.10. Fluorescently labelled cells are recruited to the site of injury in *Tg(mpeg:RFP.GFP.LC3)* embryos.

Embryos were injected with *pDEST(mpeg:RFP.GFP.LC3)* construct at 1-4 cell stage and subsequently tail transection was performed in embryos 72 hpf. Images show 2 tail fins and site of injury (white dashed line). Fluorescently labelled cells were recruited to the site of injury 6 hours post injury. This result suggests these are inflammatory cells, likely macrophages. (Scale bar 30 μ m) 40x objective.

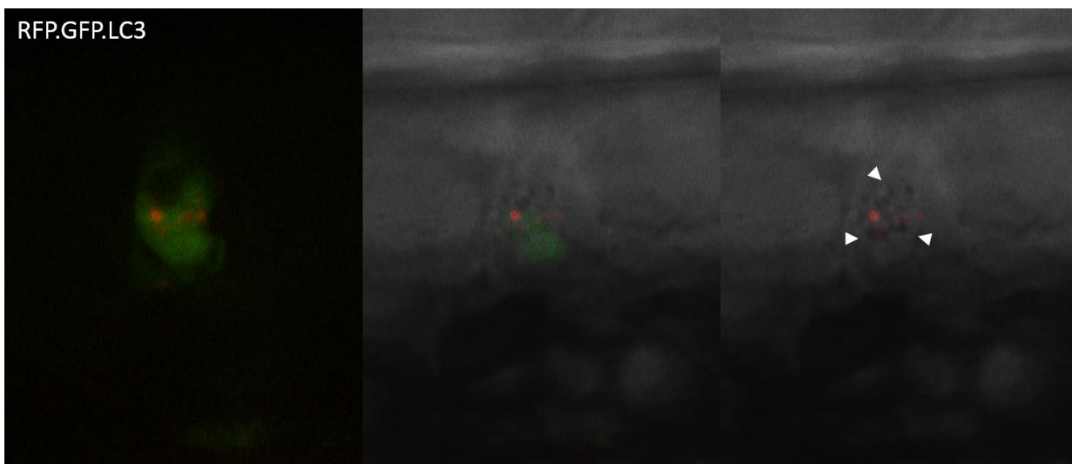


Figure 4.11. SH1000 *S. aureus* internalised by macrophages of *Tg(mpeg:RFP.GFP.LC3)*.

Larvae of F2 *Tg(mpeg:RFP.GFP.LC3)* generation were injected with 2500 CFU of wild type SH1000 and bloodstream cells were imaged on the confocal microscope to verify their ability to phagocytose bacteria. The GFP fluorescence is ubiquitous in the cytoplasm of cells, whereas RFP labelled LC3 aggregates in puncta and co-localises with phagocytosed *S. aureus* (white arrow heads). 40x objective.

4.4. Characterisation of *Tg(lyz:RFP.GFP.LC3)* transgenic zebrafish line

4.4.1. *S. aureus* internalisation in labelled neutrophils

Neutrophils in the *Tg(lyz:RFP.GFP.LC3)* line showed notably strong fluorescence. This enabled low magnification imaging (10x objective) of the neutrophil population in the entire embryo. The experiment was performed as part of the characterisation of the line, to verify whether the number of labelled cells corresponded to the number seen in the well-established *Tg(mpx:eGFP)i114* line (Renshaw *et al.*, 2006). Images were taken in 34 hpf fish in two areas populated with early neutrophils – the yolk circulation valley and the caudal haematopoietic tissue. Only cells expressing both red and green fluorescence were counted. Numbers differed from 50-130 cells per embryo, which means that on average there were more fluorescent cells counted in the *Tg(lyz:RFP.GFP.LC3)* line than in *Tg(mpx:GFP)* embryos (Figure 4.12). The variability within the *Tg(lyz:RFP.GFP.LC3)* line may be caused by natural differences between individuals. Additionally, protein expression and therefore fluorescent intensity may vary between cells, which could influence visibility during low magnification imaging. The difference between two neutrophil reporter lines may be caused by the different time points of acquisition. In the experiment held in the *Tg(mpx:GFP)* line, neutrophils were counted 31 hpf (Chapter 3), while those of *Tg(lyz:RFP.GFP.LC3)* were counted 34 hpf. The number of neutrophils in zebrafish increases between 1 and 2 dpf (Chapter 3), hence it may be possible to notice a modest increase in phagocyte counts within 3 hours. Although *lyz* and *mpx* promoter-specific lines were shown to have similar population of cells labelled with fluorophore, and those cells were described to be neutrophils (Petrie *et al.*, 2014), macrophages may also be labelled under *lyz* promoter (Pase *et al.*, 2012). During imaging experiments with the *Tg(lyz:RFP.GFP.LC3)* line, a fraction of labelled phagocytes had a different phenotype, more closely resembling macrophage. However, most of these cells were likely omitted from the final counts, which only used cells positive for both GFP and RFP; but the inclusion of a few macrophages from these data cannot be completely ruled out.

Neutrophils of embryos of the *Tg(lyz:RFP.GFP.LC3)* line were able to internalise intravenously injected bacteria in a similar manner to those of *Tg(mpx:GFP)* line used to identify internalisation rates of the cell lineage. I was therefore confident about the validation of this line for further infection-related experiments.

4.4.2. Classification of LC3 aggregates in neutrophils

It was noted during the infection of embryos transiently expressing fluorescently labelled neutrophil LC3, that LC3 protein forms various structures within cells. To determine the significance of this finding and relevance to the autophagy pathway, LC3 structures were classified based on their shape and size. *Tg(lyz:RFP.GFP.LC3)* embryos were dechorionated and injected with SH1000mCherry at 31 hpf. Larvae were mounted and imaged together with an uninjected dechorionated control group. Embryos were mounted with their ventral side facing the cover glass to allow the maximum number of neutrophils in the yolk circulation valley to be imaged in one frame. In each experiment a small group of infected (3) and uninfected (5) embryos were imaged to provide comparable time points for each acquisition.

LC3 aggregates in neutrophils were analysed by assignment of different colours of the point tool in Volocity™ Software. The classification was based on the shape of aggregate and its potential reference to subsequent steps of the process of autophagy. Points were contained in ROI manually drawn around neutrophils and saved as measurement items for further quantification. The classification and scoring system founded during characterisation served for the analysis of LC3 in neutrophils of infected and uninfected embryos and were applied in all assays involving the use of *Tg(lyz:RFP.GFP.LC3)* fish unless otherwise stated. Specified classes included: LC3 cytoplasmic puncta – point-like structures; LC3 spheroids - aggregates larger than puncta; LC3 tight vesicles (diameter < 1µM or tightly surrounding a group of bacterial cells in infected cells); LC3 spacious vesicles and spacious vesicles with puncta contained inside (Figure 4.13.). Co-localisation of *S. aureus* with LC3 structure is defined by direct association of the pathogen with aggregate, or in case of spacious vesicles, by the fact that bacterial cells are contained within the structure.

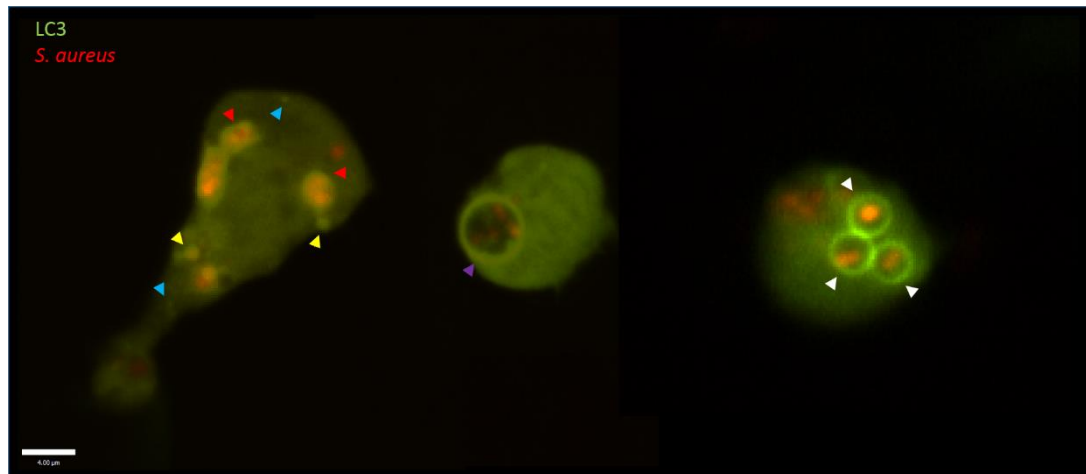


Figure 4.13. Illustration of LC3 classes.

Image shows representative neutrophils of *Tg(lyz:RFP.GFP.LC3)* embryo injected intravenously with 2500 CFU dose of SH1000-mCherry *S. aureus*. LC3 forms various aggregates in neutrophils of *Tg(lyz:RFP.GFP.LC3)* embryos. Structures vary in shape and size, and may reflect different stages of autophagic process, hence a classification was applied for quantitative analysis. Co-localisation of *S. aureus* with LC3 structure is defined by direct association of the pathogen with aggregate, or in case of spacious vesicles, by the fact that bacterial cells are contained within the structure. 40x objective.

LC3 puncta – blue arrowheads

LC3 spheroids – yellow arrow heads

LC3 tight vesicles – red arrow heads

LC3 spacious vesicles – white arrow heads

LC3 spacious vesicles with puncta – purple arrow heads

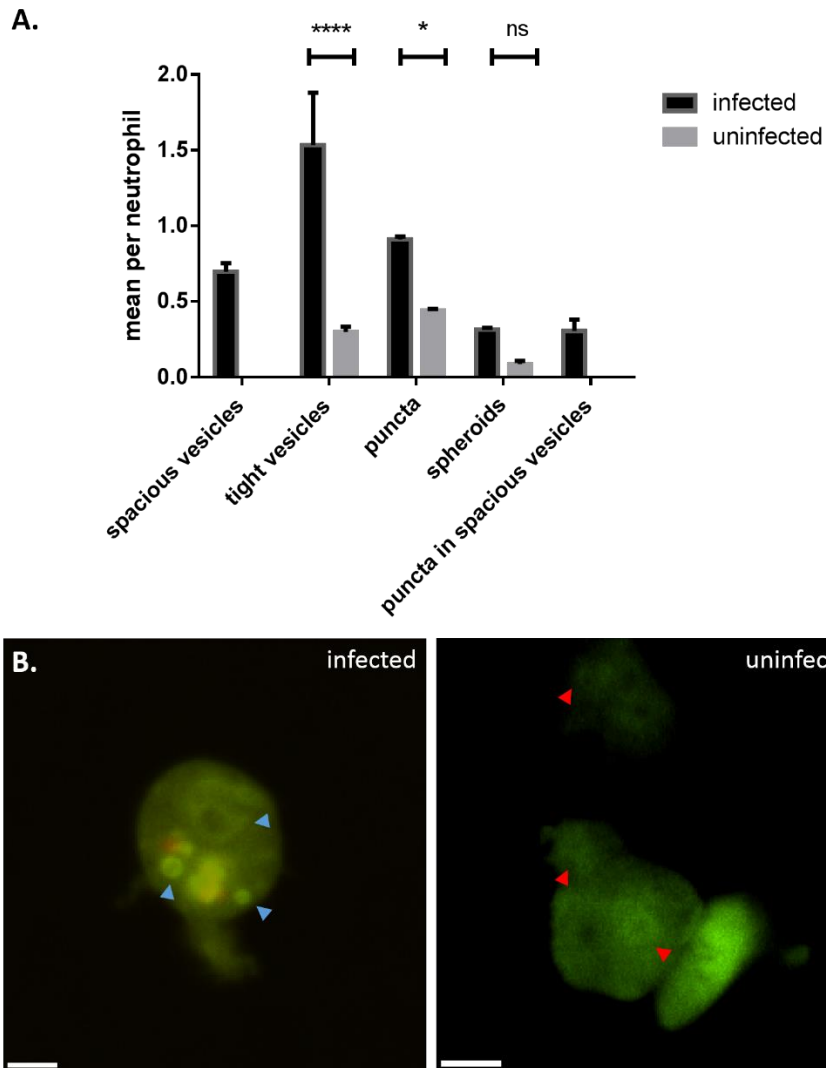


Figure 4.14. The occurrence of LC3 classes in neutrophils of infected and uninfected larvae 1 hpi.

A., Plot shows LC3 classes present in neutrophils of infected and uninjected *Tg(lyz:RFP.GFP.LC3)* embryos. Infected embryos were injected 30 hpf with 2500 CFU dose of SH1000-mCherry *S. aureus*. Two classes of spacious vesicles were not observed in the neutrophils of uninfected larvae: spacious vesicles and spacious vesicles with puncta. There was significantly more tight vesicles (p value < 0.0001) and puncta (p value = 0.0447) in infected neutrophils. The occurrence of spheroids was increased in infected neutrophils but not significantly greater (p value = 0.5517). (Two-way ANOVA multiple comparisons analysis, corrected Sidak test, n = 15 embryos per group). A representative number of embryos (and 20 phagocytes per larvae) was imaged in each experimental group, experiment repeated n = 3.

B., Panel shows representative images of infected and uninfected phagocytes. LC3 circles can be observed in both types of phagocytes, however, they have more distinctive edges and are brighter in infected neutrophils (blue arrow heads) when compared to uninfected neutrophils (red arrows). 40x objective.

The resulting analysis of the mean occurrence of particular classes per neutrophil has shown that both types of spacious vesicles seem to be present only in infected neutrophils (Figure 4.14A.). This finding could support the hypothesis that such aggregates are related to phagocytosis or other cellular processes involved in pathogen handling. Similarly, the increased presence of tight vesicles in infected neutrophils suggests bacterial capture inside of the phagophore membrane of autophagosomes (Figure 4.15.B). Furthermore, significantly higher numbers of puncta and spheroids underpin the interaction between neutrophil autophagy and *S. aureus* (Figure 4.14A.).

Puncta and autophagosomes were also observed in uninfected neutrophils, although with reduced fluorescent intensity relative to the cytoplasmic fluorescence background and smaller in size than similar structures in infected neutrophils (Figure 4.14B.). Those vesicles could be acting to remove other cellular material in neutrophils.

The analysis of *S. aureus* colocalisation with LC3 demonstrates that spacious and tight vesicles are the prevalent forms of LC3 aggregates observed around the pathogen (Figure 4.15.B). Again, the capacity of spacious vesicles does not seem to relate to the number of bacteria contained within, instead suggesting that LC3 was recruited to a previously formed vesicle rather than to bacteria themselves. Conversely, the firm structure of tight vesicles could suggest bacteria targeted recruitment. These findings could mean that both proposed interactions play a role in host's defence against *S. aureus*.

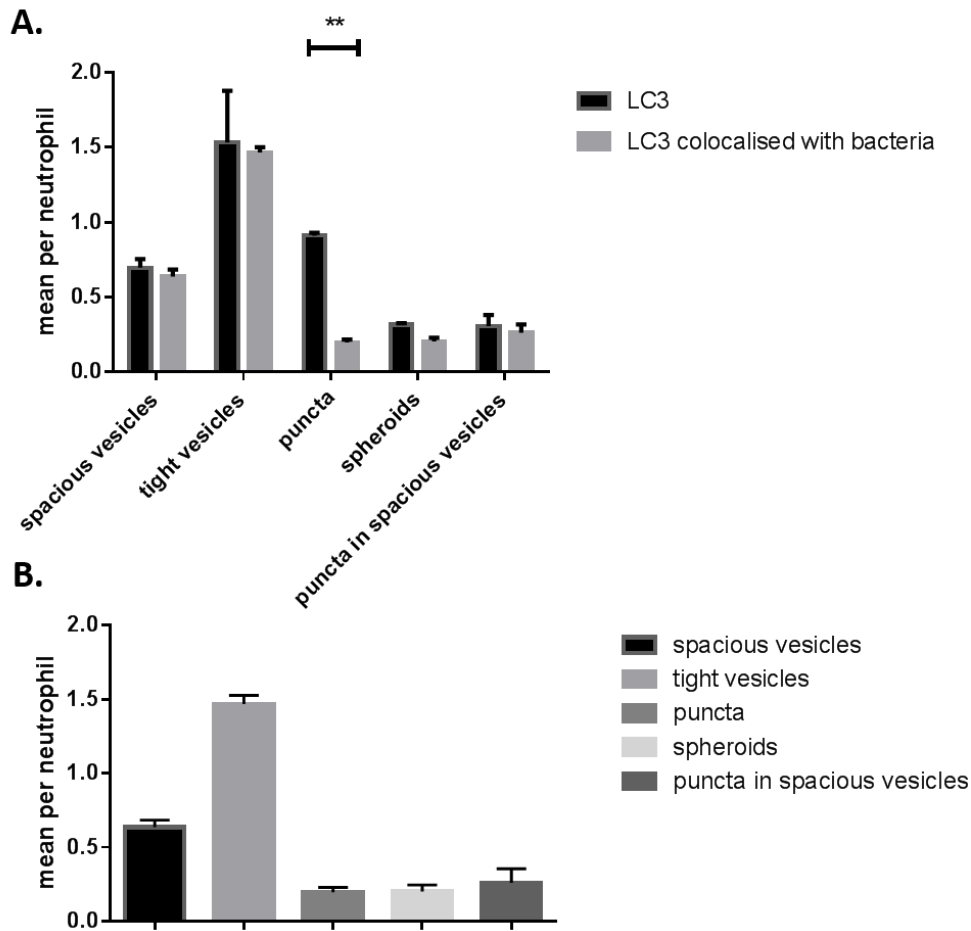


Figure 4.15. *S. aureus* co-localisation with LC3 classes in neutrophils 1 hpi.

Co-localisation of *S. aureus* with LC3 structure is defined by direct association of the pathogen with aggregate, or in case of spacious vesicles, by the fact that bacterial cells are contained within the structure.

A., Plot shows LC3 classes present in neutrophils in *Tg(lyz:RFP.GFP.LC3)* embryos infected with 2500 CFU SH1000-mCherry *S. aureus*, 1 hpi, divided in two groups: co-localised with *S. aureus* and not. The fraction of LC3 aggregates co-localised with *S. aureus* in each class was compared to the general amount of LC3 per cell (mean per cell). Significantly low number of LC3 puncta was co-localised with bacteria (p value = 0.0026, Two-way ANOVA multiple comparisons, corrected Sidak test, $n=15$ embryos per group), while other LC3 classes were associated with intracellular pathogen 1 hpi. A representative number of embryos (and 20 phagocytes per larvae) was imaged in each experimental group, experiment repeated $n = 3$.

B., Plot shows co-localisation of *S. aureus* with LC3 classes. *S. aureus* was mostly co-localised with tight vesicles LC3 class in neutrophils of infected larvae 1 hpi. There was significantly more bacteria co-localised with tight vesicles (p value < 0.0001) than with other classes. (p value < 0.0001, unpaired t test, $n=15$ embryos). A representative number of embryos (and 20 phagocytes per larvae) was imaged in each experimental group, experiment repeated $n = 3$.

4.4.3. Impact of methylene blue on LC3 function in neutrophils

It has been suggested that the presence of methylene blue can cause enhancement of the autophagy process (Congdon *et al.*, 2012). Methylene blue (MB) is commonly added to the fish embryo E3 media, in order to stop the growth of aquarium-acquired fungi. The possible impact of MB on imaging quality was briefly verified by the comparative imaging of neutrophils in embryos which were kept in media with MB and those transferred to MB-free E3 before hatching. Qualitative analysis of LC3 fluorescence in cells of approximately 5 larvae in each of two groups has demonstrated higher cytoplasmic signal in cells of MB treated fish. Cytoplasmic fluorescence constituted background noise for the LC3 aggregates, potentially impeding their proper classification. This finding led to omission of MB in future autophagy-related microscopy experiments. All embryos for subsequent autophagy studies were placed in MB containing E3 media in their first day post fertilisation and transferred to MB-free E3 before hatching or dechoriation.

4.4.4. Imaging of infection in neutrophil-specific LC3 reporter line

As previously mentioned, using *S. aureus* strains carrying GFP and mCherry plasmids affected the acquisition settings when imaging fluorescently labelled LC3. SH1000-expressed proteins were very bright, lowering general exposure times for their fluorescence channel. This caused decreased sensitivity of detection of RFP and GFP expressed in transgenic fish, when imaged together with mCherry and GFP *S. aureus* reporters, respectively. To avoid this conflict I used different fluorophores to label the pathogen. First, I infected *Tg(lyz:RFP.GFP.LC3)* embryos with a mixture of CFP and YFP-expressing SH1000 *S. aureus* and imaged on the spinning disk confocal microscope. The resulting imaging data show that altered filter setup did not enable the discrimination of the stronger LC3-GFP signal from CFP and YFP during detection, due to high exposure times applied for bacteria-encoded fluorophores and the partial overlap of CFP, GFP and YFP emission spectra (Figure 4.16.).

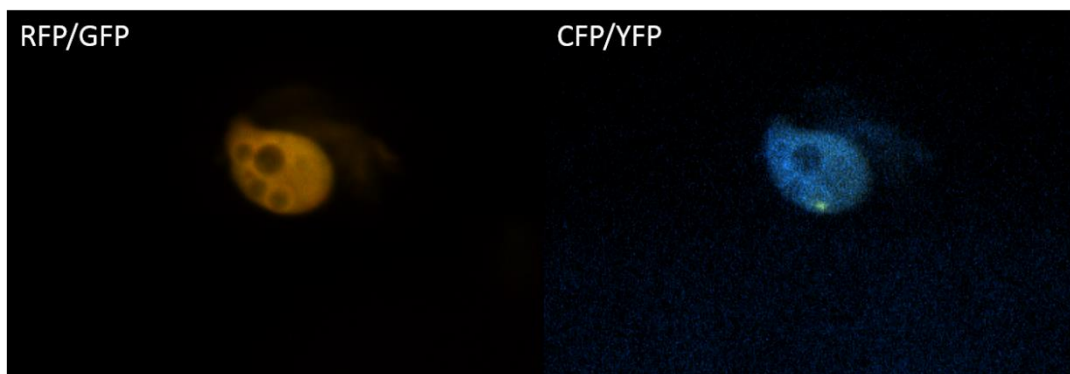


Figure 4.16. Imaging of *Tg(lyz:RFP.GFP.LC3)* embryos infected with CFP/ YFP inoculum shows overlap between spectra channels.

Tg(lyz:RFP.GFP.LC3) embryos were simultaneously injected with SH1000-CFP and SH1000-YFP *S. aureus* strains in 1:1 ratio. The image shows that filter setup did not enable the discrimination of the stronger LC3-GFP signal from CFP and YFP during detection, due to high exposure times applied for bacteria-encoded fluorophores and the partial overlap of CFP, GFP and YFP emission spectra. 40x objective.

Another alternative *S. aureus* label was tested in the infection of *Tg(lyz:RFP.GFP.LC3)* embryos by staining bacteria with fluorescent Alexa Fluor 647 dye. The dye binds to the cell wall of *S. aureus* and with the use of a thin z stack acquisition (1µm) can be visualised rather as circular rings than spherical shaped objects. Alexa Fluor 647 is strongly fluorescent when associated with *S. aureus*, even when used in the low concentrations, therefore the signal tends to be detected via the red fluorescence filters. Thus, very attentive visual analysis must be applied in order to discriminate between the *S. aureus*-bound dye rings and tight vesicles of LC3 classification. Hence, the Alexa Fluor 647 staining was only used in the experiments in the *Tg(lyz:RFP.GFP.LC3)* line, when the plasmid encoded bacterial fluorescence reporter was not available for a particular strain.

4.5. *Tg(mpeg:RFP.GFP.LC3)* transgenic zebrafish line

4.5.1. Classification of LC3 aggregates in macrophages

Unlike in the study on the *Tg(lyz:RFP.GFP.LC3)*, the full characterisation of the line and fluorescently labelled macrophages was not completed due to time constraints. Assays involving macrophage-specific LC3 line were mostly performed in comparison to the better characterised *Tg(lyz:RFP.GFP.LC3)* line. Therefore, an additional scoring assessment was applied during infection of *Tg(mpeg:RFP.GFP.LC3)* line, allowing the quantification of cellular LC3 aggregates not colocalised with internalised *S. aureus*. Macrophages of uninfected larvae were imaged as a control in experiments involving treatment of embryos with autophagy-modulating compounds and described in results Chapter 5. However, unless otherwise stated, the LC3 non-colocalised with bacteria was always scored in infected larvae.

LC3 in macrophages appears to aggregate differently than in neutrophils. Red and green fluorescence proteins seem to be separated and localised in different areas in cell. This observation could possibly be explained by quenching of the GFP protein in low pH compartments in cell. For the purpose of the macrophage analysis two groups of LC3 were distinguished based on the LC3 fluorescence protein active – red and green.

4.5.2. Imaging of infection in macrophage-specific LC3 reporter line

The macrophages of *Tg(mpeg:RFP.GFP.LC3)* seem to express both fluorescent proteins – RFP and GFP, however as previously mentioned, intracellular LC3 structures vary from those observed in neutrophils. RFP fluorescence of LC3 aggregates enabled infection with SH1000-mCherry. It was neither possible to distinguish particular elements of the image, nor to quantify the number of bacteria and their co-localisation with protein. Thus, a different fluorescent reporter of injected bacteria had to be established.

Tg(mpeg:RFP.GFP.LC3) embryos were dechorionated and injected with SH1000-CFP and SH1000-YFP at 31 hpf. Anaesthetised embryos were mounted with their ventral side facing the cover glass to allow the maximum number of macrophages in the yolk circulation valley to be captured in one frame. A qualitative analysis was completed to compare imaging performed with the use of two different fluorophores. Both CFP and YFP-labelled *S. aureus* cells internalised by macrophages were detectable (Figure 4.17.). This result is in contrast with the outcome of a similar experiment performed in *Tg(lyz:RFP.GFP.LC3)* embryos. Possibly, by reason of weaker fluorescence of the GFP protein in the macrophage-specific line, each fluorophore was well separated and detected during the imaging. Ultimately, due to lower exposure time and better imaging qualities, the SH1000-CFP strain was chosen as more appropriate for the experimental assays and was used in this study for imaging of infection in *Tg(mpeg:RFP.GFP.LC3)*.

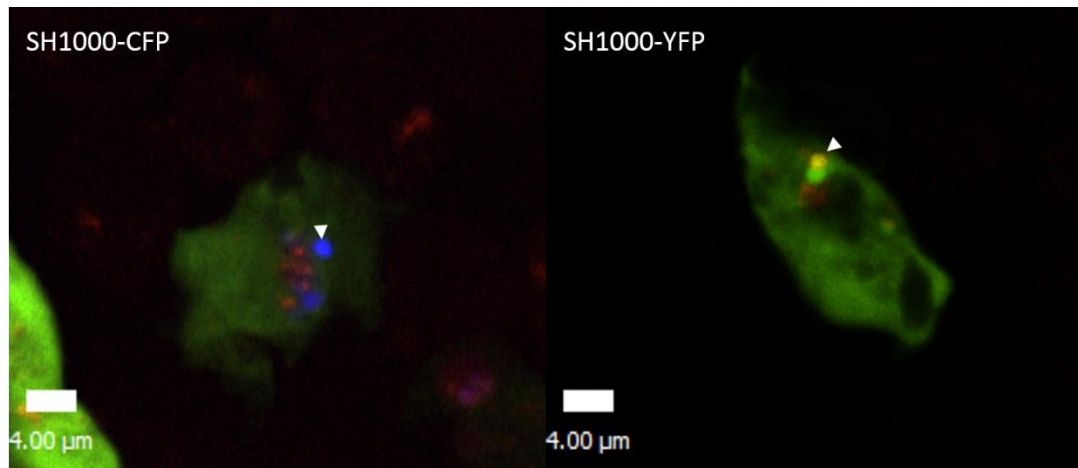


Figure 4.17. Imaging of *Tg(mpeg:RFP.GFP.LC3)* macrophages internalising differently labelled SH1000.

Embryos of *Tg(mpeg:RFP.GFP.LC3)* were infected with 2500 CFU of two different SH1000 reporter strains, one with plasmid-encoded CFP fluorescence, second with plasmid encoded YFP fluorescence. Both *S. aureus* strains are internalised by macrophages and detectable with available acquisition setup (white arrow heads). 40x objective.

4.6. Discussion

Several studies have shown that the autophagic machinery can have a great impact on the outcome of an infectious condition and a treatment with autophagy modulating drugs has a potential to help finding cures for pathogen invasion. Schnaith *et al.* (2007) identified *S. aureus* residing in autophagosomes by visualising the characteristic double membrane of *S. aureus* containing vesicles and the co-localisation of LC3 with it. Although it has been suggested that autophagy can be involved in *S. aureus* infection, there was no research performed to investigate this in an *in vivo* model. The zebrafish was shown to be a useful model to elucidate hallmarks of *S. aureus* pathogenicity (Prajsnar *et al.*, 2008, 2012). Thus we decided to make use of available tools and generate a zebrafish model for studying *S. aureus* interaction with autophagy components *in vivo*.

The RFP and GFP fluorophore label fused to LC3 in the designed constructs was incorporated to allow assessment of the maturation of LC3 positive autophagosomes. This reporter would be helpful to study the unique characteristic of the interaction of *S. aureus* and autophagy components. It has been reported that although *S. aureus* co-localised with LC3 after infection these autophagosomes were not acidified (Schnaith *et al.*, 2007). Additionally, the lack of LAMP-2 recruitment to bacteria containing autophagosomes indicates possible lack of fusion with lysosomes (Dorn, 2001). Therefore, *S. aureus* could induce an arrest of autophagosomal maturation which is more common in Gram-negative bacteria autophagy, reported for *B. abortus*, *L. pneumophila*, *P. gingivalis*, and *C. burnetii* (Sturgill-Koszycki and Swanson, 2000, Dorn *et al.*, 2001, Berón *et al.*, 2002, Pizarro-Cerdá *et al.*, 1998, Joshi *et al.*, 2001). Although the use of the mCherry labelled SH1000 strain excluded the possibility of assessing the maturation of autophagosomes with the tandem LC3 label, *Tg(lyz:RFP.GFP.LC3)* still has the potential to constitute a useful tool to study acidification aspect. The acidification of bacteria-containing autophagosomes could be visualised by staining the *S. aureus* cell wall with a low pH indicator, such as pHrodo. Detailed characteristics of the assay and indicative potential of the method are described in Chapter 5. Although in this study the *Tg(lyz:RFP.GFP.LC3)* line was primarily used to investigate the general interaction between several strains of *S.*

aureus and components of autophagy pathway, the use of pHrodo remains an interesting tool for furthering future study on the subject.

On the other hand, the parallel use of RFP and GFP fluorophores resulted in an interesting outcome in the macrophage-specific line. Red fluorescence puncta and aggregates were visualised present in macrophages, rather than a spectrum of LC3 structures, as observed in neutrophils. If we assumed that the presence of spacious LC3 positive vesicles in the neutrophils could suggest that LC3 was recruited to bacteria containing phagosomes, the lack of such structure in macrophages would indicate that phagocytosis and autophagy do not cooperate in *S. aureus*-colonised macrophages. However, this will be elaborated in detail along with the study of other components of host cell defence against *S. aureus* in Chapter 5.

In any case, the different LC3 formation in neutrophils and macrophages may imply that either autophagic machinery interacts with *S. aureus* in a distinct manner in the two cell lineages, or that macrophage LC3 performs more efficient degradation of LC3-targeted bacteria. The latter could be again related to a RFP and GFP pH indication role. In the study of Kimura *et al.* HeLa cells were transfected with a plasmid containing RFP, GFP and LC3 proteins in tandem. Further investigation showed quenching of the GFP fluorescence signal upon the autophagosome maturation, whereas RFP signal was still detectable. Fusion with lysosomes caused the rapid disappearance of the GFP signal, as no overlap of signal was indicated, and the RFP persisted, possibly due to its lower pKa value and resistance to degradation. Researchers suggested that the attenuation was caused by the protonation of the fluorophore, which allowed only a relatively short monitoring of the maturation process. Additionally, they found that both membranes of the phagosome are decorated with LC3, as the lipidated protein is bound to isolation membrane. Therefore, cytoplasm-exposed LC3 of the outer membrane, could possibly be liberated or cleaved shortly after fusion with lysosomes, for instance by a second Atg4-dependent cleavage, similar to that performed in yeast cells (Kirisako *et al.*, 2000). Such mechanisms would explain why only the RFP fluorescent signal is detected after the fusion, and why for some, both GFP and RFP proteins are spatially separated (Kimura *et al.*, 2007).

Although the creation of the LC3 fluorescence reporter transgenic lines required complex troubleshooting and general adjustments for its microscopy-based approaches, the generation of macrophage and neutrophil-specific lines opens a new path for *in vivo* infection study. By classification of different LC3 structures, we are able to increase our understanding of how individual steps of LC3 association or autophagy-driven mechanisms can interfere with intracellular pathogens. Additionally, infection studies performed in those newly generated tools may form a basis for more profound studies on autophagy-related proteins. It has been suggested that protein-protein interactions of LC3-associated proteins may determine targets selected for uptake by the autophagosome (Schwarten *et al.*, 2009). Therefore, an *in vivo* model will potentially inform our knowledge on the diverse roles of LC3 and autophagy.

Chapter 5: Investigation of intracellular pathogen processing *in vivo*

5.1. Introduction

The zebrafish infection model enables high power imaging and *in vivo* investigation of the processes occurring in a living organism during infection with *S. aureus*. Various imaging approaches can be applied to increase our understanding of the interaction of immune cells with the pathogen. Bloodstream neutrophils and macrophages internalise *S. aureus* in different ways as shown in Chapter 3. In this model, pathogen-bound and host-expressed fluorescence reporters can be employed, providing information on *S. aureus* intracellular fate. Altogether, various techniques help to clarify how the two cell lineages of professional phagocytes react to bacterial presence in the bloodstream. *S. aureus* is capable of intracellular survival, implying the evolution of strategies allowing it to escape killing by the host immune system. It can persist and grow inside different host cells, however this depends on the strain causing the infection and the defence mechanism used by the infected cell (Krut *et al.*, 2003). Data presented in this chapter show how the zebrafish model can be used to study the involvement of host intracellular mechanisms like autophagy, acidification and degradation; and how these differ following infection with different *S. aureus* strains.

Acidification is a well-known feature of the late phase of phagocytosis. Phagosomes created during uptake fuse with lysosomes, intracellular compartments containing digestive enzymes, which results in a reduction in pH and acidification of the bacteria-containing compartment. Acidification of phagosomes is followed by bacterial degradation, suggesting that acidification constitutes an important step in the pathway of bacterial internalisation and therefore a central component of the host defence. Moreover, other vesicles created during internalisation, for example macropinosomes, have also been shown to fuse with lysosomes during the late stage of maturation (Kerr *et al.*, 2006). Additionally, acidification followed by digestion of *S. aureus* is necessary for MyD88-dependent toll-like receptor responses of the host immune system (Abdelzaher *et al.*, 2010). Furthermore, intracellular acidification has

been suggested as an essential step for the optimal response to *S. aureus* infections (Ip *et al.*, 2010). Therefore this chapter includes experiments concerning the visualisation of the pH of bacteria-containing endosomes and the elucidation of the viability of those bacteria. The loss of expression of GFP in different *S. aureus* strains can be used as a tool to determine bacterial killing in host cells. During efficient killing the fluorescence intensity drops and GFP fades, while *S. aureus* is degraded in phagocytes (Schwartz *et al.*, 2009). This feature has already been used to assess the pathogenicity of different strain isolates (Schwartz *et al.*, 2009) and thus, has also been applied in this study.

As described in chapter 1, autophagy is an intracellular process that may be subverted by bacterial pathogens. The autophagosome can be used by *S. aureus* to escape host killing (Schnaith *et al.*, 2007). By destroying the autophagosomal compartment and escaping their niche, bacteria take control over the course of infection. The presence of cytosolic *S. aureus* is known to be related to host cell death (Schnaith *et al.*, 2007). Killing of the host cells relies on two proteins of autophagic pathway – Atg5 and Beclin1/Atg6. Atg5 is crucial in the development of the isolation membrane, its elongation and binding of LC3 (Mizushima *et al.*, 2001). After replication within autophagosomes, a fully cytotoxic *S. aureus* strain escapes into the cytosol, which eventually kills the host cells, making *S. aureus* capable of autophagy-dependent induction of cell death. The neutrophil and macrophage-specific LC3 reporter lines generated during this study allowed *in vivo* verification of the role of autophagy in *S. aureus* infection. Labelling of the major autophagy component, LC3, enabled assessment of pathogen-targeted autophagosome formation and other pathogen-triggered LC3 activity.

Autophagy machinery may be induced and inhibited by drug treatment. Such manipulation will affect multiple roles of the process and is commonly applied in infection-related experimental approaches. Treatment can also help to elucidate the impact of the process on the course and outcome of autophagy-dependent diseases. The use of an *in vivo* model allows observation of host response to infection with drug treatment, and helps to elucidate the differences between the strategies used by different pathogens. For instance, although the stimulation of autophagy by

rapamycin was commonly viewed as helping to fight bacterial infection (Levine *et al.*, 2011, Deretic and Levine, 2009), rapamycin treatment significantly reduced host survival during *S. flexineri* infection in zebrafish (Mostowy *et al.*, 2013). It has therefore been suggested that manipulation of autophagy can adversely affect host survival upon infection with *S. flexineri*. Herein, treatments with the autophagy enhancer carbamazepine and autophagy inhibitor chloroquine were applied. This can potentially help to verify generated LC3 reporter lines and to study how modulation of autophagic activity influences phagocyte responses to *S. aureus*.

Several classes of LC3 structures have been described during the characterisation of the *Tg(lyz:RFP.GFP.LC3)* line (Chapter 4). One of these, spacious LC3 vesicles, seem to reflect a previously published result of LC3 recruitment to the phagosome membrane (Sanjuan *et al.*, 2007). Interestingly, this form of LC3 aggregate was only observed in neutrophils of infected embryos, moreover *S. aureus* were found inside of these vesicles. LC3 association to phagosome membrane could potentially target the vesicle for lysosomal fusion and cargo degradation (Huang *et al.*, 2009). However, it remains unknown why LC3 is associated to phagosome. Several pathogens were shown to subvert immune cell killing mechanisms by escaping phagosome. Thus, such bacterial activity could constitute a potential reason for the alternative LC3 targeting.

S. aureus is capable of producing haemolysins, pore forming lipids and proteins which can destroy host cell membranes. Bacteria other than *S. aureus* have a well-documented history of using haemolysin against host immune cells, for example *E. coli* haemolysin leads to macrophage autolysis and death (Fernandez-Prada *et al.*, 1998). Leukocytes can also constitute a target for haemolysin detrimental activity. α -haemolysin, one of the 3 haemolysins produced by *S. aureus*, also called α -toxin plays an important role in *S. aureus* pathogenesis. *hla* mutant strains have decreased virulence (Bubeck Wardenburg *et al.*, 2008). α -toxin presents various types of activity, it either binds to membrane receptors and forms pores leading to host cell DNA fragmentation and apoptosis, or causes the formation of larger, Ca^{2+} permissive pores followed by cell necrosis (Bantel *et al.*, 2001). Unlike other cells confronted by α -haemolysin, human leukocytes are particularly vulnerable (Bhakdi and Trnum-

Jensen, 1991). To test whether strains with impaired haemolysin secretion will co-localise with LC3 differentially in neutrophils, *hla* mutants of SH1000 and USA300 backgrounds were injected and imaged in *Tg(Iyz:RFP.GFP.LC3)* embryos.

Furthermore, the recent study reports that PSM α toxin plays an important role in the context of phagosomal escape of *S. aureus* (Grosz *et al.*, 2014). Phenol soluble modulins (PSMs) are *S. aureus* peptides encoded in *S. aureus* in highly conserved genomic islands or in the core genome. Similarly to δ -Toxin, PSMs are also expressed in an agr-dependent manner, and play a key role in *S. aureus* virulence, which has been shown in skin infection and bacteraemia animal models (Wang *et al.*, 2007, Kobayashi *et al.*, 2011). Although PSMs can be expressed in virtually all strains, it has been shown that the pathogenicity of some of them can be enhanced, also emerging among CA-MRSA strains (Otto, 2010). Grosz *et al.* (2014) have investigated and confirmed the requirement for PSM α in genetically divergent backgrounds such as CA-MRSA LAC (USA300), MW2 (USA400) and MSSA 6850, additionally showing that the last of the listed strains is able to grow intracellularly upon escape. Importantly for this study, cytoplasmic translocation and subsequent replication takes place in professional phagocytes. The 6850 strain is strongly cytotoxic (Proctor *et al.*, 2002, Balwit *et al.*, 1994). Thus, the 6850 strain and its PSM α mutant have also been injected into *Tg(Iyz:RFP.GFP.LC3)* line embryos for study.

The zebrafish model allows us to increase our understanding of the application of autophagy mechanisms in an *in vivo* model. This is essential in investigating host-pathogen interactions, and an animal model offers the involvement of the whole immune system.

5.1.1. Hypotheses

Acidification of *S. aureus* is necessary for efficient immune system responses (Abdelzaher et al., 2010). Macrophage lysosomes are reported to be acidic, whereas neutrophil lysosomes are not (Claus et al., 1998). My hypothesis is that phagosomal pH *in vivo* in zebrafish myeloid cells determines host-cell killing capacity.

It has been suggested that *S. aureus* uses autophagosomes as its replication niche in non professional phagocytes (Shnaith et al.). I hypothesised that *S. aureus* also interact with autophagy components in immune cells, and this determines the outcome of infection.

5.1.2. Aims

Aims of experiments presented in this chapter:

- Generation of tools allowing *in vivo* indication of pH of the intracellular compartments containing *S. aureus*.
- Determination of *S. aureus* acidification and viability in neutrophils and macrophages at the early stage of infection.
- Visualisation of *S. aureus* interaction with major autophagy marker LC3 protein neutrophils and macrophages using newly generated Tg(lyz:RFP.GFP.LC3) and Tg(mpeg:RFP.GFP.LC3) lines, respectively.
- Observation of the impact of autophagy regulating drugs on LC3 co-localisation with *S. aureus* in neutrophils and macrophages.
- Observation of co-localisation of various *S. aureus* strains with LC3 structures in neutrophils.

5.2. Acidification of internalised *S. aureus*

5.2.1. Acidification of injected pHrodo particles

pH changes may be visualised by using fluorescence microscopy techniques. pHrodo™ is a specific fluorescent sensor, fluorescing red when suitably excited by appropriate wavelength illumination in low pH environments (Figure 5.1. 1). It can be used as a bacteria cell wall stain, or ready bacteria particle-dye conjugate, used in phagocytosis detection approaches.

In order to verify the ability of pHrodo to indicate acidification in zebrafish phagocytes, pHrodo™ *S. aureus* particles conjugate was injected into 30 hpf LWT embryos. To control for nonspecific acidification yielding a false positive signal, two control groups were used in which all leukocytes or just macrophages were depleted using *pu.1* and IRF8 (interferon regulatory factor 8) morpholino knockdown respectively. *pu.1* is a transcription factor essential for development of myeloid cells (Klemsz *et al.*, 1990). Using morpholino technology to knock down *pu.1* causes myeloid cell depletion in zebrafish embryos (Rhodes *et al.*, 2005). *irf8* is necessary for differentiation of progenitor cells into macrophages and in zebrafish causes the increase in neutrophil population (Li *et al.*, 2011, Prajsnar *et al.*, 2012).

Phagocyte acidification of particles was captured within 30 minutes of injection and visualised as red fluorescent puncta spread in the yolk sac circulation valley. Quantification of puncta revealed fewer spots in both morphant groups, with significantly lower number in *pu.1*-MO embryos (Figure 5.1.2). Thus the result reflected lower signal intensity observed during imaging (Figure 5.1.3). A weaker signal was observed during the imaging of the control *irf8*-MO knock down embryos, with a smaller number of acidifying phagocytes visible in the bloodstream compared to control embryos (Figure 5.1B)., There was consistent lack of signal from the control *pu.1*-MO knock down of innate immune system cells (Figure 5.1C), suggesting acidification observed in control embryos occurs in phagocytes.

Zebrafish phagocytes were able to acidify intravenously injected particles and such acidification resulted in pHrodo™ fluorescence. This led to the generation of the protocol for viable *S. aureus* cell wall staining with the use of similar indicator – pHrodo™ s-ester.

1. Image cannot be shown.

2. Acidification of particles

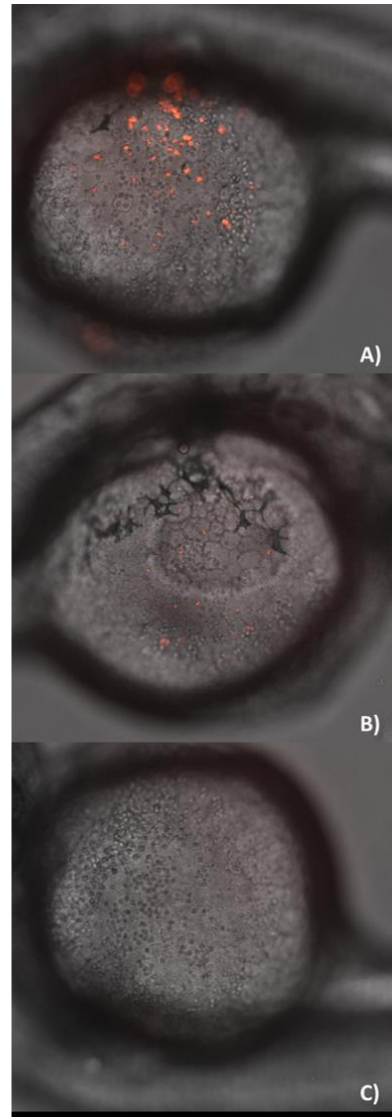
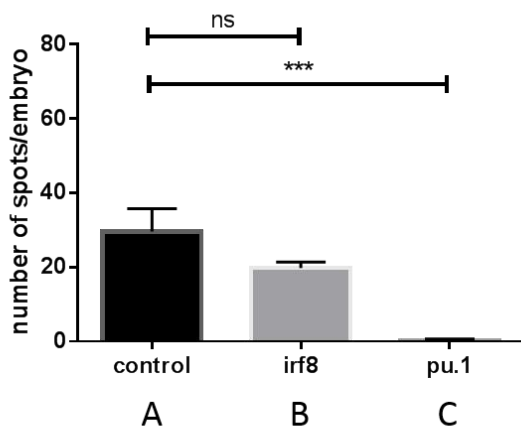


Figure 5.1. pHrodo™ Red *S. aureus* BioParticles® conjugates allow visualisation of phagocyte acidification *in vivo*

LWT embryos were divided in 3 groups A, wild type LWT zebrafish; B, irf8-MO knock down; C, pu.1-MO knock down. Embryos of all groups were further injected with the same number of *S. aureus* pHrodo™ particles 30 hpf and visualised 30 – 45 minutes post injection.

1. pH range and fluorescence emission spectra of the pHrodo™ acidification indicators (<http://www.b2b.invitrogen.com>).
2. Quantitative analysis of the number of fluorescence spots in injected embryos.
3. Example images of the fluorescence puncta in the yolk sac area of all groups of tested embryos. 10x objective.

5.2.2. *S. aureus* cell wall staining with pH indicators

pHrodo™ constitutes a useful tool for low pH indication and it allows labelling of bacteria and tracking of its environment pH during infection (Figure 5.2.). The use of viable *S. aureus* cells was necessary to visualise the process of the bacterial acidification during infection in the zebrafish model. For this purpose the SH1000 laboratory strain cells were stained with two pH sensitive dyes: fluorescein and pHrodo™. Both reagents were used as succinimidyl esters, and the staining optimisation and imaging procedures were first performed *in vitro*.

At low pH, red fluorescence signal indicated pHrodo™ sensor activation, while fluorescein was quenched according to its signal emission features and capacity. The reverse effect was observed at neutral pH. Optimising double staining *in vitro* allowed visualising and differentiating in the merge plan the pH of different *S. aureus* containing environments (Figure 5.3. 1A and 1B).

After optimisation of the staining procedure, stained SH1000 *S. aureus* cells were injected into the LWT zebrafish line, in order to assess the pH indication method *in vivo*. Figure 5.3. presents the results indicating that the protocol used for bacteria staining, produces a useful tool for *in vivo* visualisation of compartment pH. Moreover, it clearly shows that internalised bacteria reside in compartments of different pH. This suggests that either distinct internalisation modes, or various intracellular trafficking pathways, can alter *S. aureus* intracellular fate. One could also speculate that such variance results from *S. aureus* acting to subvert these pathways to its own ends.

Imaging of the early stages of infection allows acquisition of intra and extracellular bacteria, as well as uptake into bloodstream phagocytes. Strong fluorescence signal and low exposure times necessary to visualise the dyes enabled capturing image sequences during the internalisation of stained bacteria. The green fluorescence of extracellular *S. aureus* indicated the neutral pH of the bloodstream, and cellular uptake was followed by bacteria acidification illustrated by the transition of fluorescence from green to red (Figure 5.4.). Such transition has been observed in at least 3 experiments where *Tg(mpx:GFP)* line embryos were infected with

pHrodo/fluorescein stained SH1000. Based on observation during DIC imaging, and lack of GFP expression, acidifying phagocytes were proposed to be macrophages. Uptake was observed within the very first 30 minutes post injection and the gradual decrease in the pH surrounding the bacteria internalised from the bloodstream took less than 5 minutes in all cases.

Image cannot be shown

www.lifetechnologies.com

Figure 5.2. Schematic interpretation of pHrodo™ intracellular low pH indication.

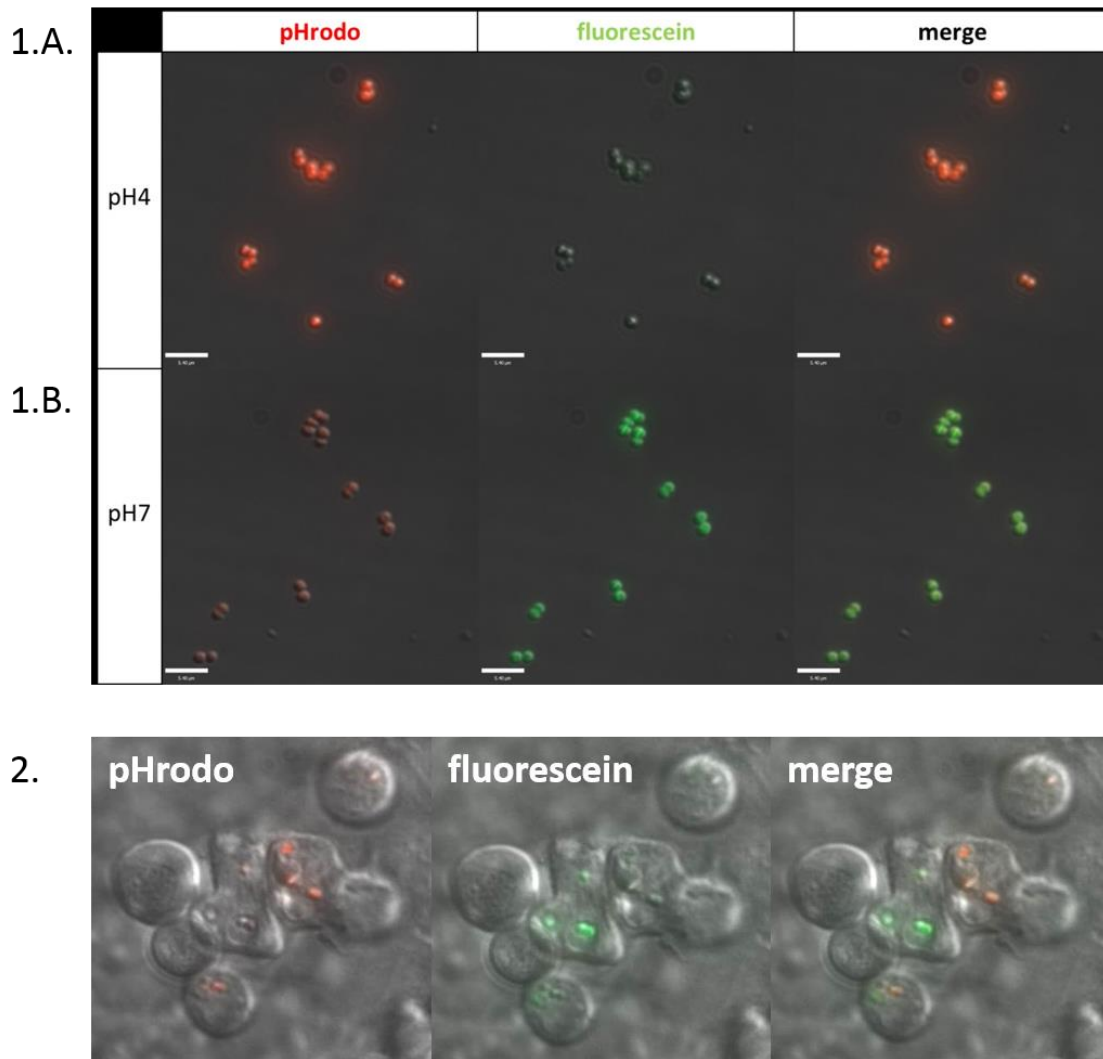


Figure 5.3. *In vitro* and *in vivo* imaging of pH sensitive dyes.

Figure shows microscopy result of the optimisation of *S. aureus* simultaneous staining with two succinimidyl esters: low pH indicator pHrodo™ and pH-sensitive fluorescein. SH1000 laboratory strain of *S. aureus* was stained and imaged in a range of different pH media to test fluorescent pH indication. Following *in vitro* validation of the protocol, stained bacteria were injected intravenously into wild type LWT embryos and imaged contained within bloodstream phagocytes using DIC technique.

1. *in vitro*, pH = 7 (1.A.) and pH = 4 (1.B.);

2. *in vivo* injected in wild-type zebrafish embryo 30 hours post fertilisation. Bacteria reside within innate immune system cells in different pH compartments. 60x oil objective.

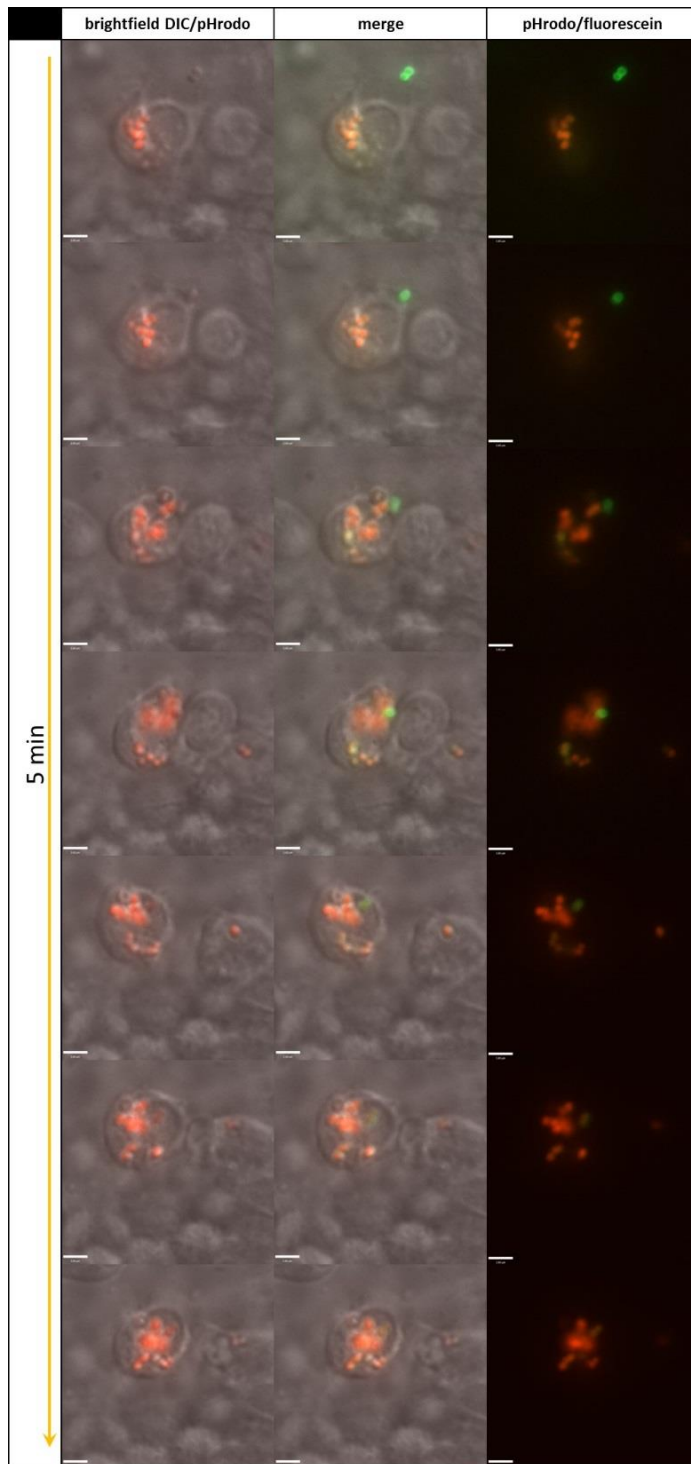


Figure 5.4. *S. aureus* uptake followed by gradual acidification.

Tg(mpx:GFP) embryos were infected with wild type SH1000 *S. aureus* stained with pHrodo™ and fluorescein pH-indicating dyes. Figure shows sequential photomicrographs demonstrating internalisation of extracellular *S. aureus* followed by gradual acidification inside of a phagocyte, likely macrophage. Acidification is illustrated by red-green fluorescence transition.

Figure consist of the three sections:

- Brightfield DIC/ pHrodo: increase in red fluorescence of internalised bacteria over time
 - Merge
 - pHrodo/ fluorescein: fluorescence transition over time.
- 60x oil objective.

Scale bar 10 µm.

5.2.3. Simultaneous visualisation of *S. aureus* acidification and viability in bloodstream phagocytes

Successful fluorescein/pHrodo™ staining allowed the dynamic acquisition of changes in the pH of *S. aureus* environments and bacteria-containing compartments. However, the experimental set up only allowed to visualise one factor, acidification. It has been shown that plasmid-encoded fluorescence can serve as an indicator of *S. aureus* viability. Killing of the pathogen results in the fading of the GFP signal and such bleaching can be used to assess the pathogenicity of different strain isolates (Schwartz *et al.*, 2009).

It was necessary to avoid fluorescein staining to incorporate the use of another green fluorescence source, plasmid-encoded GFP fluorescence. Although applying pHrodo and GFP-plasmid fluorescence allowed investigation of both factors, acidification and killing of *S. aureus*, it also generated the risk that the non-acidified, dead bacteria would not be captured. Thus, I stained *S. aureus* with pHrodo™ together with an Alexa Fluor 350 s-ester. The latter is a pH insensitive dye and played the role of an imaging control, ensuring that all bacteria present in phagocytes will be visualised.

Imaging data demonstrated that seemingly all intravenously injected bacteria were stained with Alexa Fluor 350 and could be visualised internalised in phagocytes (Figure 5.5.). Simultaneously, the use of pHrodo™ indicator highlighted which *S. aureus* cells resided in low pH compartments. A fraction of the pathogen population did not express plasmid encoded fluorescence. This result led to the use of “3 colour imaging” in the following quantification analysis, aiming to determine the viability of *S. aureus* and potential low pH degradation of the pathogen in bloodstream phagocytes.

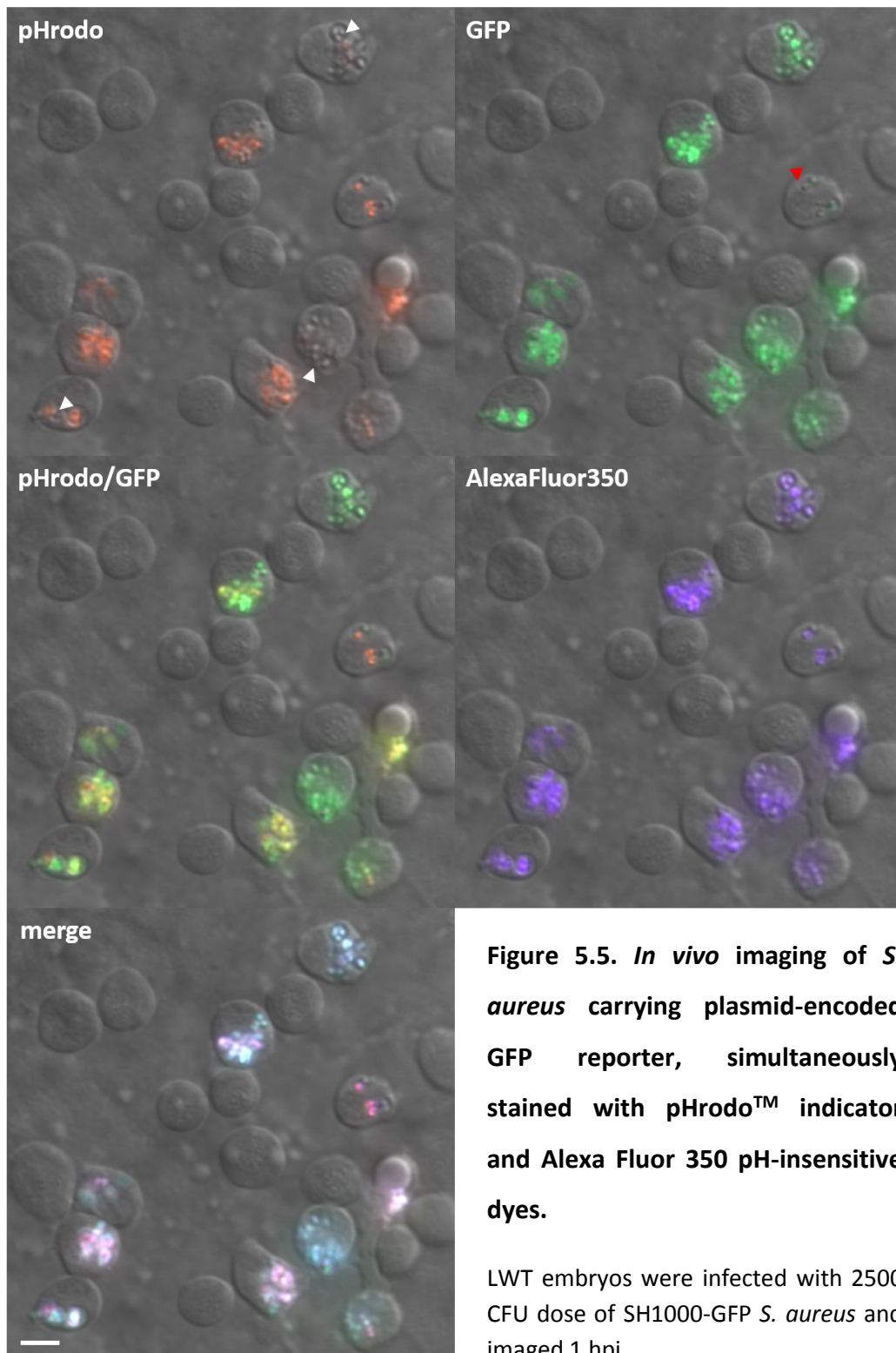


Figure 5.5. *In vivo* imaging of *S. aureus* carrying plasmid-encoded GFP reporter, simultaneously stained with pHrodo™ indicator and Alexa Fluor 350 pH-insensitive dyes.

LWT embryos were infected with 2500 CFU dose of SH1000-GFP *S. aureus* and imaged 1 hpi.

“3 colour” approach allowed visualisation of not acidified bacteria (white arrow heads) and not expressing the plasmid fluorescence less viable *S. aureus* (red arrow head).

Scale bar 10 μm. 60x oil objective.

5.2.4. *S. aureus* killing in cellular compartments of different pH

Quantitative analysis of imaging data obtained during infection with stained *S. aureus* was preceded by determination of the pathogenicity of stained bacteria. LWT embryos were injected intravenously with 2500 CFU of pHrodo and Alexa Fluor 350 stained SH1000-GFP 30 hpf, according to the standard procedure. Embryo survival was further tracked and a survival curve was generated for 3 repeats of the procedure (Figure 5.6.). The result shown that 50 % of embryos were dead by 90 hpi, which is the result expected for that dose of injected SH1000 (Prajsnar *et al.*, 2008).

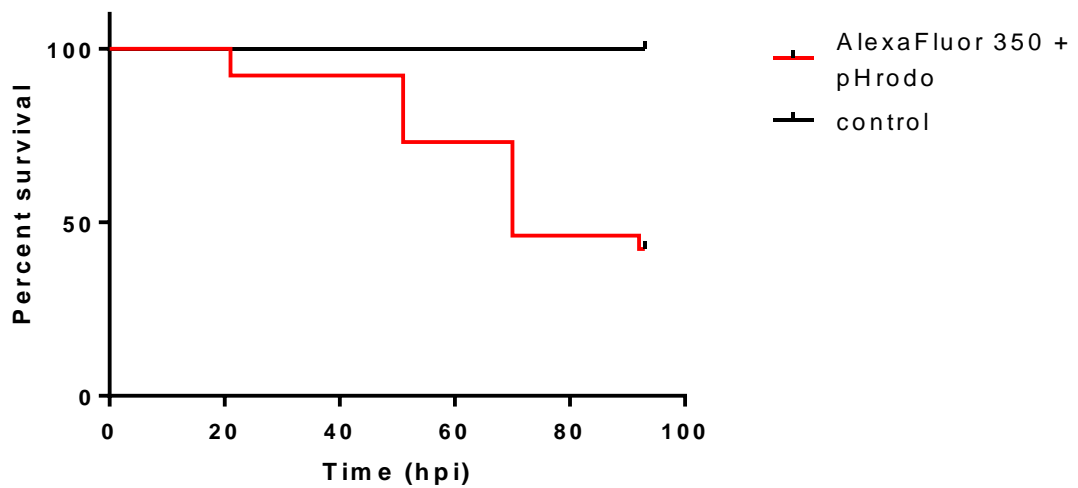


Figure 5.6. Survival of LWT embryos infected with 2500 CFU of SH1000-GFP stained with s-ester fluorescent dyes.

LWT embryos were injected 30 hpf with 2500 CFU SH1000-GFP *S. aureus*. Bacteria cell walls were stained with pHrodo™ and Alexa Fluor 350 s-ester fluorescence dyes. Staining procedure and plasmid encoded fluorescence did not impact the expected pathogenicity of the strain. (uninjected and PBS injected control, n = 3, significant difference between survival curves, log rank test, p = 0.0009).

In order to determine the viability and acidification rates of *S. aureus* in neutrophils and macrophages, the neutrophil-specific reporter line *Tg(mpx:GFP)* was infected with SH1000-GFP stained with pHrodo™ and Alexa Fluor 350. The experiment was performed in 3 independent repeats and together 24 neutrophils and 37 macrophages were studied for their bacterial content. Neutrophils were recognised based on their GFP fluorescence and macrophages, by their ability to take up intravenously injected bacteria and morphology observed with the use of DIC. Quantification of red and green fluorescence signals could not be performed automatically using Volocity® software, due to fluorescence overlapping and accumulation of bacteria in the different z-planes imaged. To overcome this limitation, bacteria were scored with the point tool and fluorescence intensity of both channels was collected for each phagocyte. It is challenging to establish a fluorescence control for each image therefore exposure times and sensitivity setup were carefully adjusted enabling similar acquisition conditions for all repeats. Values typically varied between 100 – 2500 and the lower the value for the red and green channel was, the lower acidification and viability was considered for each *S. aureus* cell (respectively) (Figure 5.7.).

Values were further pooled together and compared in neutrophils and macrophages. Imaging data analysis demonstrated that in macrophages the mean value of red fluorescence intensity was higher than green, suggesting that a larger fraction of *S. aureus* internalised in those cells was acidified and simultaneously less viable (Figure 5.8.). *S. aureus* in neutrophils showed lower mean fluorescence signal for the red channel and higher for the green, possibly implicating lower acidification rates and higher viability. Altogether the data could suggest that macrophages are more effective in killing bacteria by acidification-related degradation and that neutrophils acidify *S. aureus* less, causing prolonged bacterial survival. However, the experimental approach does not provide a clear link between the acidification and viability of cells. Although similar but not quantified observations have been made in phagocytes of various transgenic lines throughout this study and pH indication optimisation, one should consider that mean green fluorescence in neutrophils could be slightly increased by the cytoplasmic GFP signal expressed in the cells.

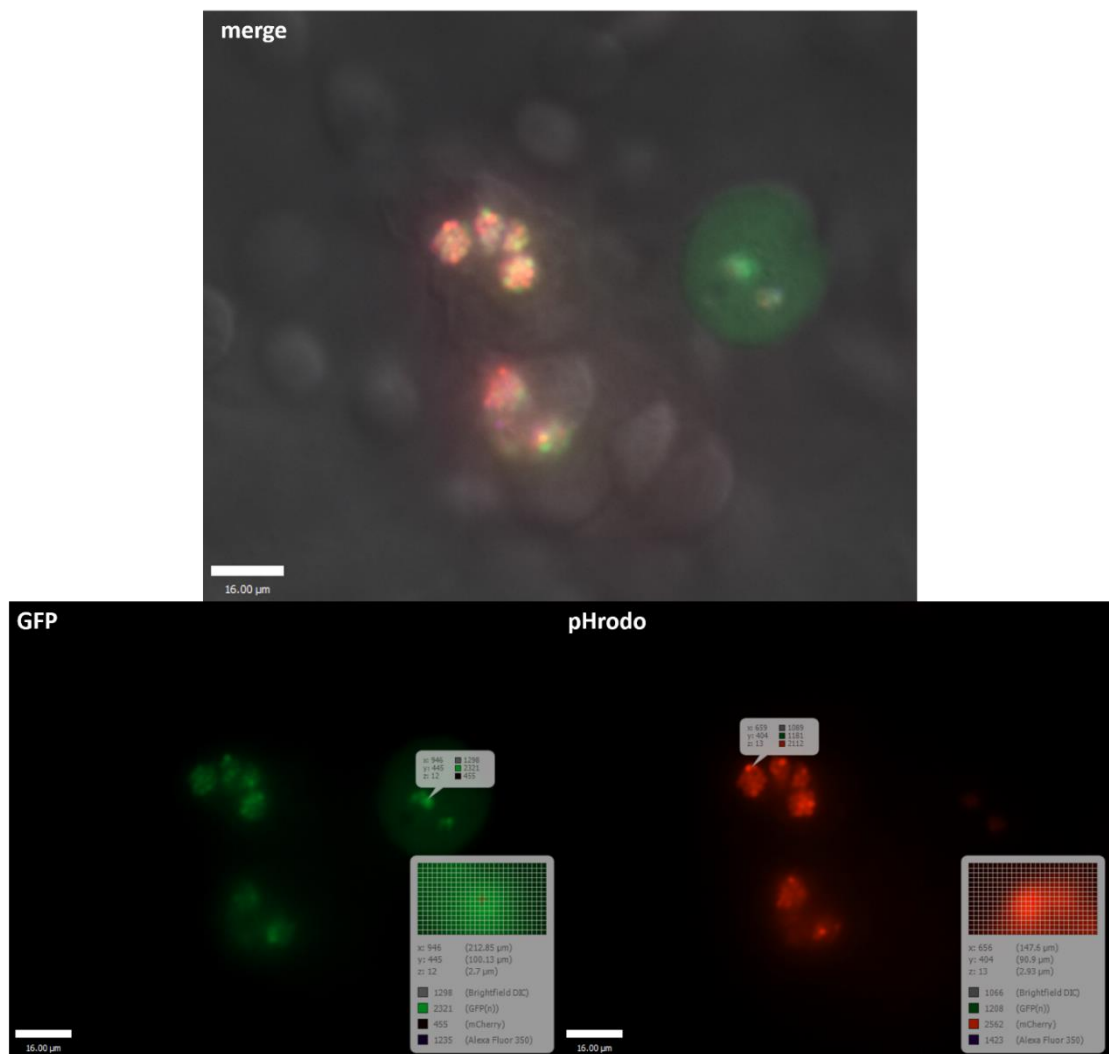


Figure 5.7. Imaging analysis of *S. aureus* viability and acidification in neutrophils and macrophages 1 hpi.

Tg(mpx:GFP) embryos were infected with 2500 CFU dose of SH1000-GFP *S. aureus* stained with Alexa Fluor 350 and pHrodo™ s-ester dyes. Image shows bloodstream phagocytes imaged 1 hpi and analysed using Volocity® software. Each bacterial cell was assigned a fluorescence intensity value for red and green channel, by manual scoring with the point tool, reflecting cell viability and acidification, respectively. Alexa Fluor 350 was used to visualise non-red and non-green bacteria (not acidified and likely killed *S. aureus*). Scale bar 15 µm. 60x oil objective.

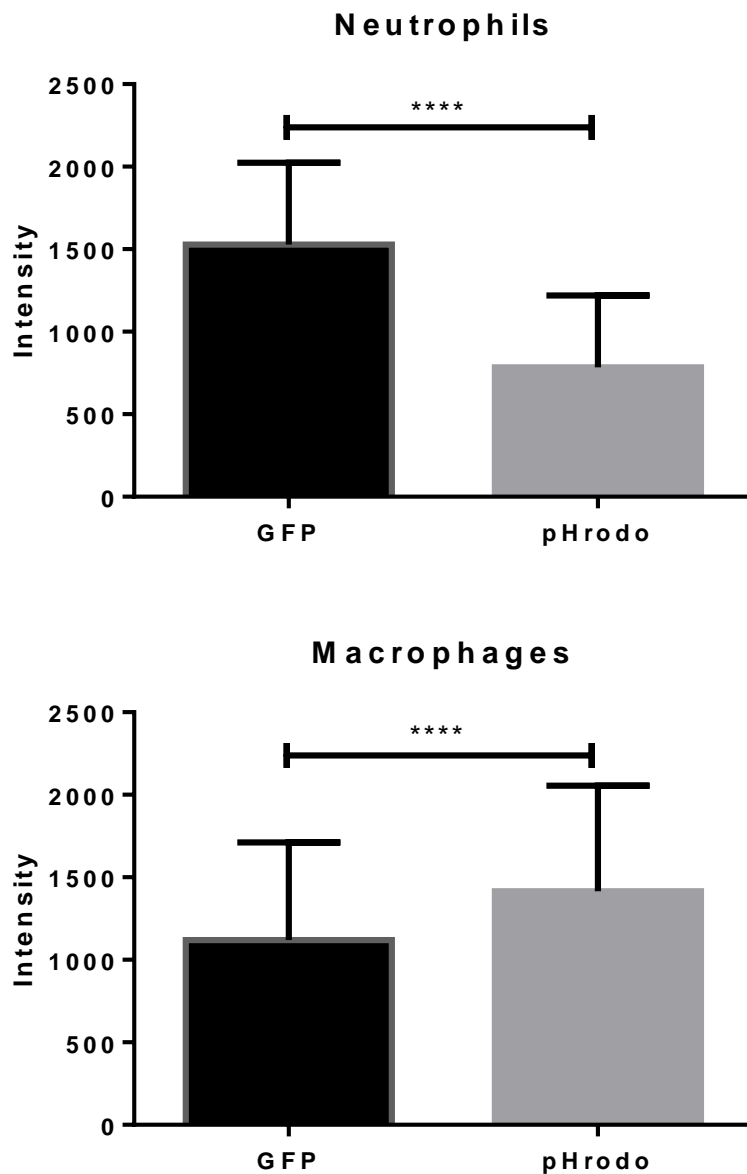


Figure 5.8. Fluorescence intensity measures of pHrodo™ stained, GFP expressing SH1000 cells internalised by neutrophils and macrophages.

Tg(mpx:GFP) embryos were infected with 2500 CFU dose of SH1000-GFP *S. aureus* stained with Alexa Fluor 350 and pHrodo™ s-ester dyes. Bloodstream phagocytes containing bacteria were imaged 1 hpi and analysed using Volocity® software. Each bacterial cell was assigned a fluorescence intensity value for red and green channel, by manual scoring with the point tool. Increased value of pHrodo fluorescence intensity implies low pH of compartment containing stained bacteria. The decrease in plasmid-encoded GFP fluorescence intensity has been used as a marker of bacteria killing. Plots show both values represented in neutrophils and macrophages (unpaired t test, significantly higher GFP values in neutrophils, $p < 0.0001$; significantly higher pHrodo values in macrophages, $p < 0.0001$). A representative number of minimum 5 embryos (and 20 phagocytes per larvae) was imaged in each experimental group, experiment repeated $n = 3$.

5.3. *S. aureus* co-localisation with LC3

The LC3 protein is widely used as a marker of autophagy machinery, and the generation of LC3 reporter transgenic lines *Tg(lyz:RFP.GFP.LC3)* and *Tg(mpeg:RFP.GFP.LC3)* (Chapter 4) allowed the analysis of *S. aureus* interaction with the autophagy pathway *in vivo*. *Tg(lyz:RFP.GFP.LC3)* embryos were infected with *S. aureus* in order to determine the involvement of the pathway in neutrophils. Several imaging approaches have also been applied to investigate the role of macrophage autophagy in *S. aureus* infection, by infecting *Tg(mpeg:RFP.GFP.LC3)* embryos. Where applicable, the role of reactive oxygen species (ROS) generation in phagocytes during infection with *S. aureus* was also investigated. ROS were visualised by simultaneous injection of bacterial inoculum and CellROX® ROS indicator (Figure 5.9. and figure 5.10).

Unless otherwise stated, 3 repeats of each experiment were performed to allow statistical analysis. Although a similar number of embryos were analysed in each experimental set up (5 larvae per group, 3 per control for each repeat), the representative group of phagocytes analysed would vary between 30 – 100. Therefore, often the comparative, quantitative analysis was related to the general population, and based on a percentage of host or pathogen cells.

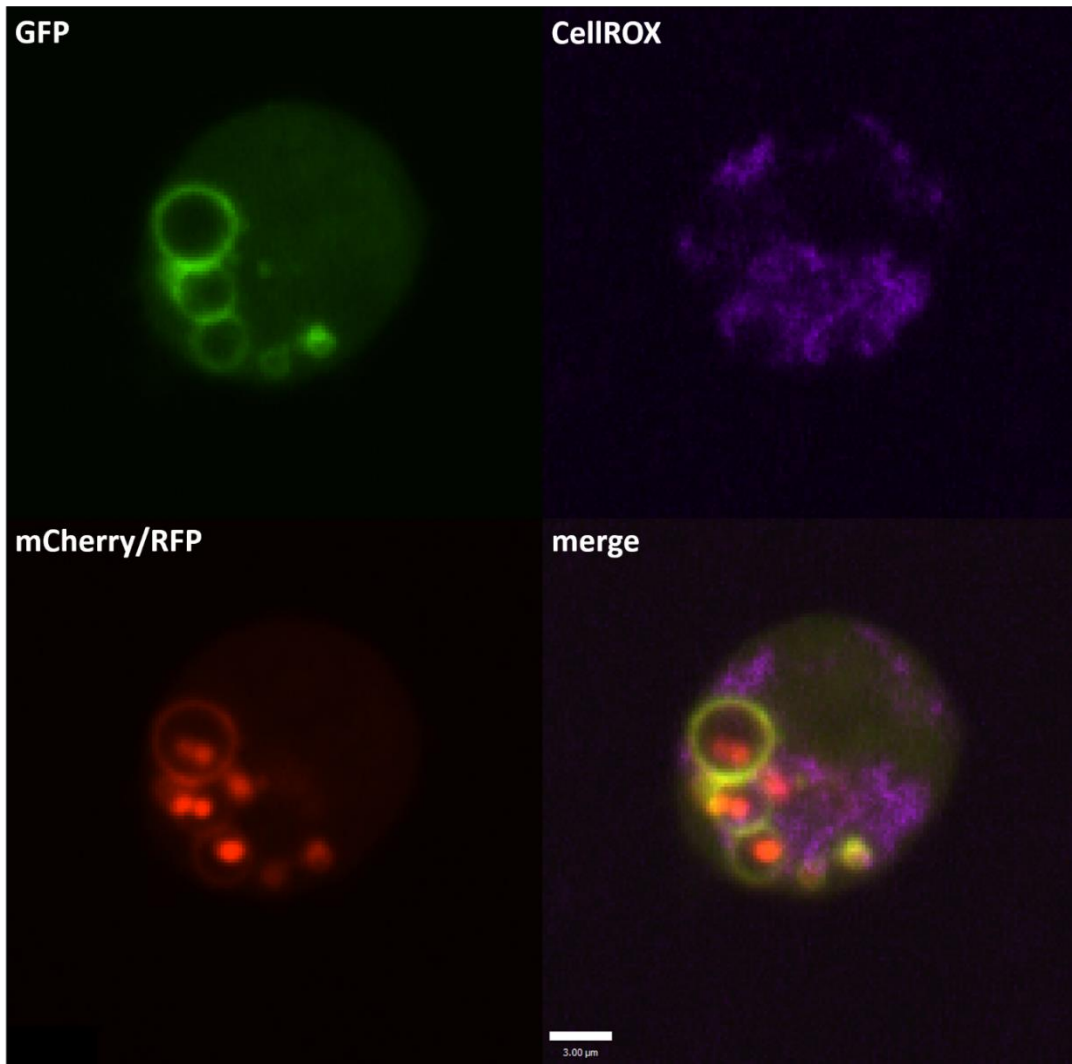


Figure 5.9. Imaging of *Tg(lyz:RFP.GFP.LC3)* embryo injected with SH1000-mCherry *S. aureus* and CellROX[®] ROS indicator.

Tg(lyz:RFP.GFP.LC3) embryos were infected with 2500 CFU SH1000-mCherry *S. aureus* inoculum with CellROX[®] ROS indicator. Image shows an example neutrophil imaged 1 hpi in the bloodstream. Presence of *S. aureus*, LC3 aggregates and ROS generation in neutrophils were analysed in Volocity[®] software. Scale bar 3 μm. 40x objective.

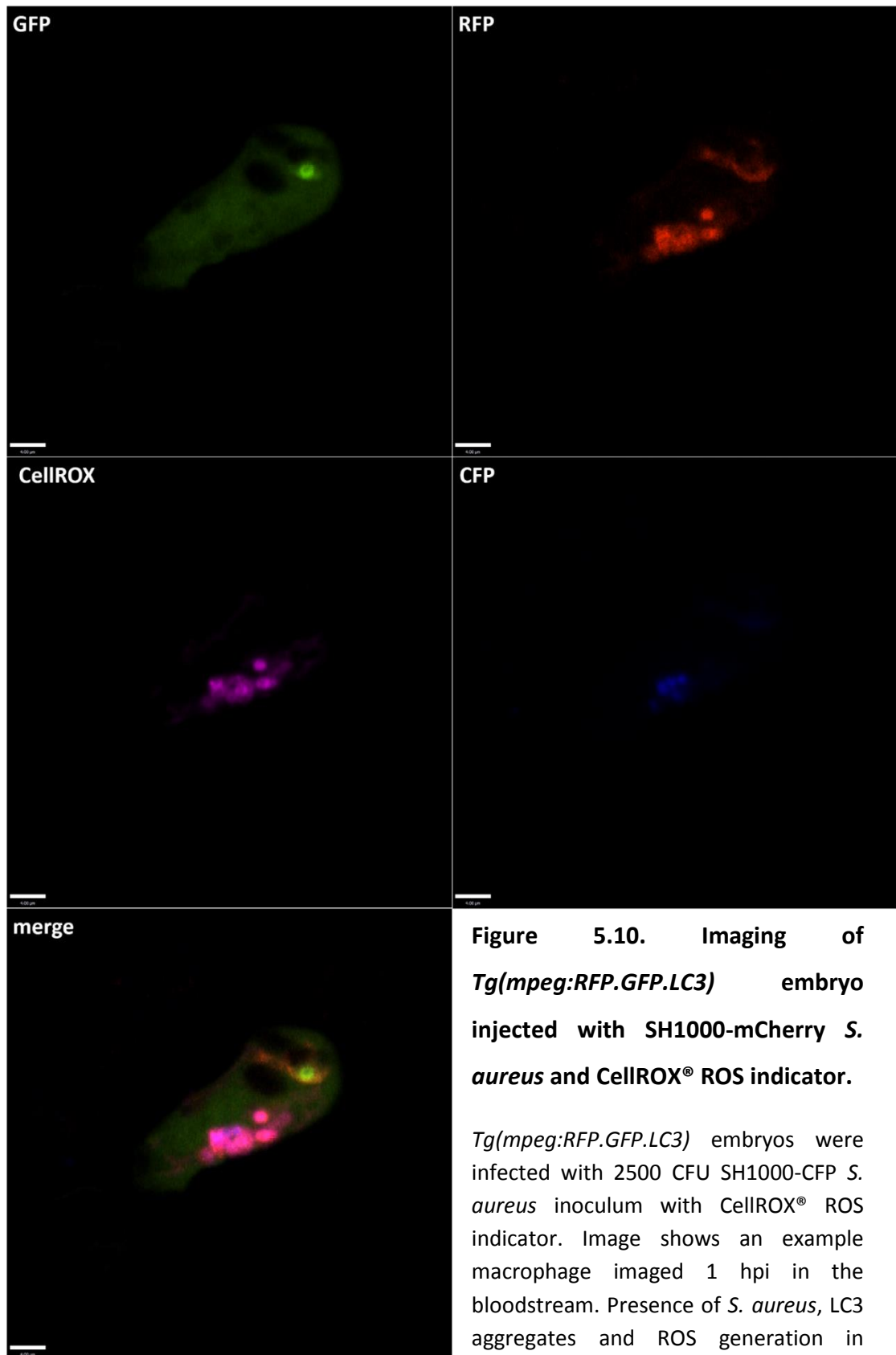


Figure 5.10. Imaging of *Tg(mpeg:RFP.GFP.LC3)* embryo injected with SH1000-mCherry *S. aureus* and CellROX® ROS indicator.

Tg(mpeg:RFP.GFP.LC3) embryos were infected with 2500 CFU SH1000-CFP *S. aureus* inoculum with CellROX® ROS indicator. Image shows an example macrophage imaged 1 hpi in the bloodstream. Presence of *S. aureus*, LC3 aggregates and ROS generation in macrophages were analysed in Volocity® software. Scale bar 4 µm. 40x objective.

5.3.1. ROS generation and co-localisation with LC3 in neutrophils during *S. aureus* infection

The generation of ROS has been suggested to have role in LC3 recruitment to phagosomes upon TLR signalling (Huang *et al.*, 2009). *Tg(lyz:RFP.GFP.LC3)* labelled neutrophils were scored for two events – *S. aureus* internalisation and ROS generation at two different time points; 1 and 20 hpi. At 1 hpi the majority of analysed neutrophils contained *S. aureus* and simultaneously showed the generation of ROS. Significantly fewer neutrophils were only ROS⁺ or *S. aureus*⁺ (Figure 5.11A). The proportion changed at 20 hpi, where no significant difference was observed between groups (Figure 5.11B). Moreover, the percentage of ROS-generating neutrophils was lower at the later time point (Figure 5.11C). The higher co-occurrence of *S. aureus* presence and ROS generation in neutrophils at the earlier time point post infection suggests that the oxidative burst occurs early after neutrophils internalise the pathogen. At 20 hpi, the signal is still generated in half of the *S. aureus*-containing neutrophils, implicating continuous *S. aureus* internalisation. The relatively high proportion of ROS⁺ uninfected neutrophils at 20 hpi compared to early stage of infection may suggest that these cells have been infected and have killed bacteria by the 20 hpi time point of acquisition (Figure 5.11D).

Although the number of bacteria residing in ROS⁺ neutrophils is higher than in ROS⁻ ones at 1 hpi it seems broadly comparable in the two groups at both time points (Figure 5.12.). Hence, pathogen-triggered ROS generation does not depend on the number of bacteria internalised in neutrophils.

The implication of ROS in *S. aureus* infection was also studied by evaluating the direct co-localisation of bacterial cells with ROS-active areas in neutrophils at 1 hpi and 20 hpi time points. Most bacteria colocalised with ROS at both time points, however, significantly more at 1 hpi than 20 hpi (Figure 5.13.). This result could also imply the significance of ROS generation in neutrophils at early time points of infection.

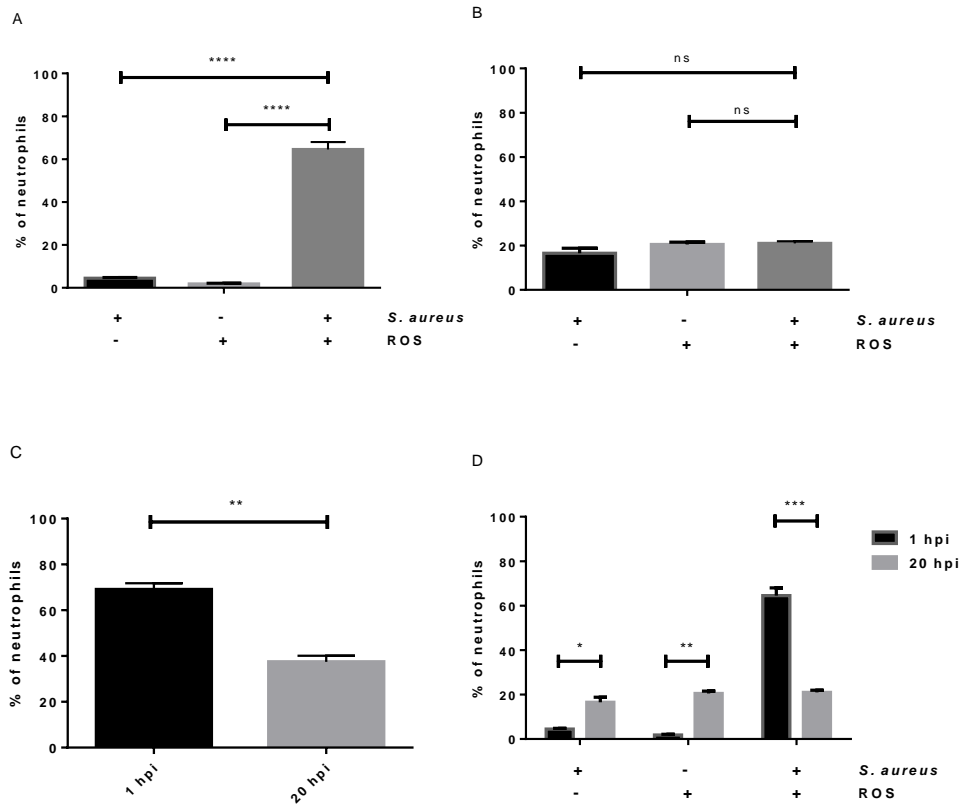


Figure 5.11. Generation of ROS in neutrophils of *Tg(lyz:RFP.GFP.LC3)* embryos.

Tg(lyz:RFP.GFP.LC3) embryos were injected with 2500 CFU dose of SH1000-mCherry *S. aureus*. ROS presence in neutrophils was assessed based on imaging data generated using CellROX® ROS indicator. Plot shows percentage of neutrophils internalising *S. aureus* bacteria and generating ROS 1 hpi (A), and 20 hpi (B). First column shows percentage of neutrophils which internalised *S. aureus* but did not generate ROS (*S. aureus*⁺). Second column shows percentage of neutrophils that generated ROS but did not contain bacteria at the time of acquisition (ROS⁺). Third column displays the percentage of bacteria-containing neutrophils that also generated ROS (*S. aureus*⁺ ROS⁺). A representative number of minimum 5 embryos (and 20 phagocytes per larvae) was imaged in each experimental group, experiment repeated n = 3.

A. Significantly more *S. aureus*⁺ ROS⁺ than *S. aureus*⁺ and ROS⁺ only (One-way ANOVA, Tukey's test, p < 0.0001) at 1 hpi.

B. No significant difference between analysed groups at 20 hpi (One-way ANOVA, Tukey's test).

C. A larger fraction of ROS-generating neutrophils was observed 1 hpi than 20 hpi (unpaired t test, p = 0.0013).

D. Significantly more *S. aureus*⁺ and ROS⁺ 20 hpi than 1 hpi (Two-way ANOVA, Sidak's test, p = 0.0190, p = 0.0037, respectively). Significantly more *S. aureus*⁺ ROS⁺ 1 hpi than 20 hpi (p < 0.0001).

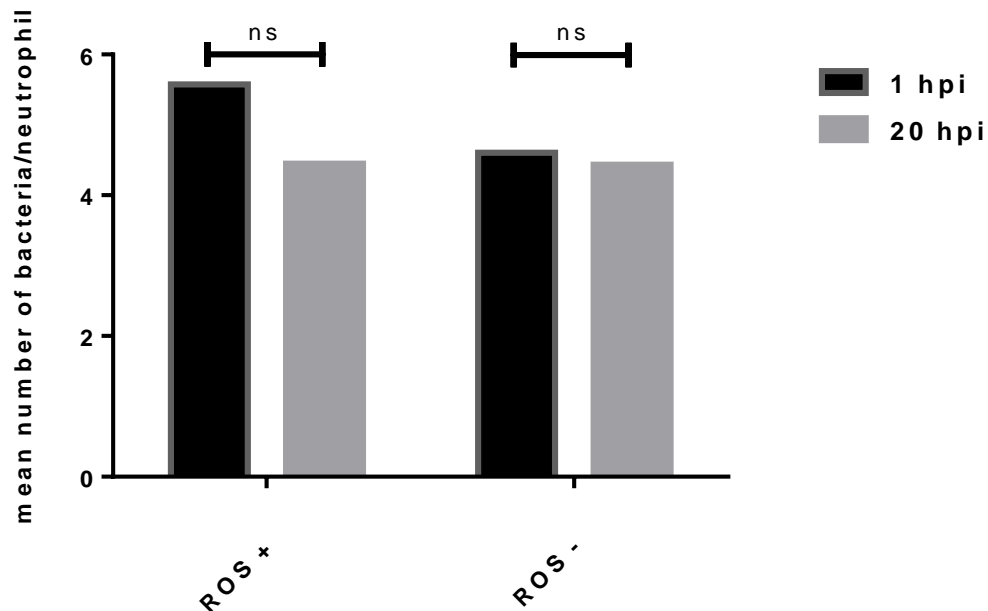


Figure 5.12. Mean number of *S. aureus* internalised by neutrophils of *Tg(lyz:RFP.GFP.LC3)* embryos.

Tg(lyz:RFP.GFP.LC3) embryos were injected with 2500 CFU dose of SH1000-mCherry *S. aureus*. ROS presence in neutrophils was assessed based on imaging data generated using CellROX[®] ROS indicator. Plot shows no significant difference in the mean number of internalised bacteria between 1hpi and 20 hpi time points in both ROS⁺ and ROS⁻ neutrophils (unpaired t test, $p=0.3796$, $p=0.9759$, respectively). A representative number of minimum 5 embryos (and 20 phagocytes per larvae) was imaged in each experimental group, experiment repeated $n = 3$.

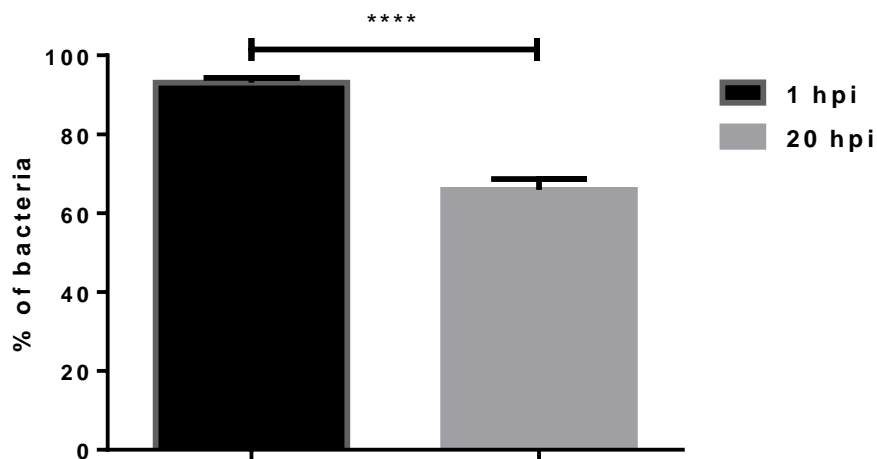


Figure 5.13. Direct co-localisation of *S. aureus* with ROS-active compartments in neutrophils of infected *Tg(lyz:RFP.GFP.LC3)* embryos.

Tg(lyz:RFP.GFP.LC3) embryos were injected with 2500 CFU dose of SH1000-mCherry *S. aureus*. ROS presence in neutrophils was assessed based on imaging data generated using CellROX® ROS indicator. Plot shows *S. aureus* cells directly co-localising with ROS compartments in neutrophils. Co-localisation was significantly higher 1 hpi than 20 hpi (unpaired t test, $p < 0.0001$). A representative number of minimum 5 embryos (and 20 phagocytes per larvae) was imaged in each experimental group, experiment repeated $n = 3$.

5.3.2. *S. aureus* co-localises with different classes of LC3 aggregates in neutrophils

The standard LC3 classification proposed during the characterisation of the *Tg(lyz:RFP.GFP.LC3)* line was applied to assess LC3 co-localisation with bacteria in neutrophils. Co-localisation of *S. aureus* with LC3 structure is defined by direct association of the pathogen with aggregate, or in case of spacious vesicles, by the fact that bacterial cells are contained within the structure. According to the result of the quantitative analysis of imaging data, 20 % of bacteria did not co-localise with LC3 in neutrophils (Figure 5.14.). 40 % of bacteria co-localised with LC3 spacious vesicles and the second largest group was bacteria co-localised with LC3 tight vesicles. *S. aureus* co-localised with spheroids and LC3 puncta together constituted less than 20 % of all bacteria. Overall this data suggests that within 1 hpi bacteria are recognised and targeted by autophagic machinery, which is reflected by puncta, spheroids or tight vesicle LC3 structures co-localised with the pathogen. Moreover, the recruitment of LC3 protein to spacious vesicles could imply that the pathway responsible for targeting of LC3 to phagocytes has been active at the early stages of infection.

Quantification data were also analysed for neutrophils divided into two distinct groups – separately for ROI⁺ and ROI⁻ neutrophils (Figure 5.14.). It has been suggested by Huang *et al.* that NOX2-generated ROS regulate phagocytosis-related autophagy by triggering the recruitment of LC3 to the phagosome membrane. Therefore one of the hypotheses of this experiment was that bacteria would co-localise with spacious vesicle LC3 more frequently in ROS⁺ neutrophils.

The results show that there was no significant difference between the numbers of bacteria co-localised with spacious and tight vesicles in ROS⁺ and ROS⁻ neutrophils, however the number of ROS⁻ neutrophils was significantly lower at 1hpi giving a smaller representative group of neutrophils. In ROS⁻ neutrophils *S. aureus* cells not co-localised in LC3 vesicles were not co-localised with either LC3 puncta or spheroids. On the other hand, in ROS⁺ neutrophils, a fraction of bacteria that was not co-localised with LC3 tight and spacious vesicles, did co-localise with these two LC3 classes. The engagement of smaller LC3 structures in ROS⁺ neutrophils could imply

that the direct targeting of intracellular *S. aureus* by autophagy is mediated by the presence of ROS.

Correspondingly, 40 % of bacteria co-localised with LC3 spacious vesicles at the later time point. Furthermore, only about 10 % of the pathogen was co-localised with tight vesicles, seemingly causing the increase of the population of not co-localised bacteria up to 40 %. Indeed, both the change in the percentage of not colocalised and tight vesicle co-localised bacteria was significant between the two time points (Figure 5.16.). Co-localisation of *S. aureus* with puncta and spheroids was still low but detectable, indicating the role of bacteria-targeted autophagy at that time point post infection. Interestingly, significantly more bacteria co-localised with spacious vesicles in ROS⁻ neutrophils (Figure 5.15), which could imply that LC3 recruitment to phagosomes is not mediated by ROS generation at that time point. However, this assumption would have to be tested in a more representative group of ROS⁻ neutrophils. Moreover, as all of the embryos were imaged at a fixed time point it is difficult to conclude whether ROS generation is constant, or if what we observe is in fact the outcome of its ongoing activity.

Taken together the 20 hpi data suggested that over the course of infection more bacteria resided in neutrophils without interacting with autophagic machinery. Moreover, the decrease in co-localisation with tight vesicles could correspond to the failure of bacteria-targeted autophagosome completion. Alternatively, at this time point tight LC3 vesicles fuse together with lysosomal compartments, creating larger, spacious vesicles. Stable, 40 % co-localisation with this LC3 class would therefore imply that a fraction of bacteria co-localised with spacious vesicles at 1 hpi was either degraded or escaped to the cytoplasm. It is likely that LC3 vesicles undergo maturation and fusion with lysosomes, which could result in the killing of bacteria or release of these cells (all or just a few) back to the cytoplasm where they have been observed during the analysis. It is difficult to determine which scenario is more likely in a dynamic *in vivo* model, however as the mean number of bacteria per neutrophil decreases in the first 20 hpi, one can speculate that at least a fraction of the internalised *S. aureus* bacteria are killed.

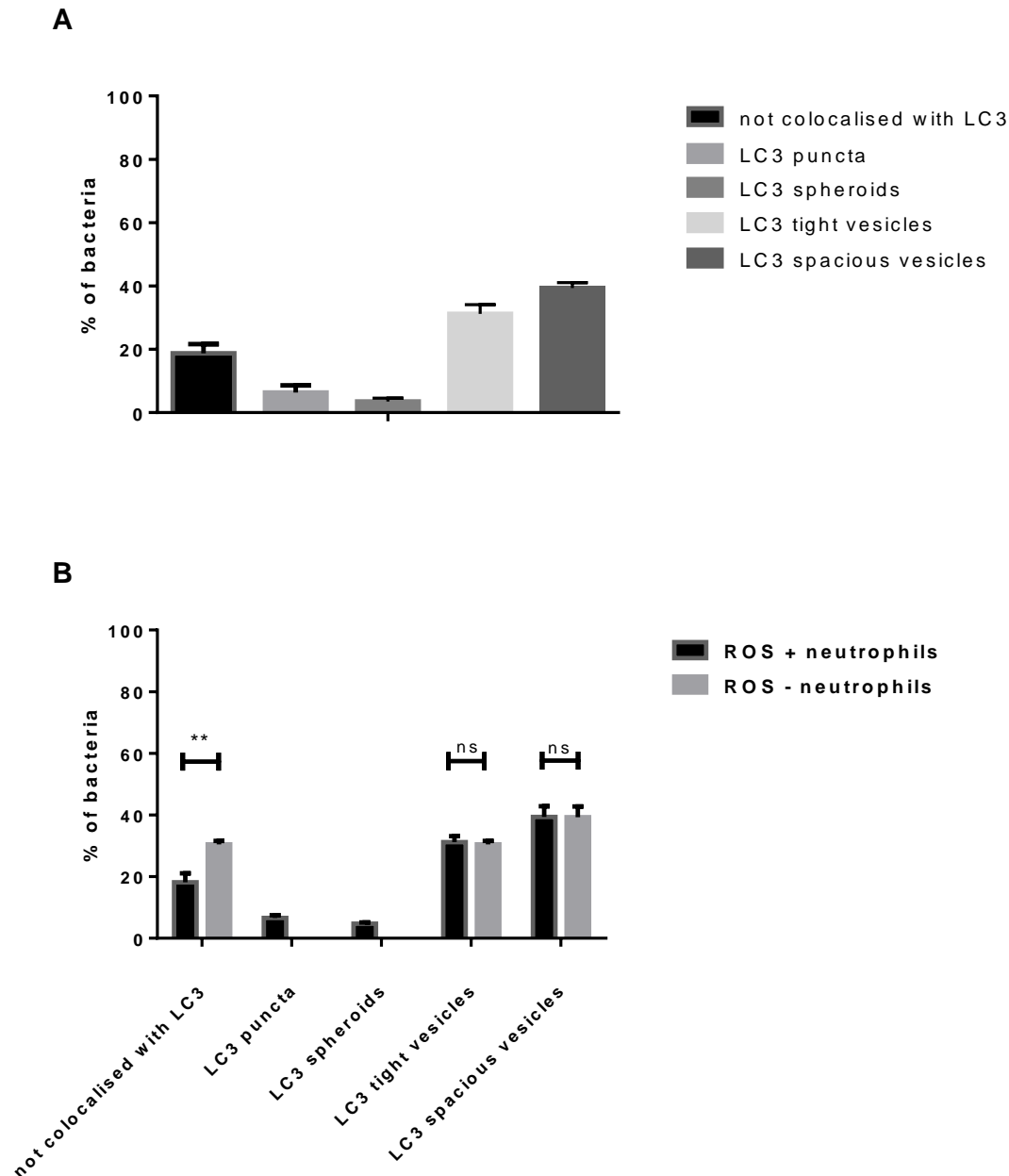


Figure 5.14. Percentage of bacteria co-localised in neutrophils with different classes of LC3 at 1 hpi.

Tg(Iyz:RFP.GFP.LC3) embryos were injected with 2500 CFU dose of SH1000-mCherry *S. aureus*. ROS presence in neutrophils was assessed based on imaging data generated using CellIROX® ROS indicator. Plot shows A, Percentage contribution of *S. aureus* co-localised with different LC3 classes in neutrophils, together with the percentage of bacteria not co-localised with LC3. *S. aureus* mostly co-localises with tight and spacious vesicles. B, Co-localisation of *S. aureus* with LC3 in ROS⁺ and ROS⁻ neutrophils. Significantly more bacteria did not co-localise with LC3 in ROS⁻ neutrophils (Two-way ANOVA, Sidak's test, $p = 0.0016$). A representative number of minimum 5 embryos (and 20 phagocytes per larvae) was imaged in each experimental group, experiment repeated $n = 3$.

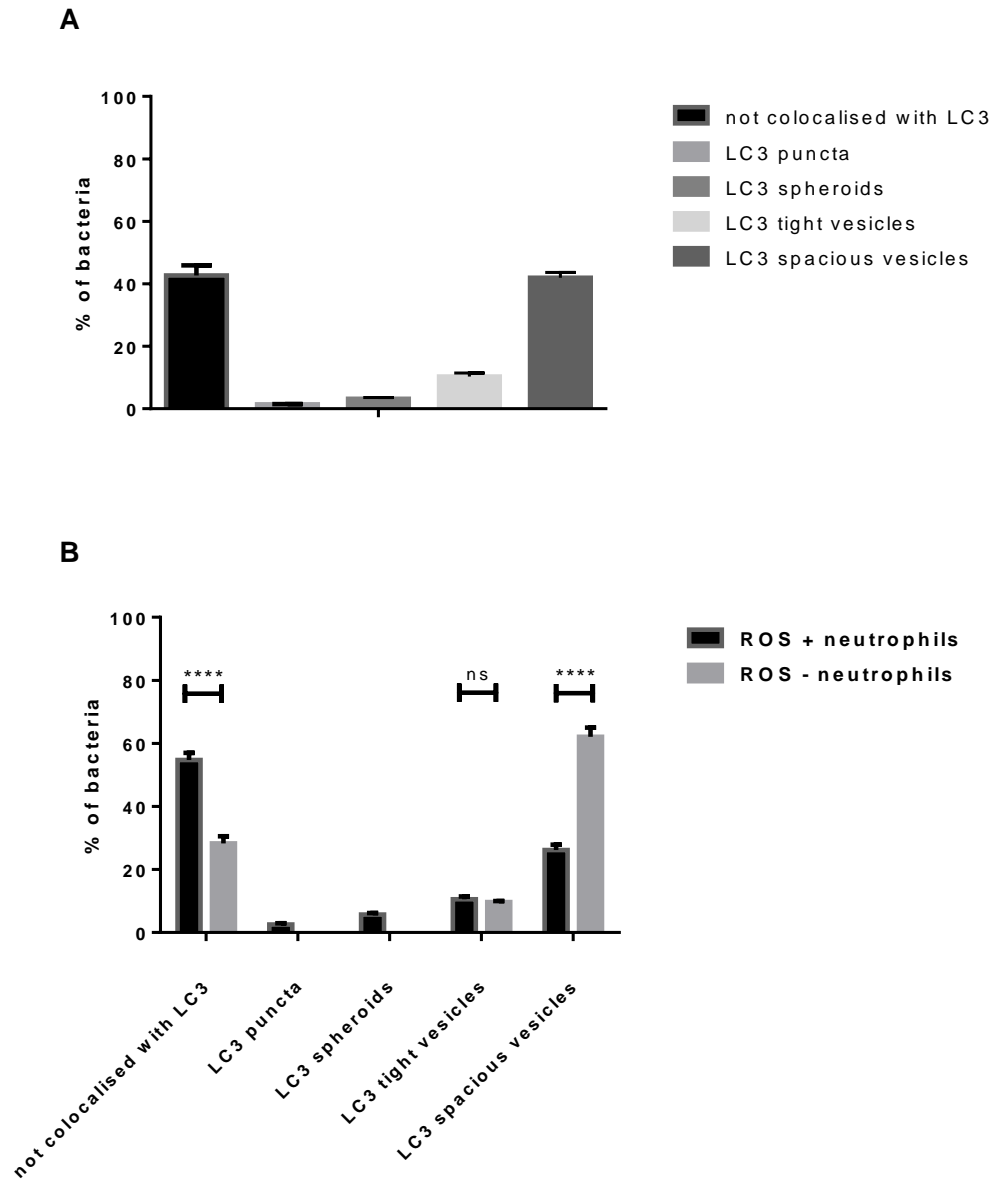


Figure 5.15. Percentage of bacteria co-localised in neutrophils with different classes of LC3 at 20 hpi.

Tg(lyz:RFP.GFP.LC3) embryos were injected with 2500 CFU dose of SH1000-mCherry *S. aureus*. ROS presence in neutrophils was assessed based on imaging data generated using CellROX® ROS indicator. Plot shows A, Percentage distribution of *S. aureus* co-localised with different LC3 classes in neutrophils, together with the percentage of bacteria not co-localised with LC3. B, co-localisation of *S. aureus* with LC3 in ROS⁺ and ROS⁻ neutrophils. Significantly more bacteria did not co-localise with LC3 in ROS⁺ neutrophils (Two-way ANOVA, Sidak's test, $p < 0.0001$). Also, more bacteria co-localised with spacious vesicles in ROS⁻ neutrophils (Two-way ANOVA, Sidak's test, $p < 0.0001$). A representative number of minimum 5 embryos (and 20 phagocytes per larvae) was imaged in each experimental group, experiment repeated $n = 3$.

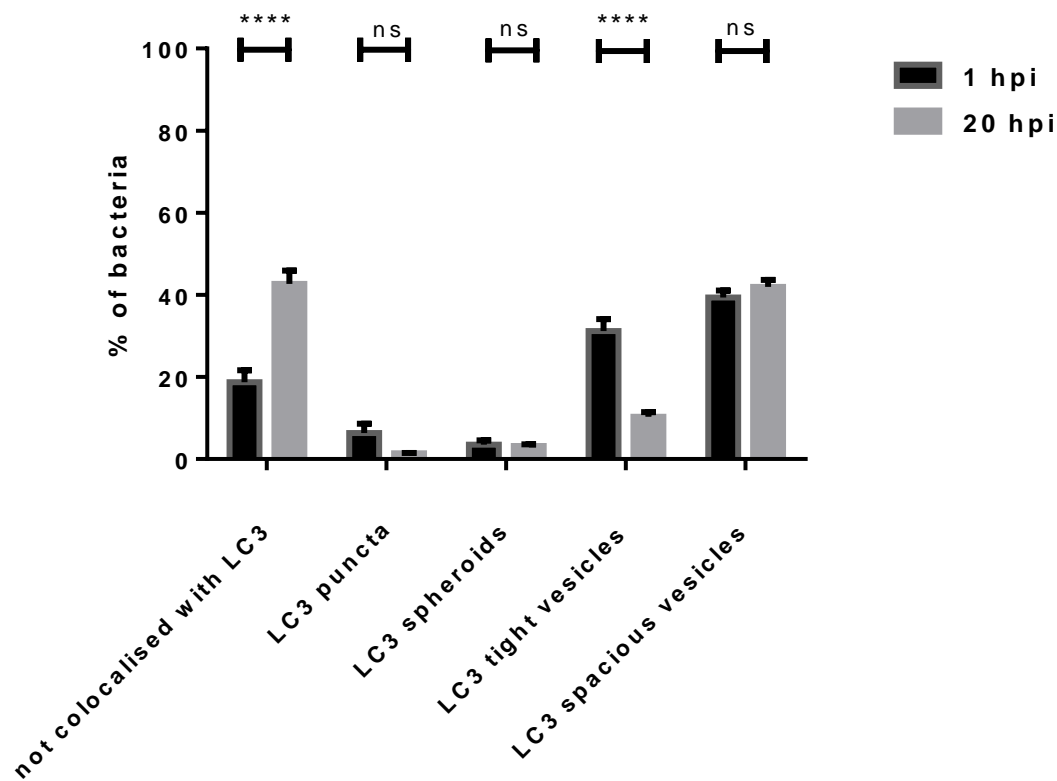


Figure 5.16. Percentage of *S. aureus* co-localised with different classes of LC3 at various time points post infection.

Tg(lyz:RFP.GFP.LC3) embryos were injected with 2500 CFU dose of SH1000-mCherry *S. aureus*. Plot shows with which classes of LC3 *S. aureus* was observed to co-localise. Significantly more bacteria did not co-localise with LC3 at 20 hpi than at 1 hpi (Two-way ANOVA, Sidak's test, $p < 0.0001$) and significantly less co-localised with LC3 tight vesicles (Two-way ANOVA, Sidak's test, $p < 0.0001$). No significant differences were observed in other LC3 classes. A representative number of minimum 5 embryos (and 20 phagocytes per larvae) was imaged in each experimental group, experiment repeated $n = 3$.

5.3.3. ROS generation and co-localisation with LC3 in macrophages during *S. aureus* infection

The *Tg(mpeg:RFP.GFP.LC3)* line was used to investigate the role of ROS generation in macrophages. As in the neutrophil-specific LC3 reporter line, phagocytes were similarly scored for two events – *S. aureus* internalisation and ROS generation. The analysis was only performed at 1 hpi time point.

Red and green fluorescent protein was distributed differently throughout the cell. This observation could possibly be explained by quenching of the GFP protein in low pH compartments in the cell. For the purpose of the macrophage analysis two groups of LC3 were distinguished based on which fluorophore appeared active, red or green.

Most macrophages infected were also ROS⁺ implicating that ROS generation plays a role in the hosts macrophage response to *S. aureus* infection (Figure 5.17A). Further analysis involved scoring of bacteria directly co-localised with LC3-active compartments in macrophages. Almost 90 % of bacteria in infected macrophages colocalised with ROS generated and about 20 % simultaneously colocalised with LC3, mostly of the red fluorescent type (Figure 5.17B).

Analysis of the imaging data demonstrated that ROS⁺ macrophages contained more bacteria than ROS⁻, although only 3.2 % of the total macrophage population was ROS⁻ (Figure 5.18.). Here again, it is difficult to conclude whether ROS generation is constant during bacterial presence in macrophage, or transiently involved in pathogen handling.

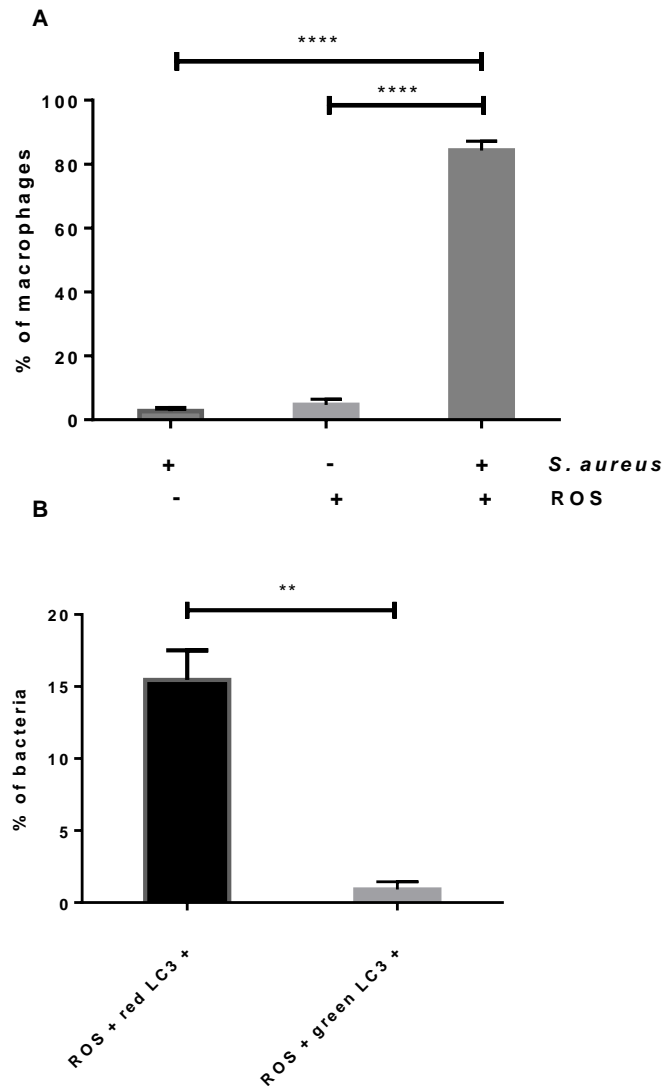


Figure 5.17. Generation of ROS in macrophages of infected *Tg(mpeg:RFP.GFP.LC3)* embryos.

Tg(mpeg:RFP.GFP.LC3) embryos were injected with 2500 CFU dose of SH1000-mCherry *S. aureus*. ROS presence in macrophages was assessed based on imaging data generated using CellROX® ROS indicator. Plots show A, Percentage of macrophages internalising bacteria and generating ROS at 1 hpi with *S. aureus*. First column shows percentage of macrophages which internalised *S. aureus* but did not generate ROS (*S. aureus*⁺). Second column shows percentage of macrophages that generated ROS but did not contain bacteria at the time of acquisition (ROS⁺). Third column demonstrates percentage of bacteria-containing macrophages that also generated ROS (*S. aureus*⁺ ROS⁺). Significant majority of macrophages was *S. aureus*⁺ ROS⁺ (One-way ANOVA, Tukey's test, $p < 0.0001$). B, 87 % of bacteria were co-localised with ROS in macrophages. Out of those 15 % were simultaneously co-localised with red LC3 (significantly more, unpaired t test, $p = 0.0024$) and 2 % with green LC3. A representative number of minimum 5 embryos (and 20 phagocytes per larvae) was imaged in each experimental group, experiment repeated $n = 3$.

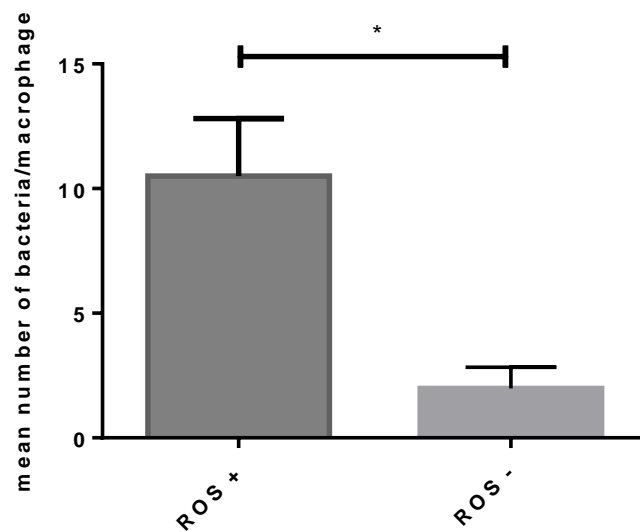


Figure 5.18. Mean number of bacteria internalised in ROS⁺ and ROS⁻ macrophages.

Tg(mpeg:RFP.GFP.LC3) embryos were injected with 2500 CFU dose of SH1000-mCherry *S. aureus*. ROS presence in macrophages was assessed based on imaging data generated using CellROX[®] ROS indicator. 3.2 % of infected macrophages were ROS⁻. Data presented on the plot shows that this fraction of macrophages contained lower number of *S. aureus* cells (unpaired t test, $p=0.0258$). A representative number of minimum 5 embryos (and 20 phagocytes per larvae) was imaged in each experimental group, experiment repeated $n = 3$.

5.3.4. LC3 interacts with bacteria internalised by neutrophils and macrophages in distinct ways

From the observation made in my study it appears that LC3 in macrophages aggregates differently than in neutrophils. Herein, LC3 was rarely observed forming a distinct fluorescent ring around bacteria and phagosomes, but otherwise forms similar structures as seen in neutrophils. This could mean that fluorescence expressed under *mpeg* promoter is dimmer or down regulated during infection, hence the detectable signal from the protein reporter is weaker.

A fraction of LC3 aggregates in macrophages was not colocalised with bacteria. The presence of both red and green LC3 may be suggesting recent antimicrobial activity, LC3 processing before recruitment to bacteria or processing unrelated to infection. Red LC3 dominates in infected macrophages suggesting that it has been involved in processes occurring in acidified environment (Figure 5.19.).

The LC3 structures co-localised with bacteria were classified based on the red or green fluorescence protein signal detectable. About 30 % of bacteria did not co-localise with LC3 in macrophages. The majority of bacteria co-localised with red LC3, significantly more than with green LC3 and more than in the not co-localised fraction (Figure 5.19.). This result could indicate that LC3 associated to the inner autophagosome membrane became acidified, and the GFP signal was quenched. The LC3 from the outer membrane would dissociate after fusion with lysosomes, and thus, only RFP fluorescence from the autolysosome lumen would be observed.

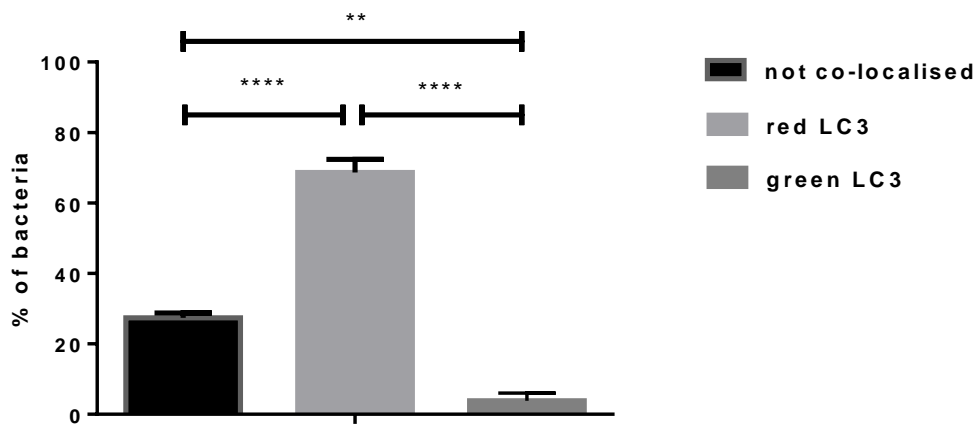


Figure 5.19. Co-localisation of *S. aureus* with LC3 in macrophages 1 hpi.

Tg(mpeg:RFP.GFP.LC3) embryos were injected with 2500 CFU dose of SH1000-mCherry *S. aureus*. Plot shows co-localisation of *S. aureus* with two classes of LC3 protein observed in macrophages, red and green. Fraction of *S. aureus* co-localised with red LC3 was significantly larger than the fraction of not co-localised bacteria and those co-localised with green LC3 (One-way ANOVA, Tukey's test, $p < 0.0001$). Significantly more *S. aureus* did not co-localise with LC3 than with green LC3 (One-way ANOVA, Tukey's test, $p = 0.0016$). A representative number of minimum 5 embryos (and 20 phagocytes per larvae) was imaged in each experimental group, experiment repeated $n = 3$.

5.3.5. LC3 vesicle content in *S. aureus* infected phagocytes

LC3 can be recruited to intracellular pathogen directly, or associated with bacteria-containing phagosomes upon TLR signalling. The latter interaction has been described as NOX2 NADPH oxidase-dependent resulting in LC3 recruitment to the phagosome membrane (Huang *et al.*, 2009). A corresponding structure, the spacious LC3-decorated vesicle, has been observed in neutrophils of infected *Tg(lyz:RFP.GFP.LC3)* line embryos.

NOX2-generated ROS are present in the phagosome lumen, unlike ROS generated in cellular mitochondria (Huang *et al.*, 2009). Therefore, additional imaging data analysis was performed to determine whether ROS species were present inside LC3 vesicles. ROS generation within LC3 vesicles was analysed 1 hpi and 20 hpi. Those vesicles would correspond to tight and spacious vesicle classes from the LC3 classification analysis. At both time points the majority of vesicles were ROS⁻ and the percentage of ROS⁺ did not change within this time (Figure 5.20.).

Some of the vesicles were observed to have LC3 puncta contained within. An additional quantitative approach was employed to help determine how often LC3 is recruited to the vesicle lumen 1 and 20 hpi. However, data resulting from the analysis demonstrated that the majority of vesicles did not contain LC3, and that the ratio did not change between the two time points (Figure 5.21)

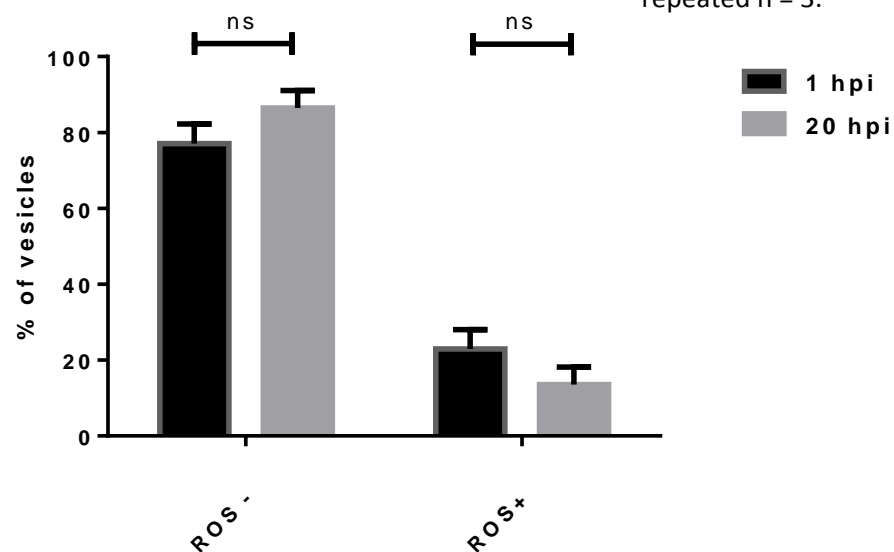
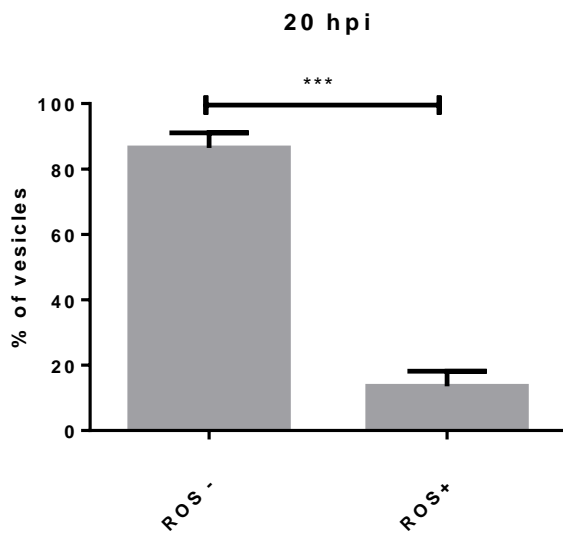
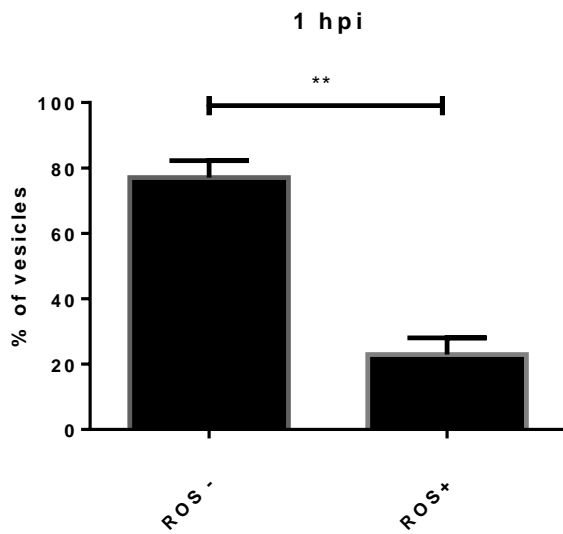


Figure 5.20. ROS generation within LC3 vesicles in neutrophils 1 and 20 hpi.

Tg(lyz:RFP.GFP.LC3) embryos were injected with 2500 CFU dose of SH1000-mCherry *S. aureus*. ROS presence in neutrophils was assessed based on imaging data generated using CellROX[®] ROS indicator. Further analysis consisted on observation of ROS within LC3 vesicles in neutrophils. Plots show that significantly more vesicles did not contain generated ROS at 1 hpi (unpaired t test, $p = 0.0017$) and at 20 hpi (unpaired t test, $p=0.0004$).

No significant difference was found in the ratio of ROS containing and not containing vesicles between 1 hpi and 20 hpi time points (unpaired t test). A representative number of embryos (and 20 phagocytes per larvae) was imaged in each experimental group, experiment repeated $n = 3$.

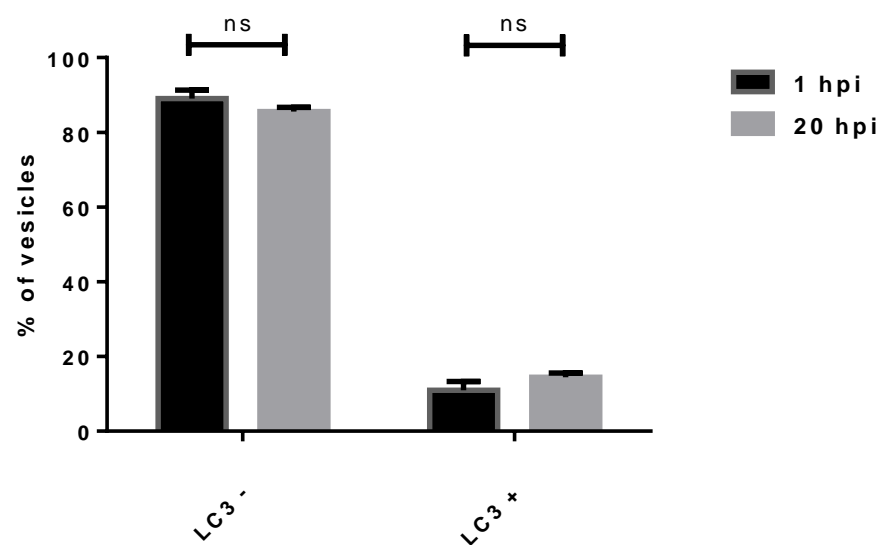
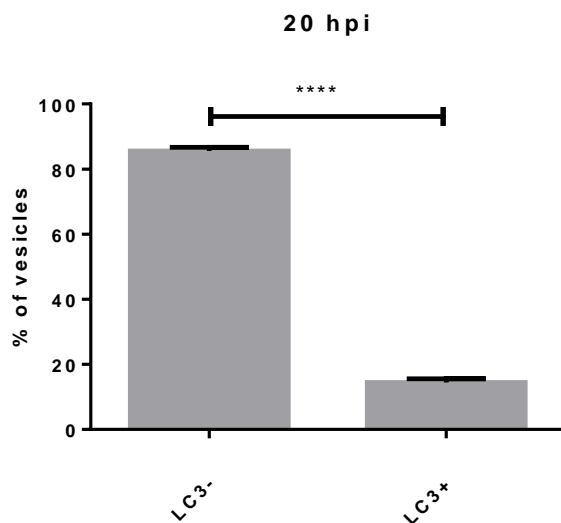
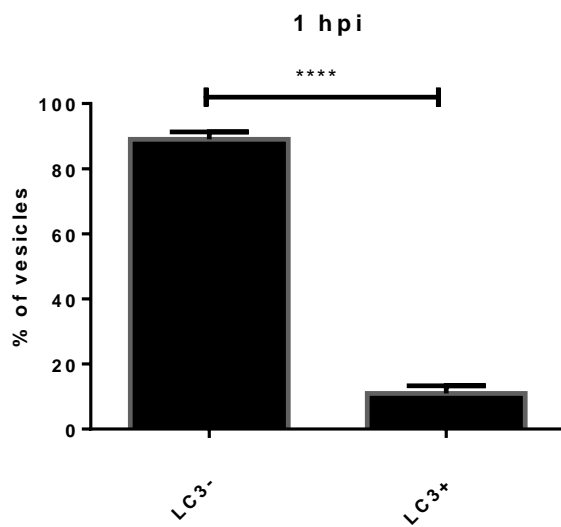


Figure 5.21. LC3 puncta presence within LC3 vesicles in neutrophils 1 and 20 hpi.

Tg(lyz:RFP.GFP.LC3) embryos were injected with 2500 CFU dose of SH1000-mCherry *S. aureus*. Further analysis consisted on observation of LC3 puncta within LC3 vesicles in neutrophils. Plots show that significantly more vesicles did not contain generated LC3 puncta at 1 hpi and at 20 hpi (unpaired t test, $p < 0.0001$).

No significant difference in the ratio of LC3 puncta containing and not containing vesicles between 1 hpi and 20 hpi time points. A representative number of embryos (and 20 phagocytes per larvae) was imaged in each experimental group, experiment repeated $n = 3$.

Although the fraction of ROS containing vesicles was relatively low, their presence could still mean that NOX2-generated ROS play a role in LC3 recruitment to *S. aureus* containing phagosomes. It was therefore useful to verify the potential implication of ROS generation and LC3 puncta recruitment in bacterial killing inside LC3 vesicles. Thus, an analysis of vesicles was performed in order to determine whether they contained bacteria.

Four groups of vesicles have been distinguished depending on their content: ROS⁺, ROS⁻, LC3⁺, and LC3⁻. The percentage of empty vesicles – those not containing bacterial cells – was calculated for each group and compared for two time points – 1 hpi and 20 hpi. At 1 hpi less than 40 % of vesicles were empty, and there was no significant difference in bacteria-killing efficiency between distinguished groups (Figure 5.22.). The number of empty vesicles increased in all groups between 1 hpi and 20 hpi, which could be caused by general intracellular killing and a decrease in the number of bacteria. Additionally it could be correlated with the previous result suggesting less bacteria co-localising with LC3 tight vesicles at 20 hpi (Figure 5.16.).

At 20 hpi, the ROS⁺ group had significantly smaller ratio of empty vesicles. It could suggest that ROS generation causes LC3 recruitment but does not increase the killing of bacteria contained in the vesicle. On the other hand that could also mean that ROS are generated while bacteria are still present in vesicles, implying that ROS⁻ vesicles have already played a role in pathogen killing.

To further analyse the involvement of both LC3 puncta and ROS presence in vesicles, I distinguished four groups of vesicles including the presence of both factors. The new classification enabled analysis of bacterial clearance from ROS⁻ LC3⁻, ROS⁺ LC3⁻, ROS⁻ LC3⁺ and ROS⁺ LC3⁺ vesicles (Figure 5.23.). At 1 hpi, ROS⁻ LC3⁻ vesicles were slightly more likely to be empty, however the result was not significant compared to most of the other groups. At 20 hpi, ROS⁺ LC3⁺ vesicles were less likely to be empty, implicating that ongoing ROS generation and LC3 recruitment to the vesicle lumen could be related to bacterial presence and intended to increase bacterial killing. Other groups would represent other stages of such interaction, with those of the ROS⁻ LC3⁺ group most likely being empty. However, the most probable scenario could only be assessed by time lapse imaging of the intermediate time points post infection.

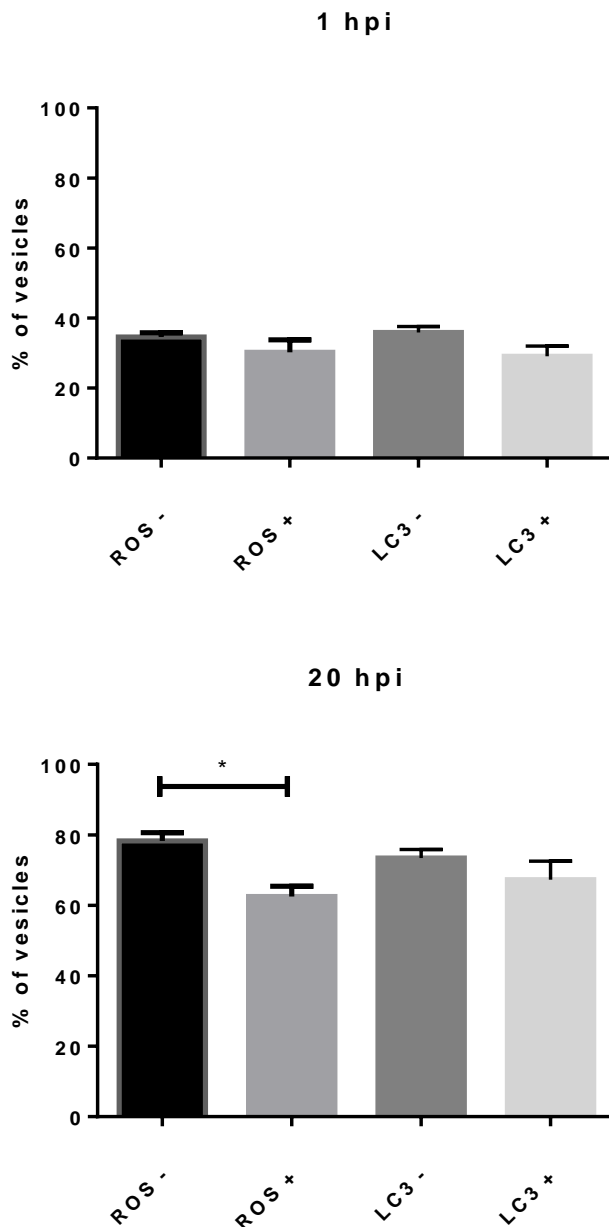


Figure 5.22. Percentage of LC3 vesicles not containing bacteria.

Tg(lyz:RFP.GFP.LC3) embryos were injected with 2500 CFU dose of SH1000-mCherry *S. aureus*. ROS presence in neutrophils was assessed based on imaging data generated using CellROX[®] ROS indicator. Further analysis consisted on observation of ROS and LC3 puncta within LC3 vesicles in neutrophils. Based on these components vesicles were marked as ROS⁺ and LC3⁺. Observation of the number of *S. aureus* in vesicles demonstrated that some did not contain bacteria. Plots show that that ROS⁻ vesicles were significantly more likely to be empty at 20 hpi (One-way ANOVA, Tukey's test, $p=0.0461$). No significant differences were found between other groups at 1 hpi and 20 hpi. A representative number of minimum 5 embryos (and 20 phagocytes per larvae) was imaged in each experimental group, experiment repeated $n = 3$.

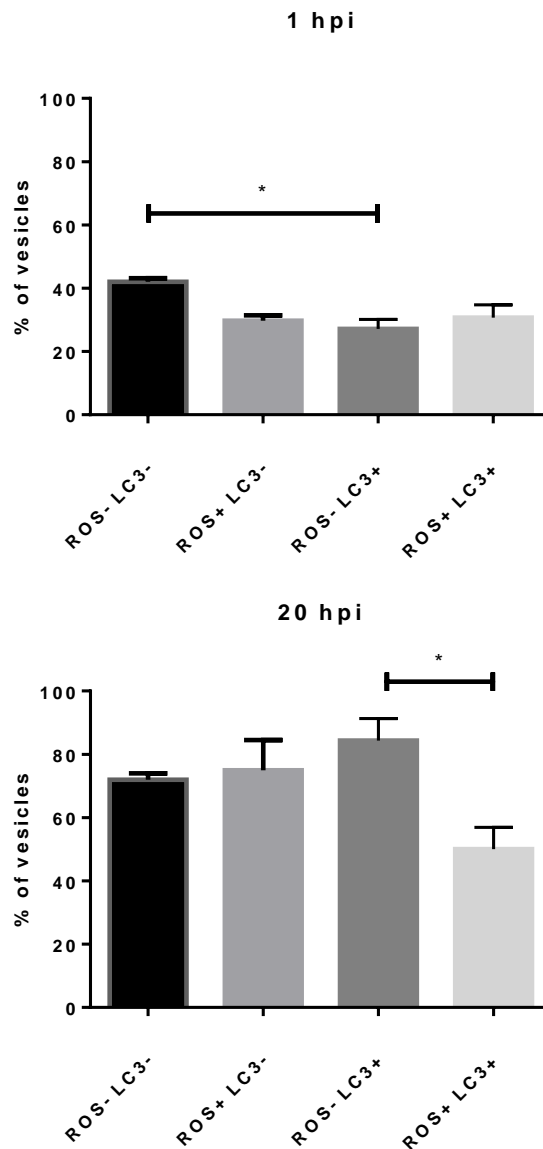


Figure.5.23. Percentage of LC3 vesicles not containing bacteria in ROS⁺ and ROS⁻ vesicles.

Tg(lyz:RFP.GFP.LC3) embryos were injected with 2500 CFU dose of SH1000-mCherry *S. aureus*. ROS presence in neutrophils was assessed based on imaging data generated using CellROX[®] ROS indicator. Further analysis consisted on observation of ROS and LC3 puncta within LC3 vesicles in neutrophils. Based on these components vesicles were marked as ROS⁺ and LC3⁺. Observation of the number of *S. aureus* in vesicles demonstrated that some did not contain bacteria. 1hpi ROS⁻ LC3⁻ vesicles were more likely to not contain bacteria (significantly more compared to ROS⁻ LC3⁺, One-way ANOVA, Tukey's test, $p = 0.02$). 20 hpi ROS⁺ LC3⁺ were more likely to contain bacteria than other groups (significantly more compared to ROS⁻ LC3⁺, One-way ANOVA, Tukey's test, $p = 0.0196$). A representative number of minimum 5 embryos (and 20 phagocytes per larvae) was imaged in each experimental group, experiment repeated $n = 3$.

Similar analysis was performed for vesicles formed in macrophages of infected *Tg(mpeg:RFP.GFP.LC3)* embryos 1 hpi. However, the formation of LC3 vesicles in macrophages is much lower, and this structure is observed in less than 5 % of macrophages, not co-localised with bacteria in most of the cases.

Quantification of imaging data has demonstrated that the minority of vesicles contained LC3 puncta and ROS species (Figure 5.24A,B). The analysis of groups distinguished for both factors indicated that all ROS⁻LC3⁻ and ROS⁺LC3⁺ vesicles were empty (Figure 5.24C). However, low numbers of analysed subjects unabled the assessment of statistical significance of this result. Red LC3 was present in all LC3 vesicles and green LC3 was present in 50 % of them (Figure 5.24D).

The analysis of LC3 vesicles in macrophages was not very comprehensive and explicit due to low numbers of vesicles generated in the phagocytes. Low numbers of LC3 vesicles may imply a lack of LC3 recruitment to phagosomes in zebrafish macrophages, or a pathway distinct from phagocytosis, playing a major role in the internalisation of intravenously injected *S. aureus*.

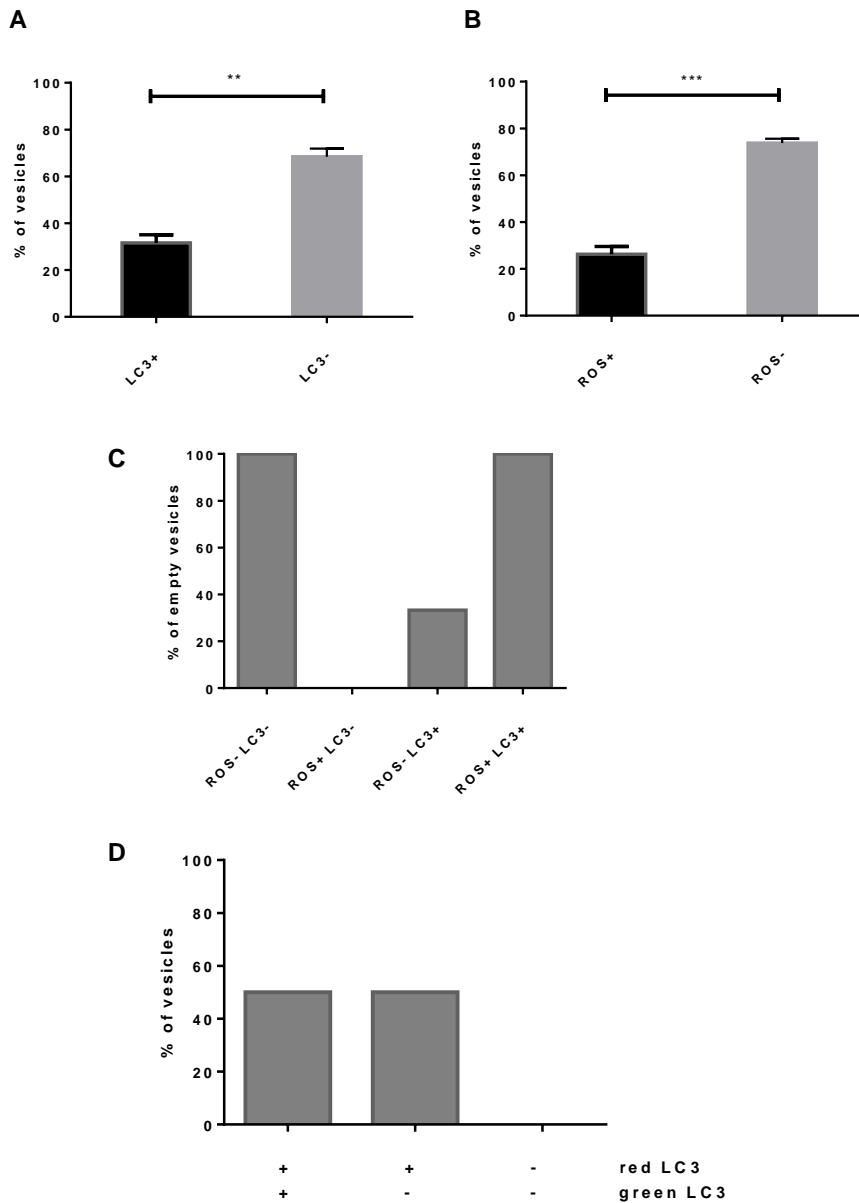


Figure 5.24. ROS and LC3 puncta within LC3 vesicles in macrophages 1 hpi.

Tg(mpeg:RFP.GFP.LC3) embryos were injected with 2500 CFU dose of SH1000-CFP *S. aureus*. ROS presence in macrophages was assessed based on imaging data generated using CellROX[®] ROS indicator. Further analysis consisted on observation of ROS and LC3 puncta within LC3 vesicles in macrophages. Based on these components vesicles were marked as ROS⁺ and LC3⁺. A and B, LC3 vesicles in macrophages were significantly less likely to contain ROS and LC3 puncta 1 hpi (unpaired t test, $p = 0.0002$, $p = 0.0017$; respectively). C, Observation of the number of *S. aureus* in vesicles demonstrated that some did not contain bacteria, 100 % of ROS⁻ LC3⁻ and ROS⁺ LC3⁺ vesicles were empty. D, Two types of LC3 were observed contained in vesicles, red LC3 was present in all LC3 vesicles and green LC3 was present in 50 % of them. A representative number of minimum 5 embryos (and 20 phagocytes per larvae) was imaged in each experimental group, experiment repeated $n = 3$.

5.4. *S. aureus* co-localisation with LC3 upon treatment with carbamazepine and chloroquine

To determine whether the formation of LC3 structures is controlled by known autophagy regulators, both *Tg(lyz:RFP.GFP.LC3)* and *Tg(mpeg:RFP.GFP.LC3)* embryos were treated with carbamazepine – an autophagy enhancer, and chloroquine – inhibiting both fusion of autophagosomes with lysosomes and lysosomal protein degradation (Chamberlain *et al.* 2013). Embryos were also treated with carbamazepine and chloroquine together, potentially resulting in elevated levels of LC3 in cells by both mechanisms: increased generation of LC3 and decreased lysosomal fusion and degradation. Drug function required embryo treatment for at least 24 hours, therefore intravenous injections were performed in larvae at 2 dpf instead of 1 dpf. Imaging took place 1 hour post infection, at a similar time point for all experimental groups, including the uninfected control group. LC3 classification was analogous to approaches applied in quantitative analysis of 1 dpf-infected neutrophil and macrophage-specific lines.

5.4.1. LC3 recruitment and ROS generation in *Tg(lyz:RFP.GFP.LC3)* embryos

For each experimental repeat, a fraction of embryos were separated and used as the uninfected control group. Control embryos were treated together with larvae predestined for injections, but an untreated fraction was also kept as a control, regardless of its origin from the infected or uninfected groups.

Initial analysis was performed on uninfected embryos. Neutrophils were analysed for their generation of LC3 aggregates and the data acquired during imaging demonstrated higher LC3 formation in neutrophils from all treated groups compared to neutrophils in untreated embryos (Figure 5.25.). LC3 aggregates were formed in similar fraction of neutrophils in all treated groups. Carbamazepine could potentially increase LC3 formation due to its autophagy enhancing activity. Chloroquine only treatment caused a similar effect, possibly because basal autophagy was occurring in uninfected neutrophils, similarly as it was shown in neutrophils of uninfected 1 dpf embryos and its components were not degraded.

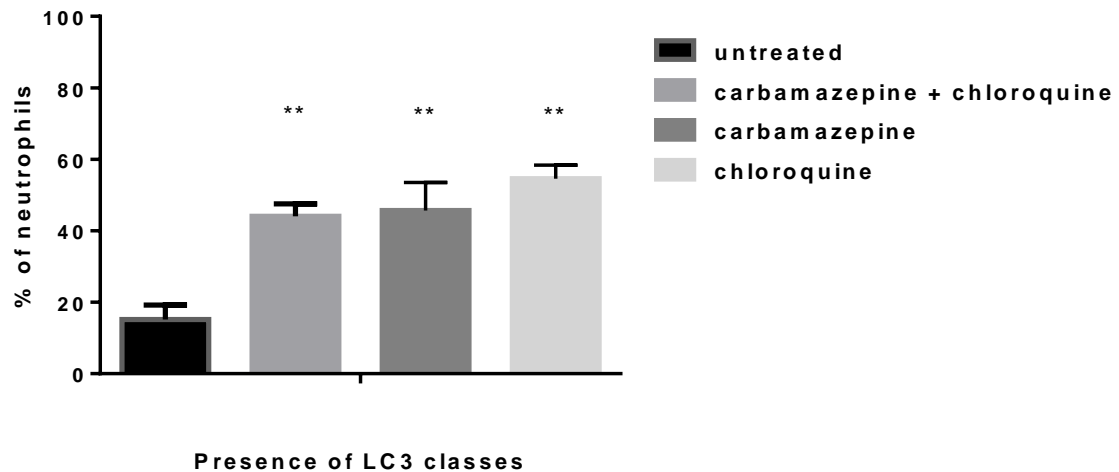


Figure 5.25. LC3 aggregates in neutrophils of uninfected 2dpf *Tg(lyz:RFP.GFP.LC3)* embryos.

Tg(lyz:RFP.GFP.LC3) embryos were treated with autophagy regulating drugs and imaged 2 dpf. The presence of LC3 classes in neutrophils was assessed based on imaging data analysis in Volocity® software. Plot shows that significantly larger fraction of neutrophils was observed to have LC3 aggregated in neutrophils of *Tg(lyz:RFP.GFP.LC3)* embryos when treated with autophagy regulating drugs (One-way ANOVA, Dunnett’s test, carbamazepine+chloroquine p = 0.0099, carbamazepine p = 0.0073, chloroquine p = 0.0015). A representative number of minimum 5 embryos (and 20 phagocytes per larvae) was imaged in each experimental group, experiment repeated n = 3.

Neutrophils in treated *Tg(lyz:RFP.GFP.LC3)* embryos were first analysed for their internalisation capacity, as the previous study was always conducted in 1 dpf larvae (Figure 5.26.). Untreated embryos were shown to have 80 % of neutrophils infected, which is less than almost 100 % in embryos infected 1 dpf (Figure 3.16., chapter 3). Interestingly, the percentage of infected neutrophils was significantly lower in both groups treated with carbamazepine (Figure 5.26.). This result can be explained by excluding roles of autophagy and phagocytosis. The former serves in intracellular housekeeping and the degradation of redundant metabolites and organelles, the latter is responsible for the engulfment of extracellular cargo. It is likely that both processes are mutually exclusive, therefore autophagic activity considerably increased by carbamazepine could slow down the internalisation processes.

Additionally, infection rates were also analysed in neutrophils, and compared to ROS generation. No significant difference between the control and treated groups was found in both ROS⁺ and ROS⁻ neutrophils (Figure 5.27.).

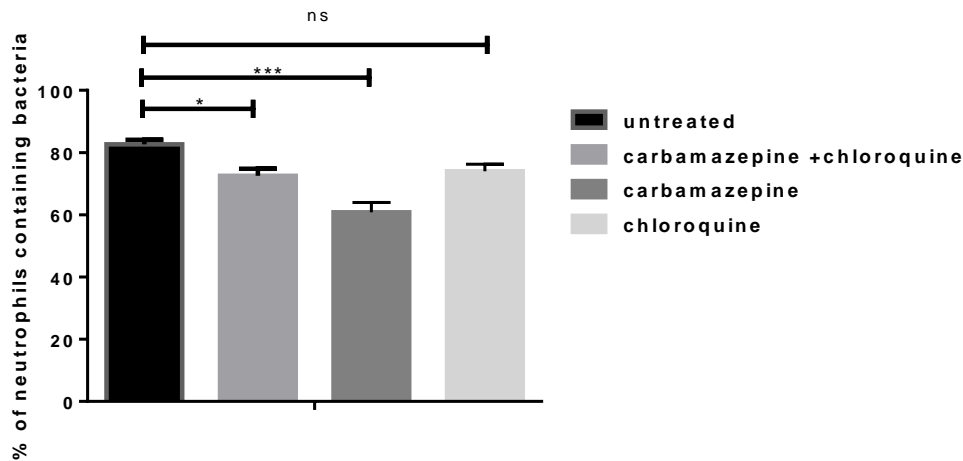


Figure 5.26. Proportion of neutrophils containing bacteria in *Tg(lyz:RFP.GFP.LC3)* embryos upon treatment with autophagy regulators.

Tg(lyz:RFP.GFP.LC3) embryos were treated with autophagy regulating drugs, infected with 2500 CFU of SH1000-mCherry *S. aureus* 2 dpf and imaged 1 hpi. The number of neutrophils containing bacteria was assessed based on imaging data analysis in Volocity® software. All neutrophils of infected embryos were scored when containing *S. aureus* at 1 hpi. Plot shows that significantly larger fraction of neutrophils was infected in untreated control embryos than in embryos treated with carbamazepine and chloroquine, or carbamazepine only (One-way ANOVA, Dunnett’s test, $p = 0.0420$, $p = 0.0005$, respectively). No significant difference was found between control and chloroquine only treatment groups. A representative number of minimum 5 embryos (and 20 phagocytes per larvae) was imaged in each experimental group, experiment repeated $n = 3$.

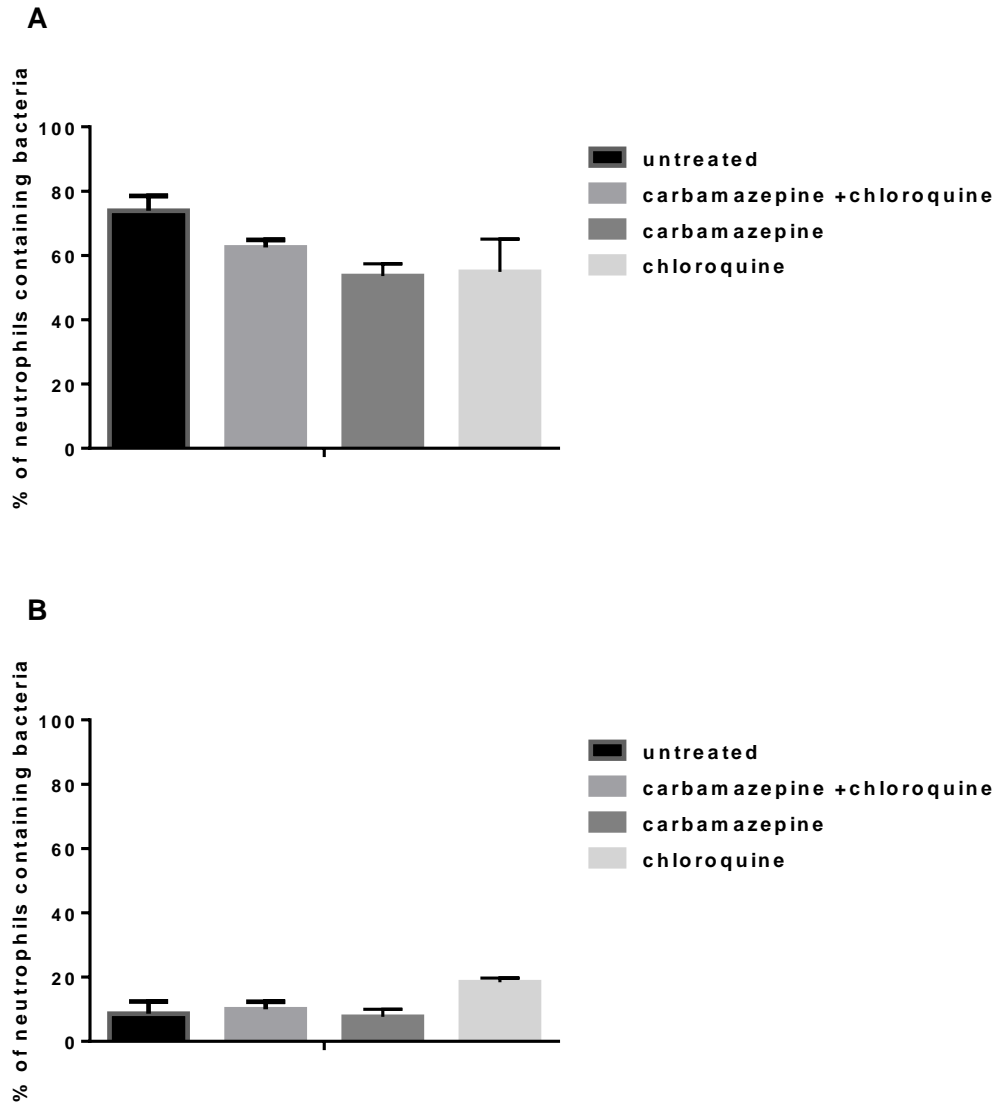


Figure 5.27. Percentage of neutrophils containing bacteria in *Tg(lyz:RFP.GFP.LC3)* embryos upon treatment with autophagy regulators with relation to ROS generation.

Tg(lyz:RFP.GFP.LC3) embryos were treated with autophagy regulating drugs, infected with 2500 CFU of SH1000-mCherry *S. aureus* 2 dpf and imaged 1 hpi. The number of neutrophils containing bacteria and ROS was assessed based on imaging data analysis in Volocity® software. All neutrophils of infected embryos were scored when containing *S. aureus* and generating ROS 1 hpi. A, ROS⁺ neutrophils. No significant difference in the amount of infected neutrophils was found in neutrophils of treated embryos compared to the untreated control. B, ROS⁻ neutrophils. No significant difference in the number of infected neutrophils was found in neutrophils of treated embryos compared to the untreated control (One-way ANOVA, Dunnett's test). A representative number of minimum 5 embryos (and 20 phagocytes per larvae) was imaged in each experimental group, experiment repeated n = 3.

The direct co-localisation of bacteria with ROS-active compartments in neutrophils was assessed for a potentially better understanding of the role of ROS generation in infected embryos. Imaging data analysis showed that nearly all bacteria co-localised with ROS in neutrophils of all groups of embryos. Therefore, there was no significant difference between untreated and treated embryos (Figure 5.28.). Although a high proportion of bacteria co-localising with ROS implies it has a role in infection, the relation of autophagy and ROS generation cannot be evaluated based on this approach.

Bacteria co-localising with ROS were also assessed for their simultaneous co-localisation with cLC3 or pLC3 (Figure 5.28). Bacteria internalised in neutrophils of embryos treated with chloroquine were significantly less likely to co-localise with phagosomal LC3 and more likely to co-localise with cytoplasmic LC3 structures. Furthermore, bacteria residing in neutrophils of carbamazepine+chloroquine treated embryos also co-localised with cytoplasmic LC3 more often than in untreated embryos. Altogether this could mean that chloroquine treatment either blocked LC3 recruitment to phagosomes or caused bacterial translocation to the cytoplasm independently or as a result of treatment. *S. aureus* residing in the cytoplasm was further targeted by autophagic machinery in both examined groups, but more efficiently in embryos also treated with carbamazepine. However, this result is based solely on the observed imaging data and the cytoplasmic presence of *S. aureus* upon treatment with chloroquine and would need to be confirmed with the use of an additional experiment, especially as the aforementioned co-localisation changes are only slightly significant.

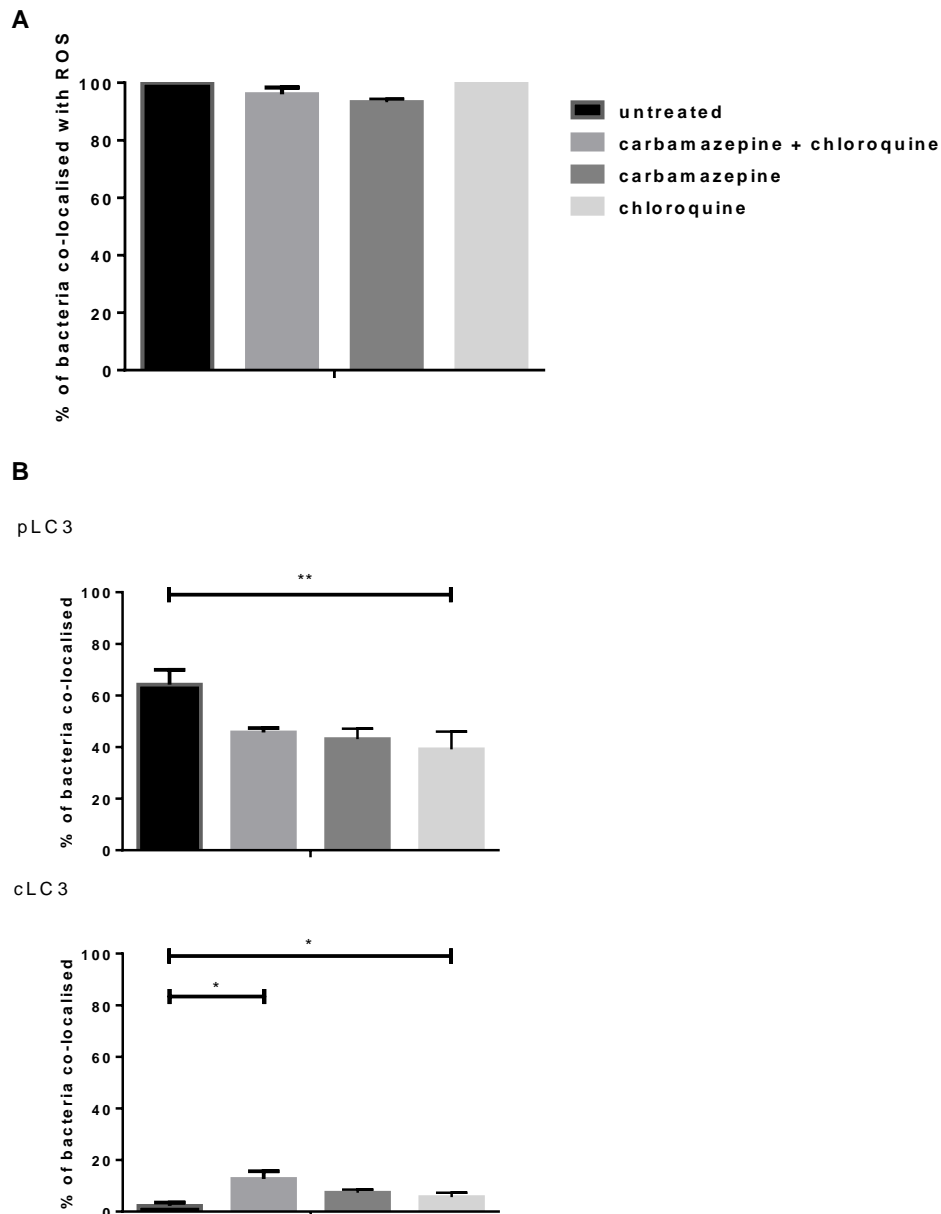


Figure 5.28. Bacteria co-localisation with ROS and LC3 in *Tg(Iyz:RFP.GFP.LC3)* embryos upon treatment with autophagy regulators.

Tg(Iyz:RFP.GFP.LC3) embryos were treated with autophagy regulating drugs, infected with 2500 CFU of SH1000-mCherry *S. aureus* 2 dpf and imaged 1 hpi. The number of bacteria co-localised with LC3 was assessed based on imaging data analysis in Volocity® software. Bacteria were also assessed for their direct co-localisation with ROS. A, in all groups almost all *S. aureus* cells co-localised with ROS-active compartments. B, smaller fraction of bacteria co-localised with pLC3 in chloroquine only treated embryos (One-way ANOVA, Dunnett's test, $p = 0.0039$). Significantly larger fraction of carbamazepine+chloroquine and chloroquine only treated embryos also co-localised with cLC3 (One-way ANOVA, Dunnett's test, $p = 0.0474$, $p = 0.0282$, respectively). A representative number of minimum 5 embryos (and 20 phagocytes per larvae) was imaged in each experimental group, experiment repeated $n = 3$.

To further investigate *S. aureus* co-localisation with particular LC3 classes, the likelihood of bacteria co-localising with puncta and spheroids, tight vesicles or spacious vesicles was assessed. Treatment with autophagy regulators caused larger fractions of *S. aureus* to fail to co-localise with any class of LC3 (Figure 5.29A). The fraction of bacteria co-localised with puncta and spheroids was larger in chloroquine treated embryos (Figure 5.29B) and *S. aureus* was less likely to co-localise with spacious vesicles in carbamazepine + chloroquine and chloroquine only treated embryos (Figure 5.29D). The fraction of bacteria co-localised with spacious vesicles was also smaller in carbamazepine only treated embryos. This result is in agreement with previous finding that *S. aureus* in the neutrophils of chloroquine treated embryos is more likely to co-localise with cytoplasmic LC3 than with phagosomal LC3 (Figure 5.28). The decreased number of bacteria co-localised with spacious LC3 vesicles might suggest that enhancement of conventional autophagy decreases LC3 recruitment to phagosomes.

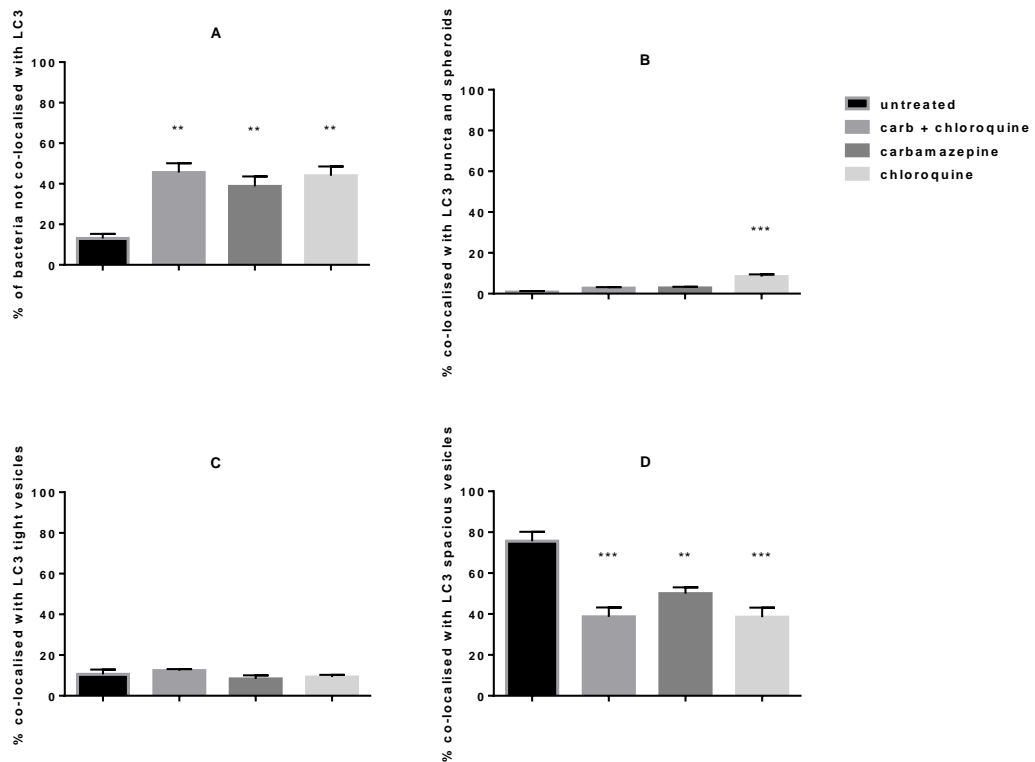


Figure 5.29. *S. aureus* co-localisation with LC3 classes in *Tg(Iyz:RFP.GFP.LC3)* neutrophils upon treatment with autophagy regulators.

Tg(Iyz:RFP.GFP.LC3) embryos were treated with autophagy regulating drugs, infected with 2500 CFU of SH1000-mCherry *S. aureus* 2 dpf and imaged 1 hpi. The number bacteria co-localised with LC3 was assessed based on imaging data analysis in Volocity® software. A, fraction of not co-localised *S. aureus*, significantly higher percentage of bacteria not co-localised with LC3 in all treated groups (One-way ANOVA, Dunnett's test, carbamazepine+chloroquine $p = 0.0016$, carbamazepine $p = 0.0067$, chloroquine $p = 0.0022$). B, fraction of *S. aureus* co-localised with puncta or spheroids, significantly larger fraction co-localised in chloroquine treated group (One-way ANOVA, Dunnett's test, $p = 0.0002$). C, fraction of *S. aureus* co-localised with tight vesicles, no significant differences in percentage of bacteria co-localised in different groups. D, fraction of *S. aureus* co-localised with spacious vesicles, significantly less bacteria co-localised with spacious vesicles in all treated groups (One-way ANOVA, Dunnett's test, carbamazepine+chloroquine $p = 0.0008$, carbamazepine $p = 0.0073$, chloroquine $p = 0.0007$). A representative number of minimum 5 embryos (and 20 phagocytes per larvae) was imaged in each experimental group, experiment repeated $n = 3$.

5.4.2. Content of LC3 vesicles in neutrophils of infected *Tg(lyz:RFP.GFP.LC3)* embryos

A different approach was designed to investigate ROS generation in phagosomes and following LC3 recruitment to the phagosomal membrane. Spacious vesicles with LC3 associated to the membrane were observed in infected neutrophils of *Tg(lyz:RFP.GFP.LC3)* embryos injected at 2 dpf. An additional analysis of the imaging data was performed to determine whether ROS and LC3 puncta were present inside LC3 vesicles in embryos infected at 2 dpf. Imaging of all groups took place from 1 hpi. Vesicles that did not contain ROS and LC3 in the lumen seemed to be more common in neutrophils of embryos treated with chloroquine only (Figure 5.30.). ROS were generated in the majority – about 80% - of vesicles in all analysed groups. Interestingly, this seems to be a high proportion given that only 20 % of vesicles contained ROS when analysed 1 hpi in embryos infected 1 dpf. This could mean that 2 dpf embryos constitute a better model for the investigation of ROS generation inside the phagosome lumen. There were significantly fewer LC3 puncta present in vesicles of both chloroquine treated groups (together with carbamazepine or not). Additionally, those vesicles were less likely to be empty (Figure 5.31.A). Vesicles in neutrophils of untreated and chloroquine only treated embryos were additionally divided into four groups: ROS⁻ LC3⁻, ROS⁺ LC3⁻, ROS⁻ LC3⁺, ROS⁺ LC3⁺ and fraction of empty vesicles was calculated in each group (Figure 5.31.B). In untreated group, all ROS⁻ LC3⁻ vesicles contained bacteria, in ROS⁻ LC3⁺ group empty vesicles represented the largest fraction, and ROS⁺ LC3⁺ vesicles were less likely to be empty. Contrarily, no ROS⁻ LC3⁺ vesicles were found in neutrophils of chloroquine treated embryos, and ROS⁻ LC3⁻ were more likely to be empty than vesicles of other groups.

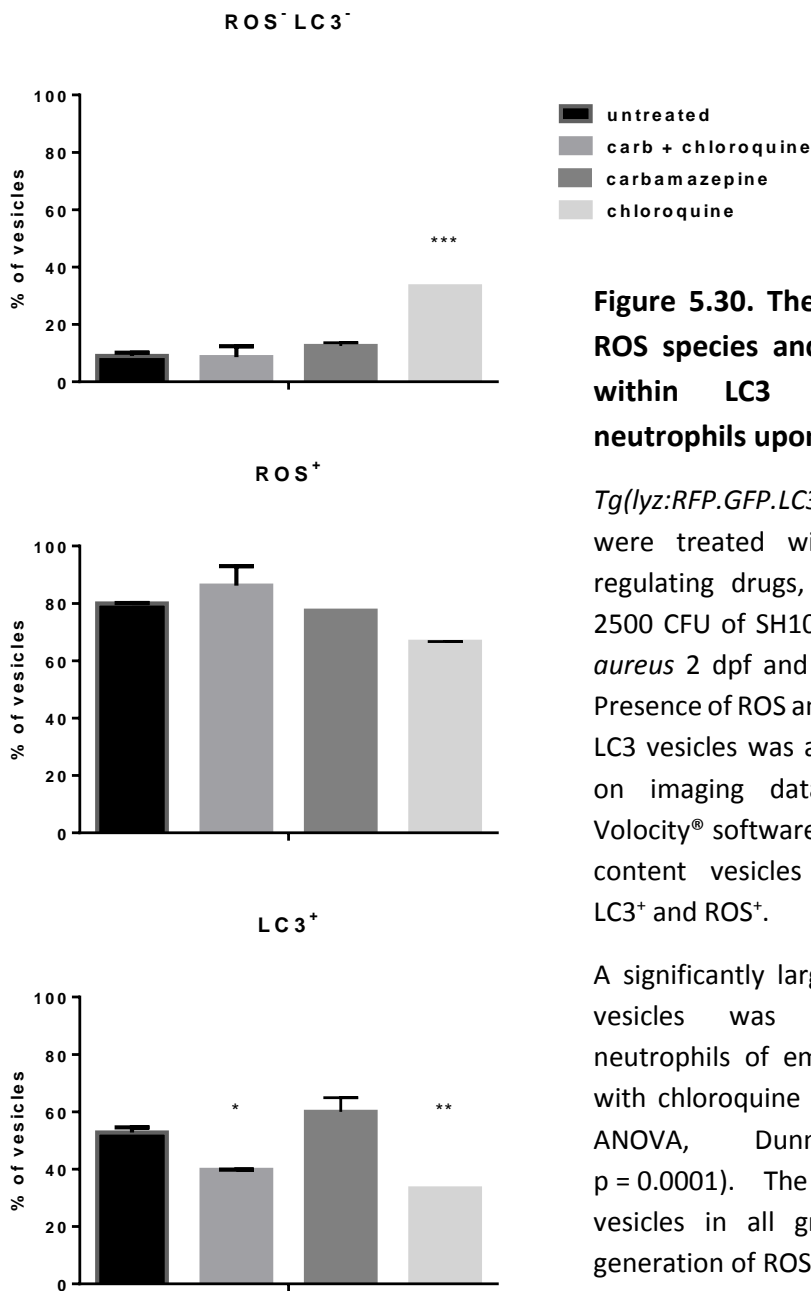
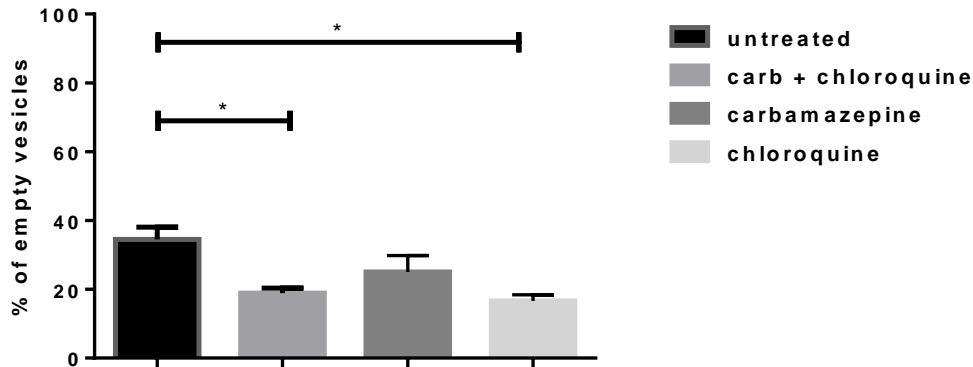


Figure 5.30. The presence of ROS species and LC3 puncta within LC3 vesicles in neutrophils upon treatment.

Tg(lyz:RFP.GFP.LC3) embryos were treated with autophagy regulating drugs, infected with 2500 CFU of SH1000-mCherry *S. aureus* 2 dpf and imaged 1 hpi. Presence of ROS and LC3 inside of LC3 vesicles was assessed based on imaging data analysis in Volocity® software. Based on the content vesicles were scored LC3⁺ and ROS⁺.

A significantly larger fraction of vesicles was ROS⁻LC3⁻ in neutrophils of embryos treated with chloroquine only (One-way ANOVA, Dunnett's test, $p = 0.0001$). The majority of vesicles in all groups showed generation of ROS. No significant difference was observed between treated groups and the untreated control. LC3 puncta were significantly less likely to be found within vesicles in carbamazepine+chloroquine and chloroquine only treated embryos (One-way ANOVA, Dunnett's test, $p = 0.0198$, $p = 0.002$, respectively). A representative number of embryos (and 20 phagocytes per larvae) was imaged in each experimental group, $n = 3$.

A



B

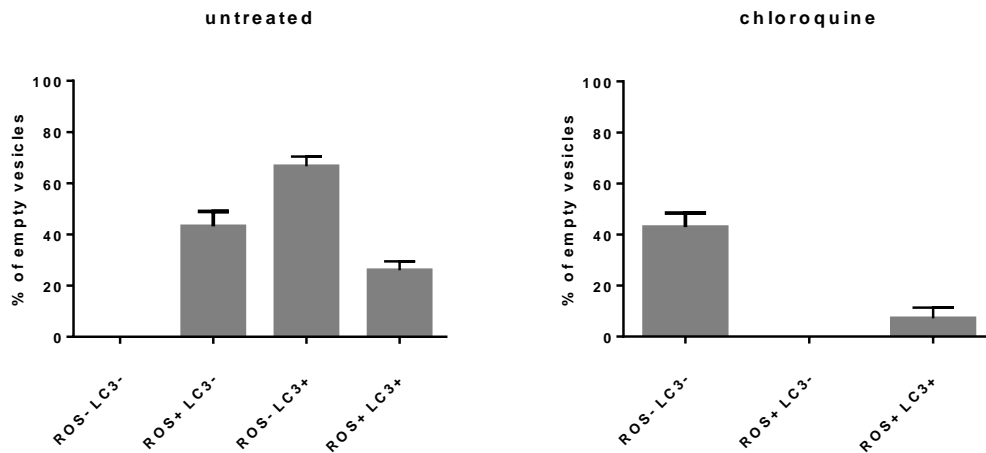


Figure 5.31. The occurrence of empty LC3 vesicles in neutrophils of *Tg(lyz:RFP.GFP.LC3)* embryos upon treatment with autophagy regulators.

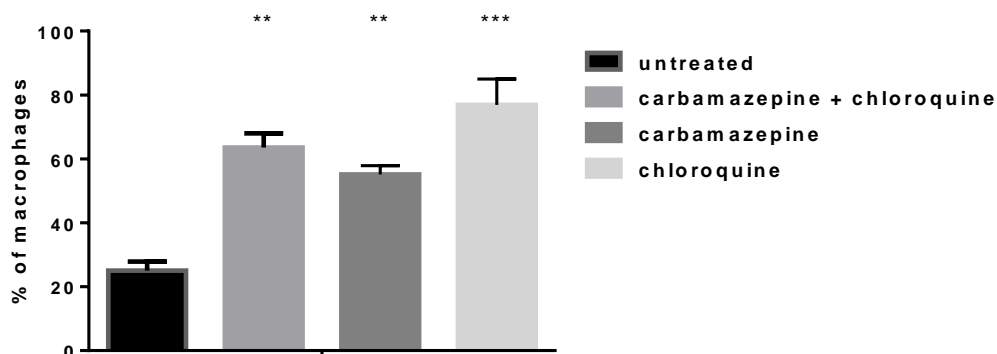
Tg(lyz:RFP.GFP.LC3) embryos were treated with autophagy regulating drugs, infected with 2500 CFU of SH1000-mCherry *S. aureus* 2 dpf and imaged 1 hpi. Presence of ROS and LC3 inside of LC3 vesicles was assessed based on imaging data analysis in Volocity® software. Based on the content vesicles were scored LC3⁺ and ROS⁺. A, significantly smaller fraction of empty vesicles was observed in neutrophils of larvae treated with carbamazepine+chloroquine and chloroquine only (One-way ANOVA, Dunnett's test, $p = 0.0211$, $p = 0.0104$, accordingly). B, all ROS⁻LC3⁻ vesicles contained *S. aureus* and ROS⁻LC3⁺ vesicles were most likely empty in neutrophils of untreated larvae. 40 % of ROS⁻LC3⁻ vesicles were empty and ROS⁻LC3⁺ were not observed in neutrophils of chloroquine treated larvae. A representative number of minimum 5 embryos (and 20 phagocytes per larvae) was imaged in each experimental group, experiment repeated $n = 3$.

5.4.3. LC3 recruitment and ROS generation in *Tg(mpeg:RFP.GFP.LC3)* embryos

As described for the neutrophil-specific line, in each repeat, a number of *Tg(mpeg:RFP.GFP.LC3)* embryos were kept as uninfected controls. Embryos of this group were treated together with larvae predestined for injections, but the untreated fraction was also kept for a control, regardless of whether it originated from the infected or uninfected group.

The first analysis concerned uninfected embryos. Macrophages were analysed for their generation of LC3 aggregates and the data resulting from imaging demonstrated that significantly more macrophages contained LC3 generated in treated groups (Figure 5.32.). The occurrence of two groups of LC3 characteristic for macrophages – red and green LC3 has also been assessed and red LC3 aggregates were more common in macrophages, than green LC3. The mean occurrence of red LC3 aggregate was also doubled in macrophages in embryos treated with carbamazepine+chloroquine and chloroquine only (Figure 5.32.).

A



B

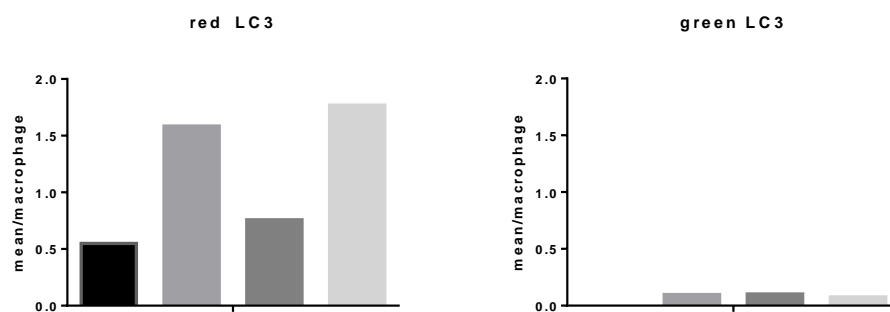


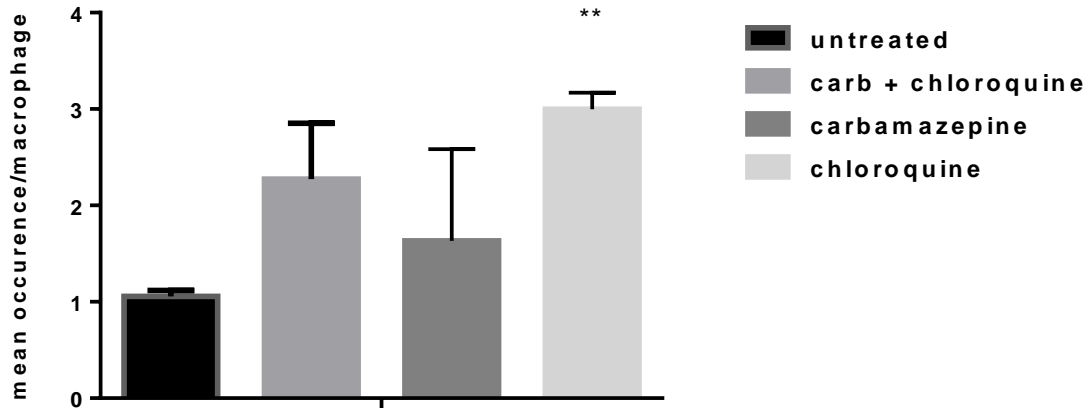
Figure 5.32. LC3 formation in macrophages of uninfected 2dpf *Tg(mpeg:RFP.GFP.LC3)* embryos upon treatment with autophagy regulators.

Tg(mpeg:RFP.GFP.LC3) embryos were treated with autophagy regulating drugs, and imaged 2 dpf. The generation of LC3 was assessed based on imaging data analysis in Volocity® software. A, plot shows that the fraction of macrophages containing LC3 structures was significantly larger in all treated groups (One-way ANOVA, Dunnett's test, carbamazepine+chloroquine $p = 0.0016$, carbamazepine $p = 0.0072$, chloroquine $p = 0.0002$). B, the occurrence of two groups of LC3 characteristic for macrophages – red and green LC3 has also been assessed, red LC3 aggregates were more common in macrophages, than green LC3. The mean occurrence of red LC3 aggregate was also doubled in macrophages in embryos treated with carbamazepine+chloroquine and chloroquine only. A representative number of minimum 5 embryos (and 20 phagocytes per larvae) was imaged in each experimental group, experiment repeated $n = 3$.

The distinction between red and green LC3 was dictated by the apparent separation of these two fluorophores in LC3 aggregates and aimed to verify whether such distribution reflects the pH of the LC3 compartments. General occurrence of both types of LC3 was assessed in macrophages, regardless of whether they co-localised with bacteria or not. Macrophages in chloroquine treated embryos were more likely to generate red LC3 (Figure 5.33.). As chloroquine is supposed to arrest autophagosome maturation and inhibit autophagy at this step, it seems that the separation of the RFP and GFP signal is not related to the compartment's pH. If there was a relationship, then according to the study performed by Kimura *et al.*, inhibition of autophagosome acidification would result in lower levels of RFP signal in the cells of treated embryos. Elevated levels of the mean occurrence of both types of LC3 were shown in macrophages of carbamazepine+chloroquine treated embryos, however these were not significantly increased compared to the control group.

Infected embryos were analysed for ROS generation and the majority of macrophages contained ROS-active areas (Figure 5.34A). Similarly, the majority showed ROS generation simultaneous with bacterial presence (Figure 5.34B). No significant difference was detected between treated groups and untreated control. The analysis of direct co-localisation of *S. aureus* with macrophages showed that all bacteria internalised in macrophages co-localised with ROS-active areas (Figure 5.35.).

red LC3



green LC3

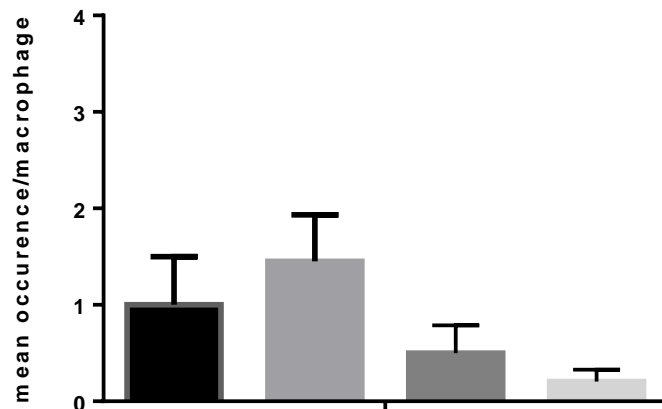


Figure 5.33. General generation of LC3 in macrophages upon infection in treated embryos.

Tg(mpeg:RFP.GFP.LC3) embryos were treated with autophagy regulating drugs, infected with 2500 CFU of SH1000-CFP *S. aureus* 2 dpf and imaged 1 hpi. The generation of LC3 was assessed based on imaging data analysis in Volocity® software. LC3 was not always co-localised with *S. aureus*, therefore LC3 structure aggregation in infected macrophages was analysed regardless of co-localisation with bacteria. The occurrence of red LC3 structures was significantly increased in macrophages when treated with chloroquine (One-way ANOVA, Dunnett's test, $p = 0.0062$). A representative number of minimum 5 embryos (and 20 phagocytes per larvae) was imaged in each experimental group, experiment repeated $n = 3$.

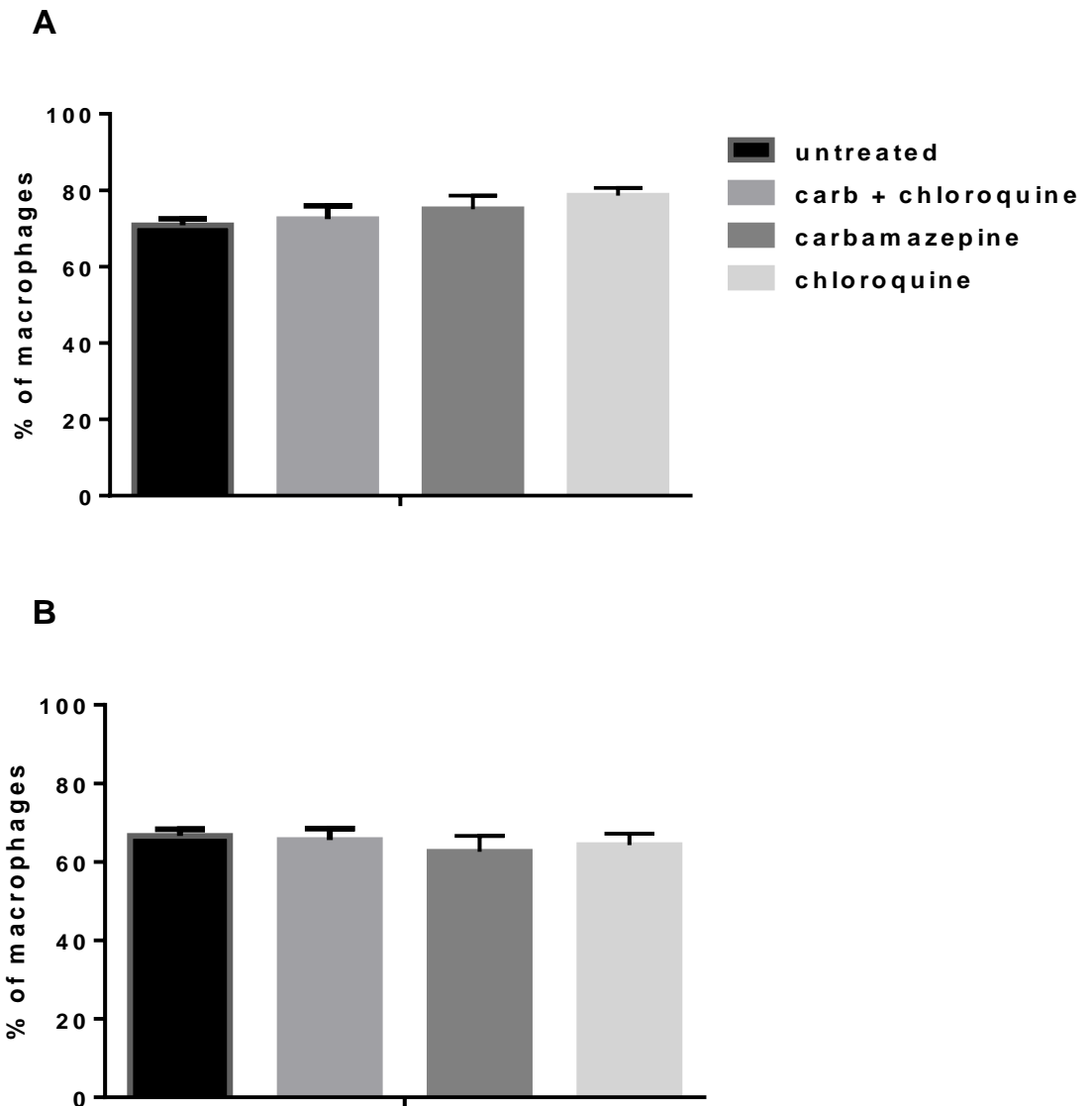


Figure 5.34. ROS generation in macrophages of *Tg(mpeg:RFP.GFP.LC3)* 2 dpf embryo upon treatment with autophagy regulators.

Tg(mpeg:RFP.GFP.LC3) embryos were treated with autophagy regulating drugs, infected with 2500 CFU of SH1000-CFP *S. aureus* 2 dpf and imaged 1 hpi. ROS presence in macrophages was assessed based on imaging data generated using CellROX® ROS indicator. The presence of *S. aureus* in macrophages was evaluated based on imaging data analysis in Volocity® software. A, percentage of macrophages in which ROS were generated. B, percentage of macrophages that generated ROS and contained *S. aureus*. A and B: No significant differences between treated groups compared to the untreated control (One-way ANOVA, Dunnett's test). A representative number of minimum 5 embryos (and 20 phagocytes per larvae) was imaged in each experimental group, experiment repeated n = 3.

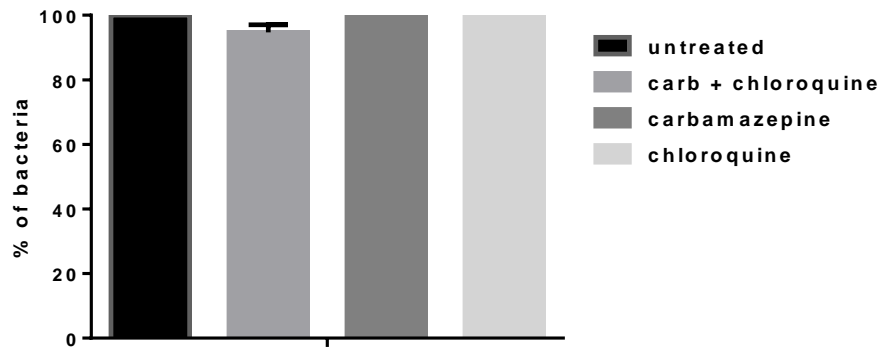


Figure 5.35. ROS co-localisation with bacteria in macrophages of 2 dpf *Tg(mpeg:RFP.GFP.LC3)* embryos upon treatment with autophagy regulators.

Tg(mpeg:RFP.GFP.LC3) embryos were treated with autophagy regulating drugs, infected with 2500 CFU of SH1000-CFP *S. aureus* 2 dpf and imaged 1 hpi. ROS presence in macrophages was assessed based on imaging data generated using CellROX® ROS indicator. The presence of *S. aureus* in macrophages was evaluated based on imaging data analysis in Volocity® software. Almost all bacteria internalised by macrophages co-localised with ROS in embryos from all analysed groups. A representative number of minimum 5 embryos (and 20 phagocytes per larvae) was imaged in each experimental group, experiment repeated n = 3.

For more detailed analysis of *S. aureus* co-localisation with LC3, bacterial cells were scored when co-localising with LC3. Treatment with carbamazepine caused reduction in non-co-localised *S. aureus* fraction and an increase of pathogen co-localisation with both red and green LC3 structures (Figure 5.36.). This implies that carbamazepine-mediated enhancement of autophagy in macrophages could increase the targeting of bacteria by components of the autophagy machinery. No significant differences in bacterial co-localisation rates with LC3 were observed in other treated groups. It may be that the autophagy enhancing effect of carbamazepine was neutralised in the presence of chloroquine. Additionally, the macrophages of carbamazepine treated embryos seemed to contain more *S. aureus* (Figure 5.37.). This could also cause an increase in bacterial co-localisation with LC3, however it does not explain why less bacteria remained not co-localised with LC3. Although the increase in the number of bacteria per cell was not significant, such correlation could indicate that active, bacteria-targeted autophagy does not guarantee increased pathogen killing.

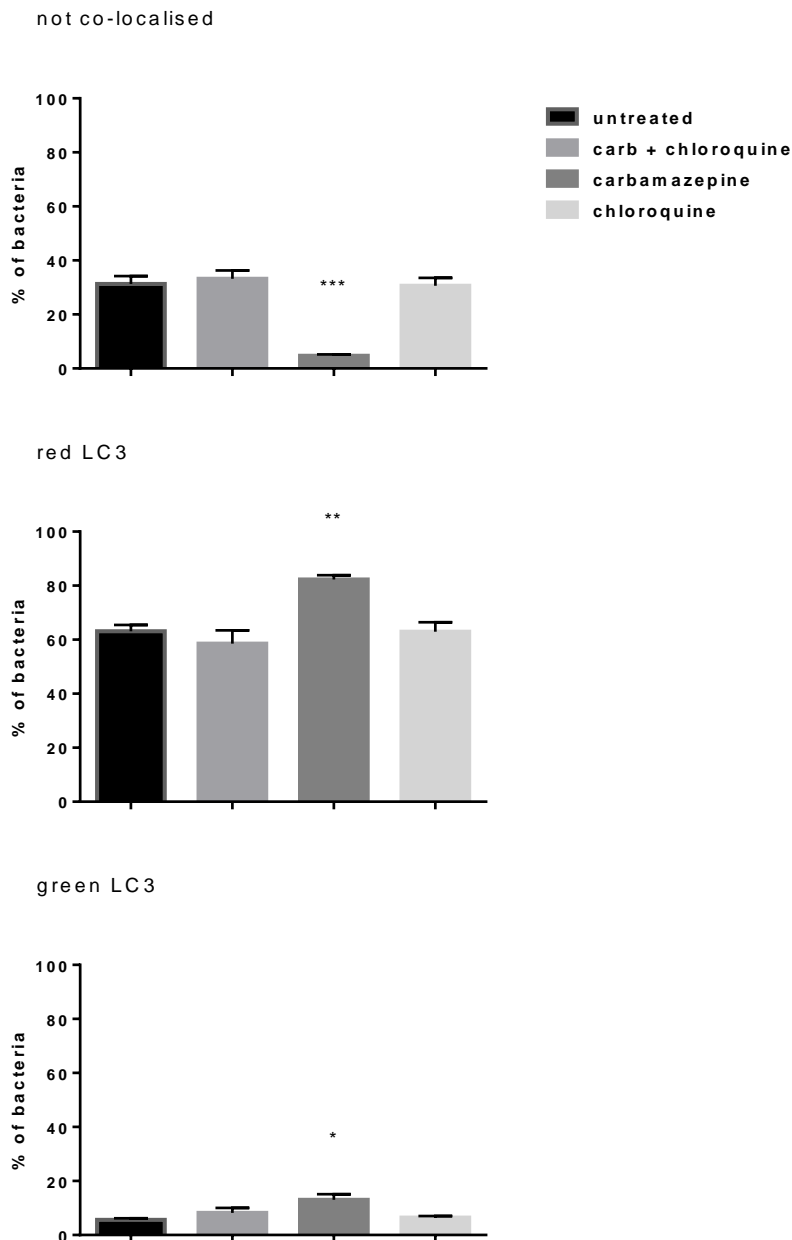


Figure 5.36. Bacteria co-localisation with LC3 in macrophages of 2 dpf *Tg(mpeg:RFP.GFP.LC3)* embryos upon treatment with autophagy regulators.

Tg(mpeg:RFP.GFP.LC3) embryos were treated with autophagy regulating drugs, infected with 2500 CFU of SH1000-CFP *S. aureus* 2 dpf and imaged 1 hpi. The co-localisation of *S. aureus* with LC3 in macrophages was evaluated based on imaging data analysis in Volocity® software. Significantly smaller fraction of bacteria did not co-localise with LC3 in macrophages of carbamazepine treated embryos (One-way ANOVA, Dunnett's test, $p = 0.0003$). *S. aureus* co-localised with red and green LC3 more likely in macrophages of those embryos (One-way ANOVA, Dunnett's test, $p = 0.0094$, $p = 0.0174$, respectively). A representative number of minimum 5 embryos (and 20 phagocytes per larvae) was imaged in each experimental group, experiment repeated $n = 3$.

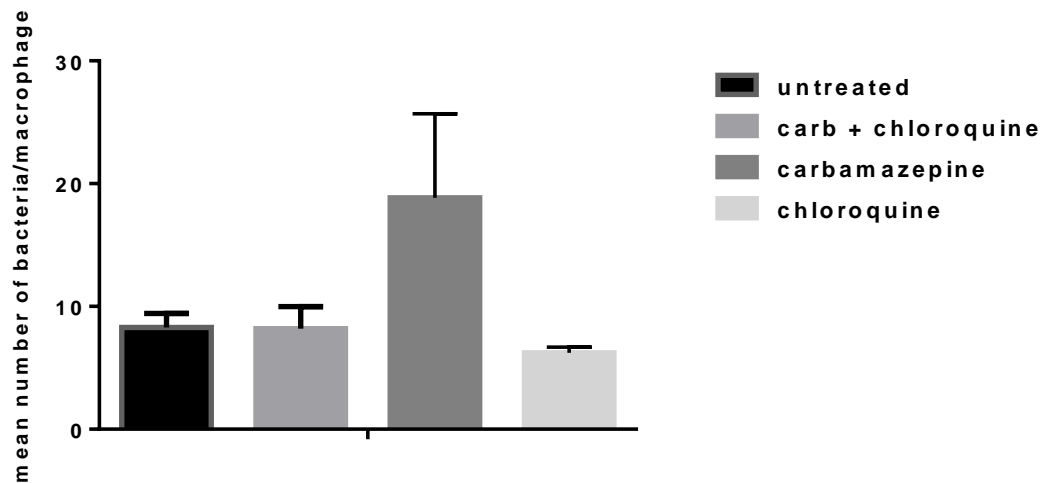


Figure 5.37. Mean number of bacteria residing in macrophages.

Tg(mpeg:RFP.GFP.LC3) embryos were treated with autophagy regulating drugs, infected with 2500 CFU of SH1000-CFP *S. aureus* 2 dpf and imaged 1 hpi. Mean number of *S. aureus* contained in macrophages was evaluated based on imaging data analysis in Volocity® software. No significant differences were found in treated embryos compared to untreated control (One-way ANOVA, Dunnett’s test). A representative number of minimum 5 embryos (and 20 phagocytes per larvae) was imaged in each experimental group, experiment repeated n = 3.

5.4.4. LC3 vesicles content in macrophages of infected *Tg(mpeg:RFP.GFP.LC3)* embryos

As described for *Tg(lyz:RFP.GFP.LC3)* embryos, an approach was designed to investigate ROS generation in phagosomes and following LC3 recruitment to phagosomal membrane in macrophages of *Tg(mpeg:RFP.GFP.LC3)* line embryos. However, unlike in neutrophil-specific line embryos, very few spacious vesicles with LC3 associated to the membrane were observed. Therefore the number of subjects was too low to perform an informative analysis.

5.5. Neutrophil LC3 co-localisation with different *S. aureus* strains

It is known that LC3 can be recruited to phagosomes during infection after the activation of autophagy by TLR signalling (Huang *et al.*, 2009). The imaging data collected from experiments in *Tg(lyz:RFP.GFP.LC3)* embryos strongly suggests that this is also the case in *S. aureus* infection. However it remains unclear what role LC3 plays once recruited to a vesicle already formed during the process of pathogen internalisation. One of the hypotheses was that *S. aureus* could try to escape from the phagosome and avoid enrolment in its maturation and processes leading to intracellular killing. To test this, I infected fish with bacterial mutants, defective in production of proteins known to facilitate escape in other bacterial infections, e.g. haemolysin, and more specifically in *S. aureus* infection – phenol soluble modulins α . Wild type strains were injected as controls in this experiment and survival tests were performed to test the effect of mutation in these proteins on bacterial virulence. However, experiments with mutant strains have only been repeated twice, thus the data presented herein could not be analysed statistically, and rather constitutes a pilot study. During each repeat a group of larvae were not imaged and were used to perform survival tests. Mutant strains were less efficient in killing infected embryos, however more detailed analysis would have to be performed with various doses of each strain to determine their pathogenicity (Figure 5.38.). The more important aim of these experiments was to use imaging data analysis in order to predict whether

the embryo model characterised in this study will have the potential to increase our knowledge on how different strains of *S. aureus* interact with autophagic machinery.

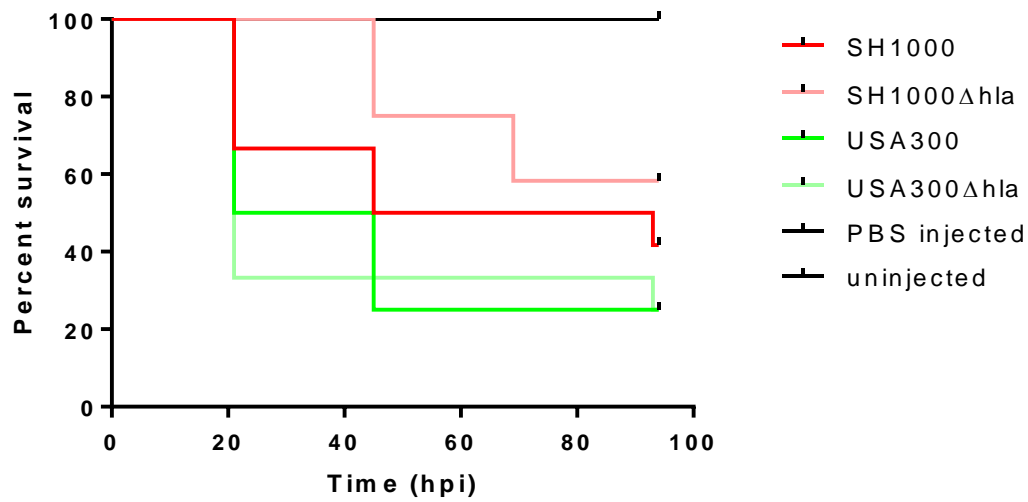


Figure 5.38. *hla* mutant strains are less efficient in killing infected embryos.

Tg(lyz:RFP.GFP.LC3) embryos were injected 30 hpf with approximately 2500-3000 CFU of different *S. aureus* strains (see legend). *hla* mutation had an impact and decreased the pathogenicity of SH1000 and USA300 strains. (uninjected and PBS injected control, n = 3, no significant difference between survival curves, log rank test).

5.5.1. USA300, USA300Δhla and SH1000Δhla strains

Tg(lyz:RFP.GFP.LC3) embryos were injected with SH1000, SH1000Δhla, USA300 and USA300Δhla strains stained with Alexa Fluor 647 dye. Further larvae of all 4 groups were imaged at 1 -3 hpi. In each experiment a small number of fish from each group (5 embryos) was imaged to provide similar time point for each acquisition. Due to fluorophore used to stain and visualise bacteria (far red fluorescence) it was impossible to incorporate ROS indication into the assay.

All studied strains infected about 75 – 85 % of neutrophils, however bacteria of the USA300Δhla strain were the most numerous in an average neutrophil (Figure 5.39.). The dose of injected inoculum was increased to 3000 CFU in this experiment, but quite remarkably it seemed that bacteria of USA300 strain are more abundant in the bloodstream, often surrounding neutrophils rather than residing inside of the phagocytes (Figure 5.40.).

The standard LC3 classification analysis was performed to assess LC3 co-localisation with bacteria in neutrophils (Figure 5.41.). No differences in co-localisation with LC3 aggregates were found between SH1000 and its *hla* mutant. In the USA300 background study, the mutant strain was more frequently colocalised with tight vesicles than the wild type strain, possibly implying that it is being effectively captured into autophagosomes from the cytoplasm. However, no clear difference in co-localisation with spacious vesicles was found for both SH1000 and USA300 background, suggesting that haemolysin expression may not contribute to phagosome expression, either not in neutrophils or in this experimental model.

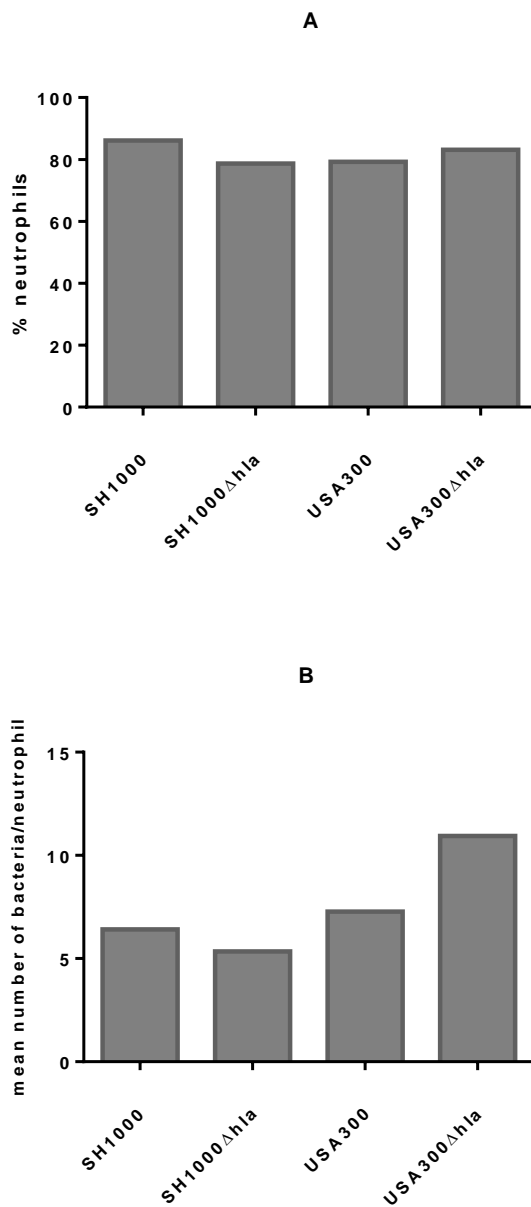


Figure 5.39. Internalisation of different *S. aureus* strains and *hla* mutants in neutrophils of *Tg(lyz:RFP.GFP.LC3)* embryos.

Tg(lyz:RFP.GFP.LC3) embryos were injected with 2500-3000 CFU dose of various *S. aureus* strains and imaged 1 hpi. The fraction of neutrophils containing bacteria and the number of bacteria in neutrophils were assessed based on imaging data analysis in Volocity® software. A, about 80% of all neutrophils contained bacteria upon infection with all tested strains. B, USA300 Δ hla strain cell were more numerous in neutrophils 1 hpi than *S. aureus* of other analysed strains. The result was not analysed statistically due to a low number of repeats (n=2, 5 embryos of each group analysed in each repeat).

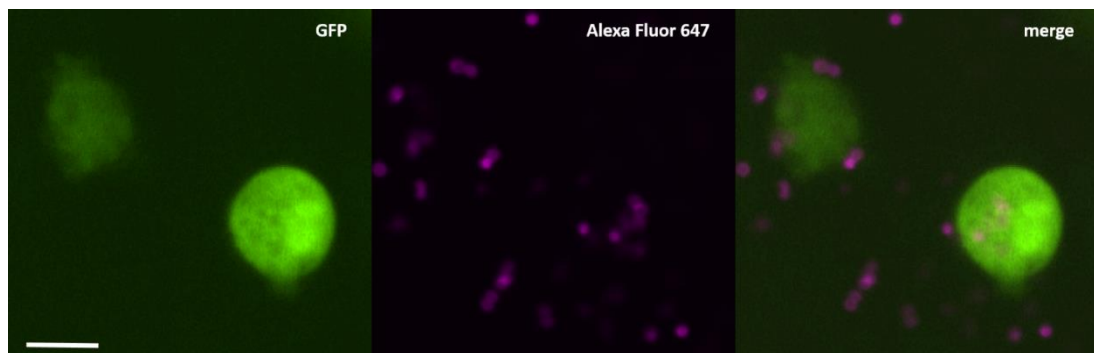


Figure 5.40. USA300 *S. aureus* is abundant in the bloodstream of infected *Tg(lyz:RFP.GFP.LC3)* larvae.

Tg(lyz:RFP.GFP.LC3) embryos were injected with 3000 CFU dose of USA300 *S. aureus* strain stained with Alexa Fluor 647 dye, and imaged 1 hpi. The image shows an example where a large number of *S. aureus* cells were not internalised in the bloodstream at that time point, which seemed to be characteristic for this particular strain. Scale bar = 10 μ m.

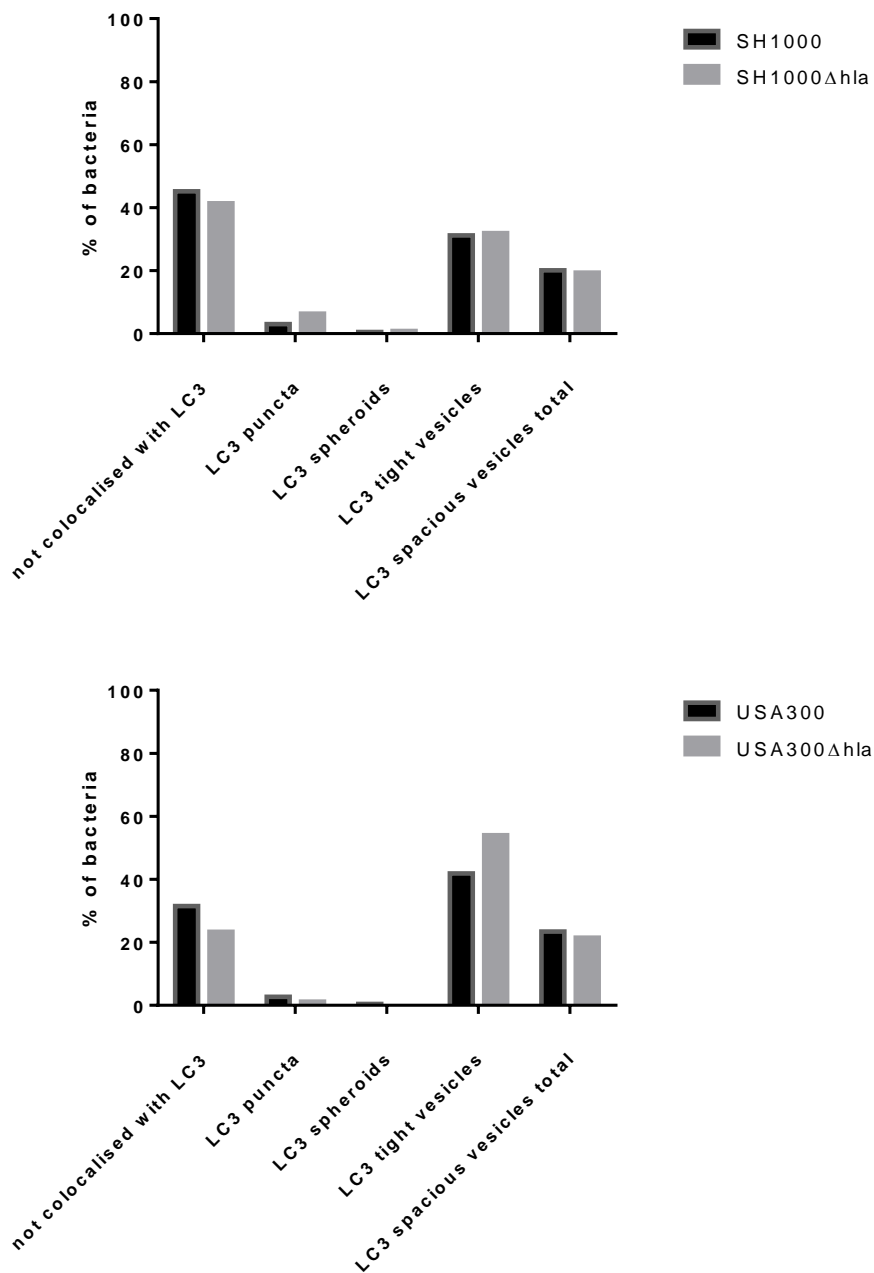


Figure 5.41. LC3 classes co-localisation with SH1000 and USA300 *S. aureus* strains and *hla* mutants.

Tg(lyz:RFP.GFP.LC3) embryos were injected with 2500-3000 CFU dose of various *S. aureus* strains and imaged 1 hpi. The fractions of bacteria co-localised with different LC3 classes in neutrophils were assessed based on imaging data analysis in Volocity® software. SH1000 and SH1000Δhla strains co-localised with LC3 structures in a similar manner. *S. aureus* of USA300Δhla co-localised with tight vesicles more frequently than wild type USA300. The result was not analysed statistically due to a low number of repeats (n=2, 5 embryos of each group analysed in each repeat).

5.5.2. 6850 and 6850 Δ psm α strains

Tg(lyz:RFP.GFP.LC3) embryos were dechorionated and injected with 6850mCherry strain and 6850 Δ psm α stained with AlexaFluor647 dye, as well as with both strains in 1:1 inoculum. Larvae of all 3 groups were further imaged at 1 -3 hpi. In each experiment a small number of fish from each group (5 embryos) was imaged to provide similar time point for each acquisition.

Data collected in the imaging analysis from the experiment where strains were injected separately was analysed first. It seems that the mutant strain was able to infect slightly more neutrophils (Figure 5.42A), however, similar number of bacteria of both types was present in neutrophils (Figure 5.42B).

The 6850 strain was more often colocalised with tight vesicles, whereas the mutant strain is often not colocalised with LC3. Together with the fact that the wild type strain is more often colocalised with puncta and spheroids - likely types of cytoplasmic LC3, it may suggest that the wild type has been captured in cytoplasm more often than the mutant strain. Nevertheless up to 50 % of the wild type strain still reside inside of spacious vesicles at this time point of infection and smaller fraction of mutant strain bacteria is co-localised with spacious vesicles at that time point.

The results of 1:1 mixed inoculum experiment demonstrates that bacteria of the wild type strain are more abundant inside of an average phagocyte (Figure 5.43.), which could suggest higher intracellular persistence or intracellular replication in the presence of mutant strain. In this assay more bacteria of 6850 Δ psm α colocalised with puncta and spheroids, and the number of not colocalised ones was decreased. Moreover, little less of wild type 6850 were still contained in spacious vesicles, and that missing group possibly shifted to co-localised with tight vesicles. However, analysis of more time points in the first hours post infection and factors such as ROS generation could help to test the hypothesis in a more comprehensive manner.

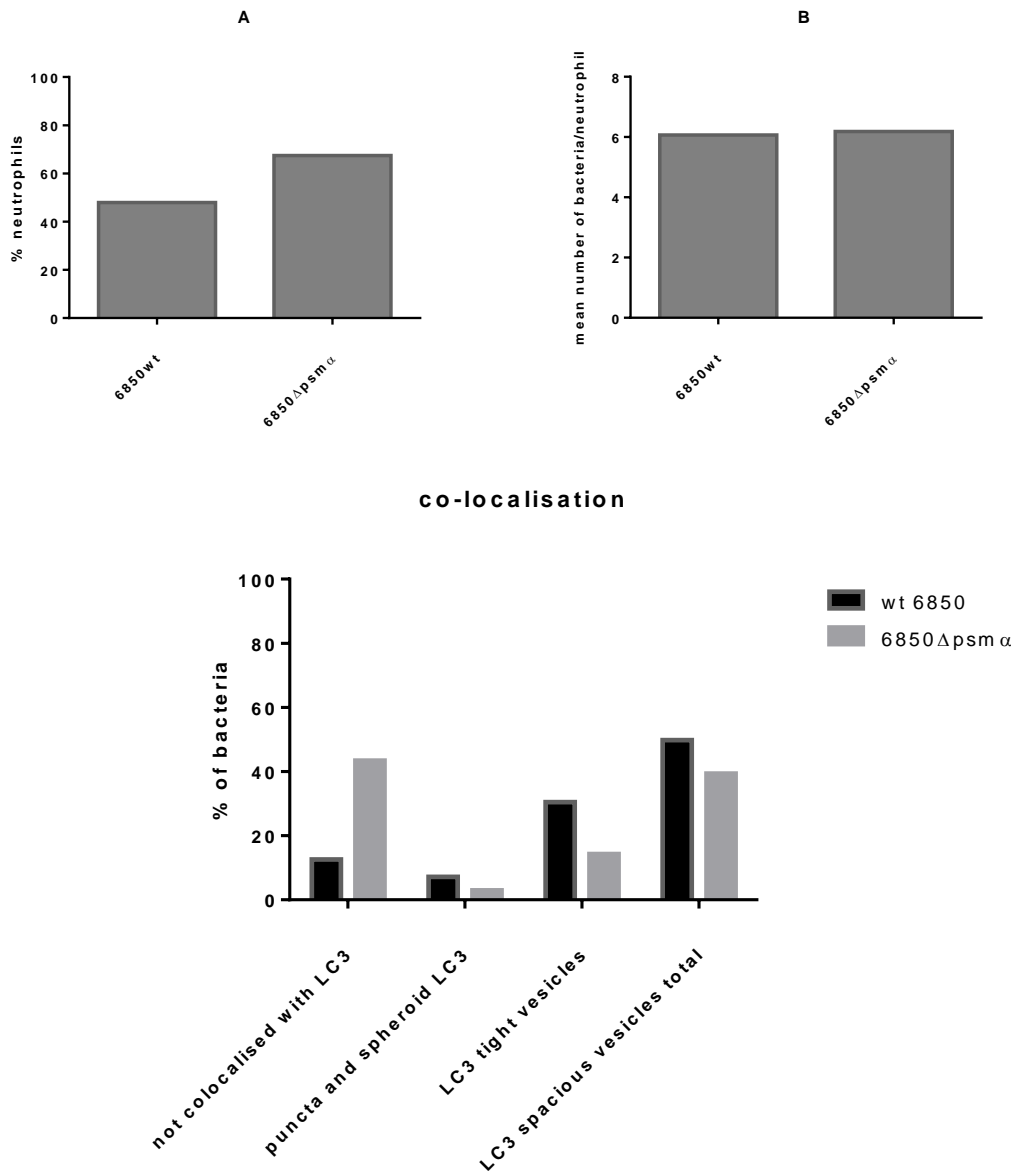


Figure 5.42. 6850 and 6850Δpsmα *S. aureus* strains internalisation in neutrophils and co-localisation with LC3 classes.

Tg(lyz:RFP.GFP.LC3) embryos were injected with 2500 CFU dose of 6850 and 6850Δpsmα *S. aureus* strains and imaged 1 hpi. The fractions of bacteria co-localised with different LC3 classes in neutrophils were assessed based on imaging data analysis in Volocity® software. A, plot shows percentage of neutrophils containing *S. aureus*. B, mean number of bacteria per neutrophil. The result was not analysed statistically due to a low number of repeats (n=2, 5 embryos of each group analysed in each repeat).

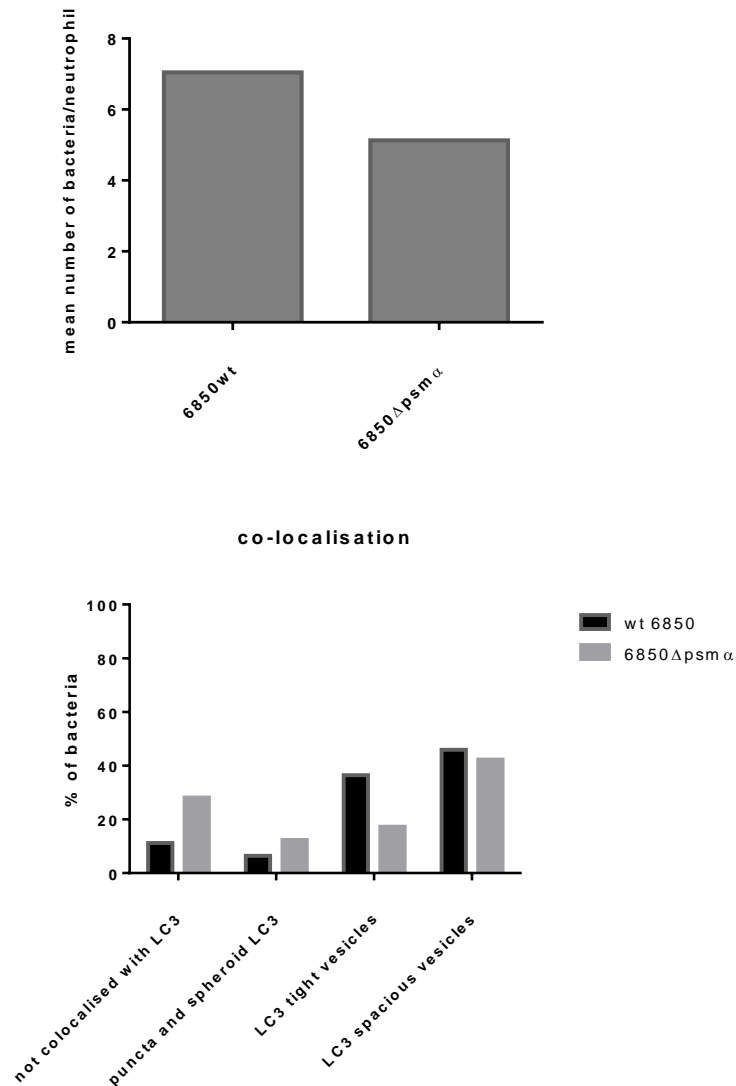


Figure 5.43. Internalisation of 1:1 mixed inoculum of 6850 and 6850Δpsmα *S. aureus* strains in neutrophils and co-localisation with LC3 classes.

Tg(Iyz:RFP.GFP.LC3) embryos were injected with 2500 CFU dose of 1:1 mixed inoculum of 6850 and 6850Δpsmα *S. aureus* strains and imaged 1 hpi. Mean number of bacteria contained in neutrophils and fractions of bacteria co-localised with different LC3 classes in neutrophils were assessed based on imaging data analysis in Volocity® software. Neutrophils contained larger number of the wild type strain when injected together with the mutant. The result was not analysed statistically due to a low number of repeats (n=2, 5 embryos of each group analysed in each repeat).

5.6. Acidification of 6850 and 6850 Δ psm α *S. aureus* strains in neutrophils and macrophages

It has been shown in the study of Grosz *et al.* (2014) that 6850 MSSA strain is capable of escape from phagosomes and replication in phagocytes cytoplasm. The intracellular growth is preceded by the lower bacteria acidification rates, indicating relocation to a neutral compartment in cell. The study in macrophage cell culture shown that the phagosomal escape started 2.5 hpi and the maximum drop of acidification occurred 6 hpi.

It is difficult to predict how such interaction would progress in *in vivo* organism, as it constitutes more dynamic and complex system. Moreover, zebrafish incubation temperature – 28 °C, is lower than optimal for growth of *S. aureus* and therefore the replication could be postponed. However, to test whether similar change in acidification rate can be observed in the zebrafish infection model, I have stained 6850 and 6850 Δ psm α *S. aureus* strains with pHrodo low pH indicator and injected them into neutrophil specific reporter lines – *Tg(mpx:GFP)*. Bacteria were also stained with Alexa Fluor 350 to allow visualisation of not acidified pathogen. Counts of acidified and not acidified bacteria were taken 2 and 6 hpi for both injected strains. Neutrophils were labelled with GFP protein, macrophages were distinguished based on their morphology observed with the DIC analysis and lack of GFP marker.

Imaging data analysis demonstrated that indeed in macrophages, a smaller proportion of the 6850 Δ psm α strain was acidified compared to the wild type strains at both time points. However, for both strains the result oscillated around 20 % (Figure 5.44.). Possibly then the published result could be confirmed in zebrafish, if the imaging took place later or after optimisation of the infected dose. In neutrophils, the acidified fraction was increased at 6 hpi compared to 2 hpi and seemed to be larger in the wild type strain population.

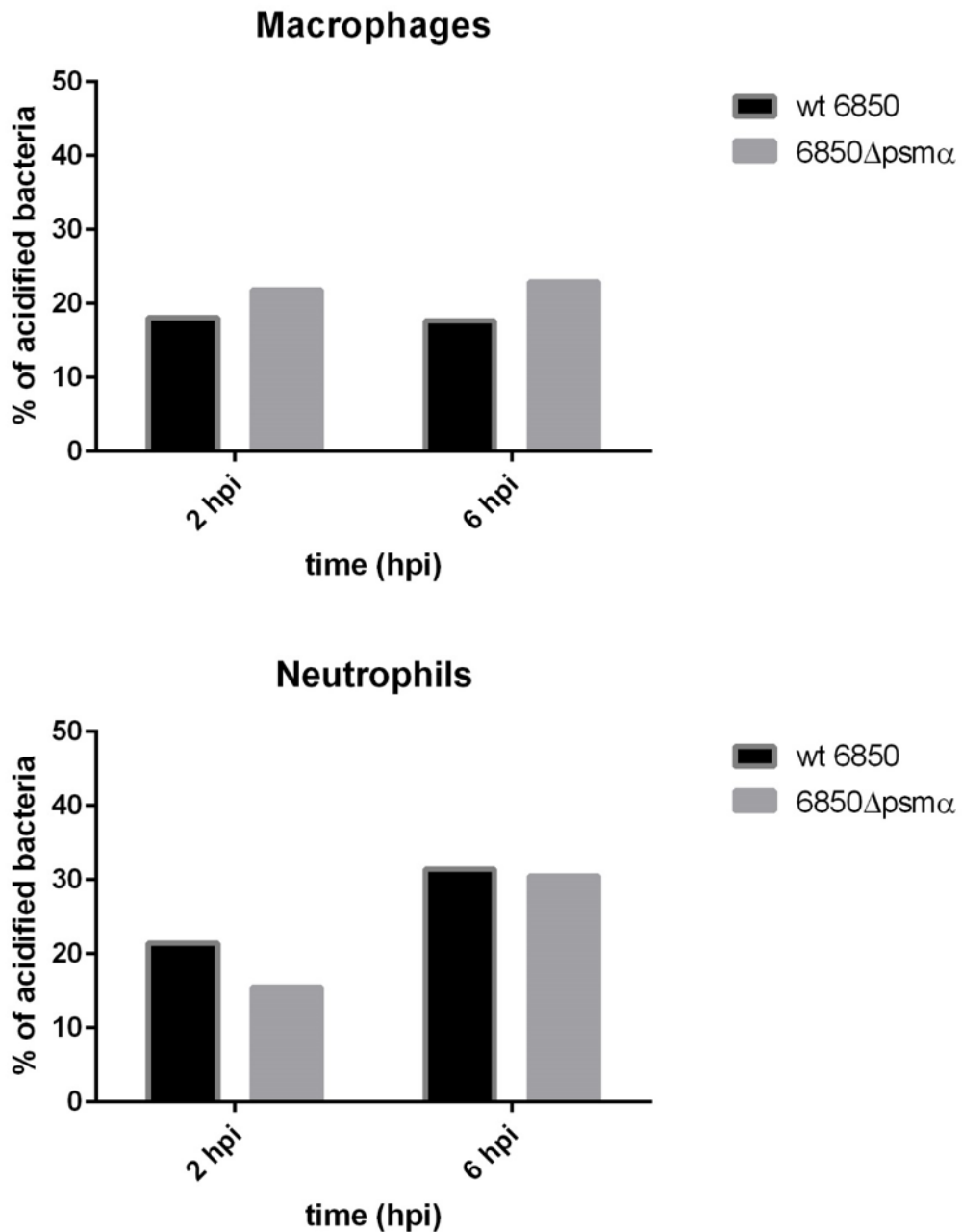


Figure 5.44. Acidification of 6850 and 6850 Δ psm α *S. aureus* strains in neutrophils and macrophages.

6850 and 6850 Δ psm α *S. aureus* strains were simultaneously stained with Alexa Fluor 350 and pHrodo™ indicator. Further bacteria were injected into *Tg(mpx:GFP)* and *Tg(mpeg:FRET)* embryos, and imaged at two time points, 2 and 6 hpi. Acidification of bacteria was assessed based on imaging data analysis in Volocity® software. In neutrophils, the acidified fraction was increased at 6 hpi compared to 2 hpi and larger in 6850 strain population. In macrophages, a smaller proportion of the 6850 Δ psm α strain was acidified compared to the 6850 strain at both time points. The result was not analysed statistically due to a low number of repeats (n=2, 5 embryos of each group analysed in each repeat).

5.7. Discussion

Acidification is a well-known feature of the late phase of phagocytosis. Phagosomes created during bacterial uptake fuse with lysosomes – intracellular compartments containing digestive enzymes, which results in a reduction in pH and acidification of the bacteria-containing compartment. Acidification of phagosomes is followed by the bacterial degradation, suggesting that acidification constitutes an important step in the pathway of bacterial internalisation and therefore a central component of the host defence. Moreover, it has been suggested that acidification followed by digestion of *S. aureus* is necessary for MyD88-dependent toll-like receptor responses of host immune system (Abdelzaher *et al.*, 2010).

An important part of this study comprises the visualisation of endosome acidification, as pH changes are an important factor for host – pathogen interactions. According to the results published by Ip *et al.* (2010) these transitions are necessary for efficient response to *S. aureus* infection, since intracellular shifting of pH conditions refers to the digestive role of lysosomes after their fusion with endosomes. Several approaches designed for this study showed that pHrodo™ staining constitutes a useful tool to visualise low pH environment in zebrafish professional phagocytes. Applied together with the second pH sensitive dye – fluorescein, this enabled first *in vivo* tracking of *S. aureus* acidification. Not all *S. aureus* cells become acidified in professional phagocytes and one could speculate that such variance results from *S. aureus* acting in order to subvert intracellular pathways to its own ends. Thus, the staining protocol established herein provides a precise, sensitive and reproducible method of environmental pH indication and constitutes a valuable tool to assess *S. aureus* intracellular fate.

The gradual change of pH was captured *in vivo* using staining of viable *S. aureus* pH sensitive dyes, allowing the demonstration of the timing and relatively short duration of the process (within five minutes after pathogen internalisation). This method allows the identification of the ability of phagosomes for intracellular acidification in a real-time visualisation experiment. The use of low pH indicator was also coupled with plasmid-expressed fluorescence allowing determination of two factors, acidification and viability of bacteria. Performing real time imaging in a living

organism impedes the use of reliable control of fluorescence intensity of indicators, such as pHrodo. Fluorescence detection observed *in vitro* can be altered *in vivo*, precluding the use of calibration. Therefore in my study, imaging set up, including exposure times and laser gain, was adjusted to allow comparable fluorescence intensity values obtained for both: indicator stain-originating fluorescence and the plasmid-encoded one. This allowed evaluation of pH and plasmid expression during *in vivo* imaging. Imaging data analysis demonstrated that in macrophages the mean value of pathogen-expressed red fluorescence intensity was higher than green, suggesting that intracellular *S. aureus* cells were acidified and simultaneously less viable (Schwartz *et al.*, 2009). Contrarily, in neutrophils lower mean fluorescence signal for the red channel and higher for the green, implies lower acidification rates and higher viability. Lower acidification could indicate arrested degradation and prolonged survival of pathogen would be more likely. However, the experimental approach does not provide clear link between acidification and viability of cells. Interestingly, in a study performed in human neutrophils, GFP fluorescence expressed by *E. coli* was inactivated rapidly following phagocytosis (Palazzolo *et al.*, 2005). Such quenching was attributed to myeloperoxidase activity within neutrophils and proposed to effect in differential survival of the GFP signal from ingested bacteria within macrophages and neutrophils. The data presented herein shows that *S. aureus* cells still express GFP fluorescence upon internalisation into neutrophils. It may be that *S. aureus* is more resistant to myeloperoxidase activity than *E. coli*. Alternatively, *in vivo* model provides different host cell-pathogen interaction, and similar *E. coli* infection experiment would yield different result if performed in the living organism.

In this chapter newly created LC3 reporter lines were used to investigate autophagic processes in bloodstream neutrophils and macrophages. Autophagic machinery may recognise pathogens and enrol them into the pathway by the interaction performed by specific components of autophagy or by other cargos designated for the degradation. Those interacting proteins play the role of autophagic adaptors and help sensing bacterial presence in cell cytoplasm (Bjørkøy *et al.*, 2005, Kirkin *et al.*, 2009). Complex confocal microscopy enabled visualisation of multiple components of intracellular pathogen handling: fluorescently labelled LC3, the key autophagy

protein; the generation of reactive oxygen species (ROS), assessed in infected phagocytes using CellROX[®] fluorescent ROS indicator and *S. aureus* expressing fluorescent reporter on plasmid.

The analysis of imaging data has demonstrated that *S. aureus* presence in neutrophils exerts ROS generation, in the way independent on the number of internalised bacteria. *S. aureus* presence triggers oxidative burst in the majority of neutrophils 1 hpi and in half of them at 20 hpi, suggesting that the pathogen re-enters the ROS generation-mediating path at this time point. This could be triggered by the second wave of internalisation, or by intracellular event leading to pathogen degradation. The direct co-localisation of bacteria with ROS-active areas in neutrophils may suggest that ROS generation triggered processes important in the course of infection. It has been shown that neutrophils depend on the production of reactive oxygen species (ROS) to kill internalized *P. aeruginosa* (Speert *et al.*, 1994) and *M. marinum* (Yang *et al.*, 2012). However, *S. aureus* strains evolved strategies for their defence against ROS, for instance staphyloxanthin allows partial resistance to killing by peroxide and singlet oxygen (Liu *et al.*, 2005). Moreover, catalase, an enzyme from staphylococcal cytoplasm contribute to resistance against ROS, by converting the degradative compound to oxygen and water (Mandell, 1975). Additionally, SOK (surface factor promoting resistance to oxidative killing) is another protein that also confers resistance to singlet oxygen (Malachowa *et al.*, 2011). The presence of these protective mechanisms could explain why *S. aureus* is still present in neutrophils 20 hpi. Nevertheless, increasing evidence shows that ROS do not have to directly interact with pathogen to influence the course of infection and ROS generation can be related to the regulation of defence mechanisms performed by host cells. For instance, a recent review concludes that ROS can interact with the generation of human extracellular traps (ETosis) in a complex manner, regulating whether ETosis shows beneficial or detrimental effects (Stoiber *et al.*, 2015). Thus, microscopy approaches established to investigate ROS generation and results presented in this chapter could constitute source of information for further investigation of the role of NETs (neutrophil extracellular traps) in *S. aureus* infection.

The direct targeting of intracellular *S. aureus* by autophagy could be mediated by the presence of ROS at the early stages of infection, as LC3 puncta, spheroids or tight vesicles co-localised with pathogen in ROS⁺ neutrophils but not in ROS⁻. However, imaging at a fixed time point makes it difficult to conclude whether ROS generation precedes co-localisation with LC3, or is constant and what we observe is in fact the outcome of its ongoing activity. Relatively high proportion of neutrophils that did not contain bacteria but shown ROS generation at 20 hpi compared to early stage of infection, could imply the presence of these compounds after recent *S. aureus* existence and its killing in those cells.

Although over the course of infection more bacteria resided in neutrophils without interacting with autophagic machinery, significant fraction of *S. aureus* would still co-localise with LC3. Over the course of infection less bacteria co-localised with tight autophagosome-like vesicles, instead tight LC3 vesicles seem to fuse with lysosomal compartments, or with each other creating larger, spacious vacuoles. Alternatively, it is also likely that tight LC3 vesicles undergo maturation and fusion with lysosomes, which could result in the killing of bacteria. However, Schnaith *et al.* (2007) proposed that the maturation of *S. aureus* containing phagosomes typically leading to the fusion with lysosomes is prevented by induction of autophagy in human epithelial cells. Moreover, protective niche constituted by autophagosomes enables pathogen escape to cytosol and replication that eventually lead to cell death (Schnaith *et al.*, 2007). However, as the mean number of bacteria in professional phagocytes decreases in the first 20 hpi, one can speculate that at least a fraction of the internalised *S. aureus* bacteria are killed, and autophagy can be more effective in these host cells.

Similar to neutrophils, infected macrophages are also show the generation of ROS and almost 90 % of bacteria in those cells directly colocalised with ROS-active areas. 20 % of *S. aureus* colocalised with red fluorescence LC3. The majority of bacteria internalised by macrophages interacted with red LC3, suggesting that the GFP signal might be quenched upon autophagosome acidification. The only detectable fluorescence would therefore come from RFP fluorophore fused to the inner membrane LC3, as the LC3 bound to the outer membrane would dissociate after this

step of autophagosome maturation (Kimura *et al.* 2007). Such results suggest that the RFP/GFP acidification reporter functions in macrophages of the *Tg(mpeg:RFP.GFP.LC3)* line, supporting the use of this line as a possible tool for macrophage autophagosome maturation study. Additionally, it indicates that macrophages can be more effective in degradation of autophagy-targeted *S. aureus* than non-professional phagocytes. Study in human epithelial cell lines shown that *S. aureus* cells presence in autophagosomes prevents their targeting to fusion with lysosomes and detrimental fate (Schnaith *et al.*, 2007). Only *agr* deficient strains undergone more conventional course of intracellular degradation, omitting the autophagy involvement (Schnaith *et al.*, 2007).

Tg(lyz:RFP.FP.LC3) and *Tg(mpeg:RFP.GFP.LC3)* embryos were treated with autophagy enhancer carbamazepine and inhibitor chloroquine. Carbamazepine treatment has already been applied in zebrafish model in a drug screen aiming the discovery of mTOR-independent treatments for diseases caused by multidrug-resistant mycobacteria (Schiebler *et al.*, 2015). Although autophagy enhancement has been shown to increase the intracellular killing of *M. tuberculosis*, through mTOR dependent stimuli (Gutierrez *et al.*, 2005), those approaches could not be tested in clinically relevant situations, as mTOR inhibition was reported to cause immunosuppression (McMahon *et al.*, 2011). In the study of Schiebler *et al.* (2015) embryos were transiently expressing RNA LC3 construct (pDestCMV:RFP.GFP.LC3), and imaged after 24h treatment with carbamazepine (50 μ M) in the presence of chloroquine (2.5 μ M), similarly as herein. The addition of the low-dose chloroquine delays the degradation of autophagosomes, therefore it prolongs the activity of autophagic machinery and increases the accumulation of autophagosomes.

Presence of LC3 protein aggregates was increased in phagocytes of embryos treated with carbamazepine+chloroquine and carbamazepine only which can be explained by carbamazepine enhancing activity. Interestingly, increased LC3 aggregate occurrence in phagocytes was also observed in chloroquine only treated embryos, although chloroquine only causes autophagosome maturation arrest, and inhibits LC3 structure degradation. However, as shown in uninfected neutrophils of 1 dpf embryos, cells engage in autophagy even without an enhancer. Thus chloroquine

treatment possibly caused the accumulation of constitutive autophagy components, observed as increase in LC3 aggregate formation. Alternatively, the use of drug could increase the activity of autophagic machinery via an unknown pathway. For instance, chloroquine could be toxic to immune cells and cause organelle damage or increased intracellular protein turnover.

Bacteria internalised in neutrophils of embryos treated with chloroquine were more likely to co-localise with cytoplasmic LC3 structures (puncta, spheroids and tight LC3 vesicles) and not with phagosome-bound LC3. This could mean that autophagosome maturation arrest had an impact on LC3 turnover and decreased LC3 recruitment to phagosomes. Independently or as a result *S. aureus* translocated to the cytoplasm where it was further targeted by autophagic machinery. In macrophage-specific line, chloroquine treatments doubled the occurrence of red LC3. As chloroquine is supposed to arrest autophagosome maturation and inhibit autophagy at this step, it seems that the separation of RFP and GFP signal may not be related to the compartment pH. If it was, according to the study performed by Kimura *et al.* (2007), inhibition of autophagosome acidification would result in lower levels of RFP signal in cells of treated embryos.

Neutrophils contained less bacteria in carbamazepine treated *Tg(lyz:RFP.GFP.LC3)* embryos. It is likely that autophagy and phagocytosis processes are performed in an exclusive manner. While the first one serves intracellular housekeeping and degradation of redundant metabolites and organelles, the other one aims engulfment of extracellular cargo. Hence, the autophagic activity considerably increased by carbamazepine possibly slowed down internalisation processes. This could imply that increased autophagy favoured bacterial infection by decrease in pathogen internalisation into neutrophils. Interestingly, although treatment with autophagy regulators increased the formation of LC3 structures in neutrophils of uninfected embryos it also caused increase in fraction of *S. aureus* cells not co-localised with those aggregates in infected embryos. Possibly the increased efficiency of autophagy did not result in specific antibacterial activity of LC3. On the other hand in macrophages from the *Tg(mpeg:RFP.GFP.LC3)* line, treatment with carbamazepine caused increase of pathogen co-localisation with both red and green LC3 structures.

This implies that carbamazepine-mediated enhancement of autophagy in macrophages shifts the process to the targeting of *S. aureus*. Nevertheless, the macrophages of carbamazepine treated embryos seemed to contain more *S. aureus*, which indicates that active, bacteria-targeted autophagy did not guarantee increased pathogen killing. Schnaith *et al.* have shown that autophagy has a characteristic function in *S. aureus* pathogenesis, and once bacteria became intracellular, their replication was reduced in the presence of wortmanin, autophagosome inhibitor (2007). Active autophagic machinery, contributed to *S. aureus* ability to subvert autophagosomes maturation and resulted in intracellular replication of the pathogen.

LC3 protein plays a key role in autophagosome formation in conventional autophagy, but also, upon TLR signalling can be recruited directly to phagosomes during infection (Sanjuan *et al.*, 2007). The latter process is regulated by NOX2-generated ROS (Huang *et al.*, 2009) present in the lumen of targeted phagosome. Herein, the analysis of spacious LC3 vesicles was conducted to test whether their presence in neutrophils of *Tg(lyz:RFP.GFP.LC3)* could imply LC3 recruitment to *S. aureus*-containing phagosomes. ROS generation in those vesicles was assessed by the presence of CellROX® fluorescence indication. Several spacious vesicles were found to contain LC3 puncta and those were scored LC3⁺ during the analysis.

My data has shown a fraction of LC3 vesicles generating ROS in their lumen at both 1 and 20 hpi time points, suggesting that the LC3 recruitment to phagosomes may occur at early time point post infection and continue over time. At 1 hpi 40 % of LC3 vesicles in neutrophils did not contain bacteria and the number of empty vesicles increased to 80 % at 20 hpi. This result implies that bacteria could be targeted for killing upon LC3 association to phagocyte. At 20 hpi ROS⁺ vesicles were less likely to be empty, which could suggest that ROS are more likely to be generated while the pathogen is still viable. The analysis of spacious LC3 vesicles was also performed in neutrophils of treated embryos. The treatment protocol used in these studies includes 24 h incubation of embryos and hence postpones infection and imaging analysis of embryos to 2 dpf. The result demonstrated that ROS generation in the lumen of vesicles was higher in older larvae and it may be that 2 dpf embryos

constitute a more effective model for the investigation of LC3 association to phagosome membrane. Constant ROS generation seems to be important to the process, as all ROS⁻ LC3⁻ still contained *S. aureus*. 40 % of ROS⁺ LC3⁺ vesicles contained bacteria, but ROS⁻ LC3⁺ vesicles were most likely empty. Upon the treatment with chloroquine the number of empty vesicles is decreased (Figure 5.31A), suggesting that the arrest of maturation can lower the ability of LC3 vesicles to clear from *S. aureus*. Moreover, ROS⁻ LC3⁺ were not observed in neutrophils of chloroquine treated embryos. Altogether it suggests that ROS and LC3 puncta present in vesicles could represent subsequent steps of the mechanism which leads to *S. aureus* degradation in spacious LC3 vesicles as proposed in the Figure 5.41. Initially, *S. aureus* presence in phagosomes would trigger ROS generation and LC3 recruitment (Figure 5.41. 1. and 2.). LC3 protein burden and fusion with lysosomes would lead to LC3 leakage to the phagosome lumen in a fraction of vesicles (Figure 5.41. 3.). Pathogen killing would further lead to switch off of the ROS generation (Figure 5.41. 4.) and LC3 puncta would be the only remaining content of the vesicle.

Experiments were not performed in *Tg(mpeg:RFP.GFP.LC3)* embryos as macrophages were not observed to contain distinct LC3 vesicles. This could imply that bacterial internalisation often occurs by a pathway distinct from phagocytosis. Autophagy and phagosome maturation could progress separately in zebrafish macrophages, resulting in the lack of LC3 recruitment to phagosomes.

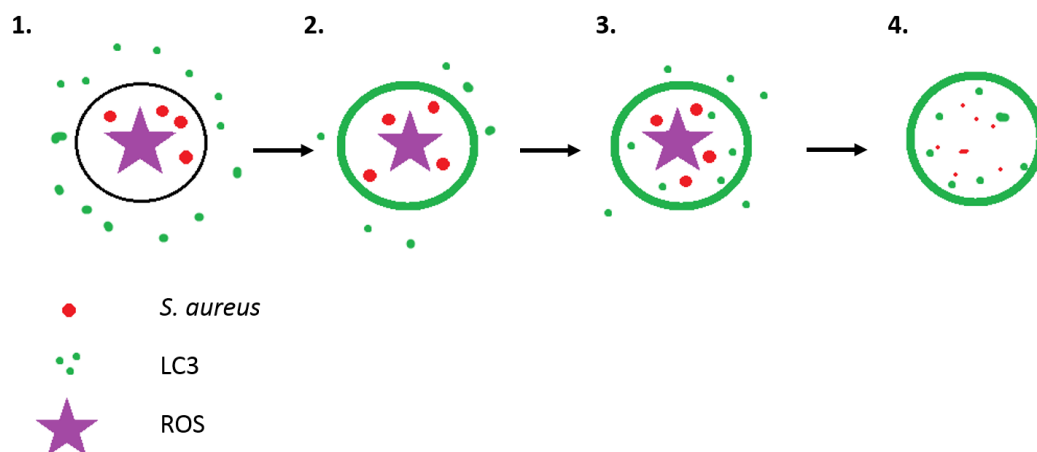


Figure 5.45. LC3 recruitment to *S. aureus* containing phagosomes upon ROS generation.

Generation of spacious LC3 vesicles in neutrophils of *Tg(lyz:RFP.GFP.LC3)* embryos suggested LC3 recruitment to phagosomes. The analysis of ROS generation in the lumen of these vesicles and the number of *S. aureus* contained within, helped to determine possible steps of bacteria killing within these structures.

1. Phagocytosis of *S. aureus* triggers ROS generation
2. LC3 is recruited to *S. aureus*-containing phagosome
3. Vesicle fusion with lysosomes could lead to LC3 leakage into the phagosome lumen
4. Generation of ROS is stopped in the absence of *S. aureus*

The imaging data collected in this study strongly suggests that in neutrophils LC3 can be recruited to phagosomes during infection with *S. aureus*, however it remains unclear what is the role of such association. Although data analysis suggested that SH1000 *S. aureus* contained within LC3 vesicles can be directed for degradation, other strains could be capable of escape from the phagosome and avoidance of intracellular killing. Therefore *Tg(lyz:RFP.GFP.LC3)* embryos were infected with various strains and their mutants of proteins known to facilitate the translocation to the cytoplasm, for instance haemolysin α . However, co-localisation of haemolysin mutants with spacious vesicles was not increased compared to wild type strain in both SH1000 and USA300 background. Although *S. aureus* haemolysins have been suggested as possible factors facilitating the escape and α -toxin was proposed to provide the pore-forming ability, still various published studies shown that increased expression of α -toxin did not exert cytoplasmic localisation of *S. aureus* in infected cells (Lâm *et al.*, 2010, Giese *et al.*, 2011, Giese *et al.*, 2009). Similarly here, the result suggests that haemolysin expression may not contribute to phagosome escape, either not in neutrophils or in this experimental model. Hence, a different escape-mediating factor had to be applied to test possible involvement of phagosomal escape to LC3 recruitment to *S. aureus*-containing phagosomes.

The recent study reports that PSM α toxin plays an important role in the context of phagosomal escape of *S. aureus* (Grosz *et al.*, 2014). Grosz *et al.* have investigated and confirmed PSM α requirement in genetically divergent backgrounds such as CA-MRSA LAC (USA300), MW2 (USA400) and MSSA 6850. MSSA6850 is strongly cytotoxic and able to grow intracellularly upon escape (Balwit *et al.*, 1994; Proctor *et al.*, 2002; Grosz *et al.*, 2014). Importantly for this study, the translocation into the cytoplasm and subsequent replication takes place in professional phagocytes. Therefore MSSA6850 and 6850 Δ psm α strains were injected into *Tg(lyz:RFP.GFP.LC3)* embryos to determine their interaction with spacious LC3 vesicles. The analysis of imaging data obtained from larvae infected with 1:1 inoculum of 6850 MSSA and 6850 Δ psm α strains demonstrated that the wild type strain bacteria are more abundant inside of an average phagocyte. Larger fraction of 6850 Δ psm α strain did not co-localise with LC3 or co-localised with spacious vesicles. To determine whether wild type 6850

escapes from LC3 phagosomes, a decrease should be observed in the proportion residing in spacious LC3 vesicles, however this was not demonstrated at 1 hpi. Grosz *et al.* (2014) suggested that the escape occurred after 2.5 hours post infection in cell line culture, thus the *in vivo* analysis should also include more time points in the first few hours post infection. The same study also shown that at 6 hpi 6850 strain was not acidified in macrophages, due to phagosomal escape and replication in the neutral cytoplasm environment. Thus, 6850 MSSA and 6850 Δ psm α strains were stained with pHrodo and imaged after injection into neutrophil and macrophage reporter lines. My data demonstrated that indeed in macrophages, a larger proportion of 6850 Δ psm α strain was acidified compared to the wild type strains at 2 and 6 hpi. However the difference was not pronounced, and it may be that *S. aureus* strains need more time to show differences in replication when incubated in lower temperature, 28°C typical for the zebrafish husbandry. Nevertheless, it is likely that the published result could be confirmed in zebrafish, after optimisation of the infected dose, and although the pilot experiments demonstrated in this chapter did not yield indisputable results, proposed *in vivo* model could potentially be useful in the future study of the involvement of autophagy in *S. aureus* phagosomal escape.

The data presented in this chapter demonstrate that the zebrafish infection model constitutes a useful tool for multi-component microscopy studies of *S. aureus*-host interaction components. Moreover, it provides dynamic model for the study on the environment of *S. aureus*, while it is invading a living organism. Methods for fluorescent indication of ROS generation and pathogen acidification were shown to be reproducible and informative and can be used in experimental work aiming to study different processes in which these factors play an important role.

Chapter 6: Observation of host-pathogen interactions in *S. aureus* infection

6.1. Introduction

The zebrafish model gives an opportunity to study differences in bacterial engulfment by neutrophils and macrophages, in a more complex environment than *in vitro* cell culture. Here, as well as the study of molecular mechanisms, it is possible to observe the impact of the bloodstream environment and co-operation with other phagocytes on the mode of pathogen internalisation. Importantly, bacterial localisation on the tissue surface favours ingestion by neutrophils in contrast to liquid media which favours macrophage internalisation (Colucci-Guyon *et al.*, 2011).

6.1.1. Mechanisms of pathogen internalisation by host cells

Cells of the host innate immune system are capable of using various pathways to internalise pathogen, and most of these are related to host defence mechanisms. Regardless of invasion mode, the interaction involves bacterial contact with the host cell membrane, followed by membrane rearrangement. Zebrafish optical accessibility enables the use of the Nomarski differential interference contrast (DIC) microscopy technique, emphasising details of observed structures and offering a “three-dimensional” display. High magnification DIC imaging permits high quality observation of the zebrafish cell membrane dynamic distortion and ruffling (Herbomel *et al.*, 1999, Le Guyader *et al.*, 2008), and hence it has been used in this study. Additionally, fluorescent reporter lines were used to visualise pathways of *S. aureus* uptake and to investigate their intracellular fate. For instance, most membrane rearrangements and pathogen internalisation pathways are considered to be actin-dependent. However, various actin-dependent processes may also influence pathogen trafficking inside of a host cell. The zebrafish model has been previously used to study infection of bacteria known to interact with the cytoskeleton and form actin tails in the cytoplasm of infected cells (Collins *et al.*, 2009, Perrin *et*

al., 2004, Mostowy and Cossart, 2011) and here it was applied to study *S. aureus* infection. Moreover, using macrophage and neutrophil specific membrane-labelled transgenic lines allowed visualisation of the diversity of *S. aureus*-containing intracellular vesicles. The CAAX motif, also known as CAAX box is a C terminal membrane targeting region, successfully used as cell membrane reporter in these studies. The best characterised eukaryotic family of CAAX motif-containing proteins is the Ras superfamily, a group of related proteins ubiquitously expressed in all cell lineages. These small GTPases function as regulators of various cellular processes at the interface of diverse membrane compartments (Wright and Philips, 2006).

Two internalisation pathways have been prioritised in this study, phagocytosis and macropinocytosis. The process of phagocytosis is an active, receptor-mediated pathway for bacterial internalisation initiated by actin remodelling and cytoskeletal rearrangements, leading to the formation of a membrane phagocytic cup which subsequently becomes a vacuole. As a consequence, a phagosome is shaped with the plasma membrane extended around the engulfed target. The understanding of phagocytosis and phagosome maturation in neutrophils is limited, as most of this information has been obtained from studies in macrophages (Lee *et al.*, 2003). However, there are multiple differences in the progress of internalisation, phagosome maturation and in the outcome of the phagocytosis process (Nordenfelt and Tapper, 2011). After internalisation, *S. aureus* is exposed to a spectrum of antimicrobial agents usually sufficient to kill the bacteria, although multiple studies have reported that *S. aureus* is capable of evading killing (Rogers and Tompsett, 1952, Gresham *et al.*, 2000, Kubica *et al.*, 2008, Thwaites and Gant, 2011). Therefore, there is a need to better understand the initial steps of *S. aureus* internalisation as well as to determine whether an alternative uptake process is involved in its prolonged intracellular existence.

Macropinocytosis can be triggered in response to growth factor stimulation, however some cells are capable of engaging in constitutive macropinocytosis (Norbury *et al.*, 1995, Racoosin and Swanson, 1989, Sallusto *et al.*, 1995, Haigler *et al.*, 1999, Dharmawardhane *et al.*, 2000, Norbury *et al.*, 1997, Watarai *et al.*, 2001). The process involves creation of membrane ruffles and protrusion of lamellipodia; both

structures are formed in an actin-dependent manner and can be retracted back into the cell. However, protrusions can also fold back creating large, circular vesicles inside of the cell containing extracellular fluid and particles. Infectious agents such as viruses and bacteria, and even protozoa and prions, have been reported to exploit macropinocytosis to gain entry into the host cells (Watarai et al., 2001, Sansonetti et al., 2001, Schroeder and Hilbi, 2008, Haraga et al., 2008, Ammendolia et al., 2004, Wanderley et al., 2006, Wadia et al., 2008, Magzoub et al., 2006, García-Pérez et al., 2003, Bermudez et al., 2004). Although such internalisation would appear to be opportunistic, some pathogens have evolved strategies to modify macropinocytic uptake to their own ends. Viruses are commonly known to subvert macropinocytic uptake, for instance by mimicking apoptotic material (Mercer and Helenius, 2008). Bacteria from *Salmonella spp.* were shown to be macropinocytosed into macrophages, and survival within these host cells is essential for their virulence (Alpuche-Aranda et al., 1994). Thus, several experiments presented in this study aimed to verify whether professional phagocytes engage in macropinocytosis while internalising *S. aureus* during zebrafish bacteraemia.

Although phagosomes and macropinosomes can both undergo maturation leading to the acidification of the vesicle and degradation of cargo, subsequent steps of their intracellular path are different. Thus, *S. aureus* fate inside of the host cell may depend on the pathway by which it is engulfed. Moreover, multiple differences in the progress of internalisation and of vesicle maturation can be observed between two cell lineages, neutrophils and macrophages, even in the common, well-conserved phagocytosis pathway (Nordenfelt and Tapper, 2011). On the other hand, macrophages may also perform macropinocytic uptake (Colucci-Guyon et al., 2011), in which the macropinosome can provide the bacterium with different, more optimal intracellular conditions, due to the simultaneous uptake of extracellular fluid. Macropinocytosis is also likely to occur in the *S. aureus* bacteraemia model, where macrophages would be more potent for the internalisation of liquid-borne bloodstream pathogens (Colucci-Guyon et al., 2011).

6.1.2. Phagocyte-phagocyte pathogen transfer

Neutrophils and macrophages cooperate during *S. aureus* infection which is important for a successful response against the pathogen (Silva, 2011). Both immune cell types are capable of phagocytosis, immunomodulation and similar kinetic behaviour under inflammatory conditions. Nevertheless, during differentiation they specialise to earn distinctive antimicrobial features, capacities and lifespan, and their complementary characteristics promote the cooperative participation in innate immunity (Silva, 2011).

Neutrophil-macrophage co-operation can have an indirect character. For instance, perivascular macrophages were shown necessary for neutrophil migration into mouse skin infected with *S. aureus*, and to constitute an important source of neutrophil-attracting chemokines (Abtin *et al.*, 2014). Of note, the same study suggested that *S. aureus* has evolved a strategy to impair this cooperation by lysis of macrophages. Another important aspect of neutrophil-macrophage interaction in *S. aureus* infection concerns neutrophil extracellular traps (NETs). *S. aureus* expresses adenosine synthase and nuclease which has been shown to result in the generation of deoxyadenosine from NETs within renal abscesses in mice. Deoxyadenosine induces apoptosis in macrophages, while they infiltrate the abscess, which increases *S. aureus* replication and expansion (Thammavongsa *et al.*, 2013). This is particularly important as macrophages are required for successful clearance of *S. aureus* ensnared within NETs (Farrera and Fadeel, 2013).

Although macrophage-neutrophil interactions demonstrate close co-operation in *S. aureus* infection, so far there is little evidence from *in vivo* animal model studies. Importantly, the direct transfer of viable bacteria between host cells has been proposed to facilitate bacterial dissemination in various diseases, but has not reported in *S. aureus* bacteraemia. During *L. monocytogenes* infection of zebrafish, bacteria were seen with a characteristic actin “comet tail”. These microbes resided in a host cell protrusion and it has been suggested that such structures in macrophages could be used to infect neighbouring nonprofessional phagocytes (Levraud *et al.*, 2009). Furthermore, it has been shown in *M. marinum* infection that neutrophils can become infected after phagocytosis of infected macrophages. (Yang

et al., 2012). Moreover, the process of phagocytosis of the whole immune cell can also occur in the opposite direction, for instance, macrophages are well known to phagocytose apoptotic neutrophils (Haslett *et al.*, 1994). Hence, bacteria can be passed from one type of host cell to another by various mechanisms.

It has been previously shown that neutrophils can actively and directly interact with macrophages in the zebrafish inflammation model (Ellett *et al.*, 2011). Experiments performed in double transgenic larvae, where both cell lineages were labelled with different fluorescent proteins, demonstrate transfer of cytoplasm portions from neutrophils to macrophages. Two additional features of neutrophil behaviour have been reported, firstly, these cells shown ongoing pseudopodial activity while transferring the cargo, and also migrated away from the site of interaction (Ellett *et al.*, 2011). Shortly after transfer, the fluorescence of the transferred cytoplasm became quenched.

6.1.3. Hypotheses

I hypothesise that neutrophils and macrophages are both capable of using a variety of internalisation pathways. I further hypothesise that both cell types, but particularly macrophages, are capable of internalising *S. aureus* via macropinocytosis; that this internalisation mode results in the formation of intracellular enlarged bacteria-containing vesicles; and that SNX5, a protein involved in macropinosome maturation (Lim and Gleeson, 2011), would affect the size of bacteria-containing vesicles.

Early in my study of *in vivo* imaging of host-pathogen interaction, I observed neutrophil to macrophage transfer of *S. aureus*. I hypothesise that such bacterial transfer is a component of pathogenesis.

6.1.4. Aims

The aims of experiments presented in this chapter are:

- Observation of internalisation pathways used by professional phagocytes using DIC and fluorescent actin reporter *Tg(mpx:Lifeact-Ruby)*.
- Determination of the size of vesicles containing bacteria in professional phagocytes.
- Study the role of SNX5 in embryo development, *S. aureus* infection and large intracellular vesicle formation using morpholino knockdown.
- Observation of phagocyte-phagocyte cooperation in neutrophil and macrophage populations during *S. aureus* infection.
- Quantification of phagocyte-phagocyte *S. aureus* transfer in a phagocyte population.

6.2. Results

6.2.1. Internalisation of bacteria in the bloodstream of zebrafish embryos.

For the *in vivo* imaging of infection and *S. aureus* interaction with host innate immune system cells, it was important to visualise the initial phagocyte-pathogen encounter. Accordingly to previous work performed in the zebrafish model of *S. aureus* infection and observations made during this study, the processes of cellular uptake of bacteria and intracellular maturation take place within first two hours post injection. In order to reveal and capture processes occurring before complete *S. aureus* clearance from the bloodstream, *S. aureus* strains were injected and visualised in embryos mounted in 1.75 % methylcellulose or in shallow layer of 0.8 % agarose (as described in materials and methods), allowing image acquisition starting from the first 5 minutes post-injection.

6.2.2.1. DIC imaging of membrane ruffling and *S. aureus* uptake

Observation of *S. aureus* internalisation processes occurring in neutrophils and macrophages was an important aim of this chapter and where applicable the two immune cell lineages were labelled with different fluorescent protein reporters. However, in the instances where only one cell type could be distinguished with a marker, the other was recognised by the ability to phagocytose intravenously injected bacteria and specific DIC appearances. It has been shown that Nomarski differential interference contrast (DIC) microscopy makes it possible to distinguish neutrophils and macrophages *in vivo* based on their cytomorphological features (Le Guyader *et al.*, 2008, Colucci-Guyon *et al.*, 2011) and such distinction has been made in several experiments comprised in this study. However, the majority of microscopy experiments using DIC were performed in *Tg(mpx:GFP)* embryos where neutrophils are GFP-positive, which facilitated the distinction between phagocyte cell types.

DIC microscopy used in this study enabled precise visualisation of shape, cell membrane ruffling and movement of bloodstream immune cells. Therefore, it also allowed observation of bacterial engulfment followed by intracellular processing

captured during first 2 hpi (Figure 6.1.). DIC imaging revealed extensive ruffling of activated macrophage membrane (Figure 6.1.). Protrusions extended into thin lamellipodia, often seemed to target *S. aureus*, and interaction between these structures and pathogen resulted in the *S. aureus* internalisation (Figure 6.2.). Such an outcome could be considered a random effect of the extensive environmental sampling characteristic for macrophages. However, macropinocytotic uptake is mostly documented by the bacteria-orientated ruffling of membrane and closing of the lamellipodia into macropinosomes containing the pathogen cargo (Alpuche-Aranda *et al.*, 1994).

Of note, not all bacterial internalisation events acquired during this study with the use of DIC technique were preceded by such definitive membrane deformation, suggesting that bloodstream phagocytes apply various mechanisms to uptake *S. aureus*. Neutrophils seemed to internalise *S. aureus* into cup-like structures, more likely representing phagocytic uptake (Figure 6.3.). In the bloodstream phagocyte population, macrophages seemed to be more active and protruding lamellipodia, and probably also thin filopodia, sampling extracellular environment, while neutrophils remained relatively still (Figure 6.4.).

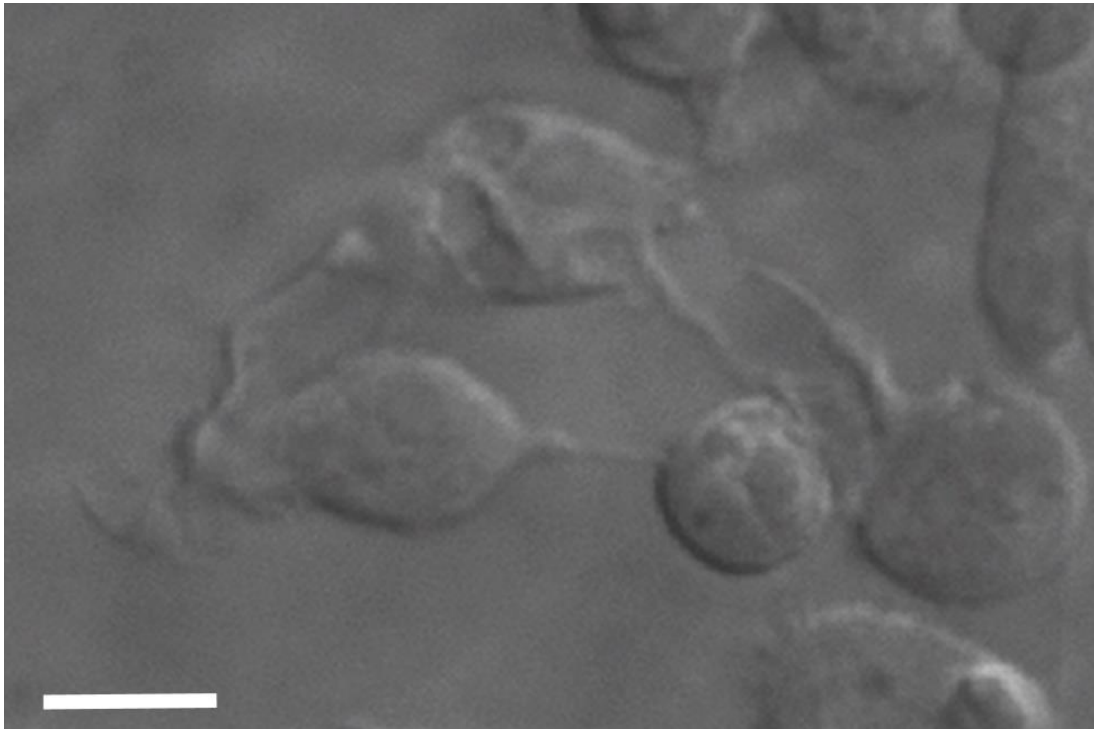


Figure 6.1. Long membrane extensions visualised in infected larvae.

Tg(mpx:GFP) embryos were infected with wild type SH1000 *S. aureus* and imaged with the use of DIC microscopy technique. Figure shows GFP-negative cells, likely macrophages, which do not contain bacteria but demonstrate an activated phenotype protruding long membrane extensions in the bloodstream of infected larvae. (Scale bar 15 μm). 60x oil objective.

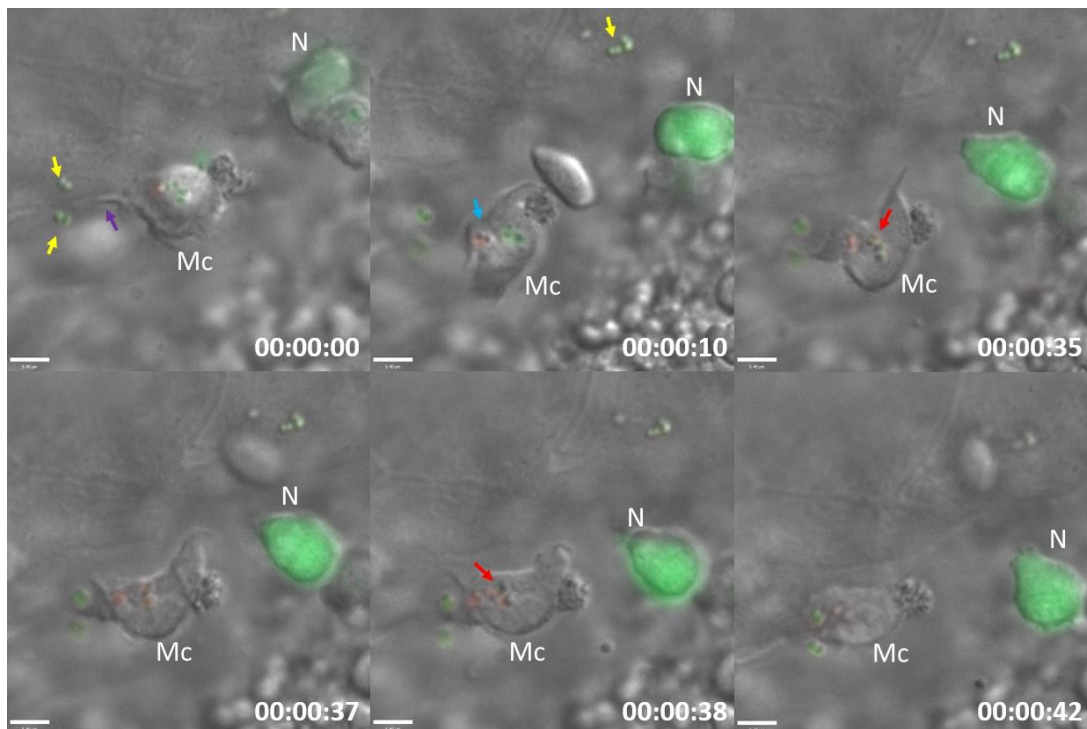


Figure 6.2. *S. aureus* uptake by macrophage.

Tg(mpx:GFP) embryos were infected with wild type SH1000. Image shows a GFP-negative phagocyte, likely a macrophage, internalising two *S. aureus* cells after protruding membrane extensions. *S. aureus* were stained with pHrodo and fluorescein, a set of dyes allowing the observation of their acidification (by green to red colour transition, see chapter 5). (Scale bar 15 μ m). 60x oil objective.

N – neutrophil

Mc – macrophage

Yellow arrow – extracellular bacteria

Blue arrow – intracellular bacteria in the low pH compartment

Red arrow – simultaneous acidification of other bacterial cells at the time of uptake

Purple arrow – cell membrane deformation towards extracellular pathogen

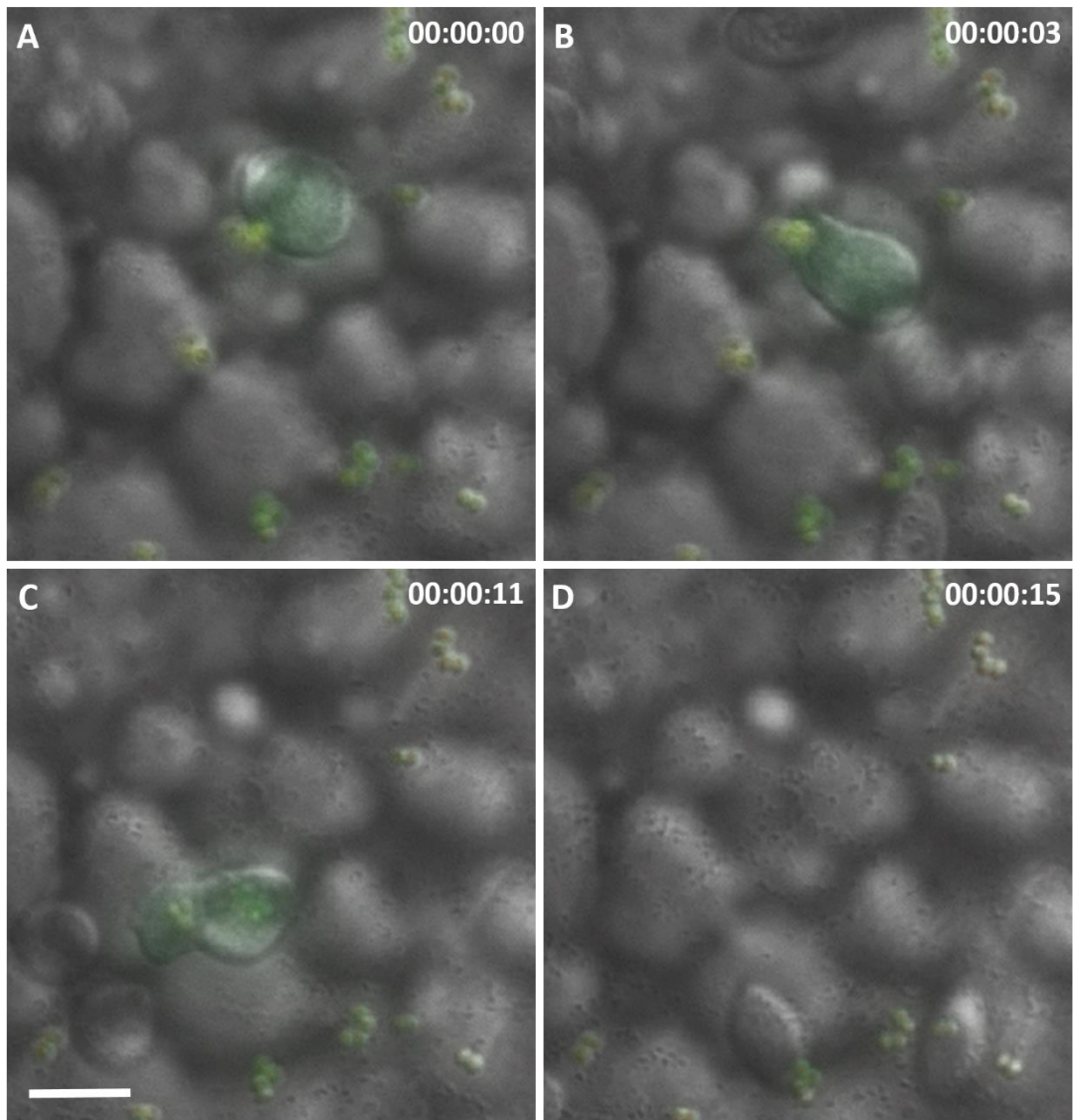


Figure 6.3. *S. aureus* uptake by neutrophil.

Tg(mpx:GFP) embryos were infected with wild type SH1000 *S. aureus*. A-D show sequential photomicrographs demonstrating a neutrophil of which initially approaches (A) internalises four (B) and further three (C) *S. aureus* attached to the endothelial surface of the zebrafish yolk sac cavity and then leaves in the bloodstream (D). Bacteria were stained with pHrodo and fluorescein, a set of dyes allowing the observation of their acidification (by green to red colour transition, see chapter 5). None of the visualised bacteria was acidified during this time lapse. During first uptake (B) a cup-like membrane structure was protruded towards the pathogen. Second uptake (C) occurred when a neutrophil moved below the observed *S. aureus*. Scale bar 15 μm . 60x oil objective.

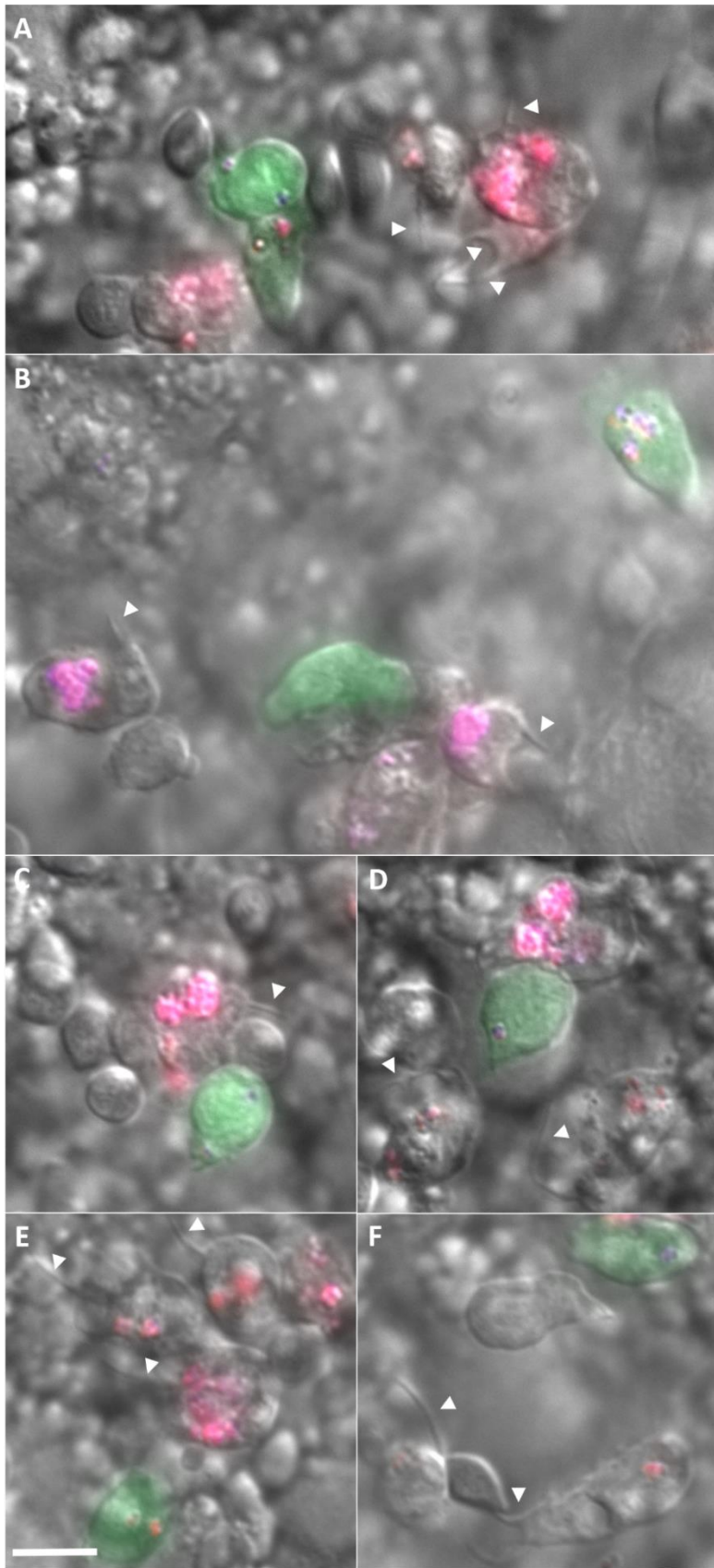


Figure 6.4.
Macrophages of
infected embryos
protrude long
membrane extensions.

Figure shows eight images taken in bloodstream of *Tg(mpx:GFP)* embryos infected with SH1000 wild type *S. aureus* strain stained with pHrodo™ and Alexa Fluor 350 dyes.

The use of DIC technique allowed visualisation of long membrane extensions (arrow heads) protruded from macrophages, but not neutrophils (GFP-positive cells).

Scale bar 15 μm.

60x oil objective.

6.2.1.2. Differences in internalisation between macrophages and neutrophils

Data collected during imaging with the use of DIC suggested that professional phagocytes can internalise intravenously injected bacteria using various pathways. Internalisation processes, for instance phagocytosis, are actin-dependent and reorganisation of the cell cytoskeleton is known to be required for phagocytic internalisation through various receptors (Kaplan, 1977; May and Machesky, 2001). Thus, a fluorescent actin reporter line was used for further study of *S. aureus* internalisation.

Using *Tg(mpx:Lifeact-Ruby)* embryos also aimed the observation of *S. aureus* interaction with cytoskeleton of phagocytosing immune cells. Fluorescent SH1000-GFP *S. aureus* were injected intravenously shortly before imaging to allow visualisation of pathogen engulfment into bloodstream phagocytes, which usually took place within the first hour post injection.

S. aureus has been previously shown to interact with actin in endothelial cells, which results in retarded bacterial invasion (Schröder *et al.*, 2006). Actin reorganisation, forming of actin cups and actin comet tails, led to propelling of bacteria to the cell surface. It has been suggested that integrin signalling promoted bacterial motility on the cell surface but hindered its internalisation into the host cell (Schröder *et al.*, 2006).

In my experiments, the formation of actin cup-like structures was observed (Figure 6.5.), however unlike in endothelial cells, it resulted in *S. aureus* engulfment. Based on the pattern of actin remodelling, it is most likely that phagocytosis was the observed uptake pathway.

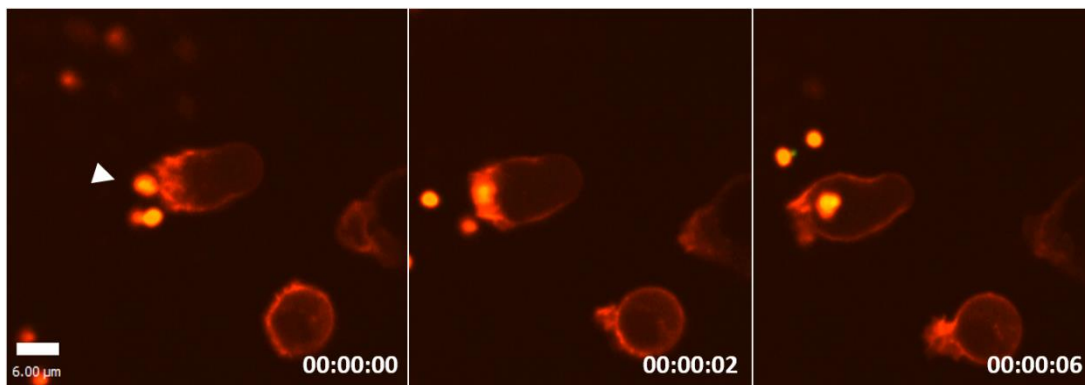


Figure 6.5. Phagocyte internalises blood-borne *S. aureus* after forming a cup-like actin structure.

Figure shows sequential photomicrographs demonstrating phagocyte cell in *Tg(mpx:Lifeact-Ruby)* embryo internalising blood-borne fluorescent *S. aureus* cell. *Mpx* promoter used in this line is less specific than in *Tg(mpx:GFP)* line as explained in Chapter 3.

S. aureus cell (arrow head) is approached by a phagocyte and internalised into a cup shaped membrane protrusion. Based on the actin remodelling pattern, it is most likely that the illustrated uptake pathway is phagocytosis. Cytomorphological features suggest that the internalising cell probably belongs to the neutrophil population. 40x objective.

Macropinocytosis involves creation of membrane ruffles and protrusion of lamellipodia, both structures are formed in an actin-dependent manner and can be retracted back into the cell body (Alpuche-Aranda *et al.*, 1994). Thus the use of actin-labelled transgenic line enabled a more complex visualisation of such remodelling during *S. aureus* uptake (Figure 6.6.). Lamellipodium and thin filopodia protruded from the cell interact with freely flowing *S. aureus* which approaches the structure and becomes “hooked” to the extended membrane. Following the interaction, the lamellipodium folds back to the phagocyte, which results in *S. aureus* internalisation. Highly active phenotype and internalisation mode could suggest that the internalising phagocyte is a macrophage.

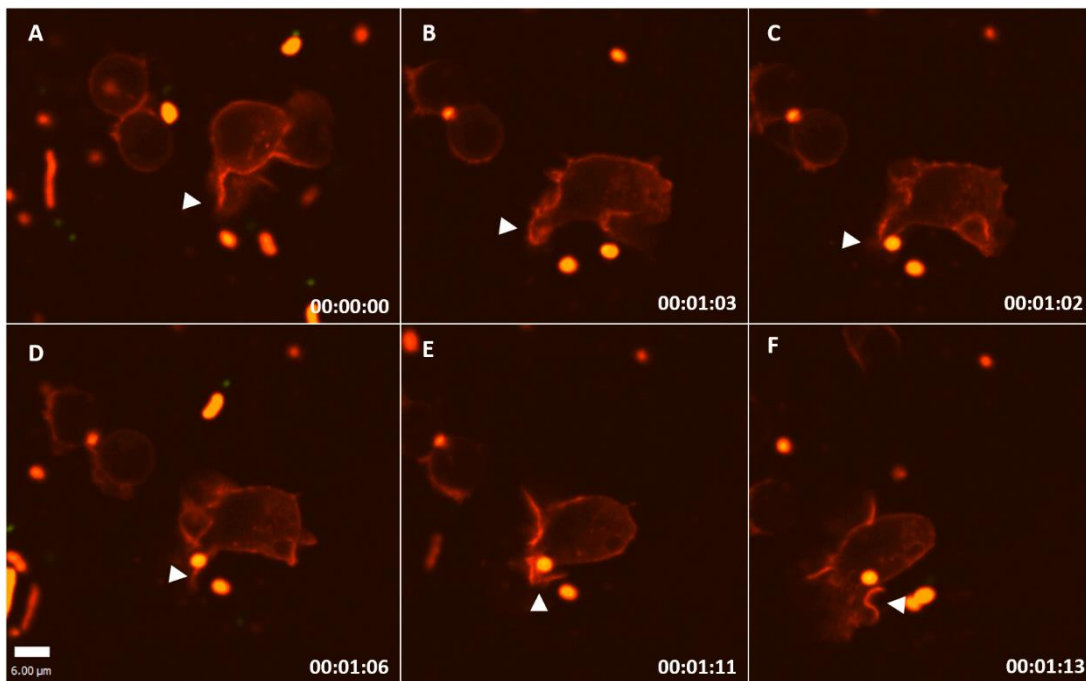


Figure 6.6. Phagocyte internalises blood-borne *S. aureus* using protruded lamellipodia.

Figure shows sequential photomicrographs (A-F) demonstrating phagocyte cell in *Tg(mpx:Lifeact-Ruby)* embryo internalising blood-borne fluorescent *S. aureus* cell.

Arrow head points at one of lamellipodia extended from the innate cell body. Lamellipodium interacts with freely flowing *S. aureus* which approaches the protrusion and becomes “hooked”. Following the interaction, the lamellipodium folds back to the phagocyte, which results in *S. aureus* internalisation. Highly active phenotype and the size of cell suggest that the internalising phagocyte belongs to macrophage population. 40x objective.

Further imaging of the GFP-expressing *S. aureus* injected into *Tg(mpx:Lifeact-Ruby)* embryos bloodstream seemed to confirm the existence of distinct internalisation phenotypes observed in professional phagocytes. A fraction of immune cells was highly activated, performing increased membrane ruffling, protruding actin lamellipodia and successively progressing along the *S. aureus*-colonised epithelium in the yolk circulation valley cavity. The second observed group remained relatively still and only phagocytosed *S. aureus* present in their proximity. Uptake mechanisms performed by cells of this population seemed to initiate from a localised membrane remodelling, a cup-like structure engulfing *S. aureus* upon contact with the phagocyte (Figure 6.7.). The third type of observed interaction, consisted on a moderately efficient uptake of endothelium-bound *S. aureus*, performed by phagocytes moving on this surface, visualised as fluorescence pulses generated by actin remodelling around *S. aureus* cells (Figure 6.8.).

Internalisation mode phenotypes of all groups seemed to be actin-dependent but could represent distinct pathways, and their membrane curvature may represent features commonly assigned to macropinocytosis and phagocytosis. Although the cytomorphology of described cell population and differences in the strength of fluorescent protein expression would suggest that macropinocytotic uptake was predominantly performed by macrophages and cup-like structures were more common in the neutrophil lineage, the *Tg(mpx:Lifeact-Ruby)* line does not constitute a tool for an unequivocal assessment. However, increased membrane ruffling was also observed in GFP-negative macrophages of *Tg(mpx:GFP)*, during acquisition using DIC technique (Figure 6.1.).

Nevertheless, lamellipodia-protruding cells, were more efficient in engulfing *S. aureus*, and a highly active cell was capable of engulfing up to 90 bacteria within 20 minutes. In the same period of time, cells of the actin-cup phenotypic group internalised only 15 *S. aureus* cells. Internalisation efficiency seemed to be dependent on the presented actin-remodelling phenotype, however a precise quantification of these events was not possible due to the high speed of the processes and relatively large area of the yolk sac cavity. Single internalisation event

takes only about 1-2 minutes, an active cell is capable of performing more than one internalisations at a time (Figure 6.7. blue arrow heads), and only a limited number of phagocytes can be captured within each z-stack frame. Additionally, membrane protrusions can be extended in multiple directions, making it impossible to capture all uptake processes in an XY plane. Although in this experimental approach, *S. aureus* was observed being internalised from a relatively flat surface, the endothelial wall of the yolk sac circulation valley, it was not always possible to determine the shape of actin structure. In multiple cases, phagocytes approached bacteria underneath the colonised tissue and engulfed cells from below the imaged surface. As described above, on these occasions actin remodelling was seen as fluorescence “pulsing” around internalised *S. aureus* cells (Figure 6.8.) and it was not possible to say whether these bacterial cells were taken up in a lamellipodium or a cup-like structure.

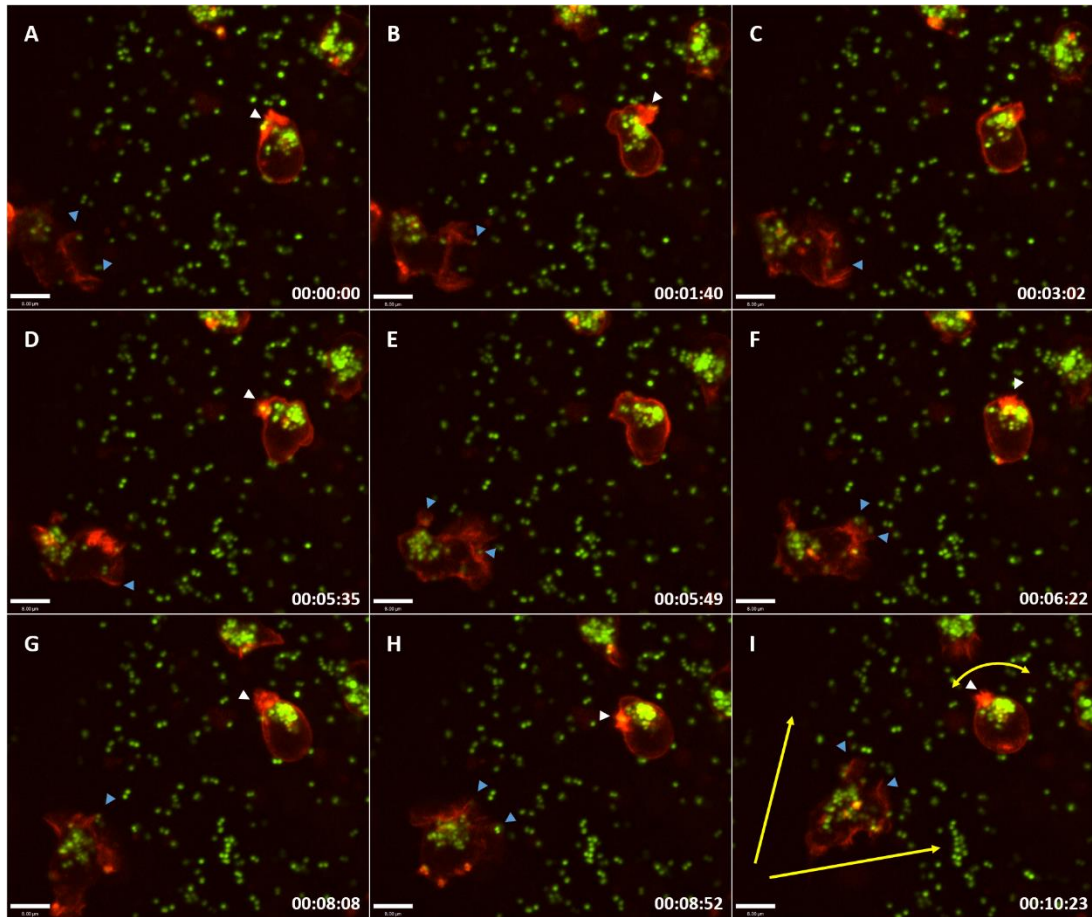


Figure 6.7. Phagocytes internalise *S. aureus* in distinct actin-dependent manners.

Figure shows sequential photomicrographs (A-I) demonstrating phagocyte cells of *Tg(mpx:Lifeact-Ruby)* embryo internalising blood-borne fluorescent *S. aureus* cell. Acquisition took place shortly after injection of SH1000-GFP *S. aureus*, and the majority of bacteria reside extracellularly on the epithelium inside of the yolk circulation valley. One of the phagocytes captured is internalising bacteria using protruded actin lamellipodia (blue arrow heads) and is progressing across the *S. aureus*-colonised surface. The other captured phagocyte remains relatively still and only phagocytoses *S. aureus* present within its proximal reach. Both internalisation modes are actin-dependent but seem to represent different pathways. (Scale bar = 15 µm). 40x objective.

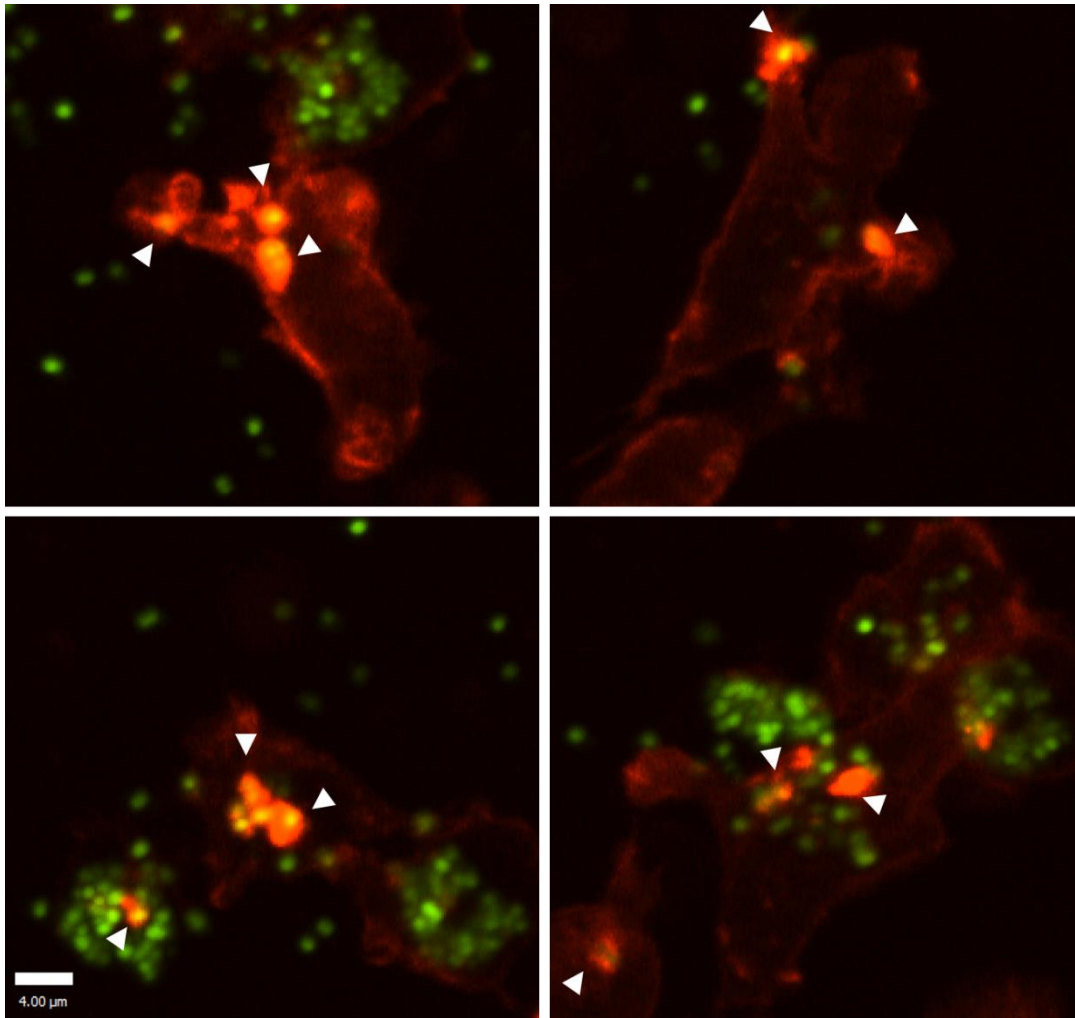


Figure 6.8. Actin “pulsing” during *S. aureus* internalisation by phagocytes of *Tg(mpx:Lifect-Ruby)*.

The image shows four examples of phagocytes internalising SH1000-GFP *S. aureus* injected intravenously into embryos of *Tg(mpx:Lifect-Ruby)*. Shortly after injection several bacterial cells resided on the epithelium layer of the yolk sac circulation cavity. When the pathogen was internalised by a phagocyte situated below the bacterium-covered layer, actin remodelling was visualised as “pulsing” fluorescence appearing around *S. aureus* cells (arrow heads). 40x objective.

6.2.1.3. Phagocyte motility and actin rearrangements during *S. aureus* uptake

Actin remodelling and membrane ruffling are known to be important for cell motility, for instance in chemotactic response of neutrophils (Carpentier *et al.*, 1991). My initial observations suggested that internalisation-related actin remodelling may influence phagocyte motility. Macropinocytosis-related membrane protrusions seem to influence the ability of the cell to relocate and reach larger number of *S. aureus* upon intravenous infection (Figure 6.7. and 6.9.). Cells with extending lamellipodia continued to engulf *S. aureus*, were motile and seemed to actively move along the bloodstream endothelium. Another phagocyte, which did not show increased membrane remodelling, remained inactive and stopped internalising *S. aureus* after engulfing approximately 30 bacterial cells. It did perform bacteria-orientated actin remodelling and seemed to reach the surrounding extracellular microbes, however, the uptake did not occur in the following 2 hours of acquisition (Figure 6.9.).

A population of phagocytes was active internalising endothelium-bound *S. aureus*. It is known that the uptake into neutrophils was more effective during engulfment of surface-bound bacteria, likely due to the coupling of internalisation and motility of these phagocytes (Colucci-Guyon *et al.*, 2011). In that study, neutrophils moved over bacteria and engulfed *B. subtilis* in a 'vacuum-cleaner'-like behaviour. Fluid-borne *S. aureus* could not be efficiently phagocytosed by neutrophils, unless it adhered to the wall of the infected yolk circulation valley, which allowed neutrophils to highly phagocytic activity. Hence, phagocytes internalising *S. aureus* from epithelium could belong to the neutrophil population.

The macropinocytic phenotype observed here is likely performed by macrophages, as these are capable of microbial internalisation, regardless if the pathogen is present in body fluids or at the cavity wall tissue surface (Colucci-Guyon *et al.*, 2011). Furthermore, the uptake capacity was higher in the lamellipodium-protruding group, than in the group of cells internalising endothelium-bound *S. aureus*.

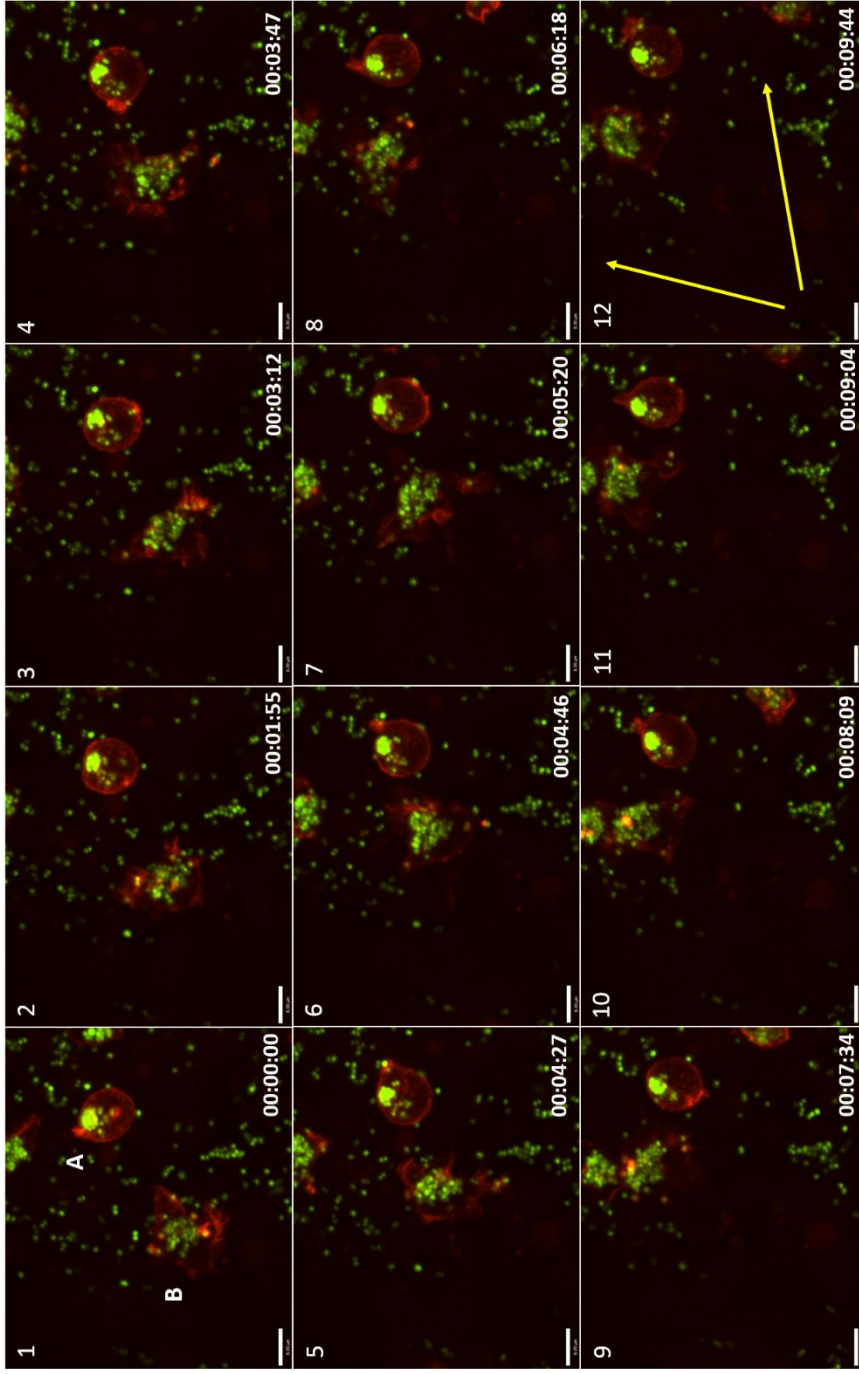


Figure 6.9. Phagocytes show different internalisation efficiency in the presence of *S. aureus*.

Figure shows sequential photomicrographs (1-12) demonstrating imaging subsequent to illustrated on the figure 6..

Cell A remains inactive after engulfing approximately 30 bacterial cells. Actin remodelling suggests reaching for surrounding extracellular pathogen, however, the uptake does not occur.

Cell B continues to engulf *S. aureus*, it is motile and seems to actively move along bloodstream wall epithelium surface. Scale bar 15 μm . 40x objective.

6.2.1.4. Size of vesicles containing bacteria at 1 hpi

Results presented above, from the study of the internalisation processes, revealed the existence of more than one pathway responsible for the uptake of substantial numbers of *S. aureus*. In this study, macropinocytosis has been hypothesised to play an important role in *S. aureus* engulfment into professional phagocytes. Such unintended uptake of *S. aureus* together with extracellular fluid, could provide the pathogen with an alternative intracellular conditions and potentially influencing its fate. Thus, I aimed to observe features indicating macropinocytic uptake.

Macropinocytotic uptake is commonly documented based on microscopy observation of bacteria-orientated membrane ruffling and closing of the lamellipodia into macropinosomes containing the pathogen cargo (Alpuche-Aranda *et al.*, 1994), and such observation has been made in my study of *S. aureus* bacteraemia. Upon membrane invagination, macropinocytic vesicles are mainly recognised by their size, which is considerably larger than the phagosomes (Hewlett *et al.*, 1994, Swanson and Watts, 1995). Therefore, herein experimental approaches have been designed to determine the size of bacteria-containing vesicles, measured within first hour post infection, at the time of increased *S. aureus* uptake.

Visual analysis of time-lapse photomicrograph series collected during multiple experiments revealed existence of differences in the shape of endosomes containing bacteria. Similarly, the size of compartments in which bacteria reside, may vary between macrophages and neutrophils and within individual phagocyte cells. Two different types of endosome shape were distinguishable, based on the observation of their physical features (Figure 6.10.): first, tight in shape, with the endosomal membrane adherent to bacterial content; second – also round in shape, but forming a “spacious vacuole”. The latter type allows bacterial movement within limited space, perceptible on recorded videos, whereas *S. aureus* in tight endosomes stay relatively static. The size alternatives are particularly noticeable when visualised in the GFP-expressing neutrophils of the *Tg(mpx:GFP)* zebrafish embryos and CFP/YFP expressing macrophages of *Tg(mpeg:FRET)* (Figure 6.11.) where the fluorescent proteins are excluded from the vacuoles.

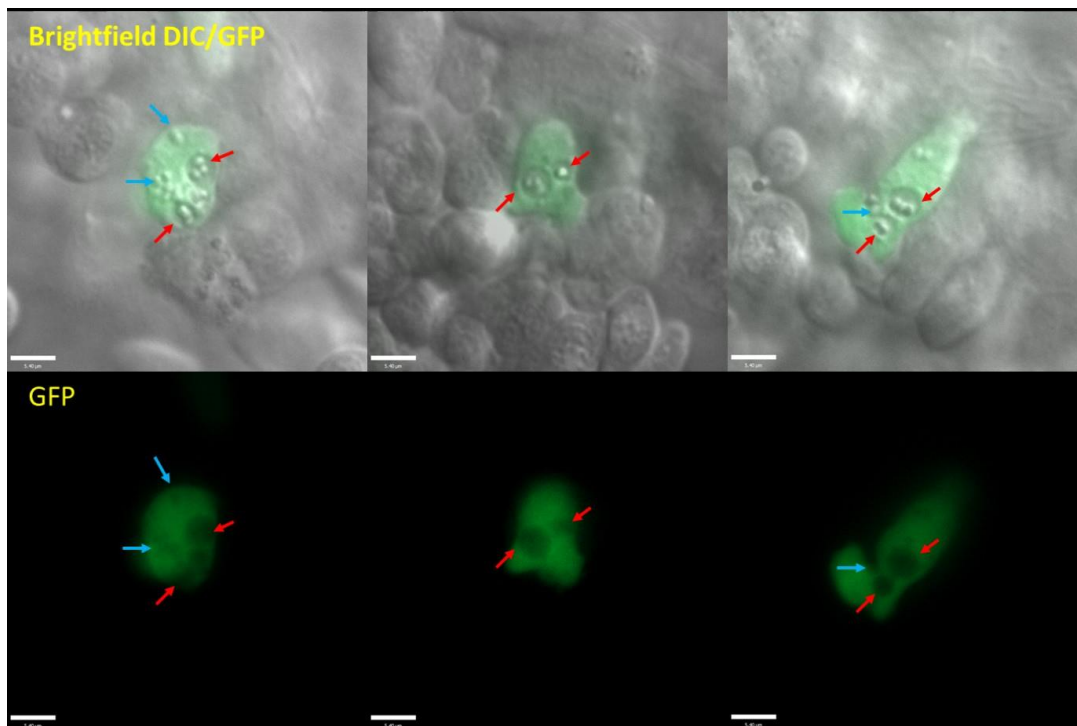


Figure 6.10. Different size of compartments containing bacteria in neutrophils

Wild type SH1000 injected into *Tg(mpx:GFP)* embryos was contained in GFP-positive neutrophils in compartments of different size. Image shows three examples of neutrophils containing *S. aureus*. Endosomes could be assessed with the use of DIC imaging and as areas of lower GFP density. Scale bar 10 μm . 60x oil objective.

Blue arrow – bacteria reside in a tight endosome

Red arrow – bacteria reside in a spacious vacuole

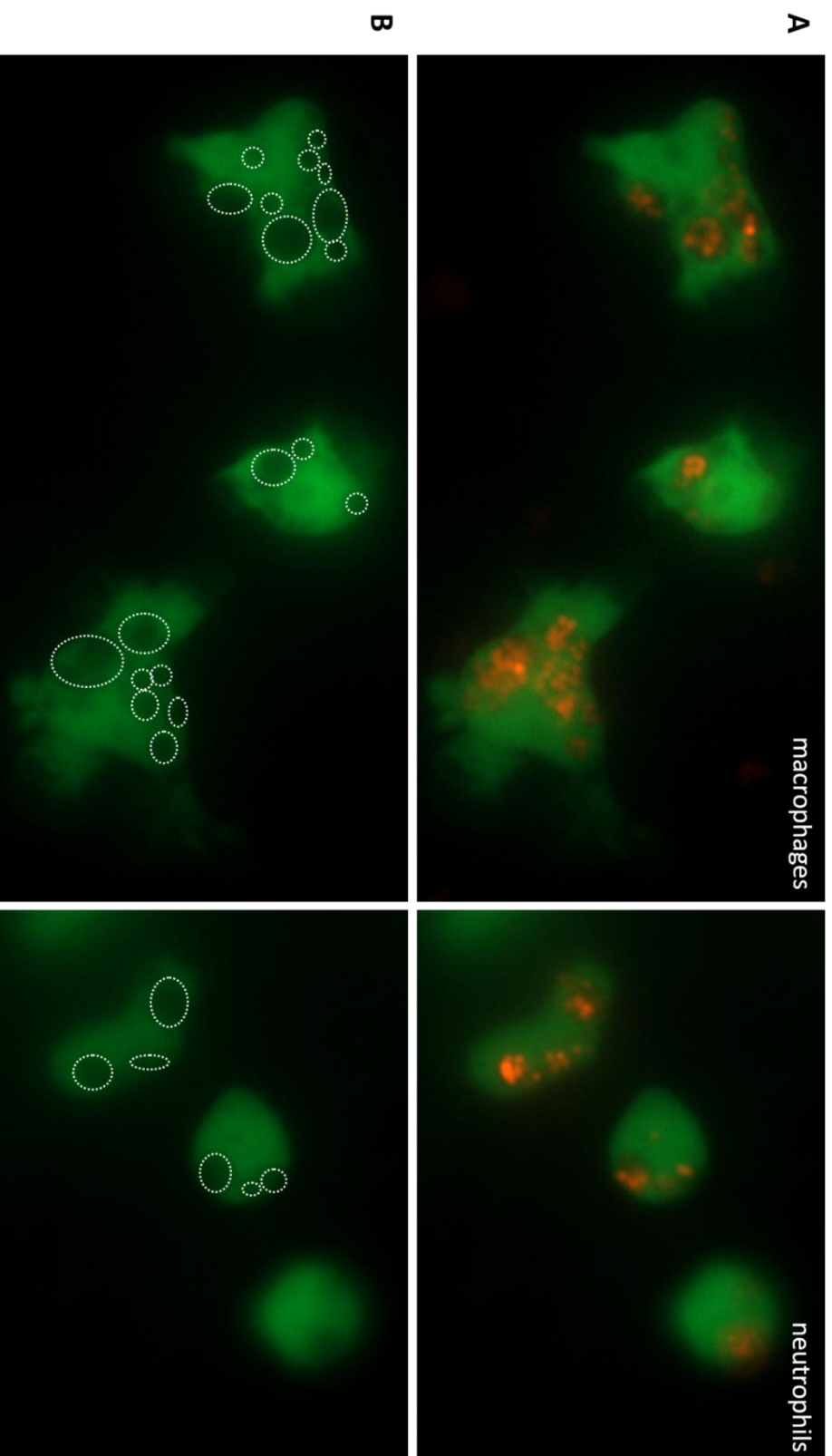


Figure 6.11. Imaging-based assessment of the size of compartments containing bacteria in neutrophils and macrophages.

SH1000-mCherry 5. *aureus* was injected into *Tg(mpx:GFP)* and *Tg(mpeg:FRET)* embryos to assess vesicles in neutrophils and macrophages, respectively.

ROI were drawn around vesicles using drawing tools of the Volocity software. Vesicles were determined as areas of lower fluorescence density. The number of bacteria residing in vesicles was determined using software measurement tool. 60x oil objective.

Tg(mpx:GFP) embryo neutrophils and *Tg(mpeg:FRET)* embryo macrophages were captured 1 hpi with fluorescent SH1000-mCherry *S. aureus*. Vesicle size (μm^3) and number of contained bacteria were analysed in Volocity™ software by drawing regions of interest (ROIs) around vesicles, visualised as areas of diluted fluorescence inside of phagocytes and marking points above *S. aureus* contained within (Figure 6.11.). The size of the vesicle is positively correlated with the number of bacteria in neutrophils and macrophages (Figure 6.12.), suggesting an increase of vesicle size caused by elevated number of internalised pathogens. However, statistical analysis demonstrated differences between the correlations of analysed groups of immune cells. In macrophages, bacteria-containing vesicles were generally larger, which could suggest that these were shaped in the uptake process engaging larger membrane surface, for instance macropinocytosis. However, enlarged size of bacteria-containing vacuoles could also be a result of the fusion of several phagosomes upon uptake. Interestingly, although neutrophils internalising surface-bound *E. coli* were shown to concentrate intracellular bacteria in a single large phagosome (Colucci-Guyon *et al.*, 2011), it seemed that *S. aureus* internalised by cells of this population remained in tight vesicles.

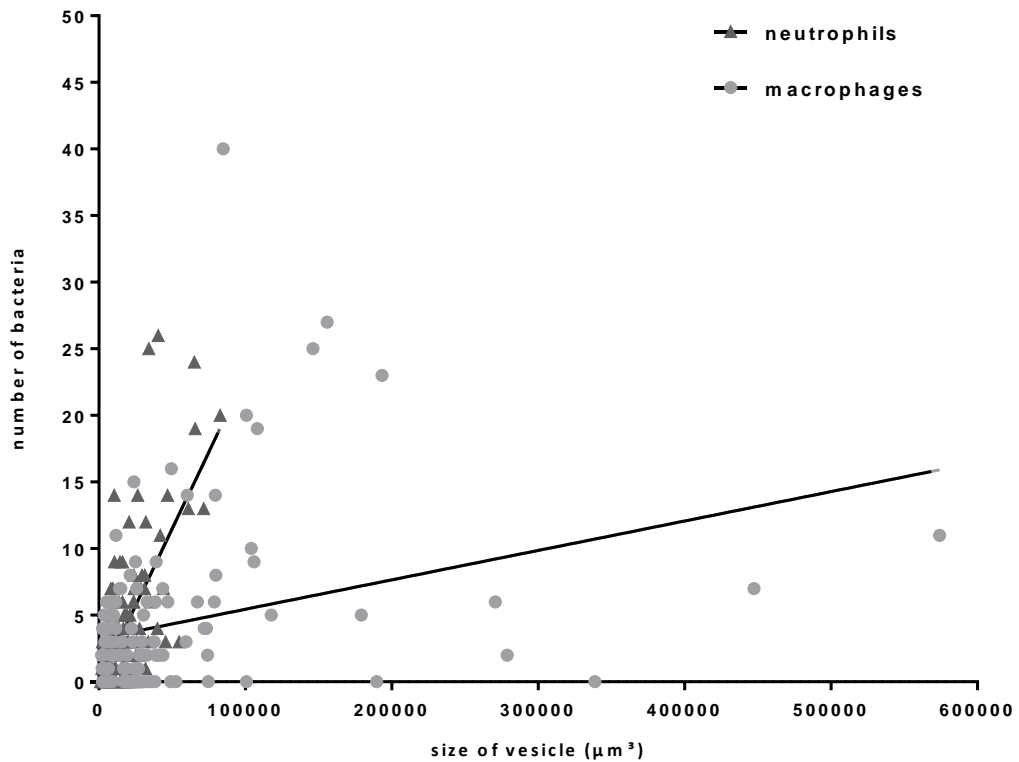


Figure 6.12. Correlation between the number of bacteria and size of the vesicle in neutrophils and macrophages 1 hpi.

Tg(mpx:GFP) embryo neutrophils and *Tg(mpeg:FRET)* embryo macrophages were imaged 1 hpi with 2500 CFU of SH1000-mCherry *S. aureus*. Vesicle size (μm^3) and number of contained bacteria were analysed using Volocity software.

Size of the vesicle is positively correlated to the number of bacteria in neutrophils and macrophages (Two-tailed $p < 0.0001$, $p = 0.0006$; Pearson $r = 0.6765$, $r = 0.2971$; respectively, $n=15$ embryos per group).

Linear regression analysis demonstrated that the slopes of both neutrophil and macrophage data sets differ significantly from zero ($p < 0.0001$, $p = 0.0006$, respectively). Additionally they significantly differ from each other ($p < 0.0001$). The result was additionally analysed for nonlinear regression and result demonstrated that one curve could not be fitted to both data sets ($p < 0.0001$).

A representative number of minimum 5 embryos (and 20 phagocytes per larvae) was imaged in each experimental group, experiment repeated $n = 3$.

An additional experiment was performed in neutrophil and macrophage-specific larvae of *Tg(mpeg1:mCherry.CAAX/mpx:GFP.CAAX)* and *Tg(mpeg1:GFP.CAAX)* to gain further insight into the shape of vesicles created in professional phagocytes upon *S. aureus* uptake. The CAAX motif is widely used as cell membrane reporter, coupling it with fluorescent proteins allows the observation of membrane-surrounded cell compartments.

Embryos were infected with fluorescent *S. aureus* SH1000 strains, labelled either with Alexa Fluor dye or by plasmid-encoded mCherry expression, and microscopy performed at 1 hpi. Imaging analysis resulted in observation of multiple vesicles present in both neutrophils (Figure 6.13.) and macrophages (Figure 6.14.). Interestingly, a substantial amount of *S. aureus* seemed to reside in relatively small vesicles, only containing a single bacterial cell. Imaging of uninfected *Tg(mpeg1:mCherry.CAAX/mpx:GFP.CAAX)* embryos demonstrated that large amount of intracellular vesicles is characteristic for neutrophils and macrophages which contain bacteria (Figure 6.15).

A fraction of vesicles was empty at the time of acquisition (1 hpi) suggesting that either bacteria were efficiently killed shortly after the uptake, or that these were created by a different pathway. Although the complex distribution and number of vacuoles impeded precise analysis of their size and content (Figure 6.14), the visualisation of intracellular membranes allowed an insight into vesicle dynamics within imaged phagocytes. Membrane structures imaged in bloodstream macrophages in the *Tg(mpeg1:GFP.CAAX)* line provided an additional illustration of folding back of lamellipodia (Figure 6.16.).

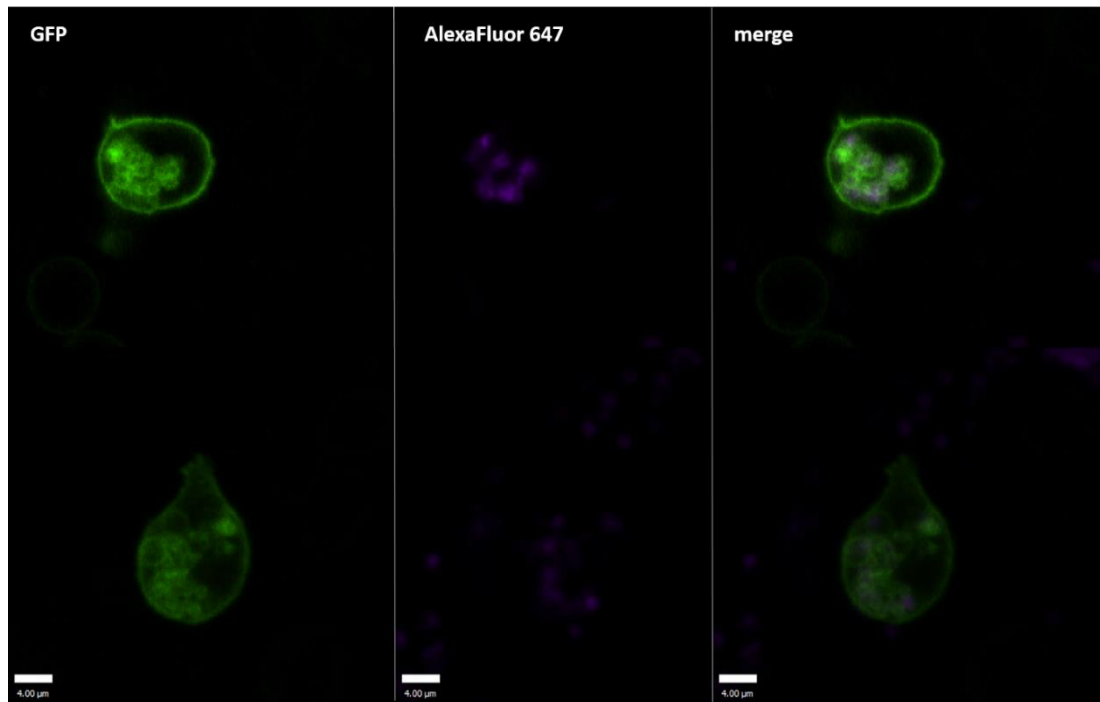


Figure 6.13. *S. aureus* resides in numerous vesicles of different sizes in infected neutrophils.

The image presents two GFP-positive neutrophil cells of infected double reporter line *Tg(mpx:GFP.CAAX/mpeg1:mCherryCAAX)* embryos. Larvae were infected with standard 2500 CFU dose of SH1000 stained with Alexa Fluor 647 dye.

Neutrophils internalised bacteria within 1 hpi. *S. aureus* can be observed residing in multiple vesicles. Although these vesicles represent various sizes, most of them seem to be relatively small, containing one *S. aureus* cell. 40x objective.

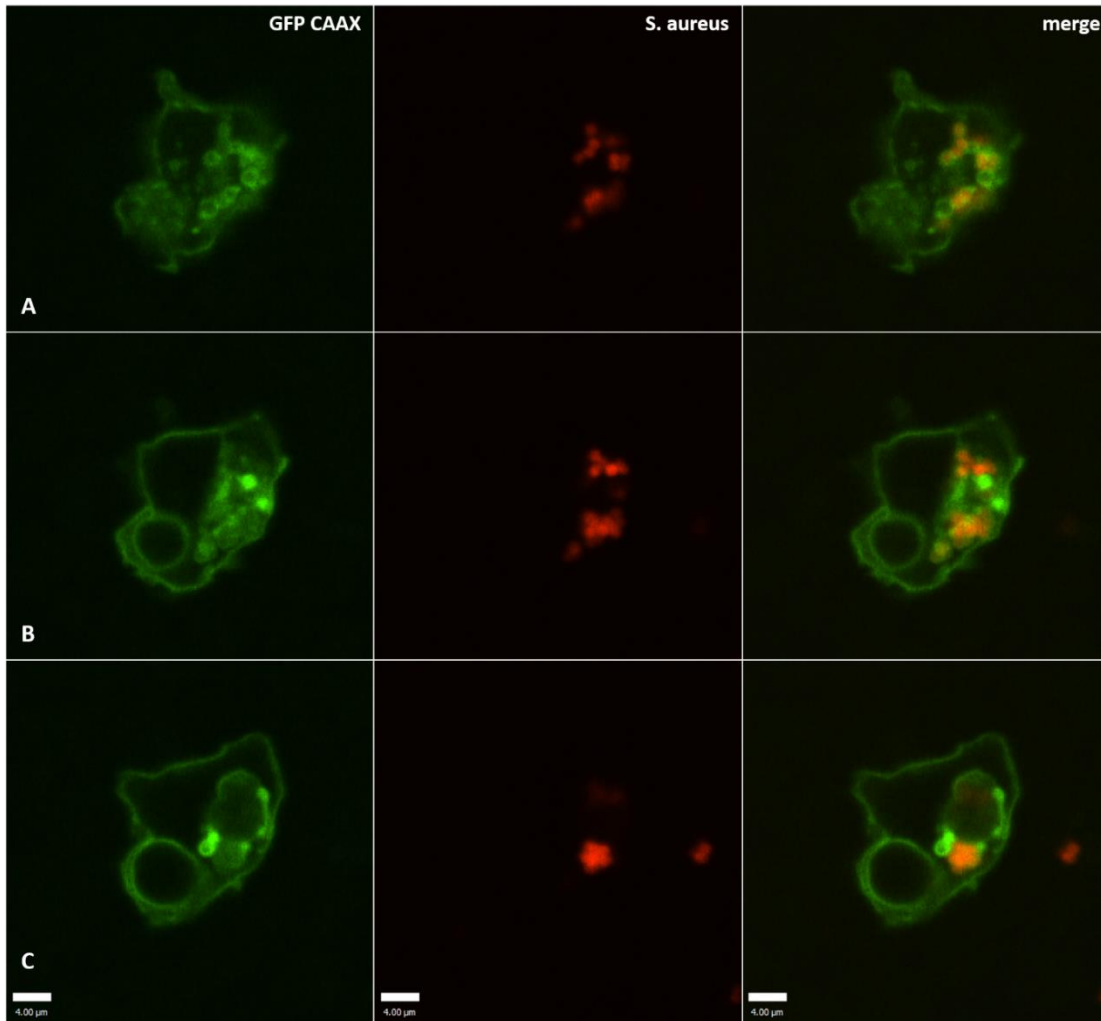


Figure 6.14. *S. aureus* resides in numerous vesicles of different sizes in infected macrophages.

The image presents 3 different z planes (A - C) of a macrophage from *Tg(mpeg1:GFP.CAAX)* embryo infected with a standard 2500 CFU dose of SH1000-mCherry *S. aureus*. Image illustrates complexity of vesicular interaction and large diversity of vesicle shape and size. 40x objective.

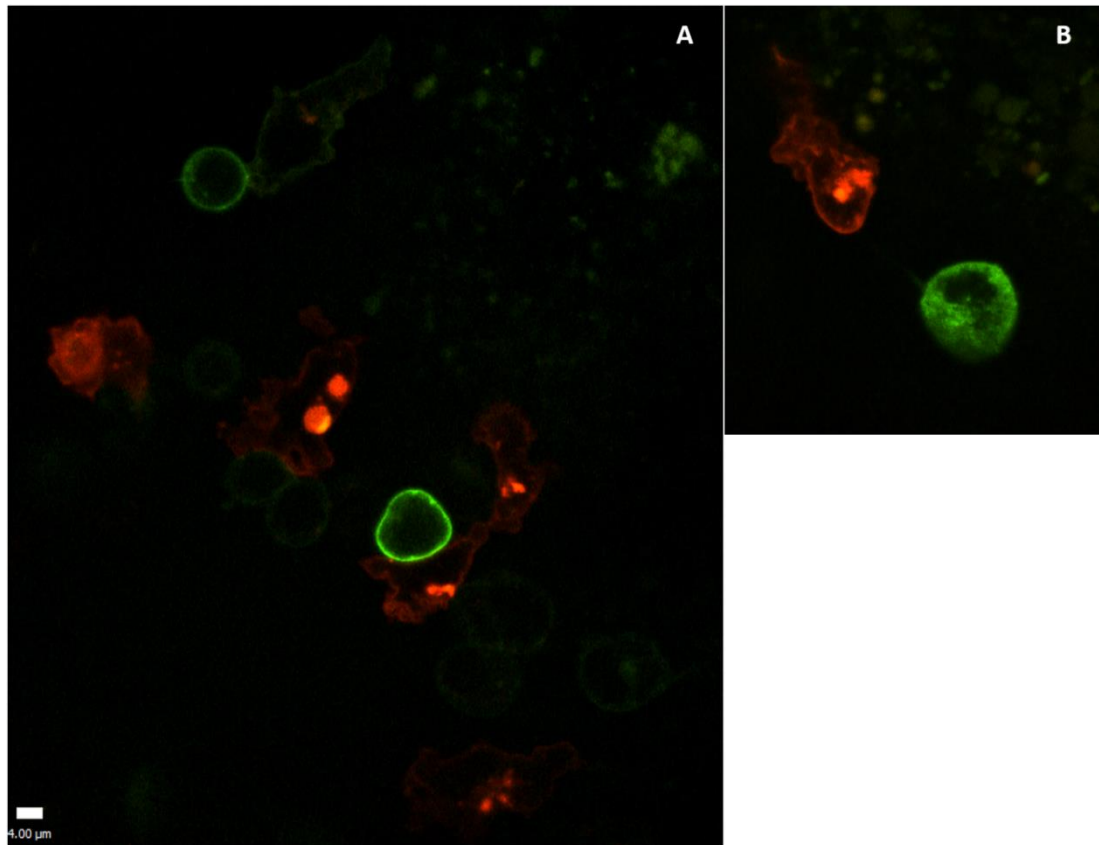


Figure 6.15. Uninfected neutrophils and macrophages show different vesicular phenotypes.

Images A and B show GFP-positive neutrophils and mCherry-positive macrophages of *Tg(mpx:GFP.CAAX/mpeg:mCherry.CAAX)* not infected embryo. Phagocytes contain lower number of intracellular vesicles compared to infected cells from the CAAX reporter lines (Figures 6.13. and 6.14.). 40x objective.

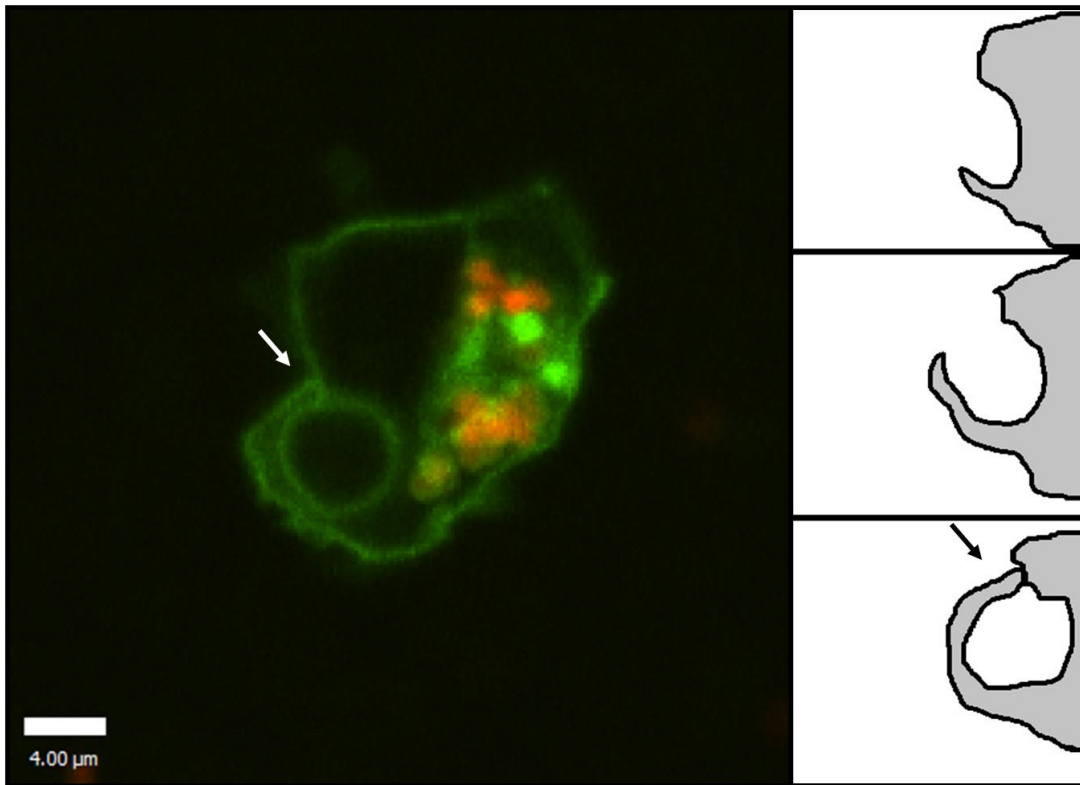


Figure 6.16. Lamellipodium structure visualised in the membrane-labelled macrophage.

Macrophage-specific *Tg(mpeg1:GFP.CAAX)* embryos were injected with SH1000-mCherry *S. aureus* and imaged 1 hpi. Fluorescent labelling of the CAAX motif enabled visualisation of phagocyte membranes. This image appears to show a lamellipodium folded back onto a macrophage, creating a large vesicle containing extracellular fluid. The panel on the right hand side demonstrates possible mechanisms of lamellipodium extending and folding back towards phagocyte cell body. 40x objective.

6.2.1.5. Infection of Snx5 morphants

The sorting nexin family members have recently been proposed to play a role in macropinosome maturation (Lim and Gleeson, 2011). Generation of fluorescently labelled SNX1 transgenic reporter did not yield a successful result as described in Chapter 4. However, a SNX-based study in the zebrafish model was still considered valuable in order to provide more specific marker for macropinocytic uptake, than descriptive analysis of membrane remodelling and vesicle size.

Morpholino knockdown techniques allow elucidation of the role of particular genes and proteins in model organisms. The use of a SNX5 morpholino in the zebrafish was previously published by Yoo *et al.* (2006). In order to see if the infection outcome would vary depending on the macropinosome maturation step in which sorting nexin 5 is involved, its function was knocked down before *S. aureus* injection. SNX5 morpholino and a control morpholino were a kind gift of Cheol-Hee Kim (Chungnam National University, Daejeon, South Korea).

LWT wild type embryos were used in the study, two groups of larvae were injected with morpholino antisense nucleotides, one with SNX5 and one with the SNX5 control morpholino. Embryo development was further observed in all three groups during 4 days (30 – 102 hpf). By 30 hpf larvae in all groups developed similarly, however at 54 hpf, embryos from uninjected group and control SNX5 morphants all hatched, while 40 % of SNX5 morphants still stayed in the chorion. The hatched SNX5MO population seemed to have curled tails and impaired brain development (Figure 6.17.). At further time point, 78 hpf, 40 % of SNX5 morphants were still in the chorion, and one of the embryos died within that time without hatching. Embryos from the control groups were still developing normally, at both time points – 78 hpf and 102 hpf. At the later time point more SNX5 morphants were found dead. The final result for 20 embryos of that group was: 15 % did not hatch and another 15 % died by 102 hpf. The phenotype of the surviving 70 % of SNX5 morphants (14 embryos) suggested a delay in development, while there were no visible difference between embryos of control groups. The impaired phenotype could be caused by defects in blood vessel development demonstrated in the study published by Yoo *et al.* (2006). This observation is in agreement with the involvement of SNX5 in

cardiovascular development and might explain why SNX5 knockdown impaired embryo survival. Nevertheless, I decided to continue the study and limit it to the early time points where larvae seemed to develop normally. Verification of SNX5 role in macropinocytosis and *S. aureus* infection was attempted with the use of high power DIC microscopy.

In the infection experiment, control SNX5 and SNX5 morpholino-injected fish was also infected with SH1000-GFP *S. aureus* at 30 hpf and imaged 2 hpi. Infection of uninjected LWT embryos was performed simultaneously to constitute a control. Survival test performed on a fraction of larvae from each group showed higher vulnerability to infection in SNX5 morphants group (Figure 6.18.). However, as described above, these fish were less viable, therefore the lower survival could be caused by impaired development, unrelated to macropinosome maturation.

High magnification imaging using DIC demonstrated that *S. aureus* could be observed in large vacuoles in all imaged groups at 2 hpi (Figure 6.19.). This could indicate that the presence of large vesicles is independent of macropinosome maturation, either because the observed vacuoles were not created during macropinocytosis, or because their shape and size is not related to the maturation process. Alternatively, SNX5 knock down did not influence the macropinosome maturation or it could not be visualised with the use of applied approach. Nevertheless, impaired development and poor survival of morphants impeded prolonged imaging and observation at the later stages of infection. Additionally, morphants were more fragile than wild type larvae and infection could result in obtaining non-specific results.



Figure 6.17. Sorting nexin 5 morphants showed impaired development.

LWT embryos were injected with SNX5 morpholino during 1-4 cell stage of development. Image presents an example of 51 hpf SNX5 morphant. Embryos showed impaired brain development (arrow head) and tail curling upon SNX5 morpholino knock down (scale bar 150 μm). 4x objective.

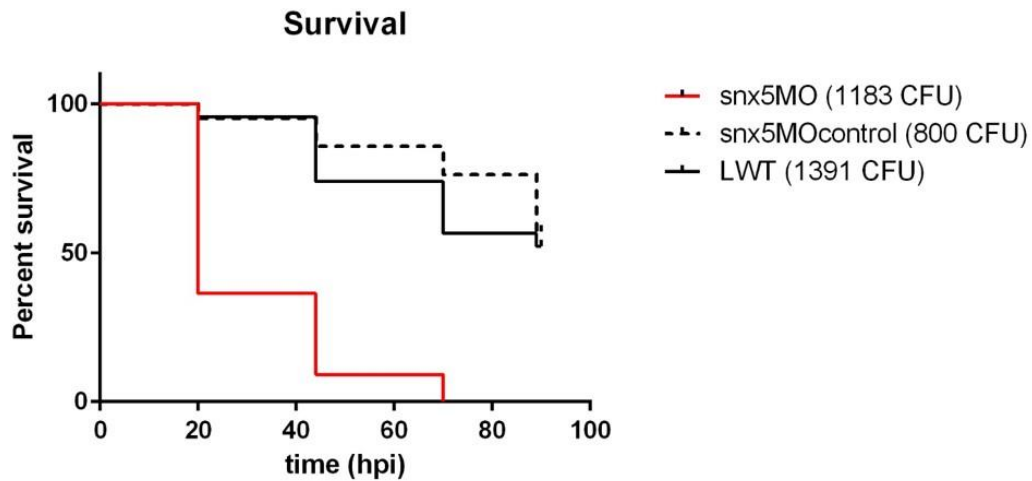


Figure 6.18. Sorting nexin 5 morphants are highly susceptible to *S. aureus* infection.

LWT (wild type) embryos were injected with SNX5 morpholino and SNX5 control morpholino at 1-4 cell stage of development. At 30 hpf fish were infected with SH1000 *S. aureus*. Control LWT embryos and control morphants shown survival rates adequate to injected dose of *S. aureus*, while SNX5 morphants were highly susceptible to infection and shown 100 % death rate within 70 hpi. A representative number of minimum 20 embryos in each experimental group, experiment repeated n = 3.

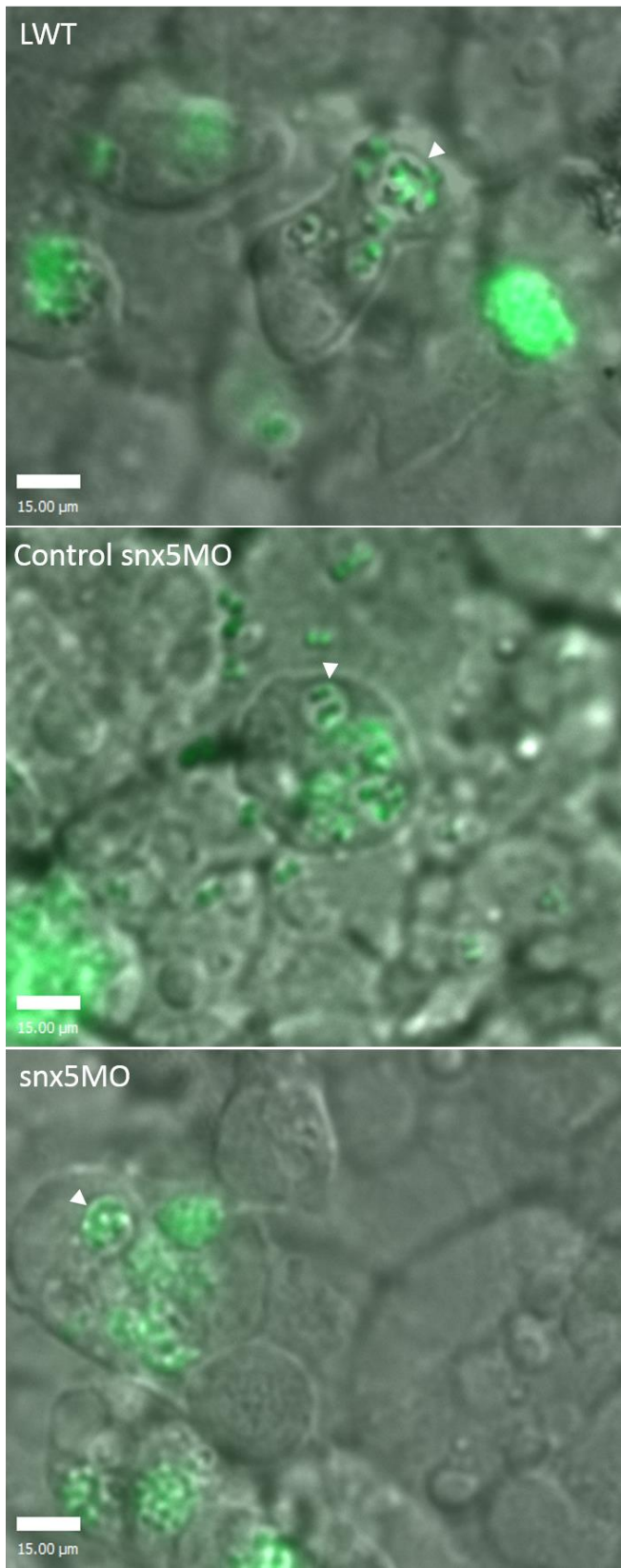


Figure 6.19. SNX5 knock down does not prevent the formation of spacious vesicles.

Images present phagocytes of LWT wild type embryos, control SNX5 injected embryos and SNX5 morphants injected with 2500 CFU dose of SH1000-GFP *S. aureus*.

SNX5 knock down did not prevent the generation of spacious vesicles and internalised pathogen was observed within those structures at 2 hpi.

60x oil objective.

6.2.2 Neutrophil to macrophage transfer of *S. aureus*

Imaging of the earlier stages of infection enabled exploration of host-pathogen interactions but also shed a light on the co-operation of innate immune system cells upon infection with *S. aureus*. Microscopy observation of the events occurring in an infected organism *in vivo* revealed the existence of mechanisms with potential impact on the outcome of *S. aureus* bacteraemia, for example the transfer of bacteria between phagocyte populations (Figure 6.20). Within first one hour post infection, an observed neutrophil transferred multiple *S. aureus* cells to a neighbouring phagocyte, most likely a macrophage. The transfer was initiated upon direct contact of the immune cells and was finalised within less than 2 minutes. This observation initiated a sequence of experiments aiming to elucidate the role and frequency of such interaction.

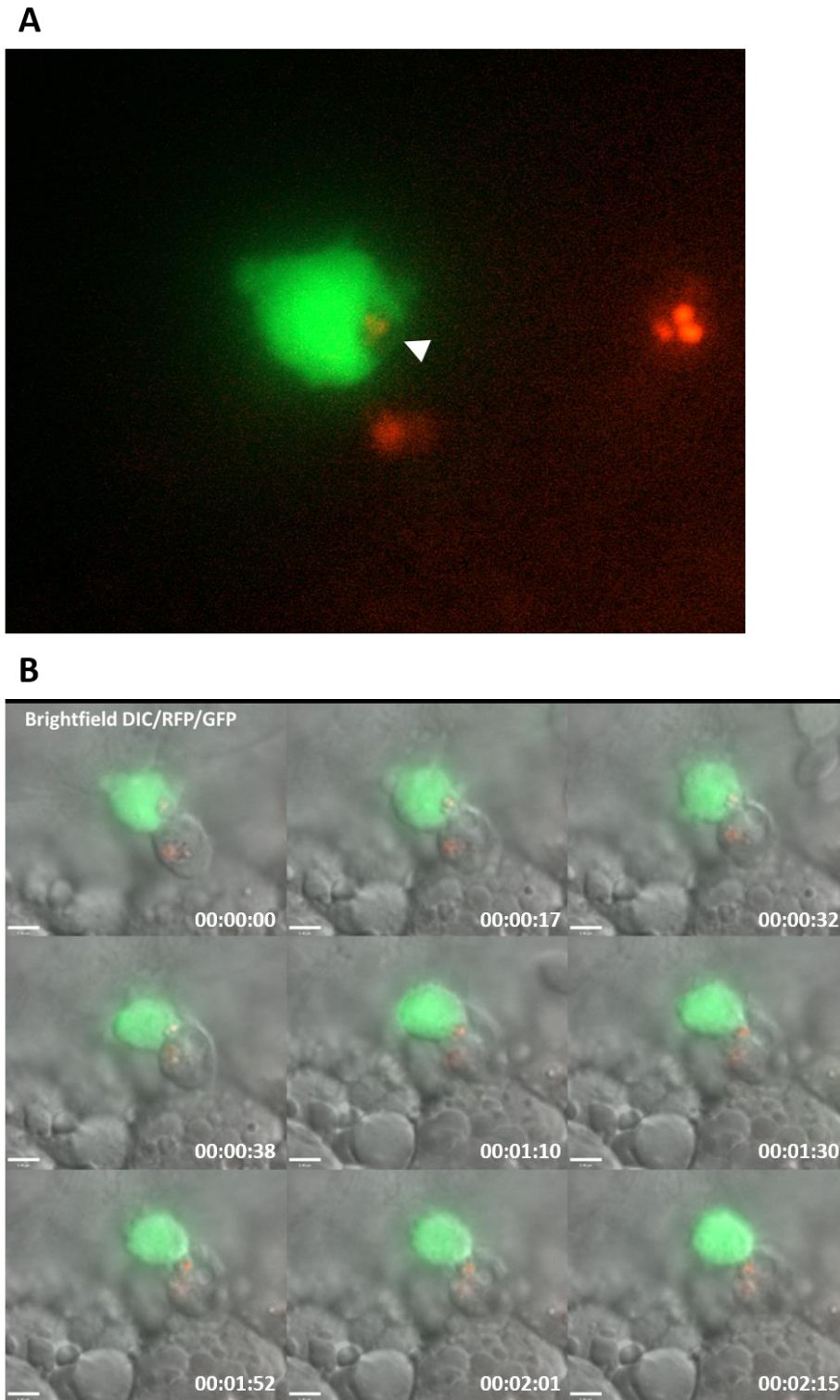


Figure 6.20. Multiple *S. aureus* cells transferred from neutrophil to macrophage.

Tg(mpx:GFP) embryos were infected with standard dose of SH1000-RFP and imaged within first hour post infection. A, *S. aureus* is contained inside of the neutrophil prior to transfer. B, Figure shows sequential photomicrographs captured during acquisition when a GFP-positive neutrophil was observed to transfer multiple *S. aureus* cells to a neighbouring cell, most likely a macrophage. (Scale bar 10 μ m). 60x oil objective.

6.2.2.1. Quantification of neutrophil to macrophage transfer in fluorescence labelled actin mRuby transgenic embryo

Quantification of phagocyte-phagocyte transfer of *S. aureus* cells was important in order to determine whether the process occurs frequently and which host cells take part in this phenomenon. It could not be performed in a large population of immune cells, as the observation of such event requires high magnification imaging, which limits the number of cells visualised at particular time point post infection. The transfer procedure requires relatively short time, and while a population of 10-20 phagocytes is visualised in an acquisition frame, it could be simultaneously occurring elsewhere in the bloodstream. Thus, it could potentially eliminate a number of events from the total counts. Moreover, aiming to image neutrophil-macrophage phagocyte pairs, could negatively influence the estimation of the population of cells which do not engage in this process, and therefore bias the evaluation of its importance. Therefore, various experiments have been designed in order to perform a credible quantification of the process. These included imaging of a random population of phagocytes at the early time points post infection, when the transfer was seen to occur, and assessment of pairing of different cell lineages in the bloodstream.

Acquisition of a random phagocyte population in the bloodstream was established in the first 4 hpi, in the yolk sac circulation valley, near the epithelium layer of the cavity wall located directly against the cover glass. Such set up enabled good optical clarity, and imaging of 20 μm of z-stacks in depth, allowing to visualise entire interacting phagocyte cells. Additionally, *S. aureus* cells adhered to the epithelium surface, which attracted both types of internalising cells, macrophages and neutrophils. The resulting videos were further analysed in the extended focus mode, as well as in each z-plane to estimate the number of transfer events.

The experiment was performed in *Tg(mpx:Lifeact-Ruby)* embryos which allowed high power visualisation of both neutrophils and macrophages and enabled short exposure times necessary for a dynamic acquisition of the process. Additionally, it aimed to determine whether the process of *S. aureus* transcellular transfer is actin-dependent, as it has been shown for other pathogens translocating between

neighbouring host cells. Intracellular bacteria *Listeria spp.* induces actin tail polymerisation at one end of the bacteria, which allows motility of the invading organisms through the host cell cytoplasm (Gouin *et al.*, 1995). Additionally, other pathogens, *Shigella Spp.* and *Rickettsia Spp.* also use similar mechanisms (Shere *et al.*, 1997, Heinzen *et al.*, 1999).

Larvae were infected with a standard 2500 CFU dose of SH1000-GFP *S. aureus*, with imaging started within 2-5 minutes after infection and lasting for approximately 4 hours. This experiment was repeated 3 times, allowing observation of a population of about 20 phagocytes, however the numbers differed due to technical limitations of such prolonged exposure. During these 3 repeats, bacterial transfer was observed 4 times, presumably in the neutrophil-macrophage direction, which was determined based on the features of the interacting cells. The position of the cells impeded verification of the role of actin in the process, despite a relatively precise in-depth acquisition (z stack thickness 1-1.5 μm). However, in one case the orientation of the donor and acceptor phagocytes allowed visualisation of increased actin remodelling at the site of the transfer (Figure 6.21.). Although such observation would have to be repeated several times to acknowledge that the process is actin-dependent, it suggests that *S. aureus* intracellular existence can exploit the phagocyte cytoskeleton and possibly use it for its mobility.

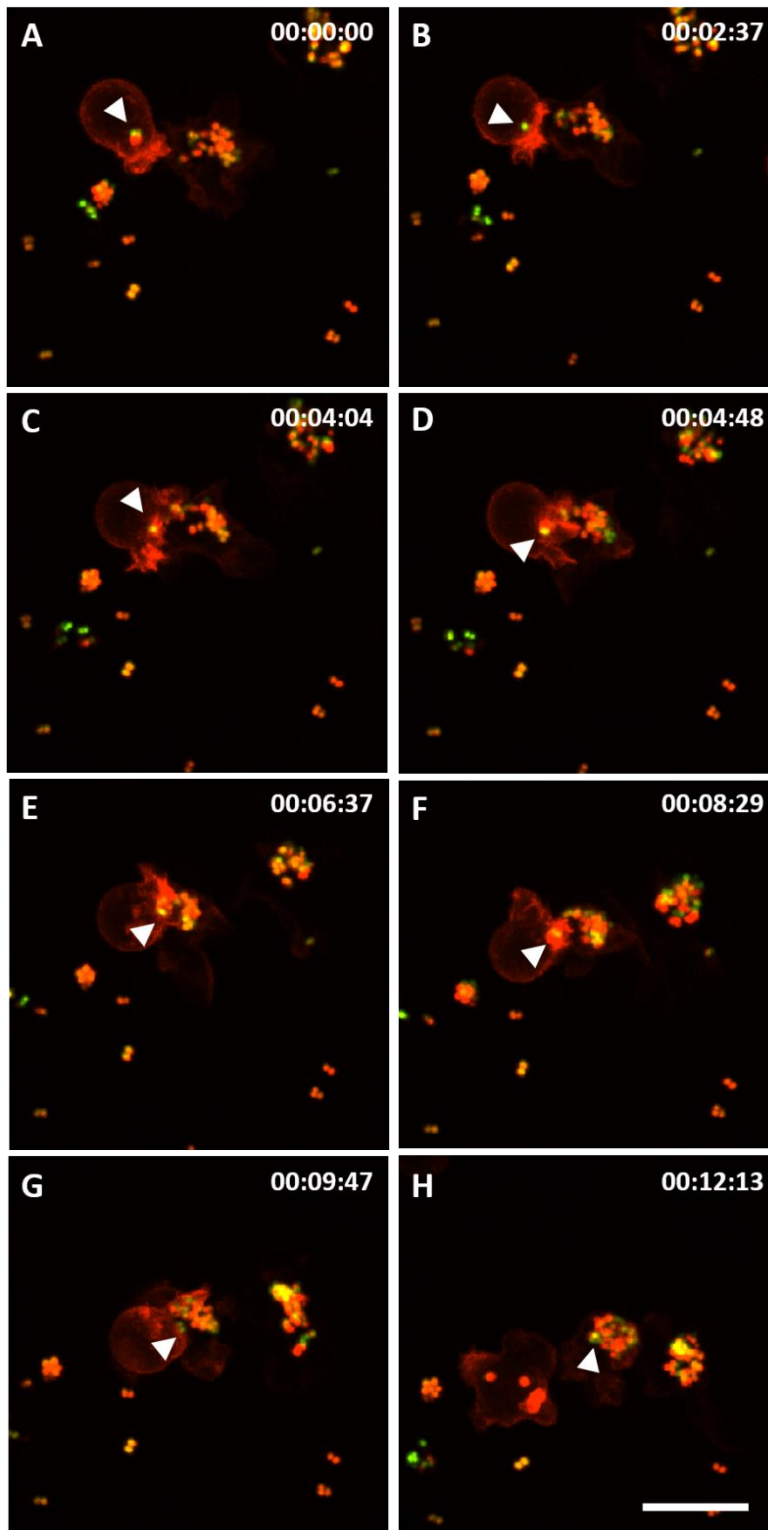


Figure 6.21. Actin remodelling during phagocyte-to-phagocyte transfer of *S. aureus* cells.

Figure shows sequential photomicrographs demonstrating SH1000-GFP *S. aureus* transfer between phagocytes in the bloodstream of *Tg(mpx:Lifeact-Ruby)* embryo.

Two *S. aureus* cells (arrow head) were transferred from neutrophil to a macrophage.

Increased fluorescence expression of labelled actin demonstrates actin remodelling at the site of transfer.

Scale bar 15 μ m.

40x objective.

6.2.2.2. Phagocyte-phagocyte colocalisation in double phagocyte-specific transgenic lines

Phagocyte-phagocyte co-localisation experiment has been established to help determine whether the phagocyte-phagocyte interaction is triggered upon *S. aureus* infection, if it is common and only occurs between different phagocyte types.

Double transgenic *Tg(mpx:GFP/mpeg1:mCherry.CAAX)* embryos were generated by pair mating of fish from neutrophil and macrophage-specific reporter lines, to visualise cells of both lineages. These were divided into three groups: uninjected, injected with PBS and infected with wild type SH1000 *S. aureus*, and examined in three independent repeats. Microscopy approach consisted on high magnification imaging of bloodstream phagocytes within the yolk sac area in a representative number of embryos (n=5) per group.

The first approach aimed to assess the number of phagocytes which did not directly contact other immune cells, neither neutrophils nor macrophages (“unpaired”). Significantly less neutrophils (Figure 6.22. A) and macrophages (Figure 6.22. B) remained unpaired in infected embryos, but not in those injected with PBS, suggesting that phagocyte-phagocyte interactions could become increased upon infection.

Subsequently, pairing rate was calculated to further evaluate, whether direct phagocyte-phagocyte contact is more likely to occur between phagocytes of the same cell lineage, or between neutrophils and macrophages. The “pairing rate” for neutrophil populations was measured by quantifying the number of pairing events between two neutrophil cells and dividing it by the total number of neutrophils. The same calculation was performed in the macrophage population. Neutrophil-macrophage pairing rate was assessed by counting the number of neutrophil-macrophage pairing incidents and dividing it by the total number of phagocytes of both populations. The analysis result has shown that neutrophil-macrophage pairing rate was significantly higher in infected embryos (Figure 6.23. C), but not neutrophil-neutrophil (Figure 6.23. A) and macrophage-macrophage (Figure 6.23. B) pairing rates. This suggests that the interaction between cell lineages is increased upon infection with *S. aureus*. However, this does not demonstrate that such interaction is related to the bacterial cell transfer.

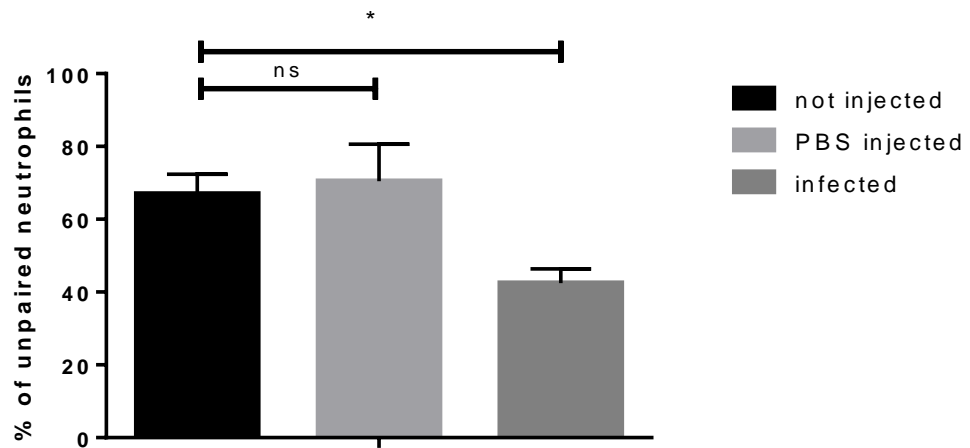
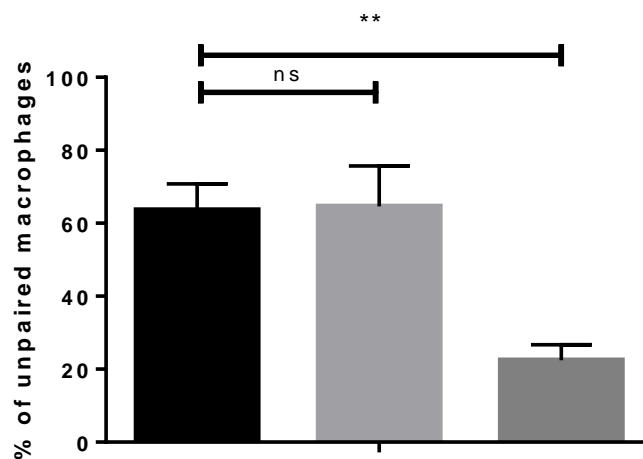
A**B**

Figure 6.22. Infection decreases the number of unpaired neutrophils and macrophages observed in the bloodstream.

Tg(mpx:GFP/mpeg1:mCherry.CAAX) embryos were divided into 3 groups: not injected, PBS injected and infected with a standard 2500 CFU dose of wild type SH1000 *S. aureus*, and imaged in the yolk sac circulation valley 1 hpi. Total numbers of GFP-positive neutrophils and mCherry-positive macrophages were counted for each group. Subsequently, a fraction of unpaired (not directly touching and contacting other phagocytes) neutrophils (A) and macrophages (B) was determined for each group. Significantly less neutrophils ($p = 0.0218$, unpaired t test, $n=15$ embryos per group) and macrophages ($p = 0.0079$, unpaired t test, $n=15$ embryos per group) remained unpaired in infected embryos suggesting increased phagocyte-phagocyte interactions. A representative number of minimum 5 embryos (and 20 phagocytes per larvae) was imaged in each experimental group, experiment repeated $n = 3$.

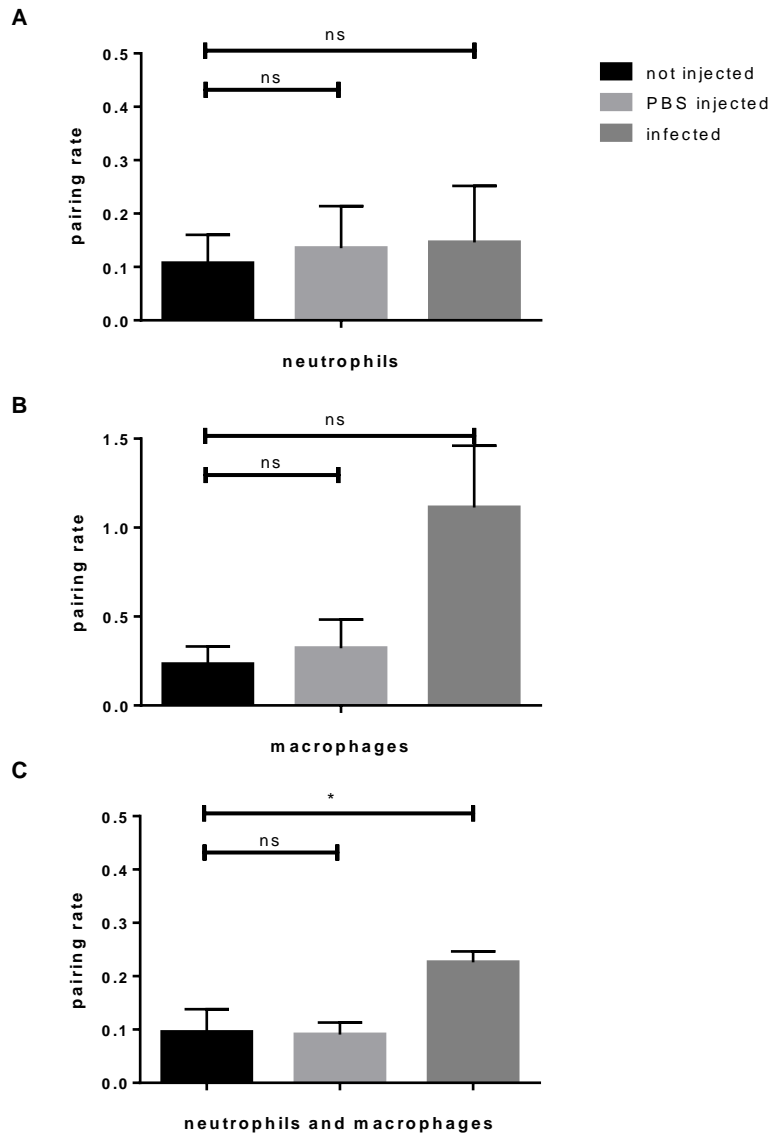


Figure 6.23. Neutrophil-macrophage pairing rate in phagocyte population is increased upon infection with *S. aureus*.

Tg(mpx:GFP/mpeg1:mCherry.CAAX) embryos were divided into 3 groups: not injected, PBS injected and infected with a standard 2500 CFU dose of wild type SH1000 *S. aureus*, and imaged in the yolk sac circulation valley 1 hpi. Total numbers of GFP-positive neutrophils and mCherry-positive macrophages were counted for each group. Subsequently, pairing rate was calculated (number of phagocyte-phagocyte pairing incidents divided by the total number of phagocytes in population) in neutrophil population (A) macrophage population (B) and for neutrophil-macrophage pairing in the mixed population. Neutrophil-macrophage pairing rate was significantly higher in infected embryos (C. one-way ANOVA, Sidak test $p = 0.0395$, $n=15$ embryos per group), but not neutrophil-neutrophil (A) and macrophage-macrophage (B) pairing rates. A representative number of minimum 5 embryos (and 20 phagocytes per larvae) was imaged in each experimental group, experiment repeated $n = 3$.

6.2.2.3. Fluorescently labelled CAAX protein transfer during *S. aureus* infection

Increased pairing of neutrophils with macrophages described in the previous paragraph suggests that immune cell lines cooperate during infection. Such cooperation could include the transfer of neutrophil contents and I therefore sought to verify whether pairing always results in transfer of *S. aureus*. Additionally, it was important to determine if transfer is unidirectional, neutrophils are always donors, and macrophages the receiving cells.

To image cell membranes from neutrophils and macrophages, I used a double transgenic: *Tg(mpeg1:mCherry.CAAX/mpx:GFP.CAAX)* embryos enabled the imaging of cell membranes, tagged fluorescently in both macrophages (mCherry reporter) and neutrophils (GFP reporter). Hence, if *S. aureus* were passed from neutrophils to macrophages, an amount of GFP-labelled CAAX would be found within macrophages. Imaging observation was performed in the same way as in the pairing experiment, however only two groups - infected and uninfected embryos were imaged, since PBS injection did not influence the pairing rate outcomes (Figure 6.23.). Representative larvae was imaged in each group, however a small fraction of imaged phagocytes has been excluded from the analysis, due to expression of both CAAX reporters (Figure 6.24) – indicating their status as early myeloid progenitor cells.

Initially, the inclusion of GFP-labelled protein within mCherry-expressing membranes was intended to be examined in the Volocity™ software environment. Drawing a line across an imaged cell enabled analysis of the profile of fluorescence within each cell. I expected that if a portion of GFP-expressing protein was contained within a mCherry vacuole, the green fluorescence peak should be registered between the red peaks (Figure 6.25). Such analysis could be performed in a fraction of cells, however a low fluorescence signal, high exposure times and the quality of the majority of the imaging data did not allow to apply it in each case.

Observation of phagocytes revealed presence of GFP-labelled protein within mCherry-expressing macrophages. Figure 6.26 shows 6 representative macrophage cells, containing GFP-positive CAAX portions, captured in not infected embryos. Similarly, macrophages containing GFP-CAAX were also visualised in infected

embryos (Figure 6.27.). In both uninjected and infected embryos, 40-50 % of macrophages contained GFP-CAAX (observation made in n=5 embryos, 3 independent repeats). However, in macrophages of uninjected larvae, these portions seemed to be larger. Interestingly, GFP-expressing membrane portions co-localised with tight vesicles characteristic for *S. aureus* presence in macrophages, visualised in the vesicle size experiment.

The experiment shows that the membrane transfer from neutrophil to macrophage occurs in both uninfected and infected embryos. Therefore it may be that the transfer of neutrophil membrane portions is a result of a process commonly occurring in zebrafish embryos. However, a group of *S. aureus* cells could benefit from it, and use as an opportunity to spread from one phagocyte to another. mCherry-labelled CAAX portions were not observed to be contained in neutrophils, suggesting that the process of transfer only occurs in the neutrophil to macrophage direction.

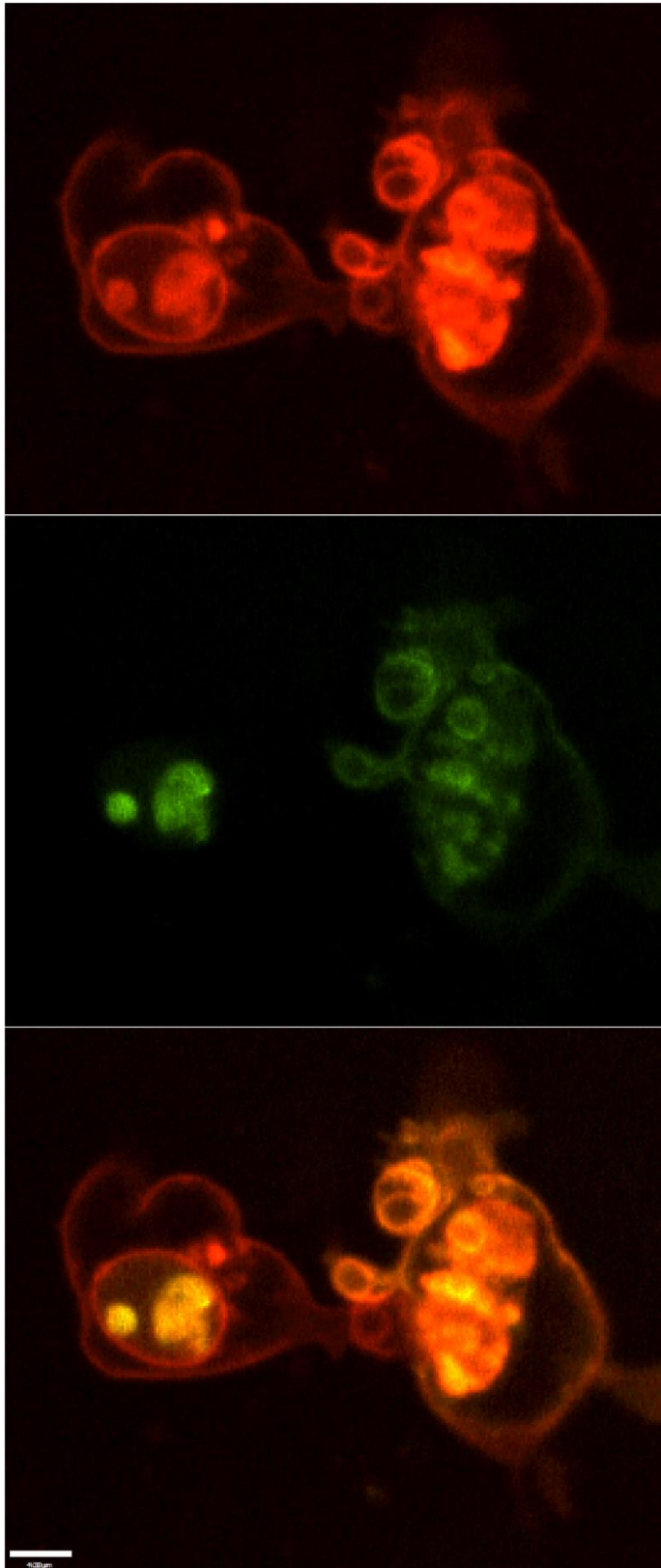


Figure 6.24. Fluorescent CAAX reporter in *Tg(mpx:GFP.CAAX/mpeg1:mCherry.CAAX)*.

Figure shows photomicrographs demonstrating phagocytes inside of *Tg(mpx:GFP.CAAX/mpeg1:mCherry.CAAX)* embryos. 5-10% of phagocytes were observed to express both GFP and mCherry fluorescence. Scale bar = 8 µm.

40x objective.

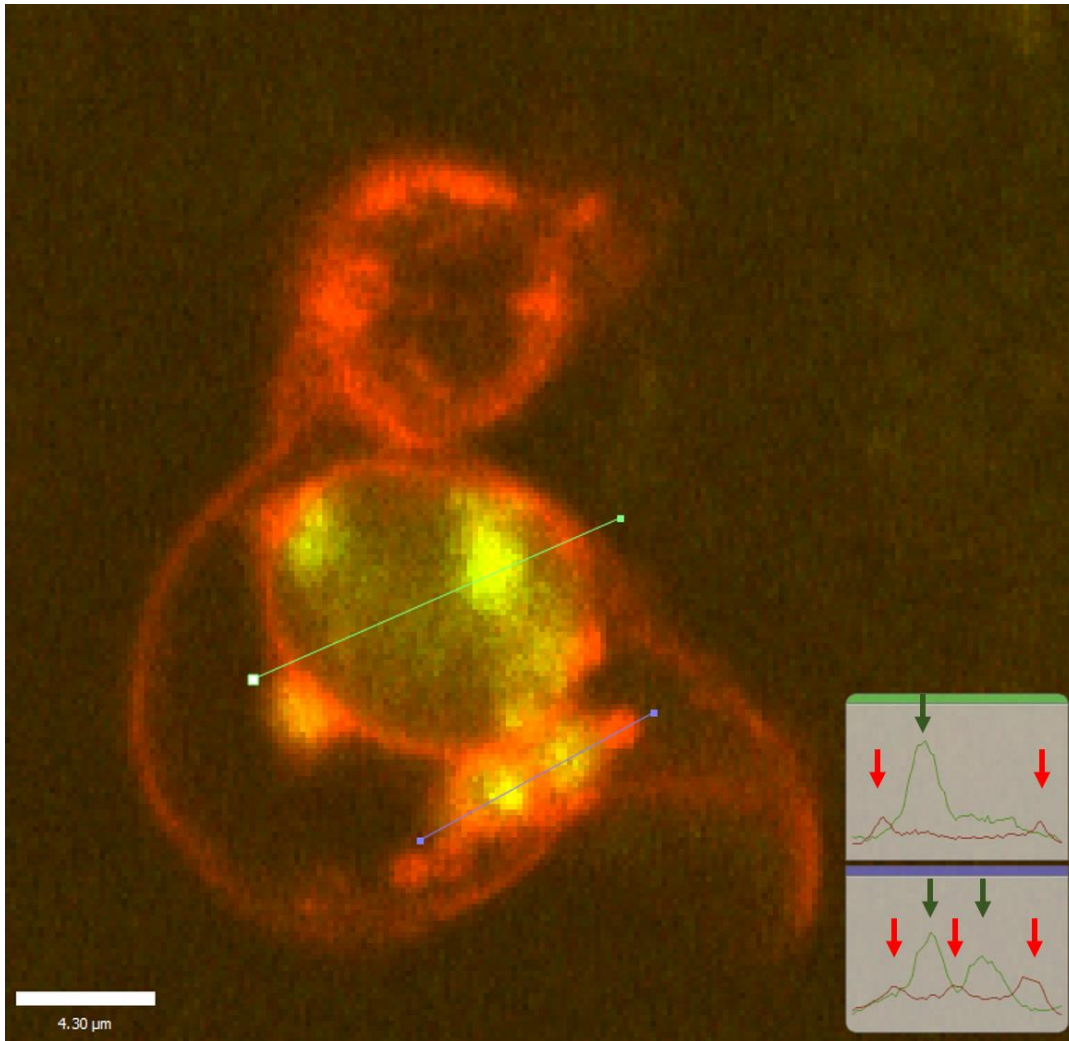


Figure 6.25. Imaging analysis of the transfer of the fluorescently labelled CAAX protein.

Image shows mCherry-positive macrophage containing GFP CAAX protein inside of a not infected *Tg(mpx:GFP.CAAX/mpeg1:mCherry.CAAX)* embryo. Volocity software tool allows drawing a line across the image and analyse fluorescence intensity profile across that line. Green arrows point GFP peaks and red arrows point mCherry peaks. Green peak contained within two red peaks suggests that green fluorescence CAAX is contained within mCherry labelled CAAX structures. GFP-positive CAAX protein seems to be contained within one large vesicle (green line) and two small (purple line). 40x objective.

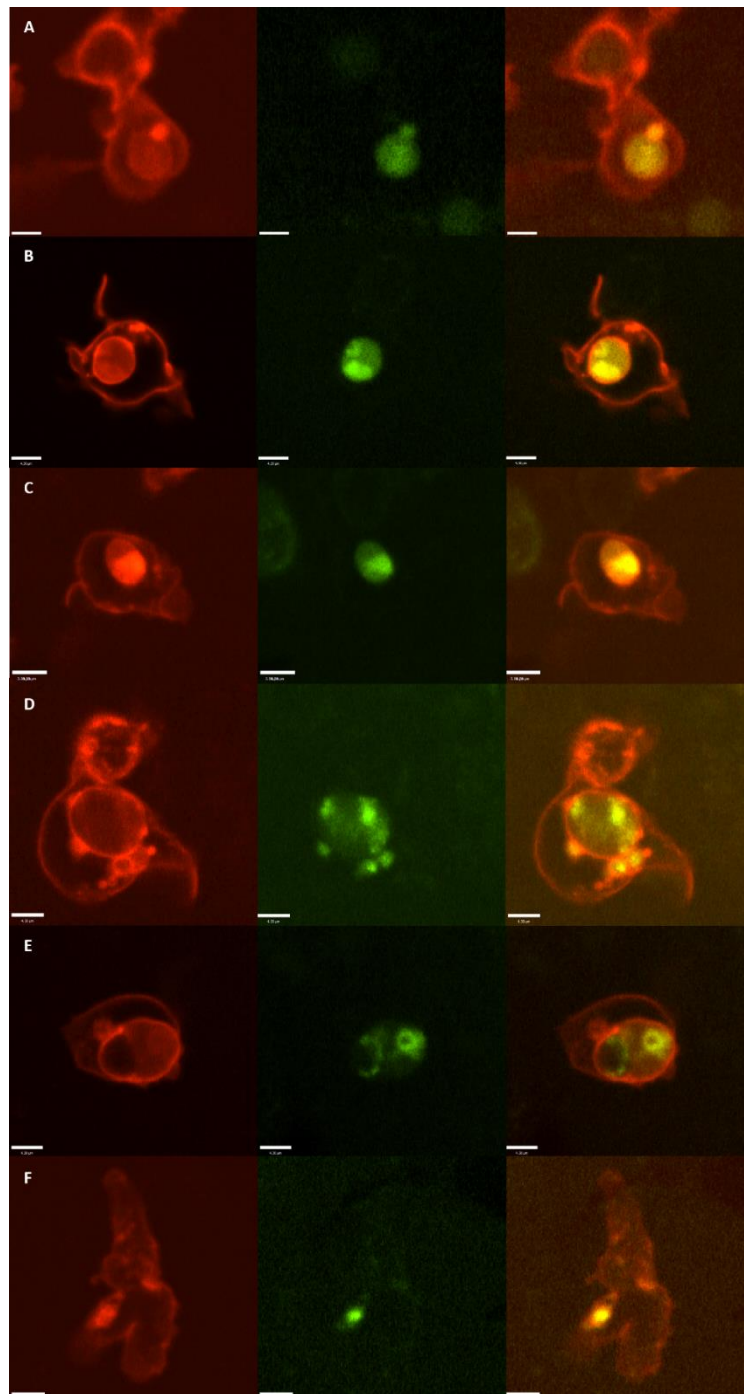


Figure 6.26. Transfer of the fluorescently labelled CAAX protein in uninfected embryos.

Tg(mpx:GFP.CAAX/mpeg1:mCherry.CAAX) uninfected embryos were imaged 30 hpf. Macrophages recognised by expressing mCherry protein contained GFP-labelled CAAX protein, likely transferred from neutrophils (Scale bar 5 μ m). 40x objective.

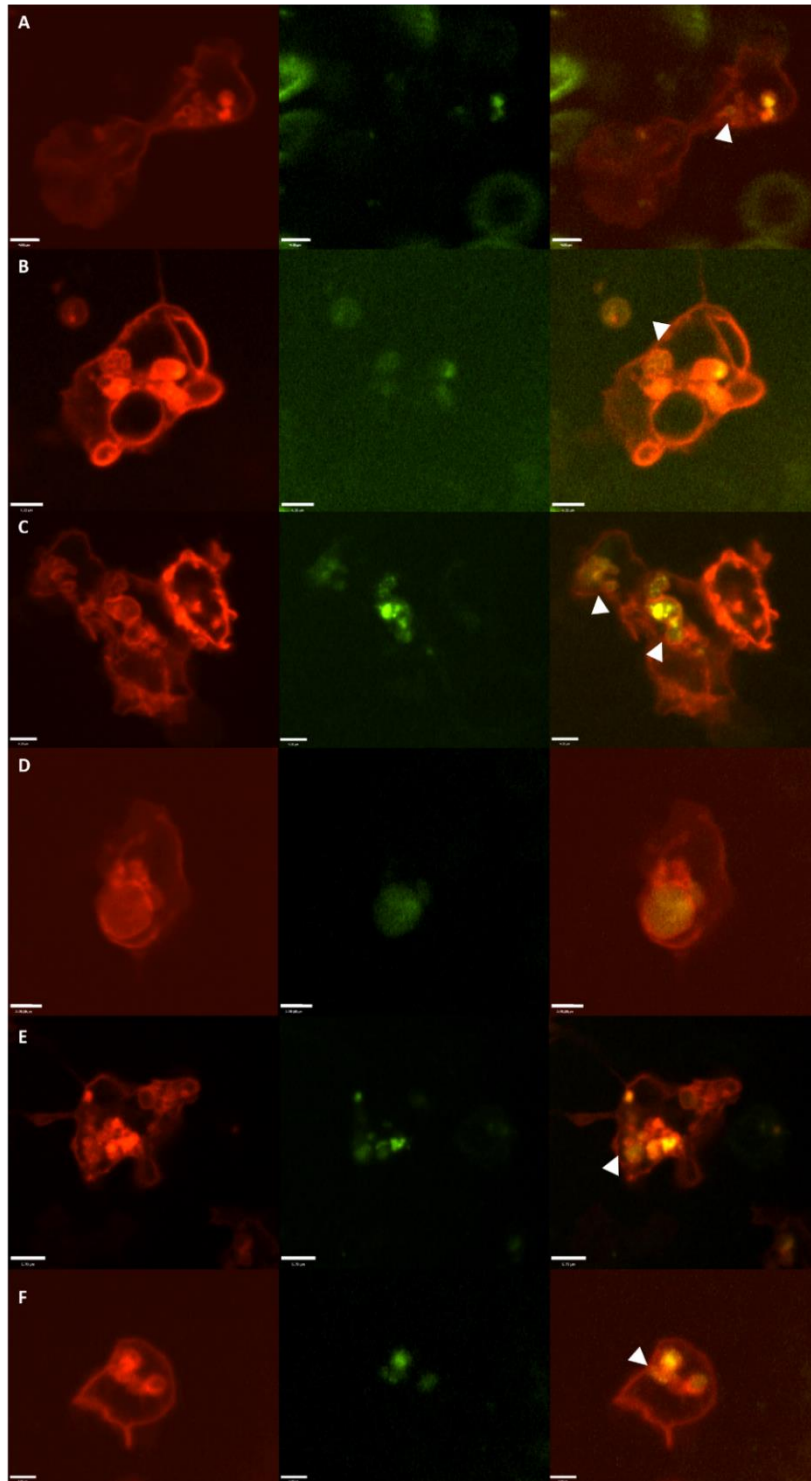


Figure 6.27. Transfer of the fluorescently labelled CAAX protein in infected embryos.

Tg(mpx:GFP.CAAX/mpeg1:mCherry.CAAX) embryos were infected with wild type SH1000 *S. aureus* and imaged 1 hpi. Macrophages were observed containing GFP-labelled CAAX protein often co-localised with vesicles characteristic for *S. aureus* infection (white arrow heads, scale bar 5 μ m). 40x objective.

6.2.2.4. Observed cases of neutrophil to macrophage *S. aureus* transfer

The initial, unintended observation of *S. aureus* transfer underlines one of the advantages of using *in vivo* study models – the potential to observe processes which are not suspected to occur during infection, and which could be missed without an insight into events in a living organism. These observations were followed by a set of additional experiments and led to several findings presented in the previous paragraphs.

Nevertheless, as the transfer of bacterial cells occurred relatively often, it has been visualised during experiments designed to study various aspects of host-pathogen interaction. Therefore, two additional interesting findings will be described in this part of the chapter.

An experiment performed with the use of pHrodoTM/fluorescein stained *S. aureus* resulted in the visualisation of the post-transfer acidification in the recipient macrophage cell (Figure 6.28.). This shows an interesting aspect of two previous findings, firstly transfer occurred from a neutrophil cell to a neighbouring macrophage, and secondly, macrophages seem to be more effective in the acidification of *S. aureus*. Transferred bacteria were not residing in a low pH compartment within the neutrophil, however, they became rapidly acidified in the macrophage.

Additionally, transfer of four cells was also observed during imaging of the neutrophil autophagy reporter, *Tg(LyzC:RFP.GFP.LC3)* (Figure 6.29.). Again, a neutrophil was the donor cell, and a macrophage was the recipient. Moreover, it could be noted that the transferred cells belonged to the population of *S. aureus* not co-localised with the autophagy marker LC3.

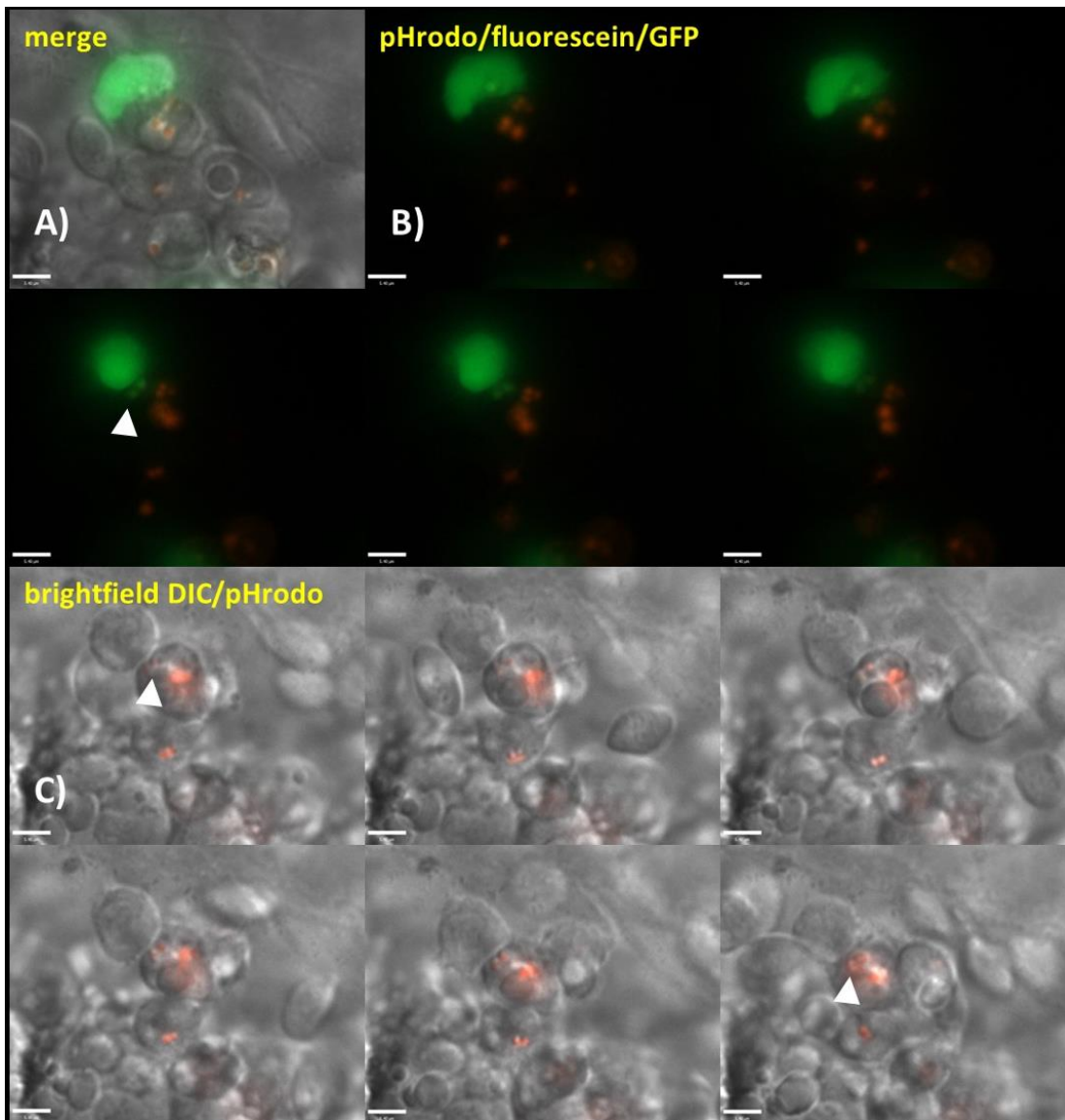


Figure 6.28. Neutrophil to macrophage multiple *S. aureus* cells transfer and subsequent acidification in the recipient cell.

Tg(mpx:GFP) embryos were infected with wild type SH1000 *S. aureus*. The figure consist of three sections of sequential photomicrographs illustrating subsequently occurring events:

- A) Merged plane image of the initial situation
- B) pHrodo/fluorescein stained bacteria secreted from GFP-expressing neutrophil (i114 zebrafish transgenic line)
- C) Increase in pHrodo red fluorescence of received/internalised bacteria over time, suggesting their gradual acidification

Scale bar 10 μ m, Time course 8 min. 60x oil objective.

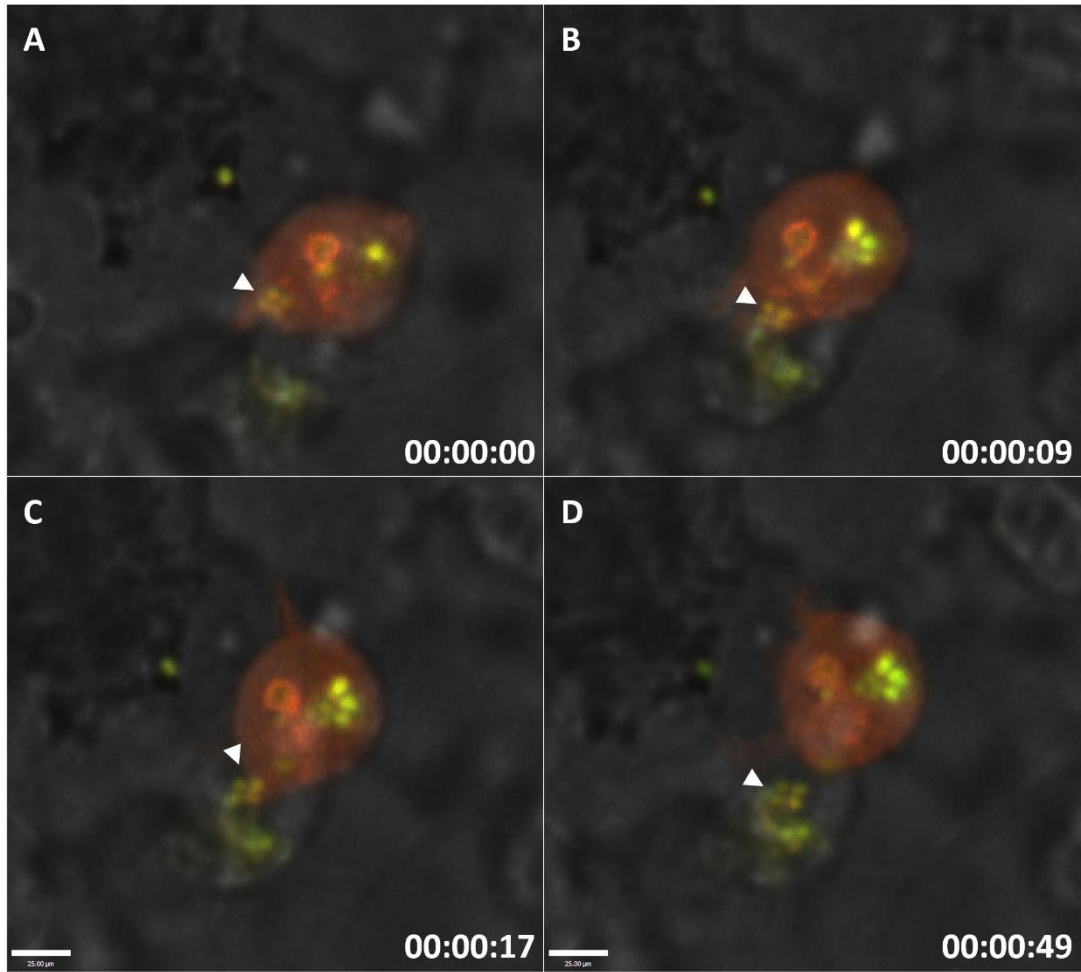


Figure 6.29. Neutrophil to macrophage multiple *S. aureus* cells transfer observed in *Tg(LyzC:RFP.GFP.LC3)* embryo.

Tg(LyzC:RFP.GFP.LC3) embryos were infected with SH1000-GFP *S. aureus* and imaged in bloodstream 1 hpi. Figure shows sequential photomicrographs (A-D) demonstrating neutrophil transferring 4 *S. aureus* cells to the neighbouring macrophage (arrow head). Scale bar 10 μm. 40x objective.

6.3. Discussion

6.3.1. Host cells internalise *S. aureus* using different pathways

Microscopy approaches and imaging data presented in this chapter constitute a spectrum of assets useful in determining *S. aureus* uptake pathways and its intracellular fate in the first hour after internalisation.

Using the DIC technique allowed visualisation of highly activated phenotype of phagocytes containing and internalising *S. aureus*. Using *Tg(mpx:GFP)* embryos allows recognition of GFP-positive phagocytes (neutrophils) and GFP-negative phagocytes (macrophages). Imaging data demonstrated that phagocytes are likely capable of internalising *S. aureus* using various pathways. Internalisation pathways were also studied in *Tg(mpx:Lifeact-Ruby)* embryos in which fluorescently labelled actin could be visualised in both neutrophils and macrophages. Actin remodelling, membrane ruffling, actin co-localisation with cup-like structures and increased activity during *S. aureus* uptake were observed. Reorganisation of actin filaments seemed to also have an impact on phagocyte motility during infection.

Three distinct phenotypes could be distinguished based on the phagocyte motility and internalisation modes observed in *Tg(mpx:Lifeact-Ruby)* embryos. A fraction of cells was relatively immobile, only internalising nearby *S. aureus*. Uptake mechanisms performed by cells of this population seemed to initiate from a localised membrane remodelling, a cup-like structure also observed in GFP-neutrophils during the DIC-based study, suggesting these cells are neutrophils. The second phenotypic group contained phagocytes that moved over bacteria on the endothelial layer of the yolk sac circulation valley and that engulfed them while progressing along the surface. Fluorescence pulsing generated by actin remodelling around *S. aureus* cells indicates that bacteria were indeed engulfed and contained inside of the phagocyte. It was not possible to unequivocally distinguish phagocyte populations in *Tg(mpx:Lifeact-Ruby)* embryos. However, both modes of internalisation have been earlier observed to be performed by GFP-positive cells in the *Tg(mpx:GFP)* reporter line, and cytomorphological features suggest that these phagocytes are zebrafish bloodstream neutrophils. It may be that the presence of two different phenotypes –

a passive one, leading to the uptake of limited number of *S. aureus* cells, and the active, surface-clearing one – results from the presence of two distinct neutrophil populations in the bloodstream of an 30-40 hpf old larvae. The first, could have differentiated from an early progenitor and would demonstrate poor internalisation rate as suggested by Le Guyader *et al.* (2008). As the embryo develops, more efficient neutrophils would be generated during granulopoiesis, and thus constitute the active fraction of observed cells. In more mature embryos, the neutrophil population would be more homogenous, and a greater part of these cells would engage in uptake of surface-bound bacteria (Colucci-Guyon *et al.*, 2011). Nevertheless, confirmation of the existence of two types of neutrophils would require to be confirmed in a reporter line, cell populations labelled in a more unequivocal manner. For instance, *Tg(mpeg1:mCherry.CAAX/mpx:GFP.CAAX)* could be used, however the fluorescence expressed in these embryos is faint, and the high exposure times required during acquisition do not allow imaging of dynamic internalisation processes. The existence of various neutrophil populations potentially indicates different modes of pathogen handling in these cells. Thus, verification of such phenomenon and elucidation of its significance will be important for our understanding of events occurring during *S. aureus* bacteraemia.

The third type of cells distinguished during imaging of *Tg(mpx:Lifeact-Ruby)* embryo phagocytes demonstrated actin remodelling and formation of multiple lamellipodia and possibly filopodia. Highly activated phenotype and significant membrane ruffling, have already been observed in the GFP-negative population in infected *Tg(mpx:GFP)* larvae, likely to be macrophages. Internalisation of bacteria present in the zebrafish body fluids by macrophages can be enhanced due to macropinocytic activity of these cells, as it has already been suggested by Colucci-Guyon *et al.* (2011). Herein, it is demonstrated that such activity also influences macrophage motility, allowing it to internalise *S. aureus* attached to the large area of bloodstream wall. The imaging data showed that this results in productive uptake.

Macrophages were shown to extend long membrane pseudopodia, which could be retracted back to the cell body, possibly facilitating their adhesion to bacteria freely circulating in the bloodstream as suggested in previous studies (Levraud *et al.*, 2009;

Colucci-Guyon *et al.*, 2011). Microbes can preferentially adhere to macrophages due to macrophage-specific expression of a range of receptors, for instance scavenger receptors (Bowdish and Gordon, 2009; Colucci-Guyon *et al.*, 2011), which could constitute another uptake-facilitating factor related to membrane remodelling. However, host cell membrane extensions, for instance filopodia and lamellipodia, were shown to allow uptake of surface-bound *E. coli* cells into macrophages, in a process distinct from macropinocytosis (Möller *et al.*, 2013). Although the described process is probably specific for *E. coli* infection, as it requires mechanical properties of the *E. coli* fimbriae, it also illustrates interesting properties of macrophage membrane rearrangements and their potential in the pathogen-targeted interaction.

Herein, most likely, lamellipodia and filopodia were generated by a macropinocytic process, presenting typical features: enhanced cell motility (Carpentier *et al.*, 1991) and bacteria-orientated ruffling of the cell membrane (Alpuche-Aranda *et al.*, 1994). Upon invagination, macropinocytic vesicles are mainly recognised by their size, which is considerably larger than the size of phagosomes (Hewlett *et al.* 1994; Swanson and Watts, 1995). It has been proposed that *S. aureus* co-localisation with spacious vesicles in neutrophils is a result of macropinocytosis (Gresham *et al.*, 2000), however detailed characterisation of vacuolar location of bacteria constitutes a gap in the *S. aureus* literature. Herein, the size of bacteria-containing vesicles was analysed, together with the number of bacteria contained within these structures to verify its impact on dimension of vesicle. Logically, the size of vesicle increased together with the number of contained *S. aureus* in both neutrophils and macrophages, however macrophages demonstrated wider range and larger vesicle volume. This could be caused by the fact that macrophages internalise greater number of *S. aureus* cells, however the result clearly shows that largest vacuoles do not necessarily contain substantial number of bacteria. It may be, that enlarged vacuoles resulted from a fusion of smaller vesicles, however imaging in CAAX membrane reporter lines demonstrated, that at least a fraction of these spacious vacuoles could result from macropinocytosis.

Herein, observation of zebrafish bloodstream phagocytes allows to speculate that macrophages internalise *S. aureus* by macropinocytosis or another actin-dependent

pathway based on generation of long membrane protrusions. The activated morphology and uptake mode resulted in increased motility and the generation of large intracellular vesicles.

6.3.2. *S. aureus* is transferred from neutrophils to macrophages

Phagocyte to phagocyte transfer observed during imaging acquisition is an example of unintended discovery. The uptake of apoptotic macrophage material has been shown to occur between two macrophages during *M. marinum* infection in the zebrafish model (Davis *et al.*, 2002), however such interaction has not been suggested to occur in *S. aureus* infection. Data presented here, collected in various quantification approaches which followed the initial finding demonstrates, that transfer is most likely unidirectional, from a neutrophil to a macrophage.

Studies performed in transgenic lines in which the membrane marker, CAAX is labelled with different fluorescence proteins in neutrophils and macrophages, show that the transfer of neutrophil portions to macrophages occurs in both uninfected and infected embryos. GFP-CAAX protein can be observed in 40-50 % of macrophages. It may be a result of the phagocytosis of the whole apoptotic neutrophils by macrophages, as shown during inflammation in previous zebrafish studies (Loynes *et al.*, 2010; Ellett *et al.*, 2011). In infected embryos a group of *S. aureus* cells could benefit on such random occasion, and use the opportunity to disseminate between host cells.

However, neutrophil pairing with macrophages is increased in infected embryos, suggesting that whether the interaction aims to help bacteria expansion or not, it occurs more often upon infection. *S. aureus* cell transfer was randomly captured during imaging experiments performed in various zebrafish lines, implying that the phenomenon is quite common in bloodstream phagocyte populations. Indeed, an imaging experiment performed in the first 4 hpi demonstrated, that approximately 1/10 of the cells engages in such process.

Although it is still questionable if the transfer of *S. aureus* is intended and pathogen-driven, and also whether it could be an actin-dependent process, it is definitely worth further investigation. It has been shown previously, that the pathogen-mediated cytoskeleton rearrangements allow active passing of pathogen between host cells (Gouin *et al.*, 1999, Steele-Mortimer *et al.*, 2000). Several pathogens, including *Listeria spp.*, *Shigella* and *Rickettsia* use host cell cytoskeleton to enable their intracellular motility (Shere *et al.*, 1997; Heinzen *et al.*, 1999). Furthermore, research on actin-mediated pathogen strategies was successfully performed using the zebrafish model. Its optical accessibility enabled discovery of *Shigella*-septin caging (Mostowy *et al.*, 2013) and visualisation of cells containing *L. monocytogenes* with an actin “comet tail” (Levraud *et al.*, 2009).

It may be that neutrophils secrete *S. aureus* to macrophages, to allow it effective killing within accepting phagocytes. Transfer recorded with *S. aureus* stained with pH-indicating dyes demonstrated that bacteria obtained from a neutral neutrophil compartment became acidified in macrophage. Additionally, the role of receiving cells could be to increase the inflammatory response, as macrophages are known to neutralise antigens and act as antigen presenting cells (APC) initiating the adaptive immune response (Murray and Wynn, 2011). Alternatively, *S. aureus* is capable of subverting intracellular processes and using host cell cytoskeleton to its own ends.

Altogether, whether *S. aureus* translocates from neutrophils to macrophages in an organised manner, or its transfer is accidental, relatively frequent occurrence and increased neutrophil-macrophage pairing during infection suggest, that this process is significant in presented bacteraemia model.

Chapter 7: Discussion

7.1. Neutrophils and macrophages interact with *S. aureus* in distinct ways during infection

The experiments in my study aimed to determine the processes occurring during *S. aureus* bacteraemia that allow the pathogen to subvert host defence and enable its survival and expansion. Previous work has shown that professional phagocytes, likely neutrophils, are responsible for an immunological bottleneck leading to *S. aureus* clonal expansion (Prajsnar *et al.* 2012). A mathematical model developed by Prajsnar *et al.* (2012), suggested that the host provides a limited number of niches which *S. aureus* uses to its own ends. This result concurred with the reported role of phagocytes in extending *S. aureus* survival (Koziel *et al.* 2009) and dissemination (Thwaites and Gant, 2011). However, it remained unclear how professional phagocytes, a main component of host defence, would provide *S. aureus* with such beneficial shelter and which process(es) performed by immune cells favour bacterial persistence. My study aimed to determine the role of neutrophils and macrophages in *S. aureus* infection and use advanced microscopy and transgenesis tools to elucidate the mechanism underlying *S. aureus* survival and clonal expansion.

In the established model, the first fish to succumb to the infection dies within first 24 hours after intravenous injection of *S. aureus* (Prajsnar *et al.* 2008). Prior to death, large *S. aureus* lesions are formed in embryos, and in 30 % of individuals these originated from only a few *S. aureus* cells (Prajsnar *et al.* 2012). This implies that a process important for *S. aureus* clonal expansion occurs before 24 hpi, and therefore 1 – 24 hpi was a targeted time frame for microscopy observation in my project.

I observed that macrophages and neutrophils clear injected bacteria from the bloodstream within one hour post infection when infected 30 hpf with approximately 2500 CFU. Macrophages seem to be more effective in this clearance role. Imaging using DIC and actin-labelled transgenic lines additionally demonstrated that macrophages are capable of engaging in an internalisation pathway distinct from phagocytosis. Lamellipodia and long filopodia protruded from the macrophage cell

body allowing efficient uptake of fluid-borne and endothelium-bound *S. aureus*. This is also associated with increased macrophage motility. This finding may explain the high macrophage internalisation capacity during the early stages of infection. Neutrophils were observed to internalise *S. aureus* without such cellular rearrangements. Neutrophils were more effective at internalising endothelium-bound than fluid-borne *S. aureus* and remained static in fluid bloodstream environment. This may suggest that neutrophils are more effective in uptake of surface-bound *S. aureus* as it has been shown for *B. subtilis* and *E. coli* (Colucci-Guyon *et al.* 2011). Since the anatomical site of infection has an impact on the phagocyte ability to efficiently internalise invading pathogens, the capacity of macrophages to engulf and degrade *S. aureus* could play an important role in the control of *S. aureus* bacteraemia.

Macrophages are not only more efficient at internalising blood-borne *S. aureus*, I also determined that these professional phagocytes may be capable of more efficient bacterial killing. The decrease in mean number of internal bacteria was more pronounced in macrophages than in neutrophils during 20 hpi. Macrophage phagosomes fuse with lysosomes resulting in acidification of the cargo (Vieira *et al.*, 2002). Zebrafish macrophages are indeed more competent in acidification of internalised *S. aureus* than neutrophils, however *S. aureus* can also reside in low pH compartments in cell of the latter group. This is an important finding given that intracellular acidification has been suggested to be essential for host response to *S. aureus* infections and necessary for MyD88-dependent toll-like receptor responses of immune system (Abdelzaher *et al.*, 2010). Nevertheless, although macrophages acidify *S. aureus* shortly after internalisation (within 5 minutes), it did not result in rapid killing of bacteria and substantial number of *S. aureus* were contained in macrophages 20 hpi.

Acidification of *S. aureus* in phagocytes is important for host defence but likely not beneficial for the pathogen. Therefore, I hypothesised that bacterial survival would be favoured if a niche at neutral pH could be established in the phagocytes. Macropinocytosis would be such a pathway with a potential to play a role in *S. aureus* survival in professional phagocytes. During macropinocytosis cell membrane

protrusions fold back creating large vesicles, containing neutral extracellular fluid. Thus macropinocytic uptake of *S. aureus* could cause establishment of alternative intracellular conditions and potentially allow pathogen survival. Macropinocytic uptake of *S. aureus* has already been proposed by Gresham *et al.* (2000) and it is important to understand the role of this process (Fraunholz and Sinha, 2012). An unsuccessful attempt to generate a macropinosome maturation transgenic reporter impeded my study on intracellular trafficking of macropinosomes and hence, macropinocytosis was investigated based on known physical features of the process: extensive membrane ruffling (Alpuche-Aranda *et al.* 1994) and size of the created vesicle (Hewlett *et al.* 1994; Swanson and Watts, 1995). High power DIC imaging enabled the demonstration that the majority of macrophages continuously extended long membrane extensions, whereas such considerable membrane ruffling was not observed in neutrophils. Moreover, it appeared that membrane ruffles were sometimes bacteria-orientated and resulted in pathogen engulfment. Macrophages seemed to either dynamically protrude lamellipodia and intensively sample the extracellular environment or extend long and stable membrane protrusions, and the latter activity being more common after *S. aureus* was cleared from the bloodstream. Actin remodelling during such uptake was confirmed in an actin reporter line. Additionally, macrophages contained larger intracellular vesicles 1 hpi with *S. aureus*, suggesting that macropinocytosis is a possible internalisation pathway performed by these phagocytes. Nevertheless, as mentioned above, macrophages were also very effective in acidifying internalised *S. aureus*. Macropinosomes fuse with lysosomes at the late stage of maturation, which has been shown to occur within 8-20 minutes after macropinosome formation in HEK293 cell line (Kerr *et al.* 2006). Thus, if *S. aureus* persistence was favoured by a neutral environment provided by macropinosome, it would have to take advantage of it in a relatively short time. Alternatively, a number of macropinosomes containing bacteria could undergo different intracellular trafficking, maintaining supportive conditions for longer. Nevertheless both explanations would require further study, and could be tested in the zebrafish *S. aureus* infection model, for instance with the use of DIC technique and pH-indicating staining protocols established in my study.

Determination of the distinct modes of pathogen handling performed by neutrophils and macrophages was important for our understanding of the role of professional phagocytes in *S. aureus* bacteraemia. Using the *in vivo* model allowed visualisation of *S. aureus* uptake resulting from membrane ruffling, which has not been previously observed. While, filopodia and lamellipodia-mediated uptake can be characteristic for a process distinct from macropinocytosis as has been shown for *E. coli* (Möller *et al.* 2013), imaging data presented herein strongly suggests macropinocytosis maybe a possible uptake mechanism for blood-borne *S. aureus*. Macrophages in bacteraemic hosts become activated as has been shown with *B. subtilis* and *E. coli* even though they do not directly contact bacteria, and such increased activity can influence internalisation pathways (Herbomel *et al.* 1999). Altogether, my observations can provide a framework to explain the intracellular fate of *S. aureus* and linking this to different outcomes *for S. aureus* persistence in host cells.

7.2. *S. aureus* is capable of intracellular replication in zebrafish professional phagocytes

Studies performed to assess population dynamics during *S. aureus* infection shown that bacteria injected into zebrafish in a 1:1 mixed inoculum of two isogenic strains will undergo an immunological bottleneck with either one of the strains significantly overrepresented in the population causing death of the embryo (Prajnsnar *et al.* 2012). Professional phagocytes appear to be responsible for the phenomenon, and it is likely that clonal expansion is initiated intracellularly within 20 hpi.

My study suggests that at 6 hpi 50 % of professional phagocytes will contain one prevalent strain, when injected with 1:1 mixed inoculum of isogenic strains expressing different fluorescence markers (which was not observed at 1 hpi). This suggests that clonal expansion starts early during infection, and the process underlying this phenomenon occurs shortly after *S. aureus* internalisation. Experiments performed in my study do not provide the answer to the question as whether the process is limited to macrophages or neutrophils. However, the zebrafish constitutes a useful model for this study. Future experimental work would

have to aim to establish phagocyte-specific reporters, carrying fluorescence marker distinguishable from fluorescent markers of *S. aureus* strains. *In vivo* microscopy of the early stages of infection would potentially inform the phagocyte role in *S. aureus* population dynamics of various strains.

The result discussed above suggest that *S. aureus* laboratory strains used in this study can potentially grow inside professional phagocytes. Replication of *S. aureus* in host cells typically occurs after it subverts an intracellular process and is released into the cytoplasm (Schnaith et al, 2007, Grosz *et al.* 2013). *S. aureus* is capable of escaping intracellular killing by subverting various mechanisms (reviewed by Fraunholz and Sinha, 2012), and autophagy is one of those mechanisms (Schnaith *et al.* 2007). Autophagy is able to restrict bacterial persistence in host cells, employing several different methods for pathogen recognition and killing. Nevertheless, in parallel, some bacteria have developed strategies in response to those mechanisms and became are to evade autophagic recognition (Mostowy et al 2011; Abdulrahman et al 2011; Choy *et al.*, 2012). Here several imaging and analysis tools were created using new transgenic zebrafish lines to assess whether autophagy could contribute to the prolonged persistence of *S. aureus* in immune system cells. Using a fluorescent LC3 reporter I was able to observe that *S. aureus* co-localises with various LC3 structures in zebrafish neutrophils. Potentially, this could mean that autophagy is involved in various aspects of *S. aureus*-phagocyte interaction. "Tight LC3 vesicles" observed during my study correspond with that of Schnaith *et al.* (2007) showing LC3 recruited to phagosomes containing *S. aureus*. The published study was performed in non professional phagocytes, showing unique interaction of *S. aureus* with autophagy components. Bacteria present in autophagosomes were not killed and were able to replicate. *S. aureus* was further released to the cytoplasm, to eventually cause host cell death and disseminate extracellularly. Replication of *S. aureus* was increased upon treatment with rapamycin, a known autophagy enhancer (Schnaith *et al.*, 2007). I observed that *S. aureus* co-localisation with tight vesicles was significantly decreased between 1 hpi and 20 hpi in neutrophils, while the proportion of cytoplasm-associated pathogen significantly expanded. Additionally, although treatment with autophagy enhancers increased the formation of LC3 structures in

neutrophils, it also caused an increase in *S. aureus* not co-localised with LC3 aggregates in infected embryos. Thus, increased autophagic efficiency did not result in a specific antibacterial activity of LC3. This implies that increased autophagy might be able to favour bacterial intracellular existence. Potentially, this could mean that *S. aureus* subverts autophagy in neutrophils, in a manner similar to that observed in non professional phagocytes. Likely, when bacteria disseminate in the bloodstream after killing non professional phagocytes at the local site of infection (Petti, C. A., and Fowler, V. G., Jr. 2003) they would further apply similar escape mechanisms upon internalisation in neutrophils.

LC3 recruitment to phagosomes in professional phagocytes has been shown in murine macrophages using zymosan (Huang *et al.* 2009). This process required the generation of ROS in the phagosome lumen triggered upon TLR signalling (Huang *et al.* 2009). Interestingly the structures formed as a result of such association did not resemble “tight LC3 vesicles” like those published in non professional phagocytes. Instead, large vacuoles visualised on imaging data presented by Huang *et al.* (2009) corresponded to “spacious LC3 vesicles” observed in my study. This could imply LC3 recruitment to vesicles formed during a pathway distinct from phagocytosis, for instance macropinocytosis, although I did not observe the presence of spacious LC3 vesicles in macrophages. However, it is not known to which type of vesicles LC3 is recruited to in zebrafish neutrophils. Structures described as tight LC3 vesicles could result from LC3 association with phagosomes, and spacious LC3 vesicles could be generated by fusion of several smaller vesicles. Nevertheless, my work suggests that the process of LC3 recruitment can be triggered by the generation of ROS, potentially mediated by TLR signalling and thus important for *S. aureus* infection.

Currently we do not know why LC3 is recruited to vesicles containing *S. aureus* in neutrophils of bloodstream infected zebrafish. It may be that the pathogen subverts autophagy to allow proliferation, as it has been shown in non professional phagocytes. Alternatively, LC3 recruitment to the phagosome could promote lysosomal fusion and degradation of the microbial cargo. The zebrafish LC3 reporter line constitutes a useful tool for further investigation of the phenomenon.

7.3. Final remarks and future work

The zebrafish infection model allows *in vivo* studies of host-pathogen interaction due to its optical accessibility. Therefore it constitutes a unique model demonstrating the role of the immune system and systemic response to *S. aureus* infection, coupled with a wide range of applicable tools. Importantly, thanks to real time observation of the events occurring in the living organism it enables visualisation and study of previously unknown processes. In my study I observed a process with potential importance to the outcome of *S. aureus* infection, neutrophil to macrophage transfer of *S. aureus*. Neutrophil and macrophage direct interaction is related to the infection, which I demonstrated by quantification of phagocyte pairing. My results also suggest that the process is unidirectional, and relatively common. It is unclear whether the transfer could favour host defence or bacterial survival. Given that macrophages are more efficient in acidifying *S. aureus*, this could increase the response of immune system, as suggested above (Abdelzaher *et al.*, 2010), and in fact *S. aureus* cells were observed to become acidified upon transfer from neutral compartments in the neutrophil.

Thus the use of the zebrafish model provides new avenues for investigation of the molecular and cellular basis of host-pathogen interaction. Findings from the model can then be used to inform studies in mammalian models (McVicker *et al.* 2014). These in turn will in long term increase our capacity to develop new control regimes for such an important and tenacious pathogen.

References

- ABDELNOUR, A., ARVIDSON, S., BREMELL, T., RYDÉN, C. & TARKOWSKI, A. 1993. The accessory gene regulator (*agr*) controls *Staphylococcus aureus* virulence in a murine arthritis model. *Infection and immunity*, 61, 3879-3885.
- ABDELZAHER, A. M., WRIGHT, M. E., ORTEGA, C., SOLO-GABRIELE, H. M., MILLER, G., ELMIR, S., NEWMAN, X., SHIH, P., BONILLA, J. A., BONILLA, T. D., PALMER, C. J., SCOTT, T., LUKASIK, J., HARWOOD, V. J., MCQUAIG, S., SINIGALLIANO, C., GIDLEY, M., PLANO, L. R., ZHU, X., WANG, J. D. & FLEMING, L. E. 2010. Presence of pathogens and indicator microbes at a non-point source subtropical recreational marine beach. *Appl Environ Microbiol*, 76, 724-32.
- ABTIN, A., JAIN, R., MITCHELL, A. J., ROEDIGER, B., BRZOSKA, A. J., TIKOO, S., CHENG, Q., NG, L. G., CAVANAGH, L. L., VON ANDRIAN, U. H., HICKEY, M. J., FIRTH, N. & WENINGER, W. 2014. Perivascular macrophages mediate neutrophil recruitment during bacterial skin infection. *Nat Immunol*, 15, 45-53.
- AKIRA, S., UEMATSU, S. & TAKEUCHI, O. 2006. Pathogen recognition and innate immunity. *Cell*, 124, 783-801.
- ALLEN, L.-A. H., BEECHER, B. R., LYNCH, J. T., ROHNER, O. V. & WITTINE, L. M. 2005. *Helicobacter pylori* disrupts NADPH oxidase targeting in human neutrophils to induce extracellular superoxide release. *Journal of immunology (Baltimore, Md.: 1950)*, 174, 3658-3667.
- AMMENDOLIA, M. G., BERTUCCINI, L., MINELLI, F., MESCHINI, S. & BALDASSARRI, L. 2004. A *Sphingomonas* bacterium interacting with epithelial cells. *Res Microbiol*, 155, 636-46.
- ARCHER, G. L. 1998. *Staphylococcus aureus*: a well-armed pathogen. *Clinical infectious diseases: an official publication of the Infectious Diseases Society of America*, 26, 1179-1181.
- BABIOR, B. M. 2004. NADPH oxidase. *Current opinion in immunology*, 16, 42-47.
- BALWIT, J. M., VAN LANGEVELDE, P., VANN, J. M. & PROCTOR, R. A. 1994. Gentamicin-resistant menadione and hemin auxotrophic *Staphylococcus aureus* persist within cultured endothelial cells. *J Infect Dis*, 170, 1033-7.
- BANTEL, H., SINHA, B., DOMSCHKE, W., PETERS, G., SCHULZE-OSTHOFF, K. & JÄNICKE, R. U. 2001. alpha-Toxin is a mediator of *Staphylococcus aureus*-induced cell death and activates caspases via the intrinsic death pathway independently of death receptor signaling. *J Cell Biol*, 155, 637-48.
- BARTON, G. M. & MEDZHITOV, R. 2002. Toll-like receptors and their ligands. *Curr Top Microbiol Immunol*, 270, 81-92.
- BARTON, G. M. 2008. A calculated response: control of inflammation by the innate immune system. *The Journal of clinical investigation*, 118, 413-420.
- BENARD, E. L., RACZ, P. I., ROUGEOT, J., NEZHINSKY, A. E., VERBEEK, F. J., SPAINK, H. P. & MEIJER, A. H. 2015. Macrophage-expressed perforins mpeg1 and mpeg1.2 have an anti-bacterial function in zebrafish. *J Innate Immun*, 7, 136-52.
- BERMUDEZ, L. E., PETROFSKY, M. & SANGARI, F. 2004. Intracellular phenotype of *Mycobacterium avium* enters macrophages primarily by a macropinocytosis-like mechanism and survives in a compartment that differs from that with extracellular phenotype. *Cell biology international*, 28, 411-419.
- BERNARD, P. & COUTURIER, M. 1992. Cell killing by the F plasmid CcdB protein involves poisoning of DNA-topoisomerase II complexes. *J Mol Biol*, 226, 735-45.

- BERÓN, W., GUTIERREZ, M. G., RABINOVITCH, M. & COLOMBO, M. I. 2002. Coxiella burnetii localizes in a Rab7-labeled compartment with autophagic characteristics. *Infect Immun*, 70, 5816-21.
- BHAKDI, S. & TRANUM-JENSEN, J. 1991. Alpha-toxin of Staphylococcus aureus. *Microbiological reviews*, 55, 733-751.
- BJØRKØY, G., LAMARK, T., BRECH, A., OUTZEN, H., PERANDER, M., OVERVATN, A., STENMARK, H. & JOHANSEN, T. 2005. p62/SQSTM1 forms protein aggregates degraded by autophagy and has a protective effect on huntingtin-induced cell death. *J Cell Biol*, 171, 603-14.
- BOSHRA, H., LI, J. & SUNYER, J. O. 2006. Recent advances on the complement system of teleost fish. *Fish & shellfish immunology*, 20, 239-262.
- BUBECK WARDENBURG, J., PALAZZOLO-BALLANCE, A. M., OTTO, M., SCHNEEWIND, O. & DELEO, F. R. 2008. Panton-Valentine leukocidin is not a virulence determinant in murine models of community-associated methicillin-resistant Staphylococcus aureus disease. *J Infect Dis*, 198, 1166-70.
- CARLTON, J., BUJNY, M., PETER, B. J., OORSCHOT, V. M., RUTHERFORD, A., MELLOR, H., KLUMPERMAN, J., MCMAHON, H. T. & CULLEN, P. J. 2004. Sorting nexin-1 mediates tubular endosome-to-TGN transport through coincidence sensing of high-curvature membranes and 3-phosphoinositides. *Curr Biol*, 14, 1791-800.
- CARPENTIER, J. L., LEW, D. P., PACCAUD, J. P., GIL, R., IACOPETTA, B., KAZATCHKINE, M., STENDAHL, O. & POZZAN, T. 1991. Internalization pathway of C3b receptors in human neutrophils and its transmodulation by chemoattractant receptors stimulation. *Cell regulation*, 2, 41-55.
- CARRYN, S., CHANTEUX, H., SERAL, C., MINGEOT-LECLERCQ, M.-P., VAN BAMBEKE, F. & TULKENS, P. M. 2003. Intracellular pharmacodynamics of antibiotics. *Infectious disease clinics of North America*, 17, 615-634.
- CHAN, P. F., FOSTER, S. J., INGHAM, E. & CLEMENTS, M. O. 1998. The Staphylococcus aureus alternative sigma factor sigmaB controls the environmental stress response but not starvation survival or pathogenicity in a mouse abscess model. *Journal of bacteriology*, 180, 6082-6089.
- CHANG, F.-Y., MACDONALD, B. B., PEACOCK, J. E., JR., MUSER, D. M., TRIPLETT, P., MYLOTTE, J. M., O'DONNELL, A., WAGENER, M. M. & YU, V. L. 2003. A prospective multicenter study of Staphylococcus aureus bacteremia: incidence of endocarditis, risk factors for mortality, and clinical impact of methicillin resistance. *Medicine*, 82, 322-332.
- CHESNEY, P. J. 1989. Clinical aspects and spectrum of illness of toxic shock syndrome: overview. *Reviews of infectious diseases*, 11 Suppl 1, S1-7.
- CHEUNG, A. L., EBERHARDT, K. J., CHUNG, E., YEAMAN, M. R., SULLAM, P. M., RAMOS, M. & BAYER, A. S. 1994. Diminished virulence of a sar-/agr- mutant of Staphylococcus aureus in the rabbit model of endocarditis. *The Journal of clinical investigation*, 94, 1815-1822.
- CHU, V. H., CROSSLIN, D. R., FRIEDMAN, J. Y., REED, S. D., CABELL, C. H., GRIFFITHS, R. I., MASSELINK, L. E., KAYE, K. S., COREY, G. R., RELLER, L. B., STRYJEWSKI, M. E., SCHULMAN, K. A. & FOWLER, V. G., JR. 2005. Staphylococcus aureus bacteremia in patients with prosthetic devices: costs and outcomes. *The American journal of medicine*, 118.
- CLAUS, V., JAHRAUS, A., TJELLE, T., BERG, T., KIRSCHKE, H., FAULSTICH, H. & GRIFFITHS, G. 1998. Lysosomal enzyme trafficking between phagosomes, endosomes, and lysosomes in J774 macrophages. Enrichment of cathepsin H in early endosomes. *The Journal of biological chemistry*, 273, 9842-9851.

- COLLINS, C. A., DE MAZIÈRE, A., VAN DIJK, S., CARLSSON, F., KLUMPERMAN, J. & BROWN, E. J. 2009. Atg5-independent sequestration of ubiquitinated mycobacteria. *PLoS Pathog*, 5, e1000430.
- CONGDON, E. E., WU, J. W., MYEKU, N., FIGUEROA, Y. H., HERMAN, M., MARINEC, P. S., GESTWICKI, J. E., DICKEY, C. A., YU, W. H. & DUFF, K. E. 2012. Methylthioninium chloride (methylene blue) induces autophagy and attenuates tauopathy *in vitro* and *in vivo*. *Autophagy*, 8, 609-22.
- COSGROVE, S. E. & FOWLER, V. G., JR. 2008. Management of methicillin-resistant *Staphylococcus aureus* bacteremia. *Clinical infectious diseases: an official publication of the Infectious Diseases Society of America*, 46 Suppl 5, S386-393.
- CULLEN, P. J. 2008. Endosomal sorting and signalling: an emerging role for sorting nexins. *Nat Rev Mol Cell Biol*, 9, 574-82.
- DAVIS, J. M., CLAY, H., LEWIS, J. L., GHORI, N., HERBOMEL, P. & RAMAKRISHNAN, L. 2002. Real-time visualization of mycobacterium-macrophage interactions leading to initiation of granuloma formation in zebrafish embryos. *Immunity*, 17, 693-702.
- DEFRES, S., MARWICK, C. & NATHWANI, D. 2009. MRSA as a cause of lung infection including airway infection, community-acquired pneumonia and hospital-acquired pneumonia. *The European respiratory journal: official journal of the European Society for Clinical Respiratory Physiology*, 34, 1470-1476.
- DELEO, F. R., DIEP, B. A. & OTTO, M. 2009. Host defense and pathogenesis in *Staphylococcus aureus* infections. *Infectious disease clinics of North America*, 23, 17-34.
- DERETIC, V. & LEVINE, B. 2009. Autophagy, immunity, and microbial adaptations. *Cell Host Microbe*, 5, 527-49.
- DHARMAWARDHANE, S., SCHÜRMAN, A., SELLS, M. A., CHERNOFF, J., SCHMID, S. L. & BOKOCH, G. M. 2000. Regulation of macropinocytosis by p21-activated kinase-1. *Mol Biol Cell*, 11, 3341-52.
- DOHERTY, G. J. & MCMAHON, H. T. 2009. Mechanisms of endocytosis. *Annual review of biochemistry*, 78, 857-902.
- DORN, B. R., DUNN, W. A. & PROGULSKE-FOX, A. 2001. *Porphyromonas gingivalis* traffics to autophagosomes in human coronary artery endothelial cells. *Infect Immun*, 69, 5698-708.
- EKMAN, A.-K. & CARDELL, L. O. 2010. The expression and function of Nod-like receptors in neutrophils. *Immunology*, 130, 55-63.
- ELLETT, F., PASE, L., HAYMAN, J. W., ANDRIANOPOULOS, A. & LIESCHKE, G. J. 2011. mpeg1 promoter transgenes direct macrophage-lineage expression in zebrafish. *Blood*, 117, e49-56.
- EWBANK, J. J. 2002. Tackling both sides of the host-pathogen equation with *Caenorhabditis elegans*. *Microbes and infection / Institut Pasteur*, 4, 247-256.
- FARRERA, C. & FADEEL, B. 2013. Macrophage clearance of neutrophil extracellular traps is a silent process. *J Immunol*, 191, 2647-56.
- FAURSCHOU, M. & BORREGAARD, N. 2003. Neutrophil granules and secretory vesicles in inflammation. *Microbes and infection / Institut Pasteur*, 5, 1317-1327.
- FERNANDEZ-PRADA, C., TALL, B. D., ELLIOTT, S. E., HOOVER, D. L., NATARO, J. P. & VENKATESAN, M. M. 1998. Hemolysin-positive enteroaggregative and cell-detaching *Escherichia coli* strains cause oncosis of human monocyte-derived macrophages and apoptosis of murine J774 cells. *Infect Immun*, 66, 3918-24.
- FIELDS, K. A., MCCORMACK, R., DE ARMAS, L. R. & PODACK, E. R. 2013. Perforin-2 restricts growth of *Chlamydia trachomatis* in macrophages. *Infect Immun*, 81, 3045-54.
- FINE, M. J., SMITH, M. A., CARSON, C. A., MUTHA, S. S., SANKEY, S. S., WEISSFELD, L. A. & KAPOOR, W. N. 1996. Prognosis and outcomes of patients with community-acquired pneumonia. A meta-analysis. *JAMA*, 275, 134-41.

- FOSTER, T. J. 2005. Immune evasion by staphylococci. *Nature reviews. Microbiology*, 3, 948-958.
- FOSTER, T. J. & HÖÖK, M. 1998. Surface protein adhesins of *Staphylococcus aureus*. *Trends in microbiology*, 6, 484-488.
- FOWLER, V. G., JR., OLSEN, M. K., COREY, G. R., WOODS, C. W., CABELL, C. H., RELLER, L. B., CHENG, A. C., DUDLEY, T. & ODDONE, E. Z. 2003. Clinical identifiers of complicated *Staphylococcus aureus* bacteremia. *Archives of internal medicine*, 163, 2066-2072.
- GARCÍA-PÉREZ, B. E., MONDRAGÓN-FLORES, R. & LUNA-HERRERA, J. 2003. Internalization of *Mycobacterium tuberculosis* by macropinocytosis in non-phagocytic cells. *Microbial pathogenesis*, 35, 49-55.
- GARZONI, C. & KELLEY, W. L. 2009. *Staphylococcus aureus*: new evidence for intracellular persistence. *Trends Microbiol*, 17, 59-65.
- GIESE, B., DITTMANN, S., PAPROTKA, K., LEVIN, K., WELTROWSKI, A., BIEHLER, D., LÂM, T. T., SINHA, B. & FRAUNHOLZ, M. J. 2009. Staphylococcal alpha-toxin is not sufficient to mediate escape from phagolysosomes in upper-airway epithelial cells. *Infect Immun*, 77, 3611-25.
- GIESE, B., GLOWINSKI, F., PAPROTKA, K., DITTMANN, S., STEINER, T., SINHA, B. & FRAUNHOLZ, M. J. 2011. Expression of δ -toxin by *Staphylococcus aureus* mediates escape from phago-endosomes of human epithelial and endothelial cells in the presence of β -toxin. *Cell Microbiol*, 13, 316-29.
- GLADSTONE, G. P. & VAN HEYNINGEN, W. E. 1957. Staphylococcal leucocidins. *British journal of experimental pathology*, 38, 123-137.
- GORDON, R. J. & LOWY, F. D. 2008. Pathogenesis of Methicillin-Resistant *Staphylococcus aureus* Infection. *Clinical infectious diseases : an official publication of the Infectious Diseases Society of America*, 46, S350-S359.
- GOUIN, E., DEHOUX, P., MENGAUD, J., KOCKS, C. & COSSART, P. 1995. *iactA* of *Listeria ivanovii*, although distantly related to *Listeria monocytogenes actA*, restores actin tail formation in an *L. monocytogenes actA* mutant. *Infect Immun*, 63, 2729-37.
- GOUIN, E., GANTELET, H., EGILE, C., LASA, I., OHAYON, H., VILLIERS, V., GOUNON, P., SANSONETTI, P. J. & COSSART, P. 1999. A comparative study of the actin-based motilities of the pathogenic bacteria *Listeria monocytogenes*, *Shigella flexneri* and *Rickettsia conorii*. *J Cell Sci*, 112 (Pt 11), 1697-708.
- GRESHAM, H. D., LOWRANCE, J. H., CAVER, T. E., WILSON, B. S., CHEUNG, A. L. & LINDBERG, F. P. 2000. Survival of *Staphylococcus aureus* inside neutrophils contributes to infection. *Journal of immunology (Baltimore, Md.: 1950)*, 164, 3713-3722.
- HAAS, A. 2007. The phagosome: compartment with a license to kill. *Traffic (Copenhagen, Denmark)*, 8, 311-330.
- HAIGLER, B. E., JOHNSON, G. R., SUEN, W. C. & SPAIN, J. C. 1999. Biochemical and genetic evidence for meta-ring cleavage of 2,4, 5-trihydroxytoluene in *Burkholderia* sp. strain DNT. *J Bacteriol*, 181, 965-72.
- HAN, J. & BURGESS, K. 2010. Fluorescent indicators for intracellular pH. *Chemical reviews*, 110, 2709-2728.
- HARAGA, A., WEST, T. E., BRITTNACHER, M. J., SKERRETT, S. J. & MILLER, S. I. 2008. *Burkholderia thailandensis* as a model system for the study of the virulence-associated type III secretion system of *Burkholderia pseudomallei*. *Infect Immun*, 76, 5402-11.
- HASLETT, C., SAVILL, J. S., WHYTE, M. K., STERN, M., DRANSFIELD, I. & MEAGHER, L. C. 1994. Granulocyte apoptosis and the control of inflammation. *Philos Trans R Soc Lond B Biol Sci*, 345, 327-33.
- HAYASHI, F., MEANS, T. K. & LUSTER, A. D. 2003. Toll-like receptors stimulate human neutrophil function. *Blood*, 102, 2660-2669.

- HE, C. & KLIONSKY, D. J. 2009. Regulation mechanisms and signaling pathways of autophagy. *Annual review of genetics*, 43, 67-93.
- HE, C. & KLIONSKY, D. J. 2010. Analyzing autophagy in zebrafish. *Autophagy*, 6, 642-4.
- HEINZEN, R. A., GRIESHABER, S. S., VAN KIRK, L. S. & DEVIN, C. J. 1999. Dynamics of actin-based movement by *Rickettsia rickettsii* in vero cells. *Infect Immun*, 67, 4201-7.
- HERBOMEL, P., THISSE, B. & THISSE, C. 1999. Ontogeny and behaviour of early macrophages in the zebrafish embryo. *Development*, 126, 3735-45.
- HERBOMEL, P., THISSE, B. & THISSE, C. 2001. Zebrafish early macrophages colonize cephalic mesenchyme and developing brain, retina, and epidermis through a M-CSF receptor-dependent invasive process. *Dev Biol*, 238, 274-88.
- HEWLETT, L. J., PRESCOTT, A. R. & WATTS, C. 1994. The coated pit and macropinocytic pathways serve distinct endosome populations. *J Cell Biol*, 124, 689-703.
- HOFFMANN, J. A. 2003. The immune response of *Drosophila*. *Nature*, 426, 33-38.
- IP, W. K. E., SOKOLOVSKA, A., CHARRIERE, G. M., BOYER, L., DEJARDIN, S., CAPPILLINO, M. P., YANTOSCA, L. M., TAKAHASHI, K., MOORE, K. J., LACY-HULBERT, A. & STUART, L. M. 2010. Phagocytosis and phagosome acidification are required for pathogen processing and MyD88-dependent responses to *Staphylococcus aureus*. *Journal of immunology (Baltimore, Md.: 1950)*, 184, 7071-7081.
- JARRY, T. M. & CHEUNG, A. L. 2006. *Staphylococcus aureus* escapes more efficiently from the phagosome of a cystic fibrosis bronchial epithelial cell line than from its normal counterpart. *Infection and immunity*, 74, 2568-2577.
- JEONG, E. & LEE, J. Y. 2011. Intrinsic and extrinsic regulation of innate immune receptors. *Yonsei Med J*, 52, 379-92.
- JOHNSON, C. M. 1993. *Staphylococcus aureus* binding to cardiac endothelial cells is partly mediated by a 130 kilodalton glycoprotein. *The Journal of laboratory and clinical medicine*, 121, 675-682.
- JOSHI, S. K., SURESH, P. R. & CHAUHAN, V. S. 2001. Flexibility in MHC and TCR recognition: degenerate specificity at the T cell level in the recognition of promiscuous Th epitopes exhibiting no primary sequence homology. *J Immunol*, 166, 6693-703.
- KASAHARA, M., SUZUKI, T. & PASQUIER, L. D. 2004. On the origins of the adaptive immune system: novel insights from invertebrates and cold-blooded vertebrates. *Trends in immunology*, 25, 105-111.
- KENNEDY, A. D. & DELEO, F. R. 2009. Neutrophil apoptosis and the resolution of infection. *Immunologic research*, 43, 25-61.
- KERR, M. C., LINDSAY, M. R., LUETTERFORST, R., HAMILTON, N., SIMPSON, F., PARTON, R. G., GLEESON, P. A. & TEASDALE, R. D. 2006. Visualisation of macropinosome maturation by the recruitment of sorting nexins. *J Cell Sci*, 119, 3967-80.
- KHERSONSKY, S. M., JUNG, D.-W., KANG, T.-W., WALSH, D. P., MOON, H.-S., JO, H., JACOBSON, E. M., SHETTY, V., NEUBERT, T. A. & CHANG, Y.-T. 2003. Facilitated forward chemical genetics using a tagged triazine library and zebrafish embryo screening. *Journal of the American Chemical Society*, 125, 11804-11805.
- KIMURA, S., NODA, T. & YOSHIMORI, T. 2007. Dissection of the autophagosome maturation process by a novel reporter protein, tandem fluorescent-tagged LC3. *Autophagy*, 3, 452-60.
- KIRISAKO, T., ICHIMURA, Y., OKADA, H., KABEYA, Y., MIZUSHIMA, N., YOSHIMORI, T., OHSUMI, M., TAKAO, T., NODA, T. & OHSUMI, Y. 2000. The reversible modification regulates the membrane-binding state of Apg8/Aut7 essential for autophagy and the cytoplasm to vacuole targeting pathway. *J Cell Biol*, 151, 263-76.
- KIRKIN, V., LAMARK, T., JOHANSEN, T. & DIKIC, I. 2009. NBR1 cooperates with p62 in selective autophagy of ubiquitinated targets. *Autophagy*, 5, 732-3.

- KLEMSZ, M. J., MCKERCHER, S. R., CELADA, A., VAN BEVEREN, C. & MAKI, R. A. 1990. The macrophage and B cell-specific transcription factor PU.1 is related to the ets oncogene. *Cell*, 61, 113-24.
- KLUYTMANS, J., VAN BELKUM, A. & VERBRUGH, H. 1997. Nasal carriage of *Staphylococcus aureus*: epidemiology, underlying mechanisms, and associated risks. *Clinical microbiology reviews*, 10, 505-520.
- KOBAYASHI, S. D., BRAUGHTON, K. R., PALAZZOLO-BALLANCE, A. M., KENNEDY, A. D., SAMPAIO, E., KRISTOSTURYAN, E., WHITNEY, A. R., STURDEVANT, D. E., DORWARD, D. W., HOLLAND, S. M., KREISWIRTH, B. N., MUSSER, J. M. & DELEO, F. R. 2010. Rapid neutrophil destruction following phagocytosis of *Staphylococcus aureus*. *Journal of innate immunity*, 2, 560-575.
- KOBAYASHI, S. D., MALACHOWA, N., WHITNEY, A. R., BRAUGHTON, K. R., GARDNER, D. J., LONG, D., BUBECK WARDENBURG, J., SCHNEEWIND, O., OTTO, M. & DELEO, F. R. 2011. Comparative analysis of USA300 virulence determinants in a rabbit model of skin and soft tissue infection. *J Infect Dis*, 204, 937-41.
- KOONIN, E. V. & ARAVIND, L. 2000. The NACHT family - a new group of predicted NTPases implicated in apoptosis and MHC transcription activation. *Trends Biochem Sci*, 25, 223-4.
- KOZIEL, J., MACIAG-GUDOWSKA, A., MIKOLAJCZYK, T., BZOWSKA, M., STURDEVANT, D. E., WHITNEY, A. R., SHAW, L. N., DELEO, F. R. & POTEMPA, J. 2009. Phagocytosis of *Staphylococcus aureus* by macrophages exerts cytoprotective effects manifested by the upregulation of antiapoptotic factors. *PLoS One*, 4, e5210.
- KUBICA, M., GUZIK, K., KOZIEL, J., ZAREBSKI, M., RICHTER, W., GAJKOWSKA, B., GOLDA, A., MACIAG-GUDOWSKA, A., BRIX, K., SHAW, L., FOSTER, T. & POTEMPA, J. 2008. A potential new pathway for *Staphylococcus aureus* dissemination: the silent survival of *S. aureus* phagocytosed by human monocyte-derived macrophages. *PloS one*, 3.
- KUEHNERT, M. J., KRUSZON-MORAN, D., HILL, H. A., MCQUILLAN, G., MCALLISTER, S. K., FOSHEIM, G., MCDUGAL, L. K., CHAITRAM, J., JENSEN, B., FRIDKIN, S. K., KILLGORE, G. & TENOVER, F. C. 2006. Prevalence of *Staphylococcus aureus* nasal colonization in the United States, 2001-2002. *J Infect Dis*, 193, 172-9.
- KURTEN, R. C., CADENA, D. L. & GILL, G. N. 1996. Enhanced degradation of EGF receptors by a sorting nexin, SNX1. *Science*, 272, 1008-10.
- LAINING, K. J., PURCELL, M. K., WINTON, J. R. & HANSEN, J. D. 2008. A genomic view of the NOD-like receptor family in teleost fish: identification of a novel NLR subfamily in zebrafish. *BMC evolutionary biology*, 8.
- LALANI, T., CHU, V. H., GRUSSEMEYER, C. A., REED, S. D., BOLOGNESI, M. P., FRIEDMAN, J. Y., GRIFFITHS, R. I., CROSSLIN, D. R., KANAFANI, Z. A., KAYE, K. S., RALPH COREY, G. & FOWLER, V. G., JR. 2008. Clinical outcomes and costs among patients with *Staphylococcus aureus* bacteremia and orthopedic device infections. *Scandinavian journal of infectious diseases*, 40, 973-977.
- LEE, W. L., HARRISON, R. E. & GRINSTEIN, S. 2003. Phagocytosis by neutrophils. *Microbes and infection / Institut Pasteur*, 5, 1299-1306.
- LEVINE, B., MIZUSHIMA, N. & VIRGIN, H. W. 2011. Autophagy in immunity and inflammation. *Nature*, 469, 323-35.
- LI, P., WONG, J. J., SUM, C., SIN, W. X., NG, K. Q., KOH, M. B. & CHIN, K. C. 2011. IRF8 and IRF3 cooperatively regulate rapid interferon- β induction in human blood monocytes. *Blood*, 117, 2847-54.
- LIESCHKE, G. J., OATES, A. C., CROWHURST, M. O., WARD, A. C. & LAYTON, J. E. 2001. Morphologic and functional characterization of granulocytes and macrophages in embryonic and adult zebrafish. *Blood*, 98, 3087-3096.

- LIM, J. P. & GLEESON, P. A. 2011. Macropinocytosis: an endocytic pathway for internalising large gulps. *Immunology and cell biology*, 89, 836-843.
- LIM, J. P., WANG, J. T. H., KERR, M. C., TEASDALE, R. D. & GLEESON, P. A. 2008. A role for SNX5 in the regulation of macropinocytosis. *BMC cell biology*, 9.
- LOWY, F. D. 1998. Staphylococcus aureus infections. *The New England journal of medicine*, 339, 520-532.
- LÂM, T.-T., GIESE, B., CHIKKABALLI, D., KÜHN, A., WOLBER, W., PANÉ-FARRÉ, J., SCHÄFER, D., ENGELMANN, S., FRAUNHOLZ, M. & SINHA, B. 2010. Phagolysosomal integrity is generally maintained after Staphylococcus aureus invasion of nonprofessional phagocytes but is modulated by strain 6850. *Infection and immunity*, 78, 3392-3403.
- MAGZOUB, M., SANDGREN, S., LUNDBERG, P., OGLECKA, K., LILJA, J., WITTRUP, A., GÖRAN ERIKSSON, L. E., LANGEL, U., BELTING, M. & GRÄSLUND, A. 2006. N-terminal peptides from unprocessed prion proteins enter cells by macropinocytosis. *Biochem Biophys Res Commun*, 348, 379-85.
- MAUTHE, M., YU, W., KRUT, O., KRÖNKE, M., GÖTZ, F., ROBENEK, H. & PROIKAS-CEZANNE, T. 2012. WIPI-1 Positive Autophagosome-Like Vesicles Entrap Pathogenic Staphylococcus aureus for Lysosomal Degradation. *Int J Cell Biol*, 2012, 179207.
- MCCMAHON, R., ZABOROWSKA, I. & WALSH, D. 2011. Noncytotoxic inhibition of viral infection through eIF4F-independent suppression of translation by 4EGI-1. *J Virol*, 85, 853-64.
- MEDZHITOV, R. 2007. Recognition of microorganisms and activation of the immune response. *Nature*, 449, 819-826.
- MEIJER, A. H., GABBY KRENS, S. F., MEDINA RODRIGUEZ, I. A., HE, S., BITTER, W., EWA SNAAR-JAGALSKA, B. & SPAINK, H. P. 2004. Expression analysis of the Toll-like receptor and TIR domain adaptor families of zebrafish. *Molecular immunology*, 40, 773-783.
- MEIJER, A. H. & VAN DER VAART, M. 2014. DRAM1 promotes the targeting of mycobacteria to selective autophagy. *Autophagy*, 10, 2389-91.
- MENZIES, B. E. 2003. The role of fibronectin binding proteins in the pathogenesis of Staphylococcus aureus infections. *Current opinion in infectious diseases*, 16, 225-229.
- MERCER, J. & HELENIUS, A. 2008. Vaccinia virus uses macropinocytosis and apoptotic mimicry to enter host cells. *Science*, 320, 531-5.
- MESTRE, M. B. & COLOMBO, M. I. 2012. Staphylococcus aureus promotes autophagy by decreasing intracellular cAMP levels. *Autophagy*, 8, 1865-7.
- MESTRE, M. B., FADER, C. M., SOLA, C. & COLOMBO, M. I. 2010. Alpha-hemolysin is required for the activation of the autophagic pathway in Staphylococcus aureus-infected cells. *Autophagy*, 6, 110-25.
- MERINO-TRIGO, A., KERR, M. C., HOUGHTON, F., LINDBERG, A., MITCHELL, C., TEASDALE, R. D. & GLEESON, P. A. 2004. Sorting nexin 5 is localized to a subdomain of the early endosomes and is recruited to the plasma membrane following EGF stimulation. *J Cell Sci*, 117, 6413-24.
- MINAKAMI, R., MAEHARA, Y., KAMAKURA, S., KUMANO, O., MIYANO, K. & SUMIMOTO, H. 2010. Membrane phospholipid metabolism during phagocytosis in human neutrophils. *Genes to cells: devoted to molecular & cellular mechanisms*, 15, 409-424.
- MIZUSHIMA, N., YAMAMOTO, A., HATANO, M., KOBAYASHI, Y., KABEYA, Y., SUZUKI, K., TOKUHISA, T., OHSUMI, Y. & YOSHIMORI, T. 2001. Dissection of autophagosome formation using Apg5-deficient mouse embryonic stem cells. *J Cell Biol*, 152, 657-68.
- MOHAPATRA, N. P., BALAGOPAL, A., SONI, S., SCHLESINGER, L. S. & GUNN, J. S. 2007. AcpA is a Francisella acid phosphatase that affects intramacrophage survival and virulence. *Infection and immunity*, 75, 390-396.

- MOSTOWY, S., BOUCONTET, L., MAZON MOYA, M. J., SIRIANNI, A., BOUDINOT, P., HOLLINSHEAD, M., COSSART, P., HERBOMEL, P., LEVRAUD, J. P. & COLUCCI-GUYON, E. 2013. The zebrafish as a new model for the *in vivo* study of *Shigella flexneri* interaction with phagocytes and bacterial autophagy. *PLoS Pathog*, 9, e1003588.
- MOSTOWY, S. & COSSART, P. 2011. Autophagy and the cytoskeleton: new links revealed by intracellular pathogens. *Autophagy*, 7, 780-2.
- MOTTA, N. 2015. Nanostructures for sensors, electronics, energy and environment II. *Beilstein J Nanotechnol*, 6, 1937-8.
- MUKHOPADHYAY, A. & PETERSON, R. T. 2006. Fishing for new antimicrobials. *Current opinion in chemical biology*, 10, 327-333.
- MULLER, W. A. 2003. Leukocyte-endothelial-cell interactions in leukocyte transmigration and the inflammatory response. *Trends in immunology*, 24, 327-334.
- MURRAY, P. J. & WYNN, T. A. 2011. Protective and pathogenic functions of macrophage subsets. *Nature reviews. Immunology*, 11, 723-737.
- MÖLLER, J., LÜHMANN, T., CHABRIA, M., HALL, H. & VOGEL, V. 2013. Macrophages lift off surface-bound bacteria using a filopodium-lamellipodium hook-and-shovel mechanism. *Sci Rep*, 3, 2884.
- NASEVICIUS, A. & EKKER, S. C. 2000. Effective targeted gene 'knockdown' in zebrafish. *Nature genetics*, 26, 216-220.
- NATHAN, C. 2002. Points of control in inflammation. *Nature*, 420, 846-852.
- NORBURY, C. C., CHAMBERS, B. J., PRESCOTT, A. R., LJUNGGREN, H. G. & WATTS, C. 1997. Constitutive macropinocytosis allows TAP-dependent major histocompatibility complex class I presentation of exogenous soluble antigen by bone marrow-derived dendritic cells. *Eur J Immunol*, 27, 280-8.
- NORBURY, C. C., HEWLETT, L. J., PRESCOTT, A. R., SHASTRI, N. & WATTS, C. 1995. Class I MHC presentation of exogenous soluble antigen via macropinocytosis in bone marrow macrophages. *Immunity*, 3, 783-791.
- NORDENFELT, P. & TAPPER, H. 2011. Phagosome dynamics during phagocytosis by neutrophils. *Journal of leukocyte biology*, 90, 271-284.
- NOVICK, R. P. 2003. Autoinduction and signal transduction in the regulation of staphylococcal virulence. *Molecular microbiology*, 48, 1429-1449.
- ODEBERG, H. & OLSSON, I. 1976. Microbicidal mechanisms of human granulocytes: synergistic effects of granulocyte elastase and myeloperoxidase or chymotrypsin-like cationic protein. *Infection and immunity*, 14, 1276-1283.
- OTTO, M. 2010. Basis of virulence in community-associated methicillin-resistant *Staphylococcus aureus*. *Annu Rev Microbiol*, 64, 143-62.
- O'KEEFFE, K. M., WILK, M. M., LEECH, J. M., MURPHY, A. G., LAABEI, M., MONK, I. R., MASSEY, R. C., LINDSAY, J. A., FOSTER, T. J., GEOGHEGAN, J. A. & MCLOUGHLIN, R. M. 2015. Manipulation of Autophagy in Phagocytes Facilitates *Staphylococcus aureus* Bloodstream Infection. *Infect Immun*, 83, 3445-57.
- PALAZZOLO, A. M., SUQUET, C., KONKEL, M. E. & HURST, J. K. 2005. Green fluorescent protein-expressing *Escherichia coli* as a selective probe for HOCl generation within neutrophils. *Biochemistry*, 44, 6910-9.
- PASE, L., NOWELL, C. J. & LIESCHKE, G. J. 2012. *In vivo* real-time visualization of leukocytes and intracellular hydrogen peroxide levels during a zebrafish acute inflammation assay. *Methods Enzymol*, 506, 135-56.
- PERRIN, A. J., JIANG, X., BIRMINGHAM, C. L., SO, N. S. & BRUMELL, J. H. 2004. Recognition of bacteria in the cytosol of Mammalian cells by the ubiquitin system. *Curr Biol*, 14, 806-11.

- PERSKVIST, N., ROBERG, K., KULYTÉ, A. & STENDAHL, O. 2002. Rab5a GTPase regulates fusion between pathogen-containing phagosomes and cytoplasmic organelles in human neutrophils. *J Cell Sci*, 115, 1321-30.
- PETER, B. J., KENT, H. M., MILLS, I. G., VALLIS, Y., BUTLER, P. J., EVANS, P. R. & MCMAHON, H. T. 2004. BAR domains as sensors of membrane curvature: the amphiphysin BAR structure. *Science*, 303, 495-9.
- PETRIE, T. A., STRAND, N. S., YANG, C. T., TSUNG-YANG, C., RABINOWITZ, J. S. & MOON, R. T. 2014. Macrophages modulate adult zebrafish tail fin regeneration. *Development*, 141, 2581-91.
- PHELAN, P. E., MELLON, M. T. & KIM, C. H. 2005. Functional characterization of full-length TLR3, IRAK-4, and TRAF6 in zebrafish (*Danio rerio*). *Molecular immunology*, 42, 1057-1071.
- PIZARRO-CERDÁ, J., MÉRESSE, S., PARTON, R. G., VAN DER GOOT, G., SOLA-LANDA, A., LOPEZ-GOÑI, I., MORENO, E. & GORVEL, J. P. 1998. *Brucella abortus* transits through the autophagic pathway and replicates in the endoplasmic reticulum of nonprofessional phagocytes. *Infect Immun*, 66, 5711-24.
- PRAJSNAR, T. K., CUNLIFFE, V. T., FOSTER, S. J. & RENSHAW, S. A. 2008. A novel vertebrate model of *Staphylococcus aureus* infection reveals phagocyte-dependent resistance of zebrafish to non-host specialized pathogens. *Cellular microbiology*, 10, 2312-2325.
- PRAJSNAR, T. K., HAMILTON, R., GARCIA-LARA, J., MCVICKER, G., WILLIAMS, A., BOOTS, M., FOSTER, S. J. & RENSHAW, S. A. 2012. A privileged intraphagocyte niche is responsible for disseminated infection of *Staphylococcus aureus* in a zebrafish model. *Cellular microbiology*, 14, 1600-1619.
- PROCTOR, R. A., DALAL, S. C., KAHL, B., BRAR, D., PETERS, G. & NICHOLS, W. W. 2002. Two diarylurea electron transport inhibitors reduce *Staphylococcus aureus* hemolytic activity and protect cultured endothelial cells from lysis. *Antimicrob Agents Chemother*, 46, 2333-6.
- RACOOSIN, E. L. & SWANSON, J. A. 1989. Macrophage colony-stimulating factor (rM-CSF) stimulates pinocytosis in bone marrow-derived macrophages. *J Exp Med*, 170, 1635-48.
- RAHME, L. G., STEVENS, E. J., WOLFORT, S. F., SHAO, J., TOMPKINS, R. G. & AUSUBEL, F. M. 1995. Common virulence factors for bacterial pathogenicity in plants and animals. *Science (New York, N.Y.)*, 268, 1899-1902.
- RAMAKRISHNAN, L., FEDERSPIEL, N. A. & FALKOW, S. 2000. Granuloma-specific expression of *Mycobacterium* virulence proteins from the glycine-rich PE-PGRS family. *Science (New York, N.Y.)*, 288, 1436-1439.
- RENSHAW, S. A., LOYNES, C. A., TRUSHELL, D. M. I., ELWORTHY, S., INGHAM, P. W. & WHYTE, M. K. B. 2006. A transgenic zebrafish model of neutrophilic inflammation. *Blood*, 108, 3976-3978.
- RHODES, J., HAGEN, A., HSU, K., DENG, M., LIU, T. X., LOOK, A. T. & KANKI, J. P. 2005. Interplay of pu.1 and gata1 determines myelo-erythroid progenitor cell fate in zebrafish. *Dev Cell*, 8, 97-108.
- ROGERS, D. E. & TOMPSETT, R. 1952. The survival of staphylococci within human leukocytes. *The Journal of experimental medicine*, 95, 209-230.
- ROOIJAKKERS, S. H. M., VAN KESSEL, K. P. M. & VAN STRIJP, J. A. G. 2005. Staphylococcal innate immune evasion. *Trends in microbiology*, 13, 596-601.
- SALLUSTO, F., CELLA, M., DANIELI, C. & LANZAVECCHIA, A. 1995. Dendritic cells use macropinocytosis and the mannose receptor to concentrate macromolecules in the major histocompatibility complex class II compartment: downregulation by cytokines and bacterial products. *J Exp Med*, 182, 389-400.

- SANDVIG, K. & VAN DEURS, B. 1990. Selective modulation of the endocytic uptake of ricin and fluid phase markers without alteration in transferrin endocytosis. *The Journal of biological chemistry*, 265, 6382-6388.
- SANSONETTI, C. J., READER, J. & VOGLER, K. 2001. Precision measurement of wavelengths emitted by a molecular fluorine laser at 157 nm. *Appl Opt*, 40, 1974-8.
- SAVILL, J. S., WYLLIE, A. H., HENSON, J. E., WALPORT, M. J., HENSON, P. M. & HASLETT, C. 1989. Macrophage phagocytosis of aging neutrophils in inflammation. Programmed cell death in the neutrophil leads to its recognition by macrophages. *The Journal of clinical investigation*, 83, 865-875.
- SCHIEBLER, M., BROWN, K., HEGYI, K., NEWTON, S. M., RENNA, M., HEPBURN, L., KLAPHOLZ, C., COULTER, S., OBREGÓN-HENAO, A., HENAO TAMAYO, M., BASARABA, R., KAMPMANN, B., HENRY, K. M., BURGON, J., RENSHAW, S. A., FLEMING, A., KAY, R. R., ANDERSON, K. E., HAWKINS, P. T., ORDWAY, D. J., RUBINSZTEIN, D. C. & FLOTO, R. A. 2015. Functional drug screening reveals anticonvulsants as enhancers of mTOR-independent autophagic killing of Mycobacterium tuberculosis through inositol depletion. *EMBO Mol Med*, 7, 127-39.
- SCHNAITH, A., KASHKAR, H., LEGGIO, S. A., ADDICKS, K., KRÖNKE, M. & KRUT, O. 2007. Staphylococcus aureus subvert autophagy for induction of caspase-independent host cell death. *The Journal of biological chemistry*, 282, 2695-2706.
- SCHRODER, K. & TSCHOPP, J. 2010. The inflammasomes. *Cell*, 140, 821-32.
- SCHROEDER, G. N. & HILBI, H. 2008. Molecular pathogenesis of Shigella spp.: controlling host cell signaling, invasion, and death by type III secretion. *Clin Microbiol Rev*, 21, 134-56.
- SCHRÖDER, A., KLAND, R., PESCHEL, A., VON EIFF, C. & AEPFELBACHER, M. 2006a. Live cell imaging of phagosome maturation in Staphylococcus aureus infected human endothelial cells: small colony variants are able to survive in lysosomes. *Med Microbiol Immunol*, 195, 185-94.
- SCHRÖDER, A., KLAND, R., PESCHEL, A., VON EIFF, C. & AEPFELBACHER, M. 2006b. Live cell imaging of phagosome maturation in Staphylococcus aureus infected human endothelial cells: small colony variants are able to survive in lysosomes. *Medical microbiology and immunology*, 195, 185-194.
- SCHWARTEN, M., MOHRLÜDER, J., MA, P., STOLDT, M., THIELMANN, Y., STANGLER, T., HERSCH, N., HOFFMANN, B., MERKEL, R. & WILLBOLD, D. 2009. Nix directly binds to GABARAP: a possible crosstalk between apoptosis and autophagy. *Autophagy*, 5, 690-8.
- SEGAL, A. W. 2005. How neutrophils kill microbes. *Annual review of immunology*, 23, 197-223.
- SELLGE, G. & KUFER, T. A. 2015. PRR-signaling pathways: Learning from microbial tactics. *Semin Immunol*, 27, 75-84.
- SENDI, P. & PROCTOR, R. A. 2009. Staphylococcus aureus as an intracellular pathogen: the role of small colony variants. *Trends Microbiol*, 17, 54-8.
- SERHAN, C. N. & SAVILL, J. 2005. Resolution of inflammation: the beginning programs the end. *Nature immunology*, 6, 1191-1197.
- SERRUTO, D., RAPPUOLI, R., SCARSELLI, M., GROS, P. & VAN STRIJP, J. A. G. 2010. Molecular mechanisms of complement evasion: learning from staphylococci and meningococci. *Nature reviews. Microbiology*, 8, 393-399.
- SHAH, V. B., HUANG, Y., KESHWARA, R., OZMENT-SKELTON, T., WILLIAMS, D. L. & KESHVARA, L. 2008. Beta-glucan activates microglia without inducing cytokine production in Dectin-1-dependent manner. *Journal of immunology (Baltimore, Md.: 1950)*, 180, 2777-2785.

- SHERE, K. D., SALLUSTIO, S., MANESSIS, A., D'AVERSA, T. G. & GOLDBERG, M. B. 1997. Disruption of IcsP, the major Shigella protease that cleaves IcsA, accelerates actin-based motility. *Mol Microbiol*, 25, 451-62.
- SHORR, A. F., TABAK, Y. P., KILLIAN, A. D., GUPTA, V., LIU, L. Z. & KOLLEF, M. H. 2006. Healthcare-associated bloodstream infection: A distinct entity? Insights from a large U.S. database. *Critical care medicine*, 34, 2588-2595.
- SILVA, M. T. 2011. Macrophage phagocytosis of neutrophils at inflammatory/infectious foci: a cooperative mechanism in the control of infection and infectious inflammation. *J Leukoc Biol*, 89, 675-83.
- SPEERT, D. P., BOND, M., WOODMAN, R. C. & CURNUTTE, J. T. 1994. Infection with *Pseudomonas cepacia* in chronic granulomatous disease: role of nonoxidative killing by neutrophils in host defense. *J Infect Dis*, 170, 1524-31.
- STEELE-MORTIMER, O., KNODLER, L. A. & FINLAY, B. B. 2000. Poisons, ruffles and rockets: bacterial pathogens and the host cell cytoskeleton. *Traffic*, 1, 107-18.
- STEIN, C., CACCAMO, M., LAIRD, G. & LEPTIN, M. 2007. Conservation and divergence of gene families encoding components of innate immune response systems in zebrafish. *Genome Biol*, 8, R251.
- STOIBER, W., OBERMAYER, A., STEINBACHER, P. & KRAUTGARTNER, W. D. 2015. The Role of Reactive Oxygen Species (ROS) in the Formation of Extracellular Traps (ETs) in Humans. *Biomolecules*, 5, 702-723.
- STURGILL-KOSZYCKI, S. & SWANSON, M. S. 2000. Legionella pneumophila replication vacuoles mature into acidic, endocytic organelles. *J Exp Med*, 192, 1261-72.
- SUMMERS, C., RANKIN, S. M., CONDLIFFE, A. M., SINGH, N., PETERS, A. M. & CHILVERS, E. R. 2010. Neutrophil kinetics in health and disease. *Trends in immunology*, 31, 318-324.
- SWANSON, J. A. 2008. Shaping cups into phagosomes and macropinosomes. *Nature reviews. Molecular cell biology*, 9, 639-649.
- SWANSON, J. A. & WATTS, C. 1995. Macropinocytosis. *Trends Cell Biol*, 5, 424-8.
- TEASDALE, R. D., LOCI, D., HOUGHTON, F., KARLSSON, L. & GLEESON, P. A. 2001. A large family of endosome-localized proteins related to sorting nexin 1. *Biochem J*, 358, 7-16.
- THAMMAVONGSA, V., MISSIAKAS, D. M. & SCHNEEWIND, O. 2013. Staphylococcus aureus degrades neutrophil extracellular traps to promote immune cell death. *Science*, 342, 863-6.
- THWAITES, G. E. & GANT, V. 2011. Are bloodstream leukocytes Trojan Horses for the metastasis of Staphylococcus aureus? *Nature reviews. Microbiology*, 9, 215-222.
- TING, J. P., LOVERING, R. C., ALNEMRI, E. S., BERTIN, J., BOSS, J. M., DAVIS, B. K., FLAVELL, R. A., GIRARDIN, S. E., GODZIK, A., HARTON, J. A., HOFFMAN, H. M., HUGOT, J. P., INOHARA, N., MACKENZIE, A., MALTAIS, L. J., NUNEZ, G., OGURA, Y., OTTEN, L. A., PHILPOTT, D., REED, J. C., REITH, W., SCHREIBER, S., STEIMLE, V. & WARD, P. A. 2008. The NLR gene family: a standard nomenclature. *Immunity*, 28, 285-7.
- TREDE, N. S., LANGENAU, D. M., TRAVER, D., LOOK, A. T. & ZON, L. I. 2004. The use of zebrafish to understand immunity. *Immunity*, 20, 367-379.
- TSIEN, R. Y. 1998. The green fluorescent protein. *Annu Rev Biochem*, 67, 509-44.
- VAN BAMBEKE, F., BARCIA-MACAY, M., LEMAIRE, S. & TULKENS, P. M. 2006. Cellular pharmacodynamics and pharmacokinetics of antibiotics: current views and perspectives. *Current opinion in drug discovery & development*, 9, 218-230.
- VAN DER SAR, A. M., MUSTERS, R. J. P., VAN EEDEN, F. J. M., APPELMELK, B. J., VANDENBROUCKE-GRAULS, C. M. J. E. & BITTER, W. 2003. Zebrafish embryos as a model host for the real time analysis of Salmonella typhimurium infections. *Cellular microbiology*, 5, 601-611.

- VENDITTI, M., FALCONE, M., MICOZZI, A., CARFAGNA, P., TAGLIETTI, F., SERRA, P. F. & MARTINO, P. 2003. Staphylococcus aureus bacteremia in patients with hematologic malignancies: a retrospective case-control study. *Haematologica*, 88, 923-930.
- VENEMAN, W. J., STOCKHAMMER, O. W., DE BOER, L., ZAAT, S. A., MEIJER, A. H. & SPAINK, H. P. 2013. A zebrafish high throughput screening system used for Staphylococcus epidermidis infection marker discovery. *BMC Genomics*, 14, 255.
- VERDRENGH, M. & TARKOWSKI, A. 1997. Role of neutrophils in experimental septicemia and septic arthritis induced by Staphylococcus aureus. *Infection and immunity*, 65, 2517-2521.
- VERDRENGH, M. & TARKOWSKI, A. 2000. Role of macrophages in Staphylococcus aureus-induced arthritis and sepsis. *Arthritis and rheumatism*, 43, 2276-2282.
- VIEIRA, O. V., BOTELHO, R. J. & GRINSTEIN, S. 2002. Phagosome maturation: aging gracefully. *The Biochemical journal*, 366, 689-704.
- WADIA, J. S., SCHALLER, M., WILLIAMSON, R. A. & DOWDY, S. F. 2008. Pathologic prion protein infects cells by lipid-raft dependent macropinocytosis. *PLoS One*, 3, e3314.
- WALHOUT, A. J., TEMPLE, G. F., BRASCH, M. A., HARTLEY, J. L., LORSON, M. A., VAN DEN HEUVEL, S. & VIDAL, M. 2000. GATEWAY recombinational cloning: application to the cloning of large numbers of open reading frames or ORFeomes. *Methods Enzymol*, 328, 575-92.
- WALMSLEY, S. R., PRINT, C., FARAHI, N., PEYSSONNAUX, C., JOHNSON, R. S., CRAMER, T., SOBOLEWSKI, A., CONDLIFFE, A. M., COWBURN, A. S., JOHNSON, N. & CHILVERS, E. R. 2005. Hypoxia-induced neutrophil survival is mediated by HIF-1alpha-dependent NF-kappaB activity. *The Journal of experimental medicine*, 201, 105-115.
- WANDERLEY, J. L., MOREIRA, M. E., BENJAMIN, A., BONOMO, A. C. & BARCINSKI, M. A. 2006. Mimicry of apoptotic cells by exposing phosphatidylserine participates in the establishment of amastigotes of Leishmania (L) amazonensis in mammalian hosts. *J Immunol*, 176, 1834-9.
- WANG, J. T. H., KERR, M. C., KARUNARATNE, S., JEANES, A., YAP, A. S. & TEASDALE, R. D. 2010. The SNX-PX-BAR family in macropinocytosis: the regulation of macropinosome formation by SNX-PX-BAR proteins. *PLoS one*, 5.
- WANG, R., BRAUGHTON, K. R., KRETSCHMER, D., BACH, T. H., QUECK, S. Y., LI, M., KENNEDY, A. D., DORWARD, D. W., KLEBANOFF, S. J., PESCHEL, A., DELEO, F. R. & OTTO, M. 2007. Identification of novel cytolytic peptides as key virulence determinants for community-associated MRSA. *Nat Med*, 13, 1510-4.
- WATARAI, M., DERRE, I., KIRBY, J., GROWNEY, J. D., DIETRICH, W. F. & ISBERG, R. R. 2001. Legionella pneumophila is internalized by a macropinocytotic uptake pathway controlled by the Dot/Icm system and the mouse Lgn1 locus. *The Journal of experimental medicine*, 194, 1081-1096.
- WEICHHART, T., HORKY, M., SÖLLNER, J., GANGL, S., HENICS, T., NAGY, E., MEINKE, A., VON GABAIN, A., FRASER, C. M., GILL, S. R., HAFNER, M. & VON AHSEN, U. 2003. Functional selection of vaccine candidate peptides from Staphylococcus aureus whole-genome expression libraries *in vitro*. *Infection and immunity*, 71, 4633-4641.
- WERTHEIM, H. F. L., VOS, M. C., OTT, A., VAN BELKUM, A., VOSS, A., KLUYTMANS, J. A. J. W., VAN KEULEN, P. H. J., VANDENBROUCKE-GRAULS, C. M. J. E., MEESTER, M. H. M. & VERBRUGH, H. A. 2004. Risk and outcome of nosocomial Staphylococcus aureus bacteraemia in nasal carriers versus non-carriers. *Lancet*, 364, 703-705.
- WRIGHT, L. P. & PHILIPS, M. R. 2006. Thematic review series: lipid posttranslational modifications. CAAX modification and membrane targeting of Ras. *J Lipid Res*, 47, 883-91.

- WYLLIE, D. H., CROOK, D. W. & PETO, T. E. A. 2006. Mortality after *Staphylococcus aureus* bacteraemia in two hospitals in Oxfordshire, 1997-2003: cohort study. *BMJ (Clinical research ed.)*, 333.
- YANG, C. T., CAMBIER, C. J., DAVIS, J. M., HALL, C. J., CROSIER, P. S. & RAMAKRISHNAN, L. 2012. Neutrophils exert protection in the early tuberculous granuloma by oxidative killing of mycobacteria phagocytosed from infected macrophages. *Cell Host Microbe*, 12, 301-12.
- YANO, T., MITA, S., OHMORI, H., OSHIMA, Y., FUJIMOTO, Y., UEDA, R., TAKADA, H., GOLDMAN, W. E., FUKASE, K., SILVERMAN, N., YOSHIMORI, T. & KURATA, S. 2008. Autophagic control of listeria through intracellular innate immune recognition in drosophila. *Nature immunology*, 9, 908-916.
- YARWOOD, J. M. & SCHLIEVERT, P. M. 2003. Quorum sensing in *Staphylococcus* infections. *The Journal of clinical investigation*, 112, 1620-1625.
- YOKOYAMA, W. M. & COLONNA, M. 2008. Innate immunity to pathogens. *Current opinion in immunology*, 20, 1-2.
- YOO, K.-W., KIM, E.-H., JUNG, S.-H., RHEE, M., KOO, B.-K., YOON, K.-J., KONG, Y.-Y. & KIM, C.-H. 2006. Snx5, as a Mind bomb-binding protein, is expressed in hematopoietic and endothelial precursor cells in zebrafish. *FEBS letters*, 580, 4409-4416.
- YOO, S. K., DENG, Q., CAVNAR, P. J., WU, Y. I., HAHN, K. M. & HUTTENLOCHER, A. 2010. Differential regulation of protrusion and polarity by PI3K during neutrophil motility in live zebrafish. *Dev Cell*, 18, 226-36.
- ZAREMBER, K. A. & GODOWSKI, P. J. 2002. Tissue expression of human Toll-like receptors and differential regulation of Toll-like receptor mRNAs in leukocytes in response to microbes, their products, and cytokines. *J Immunol*, 168, 554-61.